Imperial College London

Department of Physics

Magnetic Quivers – A New Perspective on Supersymmetric Gauge Theories

Zhenghao Zhong

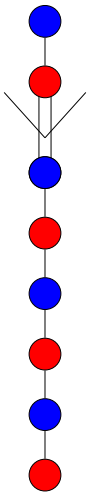

Submitted in part fulfilment of the requirements

for the degree of Doctor of Philosophy in Physics at

Imperial College London, May 2022

The research in this thesis is my own work and is the result from collaborations with several collaborators throughout the course of the PhD.

This thesis includes work from our following papers:

- [1] A.Hanany and Z.Zhong. "Highest Weight Generating function for tropical quivers. (not published)," (2019)
- [2] A.Bourget, J.F. Grimminger, A.Hanany, R.Kalveks, M.Sperling and Z.Zhong. "Magnetic Lattice for Orthosymplectic Quivers," *JHEP* **12** (2020) 092
- [3] A.Bourget, J.F. Grimminger, A.Hanany, M.Sperling and Z.Zhong. "Magnetic Quivers from Brane Webs with O5 Planes," *JHEP* **07** (2020) 204
- [4] S.Nawata, M.Sperling, H.W.Wang and Z.Zhong. "On a duality between 3d $\mathcal{N} = 4$ unitary and orthosymplectic quivers," *JHEP* **02** (2022) 174
- [5] M.Sperling and Z.Zhong. "Balanced B and D-type orthosymplectic quivers – magnetic quivers for product theories," *JHEP* **04** (2022) 145
- [6] A.Bourget, J.F. Grimminger, A.Hanany, M.Sperling, G.Zafrir and Z.Zhong. "Magnetic quivers for rank 1 theories," *JHEP* **09** (2020) 189
- [7] A.Bourget, Simone Giacomelli, J.F. Grimminger, A.Hanany, M.Sperling and Z.Zhong. "S-fold magnetic quivers," *JHEP* **02** (2021) 054
- [8] A.Bourget, J.F. Grimminger, A.Hanany, R.Kalveks, M.Sperling and Z.Zhong. "Folding orthosymplectic quivers," *JHEP* **12** (2021) 070
- [9] A.Bourget, J.F. Grimminger, A.Hanany, R.Kalveks and Z.Zhong. "Higgs branches of U/SU Quivers via Brane Locking," *submitted to JHEP* (2021) [arXiv: 2111.04745]
- [10] A.Bourget, S.Cabrera, J.F. Grimminger, A.Hanany, M.Sperling, A.Zajac and Z.Zhong. "The Higgs Mechanism – Hasse diagrams for Symplectic Singularities ," *JHEP* **01** (2020) 157

Other works that are completed during this PhD but not included in this thesis are:

- [11] A.Bourget, S.Cabrera, J.F. Grimminger, A.Hanany and Z.Zhong. "Brane webs and Magnetic Quivers for SQCD ," *JHEP* **03** (2020) 176
- [12] A.Bourget, J.F. Grimminger, A.Hanany, M.Sperling and Z.Zhong. "Branes, Quivers and the Affine Grassmannian," (2021) [arXiv: 2102.06190]

- [13] A.Bourget, A.Dancer, J.F. Grimminger, A.Hanany, F.Kirwan and Z.Zhong. "Orthosymplectic implosions," *JHEP* **08** (2021) 012
- [14] A.Bourget, A.Dancer, J.F. Grimminger, A.Hanany and Z.Zhong. "Partial implosions and Quivers," *submitted to JHEP* (2021) [arXiv: 2112.10825]
- [15] A.Bourget, J.F. Grimminger, A.Hanany and Z.Zhong. "The Hasse Diagram of the Moduli Space of Instantons," *submitted to JHEP* (2022) [arXiv: 2202.01218]

Zhenghao Zhong (2022)

The copyright of this thesis rests with the author and is made available under a Creative Commons Attribution Non-Commercial No Derivatives licence. Researchers are free to copy, distribute or transmit the thesis on the condition that they attribute it, that they do not use it for commercial purposes and that they do not alter, transform or build upon it. For any reuse or redistribution, researchers must make clear to others the licence terms of this work.

Abstract

We focus on supersymmetric gauge theories with eight superchrages in spacetime dimensions $d = 3, 4, 5, 6$. These theories have very rich vacuum structures so our focus will be on their moduli spaces of vacua. For $d =, 4, 5, 6$, we look at the *Higgs branch* moduli space. The usual story is that the Higgs branch is a classical object that can be easily computed from its Lagrangian. However, non-perturbative contributions can enhance the Higgs branch and a classical description no longer works. In $6d$ $\mathcal{N} = (1, 0)$ and $5d$ $\mathcal{N} = (1, 0)$, these contributions originate from tensionless BPS-strings and massless gauge instantons respectively as we tune gauge coupling(s) to infinity. For $4d$ $\mathcal{N} = 2$ theories, many gauge theories, and in particular superconformal field theories (SCFTs), do not even have a Lagrangian description. We offer a unifying solution to these problems in the form of *magnetic quivers*. These are $3d$ $\mathcal{N} = 4$ gauge theories whose *Coulomb branch* is the same as the Higgs branch of the higher dimensional theories. Using brane systems of $\mathrm{D}_d - \mathrm{D}_{d+2} - \mathrm{NS5}$, with the possible inclusion of O_d orientifold planes, we show how the magnetic quivers of these theories can be extracted. Then, a) using the monopole formula we study the moduli space as an algebraic variety by computing its Hilbert series and b) using the new concept of *Quiver subtraction* we extract the phase diagram (Hasse diagram) of these moduli spaces. Examples we explore include 5d SQCD theories at UV fixed point, 4d rank one SCFTs, class $\mathcal{S}$ theories, $\mathcal{S}$-fold theories etc. For the second outcome of the thesis, we focus on new features of gauge theories with orthosymplectic gauge groups such as discrete subgroups and non-simply laced edges, leading to a general classification of such theories. For the final outcome, we study gauge theories with a mixture of unitary and special unitary gauge groups which lead to a slew of new gauge theories related by 3d mirror symmetry.

Acknowledgements

能够有今天，我感谢我的爸爸妈妈，外公外婆，爷爷奶奶的支持！还要感谢Andrew在英国那么多年以来一直帮助我！

My academic journey began back in December 2015. I saw a (Youtube) lecture by Ami in Thailand talking about group theory and particle physics. It was quite the awe inspiring talk. I contacted Ami for a summer project and he agreed! An actual research project in theoretical physics. At the time no one else was willing to give such an opportunity to a second year undergrad. I remember my first task was to compute the Coulomb branch Hilbert series of a $U(1)$ gauge theory with two electrons. And *that* was when my journey in quiver gauge theory began. If I didn't send Ami that email all those years ago, life would have been quite different. Perhaps I wouldn't even have gotten a chance to work in theoretical physics. It is really quite remarkable how life can change by just one email.

To have a PhD supervisor who was always there when I needed help and always encouraged, but not pressured, me to do my best. And in the end, all of these lead to an enjoyable, flexible but yet, very productive PhD lifestyle. What more can a PhD student ask for? Thank you Ami!

I would like to thank all the Quiver Family members (in chronological order of me physically meeting them):

Santiago (2016): when Ami assigned me a quiver project all the way back in 2015, I honestly was not sure how to proceed. But then I met you! Back then, you just started as a PhD student and already knew so much about the subject. Your intuitiveness with physics, your passion, and how you bend branes to your will (pun intended) is absolutely remarkable. Really! The way you solve difficult gauge theory questions with just brane manipulations is just magical. I mean everything we did with magnetic quivers were based so heavily on your previous works of Kraft-Procesi transition, Quiver subtractions etc. In fact, during your last day as a PhD student at imperial, you came up with the amazing idea of 5d Kraft-Procesi transitions that led to the Hasse paper and subsequent publications on magnetic quiver!

I've never seen such a kind and passionate physicist and I will also never forget our cartoon discussions! Muchas gracias amigo!

Rudolph (2017): Thank you so much for developing all the awesome `Mathematica` codes we use to compute Hilbert series. To be honest, without all these amazingly efficient and powerful codes I don't know how I would have computed like 95% of all of Higgs branch Hilbert series and HWGs! And your knowledge in group theory is absolutely unparalleled.

Dominick (2018): For being a great AQFT rapid feedback tutor and an absolute computer wiz. It was unfortunate that we didn't have enough time before you left to do some really cool stuff with Machine learning and speed up the monopole formula. But it was always great to chat with you when you're around!

Anton (2018): I will never forget the time you invited us to Bratislava and to the dinner with Roger Penrose. That was so dope!!! It was unfortunate that our trips didn't continue due to Covid. Otherwise I'm certain we could have some amazing times and done some insane Hilbert series computations by paralellizing the summation on the 100 core computer! Those would have generated some really nice results! Will also never forget the time we explored the wild in South africa after midnight! That was quite the thrilling experience!

Julius (2018): My quiver brother! Maybe it is fate but somehow when we do research it is just so in sync! Back in 2019 summer, no one was keen on doing magnetic quiver with O5 branes and you're the only one that just keep pushing us to work on this project. And when all of us buckled down, we got something beautiful that kicked started the orthosymplectic program. Without this paper I would never have wanted to push for the Magnetic lattice paper. And now, we have like 5 subsequent orthosymplectic quiver papers! What an absolute haul! And bro I will always remember our conference trips. I mean, like if we didn't do all the traveling back in 2019, Covid would have meant that I never travel at all during my PhD! It also got me totally hooked to traveling to places now which I absolutely embrace!

Antoine (2018): I remember the day we first met. I never thought this random person sitting in the chair in Huxley common room will become such a close friend and colleague! The knowledge you have about mathematics and your intuitiveness in coding is absolutely jaw dropping. I mean who on earth is able to code in real time whilst having a conversation and then actually solve the problem??? Wht the heck??? And if I give you 10 more minutes, you can make that code 100x more efficient! But aside of all your research achievements, I think your Youtube channel is just such a remarkable thing. To commit to teaching advanced mathematics to the public and in an entertaining and clear fashion is just so dope. I just wish it was in English... I mean if its in English I'd volunteer to be your Youtube manager!

Marcus (2018): My Chinese brother! It is one thing to have a friend abroad, but to have a friend at home, by which I mean in China, is such a blessing. I suppose we physically met in 2018 but I've first studied your work in great detail all the way back in 2016! I was always amazed just how incredibly fast you can learn and absorb things! When confronted with a completely

new topic you will say "Let me do some reading" and the next day afternoon you explained the details to me like an expert of that field! And somehow, no matter how complicated the concept, you can always explain it in such a way that I can quickly understand! It's like magic! And you are always a shoulder to lean on when I need help whether it is academic or in life. And our time in China, especially in Beijing was so fantastic! The Yanqi lake and Tsinghua trip really is a dream come true. Also, you're my only quiver family who is cool enough to watch the same anime+cartoons as me! Great tastes bro!

Kirsty (2020): First time I have a younger member in the quiver family! It was so bizzare that we know each other for a whole year via zoom before actually meeting in person in 2021! And yet in such crazy times you were able to do amazing research and discover an infinite number of quivers that subverts expectation of global symmetry. Very proud of you and also you convinced me a vegan cake can be really delicious! Hope all the best in your future journeys!

Giulia (2014): I rarely met Giulia during my PhD since she technically graduated the moment I entered my PhD. But nevertheles, she was my 1st year undergraduate tutor! I remember asking her about her research back in 2014, and she replied:"Oh, my research is very mathematical". It is so unbeliavable that a few years later I am doing the same research as she is!! I cannot overstate just how much her MSc dissertation have helped me in my journey.

I would like to thank all my other collaborators Andrew Dancer, Simone Giacomelli, Wang Hao, Frances Kirwan, Salvo Mancani and Satoshi Nawata for all the help and awesome collaborations over the years.

In particular, I would like to thank Gabi Zafrir for collaboration as well as many amazing conversations that led to the developments in orthosymplectic quivers.

I would also like to thank Stefano Cremonesi, Yanghui-He, Noppadol Mekareeya, Daniel Juteau and Rak-Kyeong Seong both for developing all the fantastics tools to study moduli spaces as well as invaluable discussions throughout the years.

Undergrad

I've been at imperial college for my undergrad starting in 2014 all the way till I finish my PhD in 2022. During my undergrad, which certainly was no cake walk, I was grateful to have Andreas Georgakis, Sean Barrett, Guillaume Dideron to accompany me in this journey. I would also like to thank Victor Chen and Kwok Ho Wan who were the first to convince me to do a summer project back in my second year in undergrad! Otherwise I never would have the courage

to do so. I am also glad to still stay in touch with so many of you!

I would also like to thank Rahim Leung and Sumer Jaitly who were with me since undergrad and all the way to PhD! In fact, Rahim and I met all the way in our first year student accomadation at Xenia! I bet neither of us in 2014 would have thought we are still colleagues in the same building 8 years onwards!

I am also grateful for Vijay Tymms who interviewed me and accepted me into Imperial college undergrad in the spring of 2014. Oliver Buchmueller for being my personal tutor for my undergrad.

And especially my senior tutor Zhang Jing who was always there when I needed someone to talk to both during my undergrad and my masters. Looking back, I'm really glad to have a mentor and a friend to support me through those times.

QFFF

The MSc in QFFF here is no picnic. But once again I'm glad to have such amazing friends. My dear friend Arshia who is now my PhD colleague as well. I think out of everyone we think the most alike and enjoy the most similar things. I will miss those insightful physics discussions but also our Call of Duty zombie nights! This is one thing I never had in my past, a FPS gaming friend! And only you would have thought of that absolutely ridiculously fun journey in the middle of nowhere in Norway! That was such a beautiful experience!!!

I will also remember my friends Zhang Yan Bai, Song Shi Cong, Wu Wei and Wang Jie Yu. To be honest, growing up in an international school means I never really had Chinese friends when I was young. Before hanging out with you guys I never realized I missed out on so much about our culture.

And Sun Pu Wen, my friend since we were students in undergrad. I think out of everyone I know, you were the most passionate about physics. It was just absolutely awesome that you followed your dream to do particle physics and then you made it!

I would also like to thank all my lecturers during my studies. In particular, I really enjoyed the unification course by Arttu Rajantie, particle symmetries course by Dan Waldram and the differential geometry course by Chris Hull .

PhD

After years of looking up to the PhD students in the theory group, I am glad to finally join them in 2018.

Ed Tasker was not just a great friend but also an absolutely amazing teacher. When I was in undergrad, Ed taught the rapid feedback class for Foundations of Quantum Mechanics. That was... just the best course ever. I think there were more students in the feedback course than in the actual lecture (and the lecture already has a lot of people, which says something about how many people that went to the feedback!). The amount of effort that Ed put in into each and every answer in the problem sheet was incredible. He didn't just write down the official solutions but *in addition* gave his own solutions as well. And this is not just me saying this but all my colleagues back in undergrad agreed as well! Ed also taught me in the rapid feedback for differential geometry. He marked all the questions in all of our problem sheets with very detailed feedbacks. Having done a rapid feedback myself, I can really see just how much extra effort and dedication Ed put in. And I absolutely mean it when I say **no one** else did a better job in teaching than he did. You can really feel his passion teaching those courses. I wish I had more chances to tell him just how amazing he is...

When I first started by PhD, some of my new PhD colleagues I already knew from QFFF rapid feedbacks: Alex harrold teaching us black holes, Simon Nakach for QED and Lucas Wallis for QFT. I am glad to know them both as teachers and as friends.

I have more time to spend with David Tennyson and Nat Levine, since they are younger, and glad we went to cool trips to France and Spain together!

Krai Cheamsawat and Nipol Chaemjumrus, thank you for all your recommendation on reading materials on Brane Dynamics and U-duality! They really helped me during my PhD!

Matthew Cheung, you're just such a knowledgeble guy! Not only are you an expert in your own field, you even know like 90% of the topics that I deal with in my research! I wish you all the best for your future and will never forget the honest chats we have on the long walks back from college. Thank you for being a great friend and colleague!

Justinas Rubumtis, I won't forget all our movie nights together! Now that you are going to Taiwan I wish you the best and since it is pretty close to home, I hope we meet often in the Taiwan night markets!

Andreas Mantziris, it was so cool hanging out with you. But sadly Covid meant we basically didn't see each other for like 30 months! But I'm glad we got to chat in the last few months!

I am of course glad to have all my other PhD colleagues Ariana Renzini, Stav Zalel, David Ho, Chris Erickson, Clement Mawby and Henry Price. And all the younger PhD students as well! I gotta admit, the younger generations might know how to party better than us older ones! All of you really made the theory group a fun and memorable experience.

Cartoons!

I know this is quite unusual but it is not just humans that got me through my PhD. I am glad be living in the renaissance of cartoon shows in the last few years. PhD life isnt walys rainbows and sunshines but these shows really got me through the some hard times. In particular: The Simpsons, My Little Pony: Friendship is Magic, Animaniacs, Star vs The Forces of Evil, She-ra, Castlevania, The Amazing World of Gumball, Gravity Falls, The Owl House, Amphibia and last but not least, Sonic X. And I am very glad to enjoy many of them with my colleagues as well!

To my parents and my grandparents

. . . and to $\mathcal{L}.\mathcal{M}.\mathcal{S}$

If you are receptive and humble, mathematics will lead you by the hand.

- Paul Dirac

Contents

List of Tables

List of Figures

Introduction

When Paul Dirac wrote down his equation that describes a quantum theory of electrons [26], he opened the door to the rich and prosperous subject that is quantum field theory. Throughout the decades, QFT became a household name and a focal point of the theoretical physics community. To underscore how precisely field theories prediction match experimental results, Feynman made the famous analogy that it is akin to the thickness of a single strand of hair when measuring the distance between New York and Los Angeles [27].

Perturbative expansions using Feynman diagrams, which have remarkable success with theories such as QED, proved to be instrumental in arriving at such precise results. However, with the inclusion of non-Abelian gauge groups, quantum field theories become significantly more complicated. Non-perturbative effects such as confinement and chiral symmetry breaking makes QCD a difficult problem to tackle. Dealing with non-perturbative effects is one of the main objectives of high energy physics today. In fact, the strand of hair analogy made above was referring to the $g-2$ muon moment measurement at CERN in the 1970s [28]. A much more recent and precise measurement from Fermilab [29] hints at a discrepancy between the experimental data and predictions by the standard model. The result could be due to beyond standard model effects but it could also be the uncertainty in the theoretical computation. In particular, the non-perturbative contributions from the hadronic vacuum polarization process prove to be very difficult to compute and choosing a different lattice QCD model can in fact reconcile the experimental data with the standard model [30]. This, again, underpins the importance of understanding non-perturbative physics if wish to understand our universe.

Non-perturbative effects often arise at strongly coupled regions in the theory where perturbative methods fail. String theory offers a solution to dealing with strongly coupled theory

through various sets of dualities (S-duality, T-duality, U-duality). A theory that is a strongly coupled can be dualized to a theory that is weakly coupled where perturbative methods are applicable. Supersymmetric gauge theories realized using string/brane construction also enjoy such dualities. This, along with many other properties such as useful constraints imposed by supersymmetry, is what make SUSY gauge theories such a desirable object to study and the main focus of this thesis.

Given a supersymmetric gauge theory, one can compute many interesting properties. Traditionally, one would compute path integrals and correlation functions as with any other quantum field theory. In four dimensions, the maximal amount of supersymmetry one can have for a gauge theory is 16 supercharges (or 4d $\mathcal{N} = 4$). These theories are super Yang-Mills theories (SYM) where the number of supersymmetry is highly constraining and the field content is entirely determined by the gauge group. Studies of such theories began in the early days of supersymmetry and continues today, where techniques field theorists are familiar with such as computing scattering amplitudes with Feynman diagrams are still commonly used. However, the lack of matter fields (other than those transforming in the adjoint) creates incentive for one to study theories with lower amount of supersymmetry. With 8 supercharges, matter fields can now transform in bifundamental representations between different gauge groups. However, as the field content becomes richer, traditional methods become less effective. In fact, even writing down the Lagrangian becomes a tedious task.

Perhaps, rather than including every field in the gauge theory, one can focus on the simplest fields: *scalars*. At first sight, scalar fields seem uninteresting and do not lead to exotic behaviors such as quark confinement, asymptotic freedom, chiral symmetry breaking etc. In the standard model, we have a single scalar field (Higgs boson). Before symmetry breaking, the geometry of the moduli space of vacua is just S^1 which doesn't look too interesting. However, for supersymmetric gauge theories with 8 supercharges, the field content is comprised of vector multiplets and hypermultiplets and in $d = 3, 4, 5, 6$, most of these multiplets contain scalar fields. As a result, the geometry of the moduli space of vacua, defined by all configurations of scalar fields where the scalar potential vanishes, can be very rich and an interesting object

to study[1]. Furthermore, scalar fields are responsible for the Englert-Brout-Higgs-Guralnik-Hagen-Kibble mechanism or Higgs mechanism for short. As the Higgs boson acquires a VEV of 125 GeV, the Higgs mechanism kicks in and the electroweak gauge symmetry is broken from $SU(2) \times U(1) \to U(1)_{\text{diag}}$. When there are more gauge groups and scalar fields, the Higgs mechanism become richer as well, with the possibility to partially Higgs the theory into multiple subgroups.

In the 90s, more focus had been diverted to studying the moduli spaces of vacua. In 8 supercharges, this is divided into the Higgs branch, Coulomb branch and mixed branch. The Coulomb branch receives quantum corrections and is notoriously difficult to study. Traditionally, the Coulomb branch was studied by computing the prepotential which in turn gives the metric of the moduli space. Such techniques are very effective when studying Coulomb branches of 5d theories and had subsequently been used to classify 5d theories with non-trivial superconformal fixed points. However, a 5d $\mathcal{N} = 1$ Coulomb branch is a real manifold and much simpler than its lower dimensional counterparts. A 4d $\mathcal{N} = 2$ Coulomb branch is a special Kähler manifold that has a more complicated structure. The seminal work of Seiberg and Witten [32, 33] developed the Seiberg-Witten curve which studies this Coulomb branch by computing the quantum prepotential in the IR fixed point. In 3d $\mathcal{N} = 4$, however, the Coulomb branch becomes a hyperKähler manifold and previous techniques become less effective and new approaches are needed.

On the other hand, the Higgs branch is a classical object due to non-renormalization theorems [34]. If the Lagrangian of the theory is known, the Higgs branch can be easily constructed and studied as a hyperKähler quotient. However, this is not the case in 5d and 6d where non-perturbative contributions can arise in the UV fixed point which enhance the Higgs branch. Furthermore, in 4d, most of the SCFTs do not have a Lagrangian description. For these reasons, the Higgs branches of many interesting $d = 4, 5, 6$ theories cannot be studied using a hyperKähler quotient and once again, new approaches are needed.

[1]The reason we stopped at 6d is because it is the maximal dimension that you can have a theory with 8 supercharges. Furthermore, when studying SCFTs, it is also the maximal dimension where you can have conformal extension of super Poincaré algebra [31]. One can also discuss theories in $d \leq 2$ but this will not be in the scope of this thesis.

In the last few decades, there have been much developments in understanding moduli spaces. Some of the developments that are more relevant to this thesis are as follows:

- First of all, rather than writing down the Lagrangian of a SUSY gauge theory explicitly, we use concise diagrams called *quivers* instead. For theories with eight supercharges, a quiver gauge theory consists of *nodes* which represent gauge groups, *squares* which represent flavor groups and *edges* which represent matter fields [35]. In terms of the supermultiplets in the theory, the vector multiplets always transform under the adjoint representation of the gauge groups and the hypermultiplets transform under bifundamental representation of the two adjacent gauge/flavor groups it is connected to. In eight supercharges, the superpotential is fixed and can be read off from the quiver straightforwardly when it is rewritten in a four supercharge notation with directed arrows. As we will be dealing with theories with several gauge/flavor groups, it is ideal to express them using a quiver notation.

- Rather than focusing on the metric of moduli spaces, we view the moduli spaces as algebraic varieties and compute relevant generating functions. In particular, we focus on the *Hilbert series* which counts holomorphic functions on the moduli space. Since the scalar fields that parameterize our moduli spaces are chiral operators, one can equivalently study the moduli space as the ring of chiral operators, or *chiral ring*. Then, the Hilbert series will be counting gauge invariant chiral operators graded by their conformal dimension. The Hilbert series $\mathrm{HS}(t)$ is expressed in terms of a counting fugacity t. However, it can be *refined* where the irreducible representations of the operators transforming under the global symmetry group is specified. A refined Hilbert series can be concisely encoded in a different generating function called highest weight generating function (HWG).

- The classical Higgs branch of $d = 3, 4, 5, 6$ theories with eight supercharges are hyperKähler quotients and can be computed using the Molien-Weyl formula.

- The Coulomb branch Hilbert series of $3d$ $\mathcal{N} = 4$ can be computed directly[2] using the

[2]This is an important distinction as in the past they are usually computed indirectly by computing the Higgs branch Hilbert series of the 3d mirror dual.

monopole formula developed in the seminal paper [36]. This is an essential development and will be the main tool we use throughout this thesis. Furthermore, it turns the $3d$ $\mathcal{N}=4$ Coulomb branch, which used to be a difficult object to study, into something that we can easily extract non-trivial information from.

- Following the development in [37], brane systems were developed as a means to study gauge theories and their moduli spaces. The original D3-D5-NS5 model to study $3d$ $\mathcal{N}=4$ theories was subsequently extended to $d=4,5,6$ dimensions with a set of $\mathrm{D}_p-\mathrm{D}_{p+2}-\mathrm{NS5}$ branes. Furthermore, it was shown in [37] that performing 3d mirror symmetry in the brane system is just taking the S-dual followed by a rotation of coordinates, allowing us to readily create mirror pairs. As we will see later, this identification also allows us to identify the Higgs branch of higher dimensional theories with the Coulomb branch of $3d$ $\mathcal{N}=4$ theories. The possible inclusion of orientifold planes also extends the gauge theories represented by brane systems from unitary/special unitary gauge groups to (special) orthogonal and symplectic gauge groups as well [38, 39, 40].

- Depending on the arrangement of the branes, a brane system can describe the Higgs branch phase, Coulomb branch phase or the mixed branch phase of the moduli space. If one start with the Higgs branch phase and starts opening up directions corresponding to Coulomb branch moduli, the brane system will under go a phase transition into a more singular loci in the Higgs branch. If the transition is *minimal* then it is called a Kraft-Procesi transitions [41, 42]. These phase transitions are related to the pattern of partial Higgsing of the gauge theory. Constructing *Hasse diagrams* which encode such Higgsing pattern is important to help understand the geometric structure of the moduli space [43, 10].

These cumulative knowledge led to the central theme of this thesis: **Magnetic Quivers**. A magnetic quiver is a $3d$ $\mathcal{N}=4$ quiver gauge theory whose Coulomb branch is the same as the Higgs branch of the corresponding **electric quiver** which is a $d=3,4,5,6$ theory with eight supercharges. We seek out these magnetic quivers because $3d$ $\mathcal{N}=4$ Coulomb branches are now very accessible owing to developments in the last decade. This 'duality' allows us to study

the Higgs branch of electric quivers both at the superconformal fixed point and away from it even if they cannot be constructed as hyperKähler quotients. Once the magnetic quiver of a theory is obtained, one can a) define the moduli space as an algebraic variety by computing the Hilbert series using the monopole formula and b) study the Hasse diagram using an algorithm called **Quiver subtraction**.

The new approach to supersymmetric gauge theories is to redirect the focus to the Higgs branch and the new tool of execution is the magnetic quiver. Throughout this thesis, we use magnetic quivers to extract much more useful information about complicated and exotic gauge theories and SCFTs than traditional methods which often just give the dimension and global symmetry of the moduli space.

The current stage of this program is still at the data collection. We will leave a more in depth analysis of the generating functions and Hasse diagrams we gathered for future work. Nevertheless, even at this phase we had already found many interesting new phenomenons whilst at the same time confirming conjectures in the literature.

Prelude Brief introduction to the tools we will be using in this thesis such as quivers, Hilbert series, highest weight generating function.

Chapter 1: We explore how the field content and moduli spaces of SUSY gauge theories with eight supercharges vary in each dimension from three to six.

Chapter 2: We introduce the concept of magnetic quivers and the motivation to study them.

Chapter 3: The purpose of this chapter is to construct brane systems that describe gauge theories in $d = 3, 4, 5, 6$. This include gauge theories with unitary/special unitary gauge groups and, upon including orientifold planes, gauge theories with (special) orthogonal/symplectic gauge groups as well. Once the brane system is constructed, we then show how the magnetic quivers can be extracted from them.

The remaining chapter describes gauge theories in $d = 3, 4, 5$ and their magnetic quivers.

Chapter 4: The focus is on 5d $\mathcal{N} = 1$ gauge theories. The first part looks at SQCD theories with special unitary gauge groups. The magnetic quivers for these theories were already

derived in the literature. Instead, we provide the highest weight generating functions (HWGs) which fully encode the Hilbert series of the moduli spaces.

The second part, we focus on SQCD theories with symplectic gauge group. The corresponding magnetic quivers are orthosymplectic (contains (special) orthogonal and symplectic gauge groups). Interestingly, for these theories there exists of a $(\mathbb{Z})_{\text{diag}}$ subgroup and the choice of whether or not to gauge this subgroup will change the moduli space. We show that only by decoupling this subgroup do we can the magnetic quiver that corresponds to 5d theories at the UV superconformal fixed point.

We also study a duality between unitary and orthosymplectic $3d$ $\mathcal{N} = 4$ quivers by computing topological twisted indices, superconformal indices and including extended operators (Wilson lines).

Chapter 5: This chapter discusses magnetic quivers of 4d $\mathcal{N} = 2$ theories. The first part focuses on the magnetic quivers of rank one 4d SCFTs. All these rank one theories were classified in the literature, and using a Bottom-Up procedure, we were asble to obtain their magnetic quivers. These magnetic quivers are then extended into two different infinite families, the latter are magnetic quivers of a class of SCFTs called $\mathcal{S}$-fold theories.

The second part looks at folding orthosymplectic magnetic quivers we obtained in Chapter 4. This marks the first appearance of non-simply laced orthosymplectic quivers. We discuss some of its properties and relations to 4d $\mathcal{N} = 2$ theories.

The third part looks at the magnetic quiver of class $\mathcal{S}$ theories. This vast landscape of SCFTs produces magnetic quivers that are star-shaped. We find infinite families of star-shaped quivers whose Coulomb branch displays a product structure.

Interlude chapter: Orthosymplectic quivers have been a main player in this thesis. This chapter aims to group together all the orthosymplectic quivers discussed in previous chapters into a Dynkin classification. The unique features of ABCD-Dynkin type orthosymplectic quivers are discussed.

Chapter 6: This chapter focuses on 3d $\mathcal{N} = 4$ theories only. In this case, many of the magnetic

quivers are also the 3d mirror dual. We studied *all* linear type quivers with a mixture of unitary and special unitary gauge groups and their 3d mirrors/magnetic quivers. The results in this chapter greatly expands the known landscape of 3d mirror pairs in the literature.

Chapter 7: This chapter looks at Hasse diagrams which detail the phase transitions in the moduli space. We investigate how the pattern of partial Higgsing of $d = 3, 4, 5, 6$ gauge theories can be obtained through a *quiver subtraction* algorithm on the magnetic quiver. The Hasse diagrams of the magnetic quivers in the previous chapters are then listed.

Prelude

Given a gauge theory, what do we compute? Rather than looking at path integrals, correlation functions or indices, we will be looking at a set of generating functions. To be specific, we compute the Hilbert series and highest weight generating function associated with a given moduli space of vacua of the gauge theory. These tools are ubiquitous in this thesis and is therefore appropriate to have a prelude chapter discussing some of the basics of these combinatorial tools. Readers that are familiar with these concepts can skip this section.

Hilbert Series

The Hilbert series counts holomorphic functions on the moduli space of vacua $\mathcal{M}$ and is parameterized by the counting fugacity[3] t. This is equivalent to counting gauge invariant chiral operators in the **chiral ring** (see [45] for a review). In general, it is a rational function that takes the form:

$$HS_{\mathcal{M}}(t) = \sum_{d=0}^{\infty} m_d t^d = \frac{Q(t)}{(1-t)^{\dim(\mathcal{M})}} \tag{1}$$

where m_d is the Hilbert function and $Q(t)$ is a polynomial [46]. When written as a Taylor expanded infinite series, the coefficient m_d gives the number of linearly independent homogeneous polynomials at degree d. The dimension of $\mathcal{M}$ is given by the order of the pole at $t \to 1$. As we shall see later on, the expression for $Q(t)$ is in general a very complicated polynomial. We refer readers to [46] for a more detailed introduction on Hilbert series in relation to quiver gauge theories and [47] for a more mathematical introduction.

In this paper, we will use the Hilbert series as a generating function for counting gauge invariant chiral operators that parameterize the moduli space of vacua and grade them according

[3]From a statistical mechanics point of view, this fugacity can be seen as the chemical potential [44].

to their quantum numbers. For unrefined Hilbert series, these quantum numbers are the R-charges associated with the R-symmetry groups. We can then interpret the Hilbert function m_d as the number of linearly independent chiral operators of R-charge d. Once we computed the Hilbert series, we can define the moduli space as an algebraic variety[4] and extract the generators and the relations between. One important observation is that for all the Hilbert series in this thesis, $Q(t)$ is palindromic which means the moduli space is a Calabi-Yau variety [5]. This is consistent with the expectation that the moduli spaces are all hyperKähler cones.

Highest Weight Generating function (HWG)

A refined Hilbert series includes more fugacities that capture other quantum numbers in the theory such as topological charges. For our purposes, the refined Hilbert series can always be mapped into the form $\mathrm{HS}(x_i, t)$ where x_i are characters of irreducible representations of the global symmetry group of the moduli space G_{global}. We can always express the refined (or unrefined) Hilbert series as a rational function. From here on, we will refer to Hilbert series expressed in rational form as *exact*, as oppose to its Taylor expanded form. For gauge theories with several gauge groups, however, the exact refined Hilbert series is a very long expression that is difficult to even write down. In [49], a new generating function was introduced called the *highest weight generating function* $\mathrm{HWG}(\mu_i, t)$ which easily encapsulates the exact refined Hilbert series $\mathrm{HS}(x_i, t)$.

If we Taylor expand $\mathrm{HS}(x_i, t)$, at each order in t the characters can be grouped together into Dynkin labels of irreducible representations $[n_1, ..., n_r]_{G_{\text{global}}}$ [6] of the global symmetry group G_{global} with rank r. The novelty of HWG is that it rewrites the Dynkin labels in terms of μ_i, which we call the highest weight fugacities:

$$[n_1, ..., n_r]_{G_{\text{global}}} \leftrightarrow \prod_{i=1}^{r} \mu_i^{n_i} \tag{2}$$

[4] We very briefly review algebraic variety in Appendix D.

[5] By virtue of Stanley's theorem [48].

[6] $[n_1, ..., n_r]_{G_{\text{global}}}$ labels the highest weights within an irrep and since we can always identify an irrep by its highest weights, the Dynkin label uniquely identifies the irrep.

[50]. We make clear this correspondence through a simple example with $G_{\text{global}} = SU(5)$:

$$[n_1, n_2, n_3, n_4]_{SU(5)} \leftrightarrow \mu_1^{n_1}\mu_2^{n_2}\mu_3^{n_3}\mu_4^{n_4}. \tag{3}$$

Explicitly, $[3, 2, 1, 6]_{SU(5)}$ corresponds to $\mu_1^3\mu_2^2\mu_3\mu_4^6$ etc. As it turns out, this simple repackaging allows a complicated expression $\text{HS}(x_i, t)$ to be expressed in a much more compact form. Furthermore, we will see many examples in this thesis where an infinite number of gauge theories that belongs to the same family can be expressed by a single general HWG. A more in-depth look into the structure of HWG can be found in [49].

Plethystic Program

Now that we have a way of counting gauge invariant chiral operators in the moduli space, we introduce some tools to extract the number of generators and the relations between them. These tools are part of the plethystic program [51, 44].

We first introduce the **Plethystic Exponential** (PE) of some function $f(t_1, t_2, ..., t_n)$ with variables $t_1, t_2, ..., t_n$:

$$\text{PE}[f(t_1, t_2, ..., t_n)] := \exp\left(\sum_{k=1}^{\infty} \frac{f(t_1^k, t_2^k, ..., t_n^k)}{k}\right) \tag{4}$$

The PE gives symmetric products of the variables and plays a key role in computing the Higgs branch Hilbert series [11, 52, 53]. For our purposes, we will only be using PE as a way of simplifying our expressions.

The plethystic exponential (PE) has an inverse function called the **Plethystic Logarithm** (PL):

$$\text{PL}[f(t_1, t_2, ..., t_n] = PE^{-1}[f(t_1, t_2, ..., t_n)] = \sum_{k=1}^{\infty} \frac{\mu(k)\ \log(f(t_1^k, t_2^k, ..., t_n^k)}{k} \tag{5}$$

where $\mu(k)$ is the Möbius function given as:

$$\mu(k) := \begin{cases} 0 & k \text{ has repeated prime factors} \\ 1 & k = 1 \\ (-1)^n & k \text{ is a product of } n \text{ distinct primes} \end{cases} \tag{6}$$

If $f(t_1, t_2, ..., t_n)$ is a Hilbert series for the moduli space, then by taking the PL we get the defining equation of the moduli space [44]. By viewing the moduli space as an algebraic variety, we can uniquely define it by identifying the generators and relations[7] [54]. The first few positive terms are the generators of the moduli space whereas the first few negative terms are the relations.

If the PL is a finite series (i.e terminates), the moduli space is a complete intersection. Gauge theories whose moduli space of vacua is a complete intersection has many interesting properties such as its connection to closures of maximal nilpotent orbits [55, 56] and Slodowy slices [57]. However, most of the moduli spaces that we will be studying in this thesis have non terminating PLs where higher order terms are dominated by higher syzygies[8] that obscures the generators and relations.

[7]We follow the assumption that there exists a one-to-one correspondence between the Hilbert series of the moduli space and the generators and relations that defines the algebraic variety. This statement has not been proven to the best of our knowledge. But from all the cases we observed, by taking the plethystic logarithm of the Hilbert series, we can uniquely identify the algebraic variety. And vice-versa, by giving the generators and relations of the algebraic variety, we can obtain the Hilbert series using tools such as `Maclaulay2`.

[8]Also known as relations of relations.

Chapter 1

Supersymmetric Gauge Theories

In this chapter, we will review some basics about supersymmetric gauge theories in $d = 3, 4, 5, 6$ with eight supercharges as well as different techniques to study their moduli spaces. This is not at all a comprehensive study of the rich physics occurring in each of these dimensions. Instead, using $SU(2)$ with 4 flavors as a particular example, we see how its Higgs branch and Coulomb branch changes in different dimensions.

1.1 Quiver gauge theories

In this thesis, rather than writing down the Lagrangian of a supersymmetric gauge theory explicitly, it will be encoded inside a *Quiver diagram*.

Quivers take different forms depending on the number of supercharges. Since we are interested in theories with eight supercharges, the quivers are made of circles, squares and edges connecting them which encode the gauge symmetries, flavor symmetries and matter fields in the theory respectively [35]. The different fields in these theories are contained in **vector multiplets** and **hypermultiplets** whose field content are different depending on the dimension d.

For example, a U(2) gauge theory with four flavors is given by the following quiver diagram:

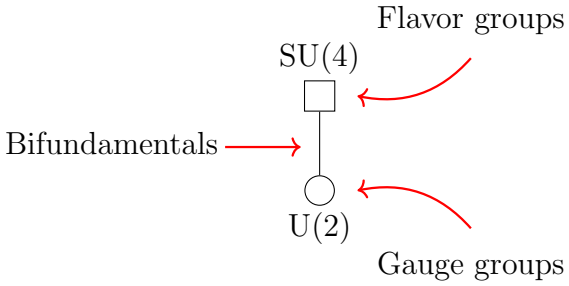

(1.1)

Importantly, the quiver diagram encodes the different representations the gauge and matter fields transform under. The vector multiplets transform under the adjoint representation of U(2) and the hypermultiplets transform under the bifundamental representation of U(2) and the flavor group SU(4) .

Superpotential

For theories with eight supercharges, the superpotential of the theory is fixed. To extract it, one should rewrite the quiver in four supercharges notation. An undirected line that represented a bifundamental hypermultiplet is now two arrows pointing in opposite directions representing a fundamental chiral and an anti-fundamental chiral multiplet. The vector multiplet also decomposes into a vector multiplet and an adjoint chiral multiplet. The same quiver above now takes the form:

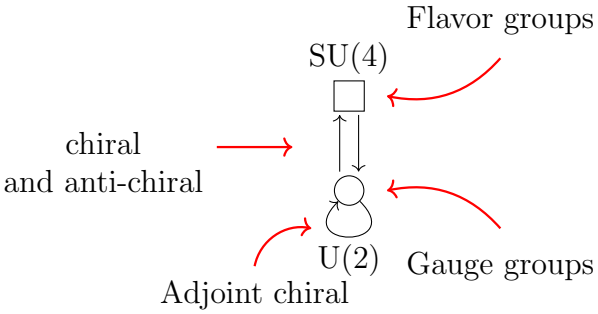

(1.2)

The superpotential is then given by:

$$W = \mathrm{Tr}(A_i^\alpha \Phi_j^i B^{j\beta}) \tag{1.3}$$

where A_i^α, $B^{i\beta}$ and Φ_j^i are the fields associated with the chiral, anti-chiral and adjoint chiral multiplets respectively. $i, j = 1, 2$ are indices for the U(2) gauge group whereas $\alpha, \beta = 1, 2, 3, 4$ are indices for the SU(4) flavor group. We will very rarely discuss quivers in four supercharges notation but in general they are useful in studying the Higgs branch of the theory.

Orthosymplectic quivers

Whilst most quiver gauge theories found in the literature are restricted to quivers with unitary gauge groups, the study of quivers made of (special) orthogonal and symplectic gauge groups has proven to be very fruitful as well. These quivers are colloquially called *orthosymplectic quivers* [38] and will be featured prominently in this thesis. A signature property is the alternating sequence of (special) orthogonal and symplectic groups.

For example, a USp(2) gauge theory with SO(8) fundamental flavor symmetry takes the following form [1]:

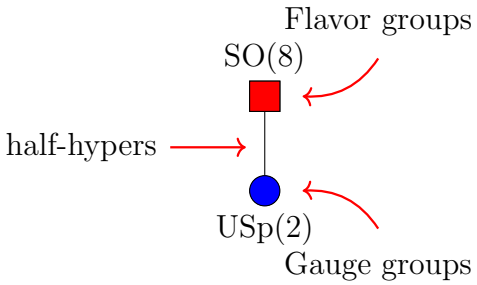

(1.4)

The line in the quiver consists of 8 half-hypers[2] transforming in pseudo-real fundamental representation of $\mathrm{USp}(2)_{\text{gauge}} \times \mathrm{SO}(8)_{\text{flavor}}$.

[1]Here, we use the compact symplectic group Sp(n) (or equivalently USp(2n)) which is defined as the intersection of SU(n) and $\mathrm{Sp}(2n, \mathbb{C})$. USp(2n) is often used to be consistent with the usage of SO(2n) and SO(2n+1). To prevent confusion of notation, it is understood that $\mathrm{SU}(2) \cong \mathrm{Sp}(1) = \mathrm{USp}(2)$.

[2]In the previous case of U(2), the bifundamental representations are complex and therefore the line represents *full* hypers. Thus, if we have N_f even number of half-hypers, we can equivalently call them $N_f/2$ full hypers.

Quiver notations

We will henceforth adopt the following color coding for the gauge and flavor groups for the rest of the thesis:

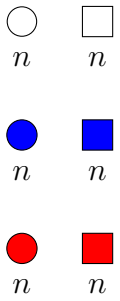

(1.5)

Special unitary gauge nodes (which we will see later on) will be explicitly labelled.

1.2 Three-dimension ($3d$ $\mathcal{N} = 4$)

Moduli spaces of vacua of gauge theories differs greatly in different dimensions. This is due to different number of scalar fields in the vector and hypermultiplets as well as the R-symmetry group. In the remainder of this chapter, we will always identify these three objects before diving into the moduli space itself.

R-symmetry

For 3d $\mathcal{N} = 4$ theories, the R-symmetry is $\mathrm{SU}(2)_L \times \mathrm{SU}(2)_R$.[3]

Vector multiplet (A_μ, ϕ^i, spinors)

Contains a gauge field A_μ with $\mu = 0, 1, 2$, three real scalar fields ϕ^i with $i = 1, 2, 3$ and (Majorana) spinors. The three scalar fields transform under the $[2]_{\mathrm{SU}(2)_L}[0]_{\mathrm{SU}(2)_R}$ representation. Thus, the scalar fields transform under the adjoint representation of $\mathrm{SU}(2)_L$ but trivially under $\mathrm{SU}(2)_R$.

[3]The best way to arrive at this symmetry group is to dimension reduce from 6d $\mathcal{N} = (1, 0)$ theories. The $\mathrm{SU}(2)_L$ is the double cover of the rotational group that rotates the three coordinates that are compactified. The $\mathrm{SU}(2)_R$ symmetry is simply the same R-symmetry that rotates the supercharges in 6d [58].

Hypermultiplet $(q, \tilde{q}^\dagger,$ spinors$)$

Contains the complex scalar q, its complex conjugate $\tilde{q}^\dagger$ and (Majorana) spinors. The complex scalars transform under $[0]_{\mathrm{SU}(2)_L}[1]_{\mathrm{SU}(2)_R}$ of the R-symmetry group. In other words, they transform trivially under $\mathrm{SU}(2)_L$ and as a doublet under $\mathrm{SU}(2)_R$.

1.2.1 Coulomb branch (Monopole operators)

The moduli space of vacua is parametrized by scalar fields. The **Coulomb branch** is parameterized by the scalar fields ϕ^i with non-zero VEV living in the vector multiplet, which transform under the adjoint representation of the gauge group. As they transform non-trivially under $\mathrm{SU}(2)_L$, this is the R-symmetry subgroup that acts on the Coulomb branch. Let us first focus on the classical Coulomb branch of a gauge theory with gauge group G. The scalar potential from the real scalar fields takes the following form:

$$V = \frac{1}{g^2} \sum_{i<j} \mathrm{Tr}[\phi^i, \phi^j]^2 \tag{1.6}$$

with g being the gauge coupling. At the supersymmetric vacuum state, the scalar potential needs to vanish which occurs whenever the scalar fields commutes. This is equivalent to saying that the scalar fields take values in the Cartan subalgebra of the gauge group G. At generic VEVs, Higgs mechanism will break the gauge group G to its maximal torus $U(1)^r$ where r is the rank of G. This gives rise to r photons which can be dualized to r real scalar fields, and, along with the $3r$ real scalar from ϕ^i, the Coulomb branch carries $4r$ degrees of freedom. Equivalently, the $4r$ real degrees of freedom can be viewed as r quaterionic degrees of freedom. The Coulomb branch is then a hyperKähler manifold with $\mathrm{SU}(2)_L$ action. For a general $3d$ $\mathcal{N} = 4$ quiver, the quaterionic dimension of the Coulomb branch is the sum of the ranks of the gauge group (since this give the number of scalars in the vector multiplets).

The Coulomb branch of $3d$ $\mathcal{N} = 4$ SUSY gauge theories is notoriously difficult to study as it is not protected against quantum corrections. More traditional approaches include computing the one-loop Coulomb branch metric by integrating out massive fields which are only reliable

at weakly coupled regions. It will be ideal to come up with a method in computing the Coulomb branch that also gives the exact answer in the strongly coupled IR fix points. Furthermore, the procedure mentioned above in dualizing photons (obtained from taking the Hodge dual) to get real scalars is only known when G is completely broken into abelian subgroups $U(1)^r$. For less generic VEVs, G is broken to a non-Abelian subgroup $H \subset G$ and it is not known how to dualize the non-Abelian vector multiplets [36]. To deal with these problemsome features effectively, a modern approach is developed using the idea of *monopole operators*.

Dressed monopole operators

In modern QFT, one not only looks at traditional local operators that are ordered but at disorder operators as well. For our purpose, the disorder operators we are interested in are t'Hooft monopole operators [59]. These monopole operators $V_m(x)$ can be defined by specifying the singularity of the fields in the Euclidean path integral at the insertion point x. Using spherical coordinates (r, θ, ψ), the gauge field $A_\pm$ and scalar field σ have the following singular boundary conditions as $r \to 0$:

$$\begin{aligned} A_\pm &\sim \frac{m}{2}(\pm 1 - \cos\theta)d\psi \\ \sigma &\sim \frac{m}{2r} \end{aligned} \tag{1.7}$$

where m is the *magnetic charge* obtained by integrating over the S^2 that encloses the singularity. $A_\pm$ are the gauge connection 1-form in the northern and southern patched of the S^2. The boundary conditions enforces we are dealing with supersymmetric $\frac{1}{2}$-BPS monopole operators.

Importantly, m is also an element of the Lie algebra of the gauge group G of our theory. Dirac quantization condition [60]:

$$e^{2\pi i m} = \mathbb{1}_G \tag{1.8}$$

ensures that the magnetic charges live in the weight lattice $\Gamma_{G^\vee}$ of the GNO (Langlands) dual group of G [61]. Since we are interested in gauge invariant operators, the lattice of charges we choose from is given by the quotient $\Gamma_{G^\vee}/\mathcal{W}_{G^\vee}$ where $\mathcal{W}_{G^\vee}$ is the Weyl group of $G^\vee$.

Now that we introduced the monopole operators, how is it related to the Coulomb branch?

It turns out, if we decompose the $3d$ $\mathcal{N}=4$ vector multiplet $(A_\mu, \phi^1, \phi^2, \phi^3, \text{spinors})$ into 3d $\mathcal{N}=2$ multiplets, we will get a $\mathcal{N}=2$ vector multiplet and an $\mathcal{N}=2$ adjoint chiral multiplet. The vector multiplet contains a gauge field which can be dualized to a scalar field A and real scalar $\phi^1=\sigma$ which contribute to parameterizing the Coulomb branch. The above definition of the monopole operator and the boundary conditions basically replaces the $3d$ $\mathcal{N}=2$ vector multiplet with the set of monopole operators V_m. These monopole operators are called *bare* monopole operators. As for the $\mathcal{N}=2$ adjoint chiral multiplet, it contains two real scalar fields which can be complexified to $\Phi=(\phi^2,\phi^3)$ and serves to *dress* the bare monopole operator. In summary, the resulting *dressed monopole operator* becomes the object that parameterizes the Coulomb branch. This is schematically summarized in the diagram below:

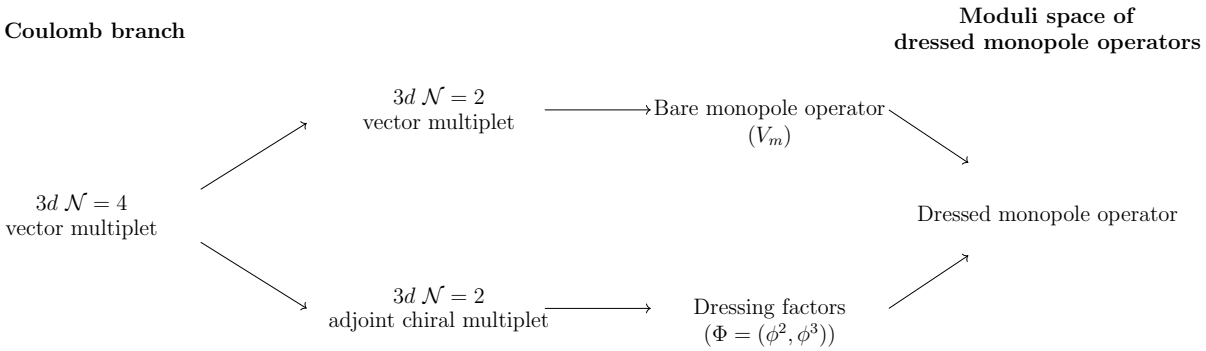

(1.9)

Therefore, the Coulomb branch is equivalent to the moduli space of dressed monopole operators. An excellent review on monopole operators can be found in [45].

Monopole formula

By identifying dressed monopole operators as the objects that parameterizes the Coulomb branch, the next step is to enumerate them using a generating function. The boundary conditions allows the monopole operators to be treated as $\mathcal{N}=2$ chiral multiplets. As a result, they will populate the chiral ring and can be counted using a Hilbert series $\text{HS}(t)$. Here, t is the counting fugacity whose power gives the R-charge[4] of the monopole operators. The R-charge $\Delta(m)$ of the bare monopole operator of magnetic charge m for a gauge theory G with N_f hypermultiplets in

[4]The R-charge is given by the $\text{U}(1)_C$ Cartan subgroup of the $\text{SU}(2)_L$ R-symmetry subgroup that acts on the Coulomb branch.

the representation $\mathcal{R}_i$ is given in [62] which we reproduce here:

$$\Delta(m) = -\sum_{\alpha\in\Delta_+} |\alpha(m)| + \frac{1}{2}\sum_{i=1}^{N_f}\sum_{\rho\in\mathcal{R}_i} |\rho_i(m)| \tag{1.10}$$

where α are the roots of the algebra $\mathfrak{g} = \text{Lie}(G)$ of which only the positive roots Δ_+ are selected. The first term are contributions from the vector multiplets transforming under the adjoint representation of G. The second term are contribution from the N_f hypermultiplets where ρ are the weights of the representation $\mathcal{R}_i$.

The R-charge is defined by the UV $\text{U}(1)_C$ R-symmetry but in the case where $\Delta(m) \geq \frac{1}{2}$, the value coincides with the IR superconformal R-symmetry as well, which is also the conformal dimension of the monopole operators. Theories where all monopole operators follow this condition are called *good* for $\Delta(m) > \frac{1}{2}$ and *ugly* for $\Delta(m) = \frac{1}{2}$ [62]. If $\Delta(m) < \frac{1}{2}$, the R-charges in the UV do not coincide with those in the IR and one obtains a divergent Hilbert series. In this paper, we will mainly be focusing on good quiver gauge theories.

With the R-charge grading of the bare monopole operators identified, we turn our attention to the contributions from the complex scalar field $\Phi = (\phi^2, \phi^3)$ in the dressing factors. Generic magnetic fluxes will break the gauge group G to its maximal torus. In particular, the contribution when all magnetic charges are inequivalent and larger than zero, the dressing factor P_G for a rank r gauge group contributes:

$$P_G(m_i \neq m_j > 0, t) = \frac{1}{(1-t^2)^r} \tag{1.11}$$

However, particular configurations of magnetic charges m can also break G to a subgroup H_m. In general, the dressing factor $P_G(m,t)$ is given by:

$$P_G(m,t) = \prod_{i=1}^{r} \frac{1}{1-t^{2d_i(m)}} \tag{1.12}$$

where $d_i(m)$ is the Casimir invariant of G. The classical dressing factor for classical gauge groups is written explicitly in Appendix A of [36].

Putting the pieces together, the Coulomb branch Hilbert series of a G gauge theory with

N_f hypermultiplets is given by:

$$\mathrm{HS}(t) = \sum_{m \in \Gamma_{G^\vee}/\mathcal{W}_{G^\vee}} t^{2\Delta(m)} P_G(m,t) \tag{1.13}$$

where, as mentioned earlier, we are interested in gauge invariant operators so the magnetic charges are summed over the lattice $\Gamma_{G^\vee}/\mathcal{W}_{G^\vee}$.

To summarize, the Hilbert series enumerates gauge invariant dressed monopole operators graded by their R-charge. The generating function gives the Hilbert series of the Coulomb branch chiral ring, from which the generators and relations that defines the moduli space as an algebraic variety can be extracted.

The formula for $\Delta(m)$ and $\Gamma_{G^\vee}/\mathcal{W}_{G^\vee}$ for classical groups are detailed in Appendix A.

Refinement

The Hilbert series can be further *refined* by detailing how the operators transform under irreducible representations of the Coulomb branch global symmetry group G_{global}. This can be obtained from the monopole formula by assigning fugacities z to non-simply connected gauge groups G which counts the charges of $\mathrm{U}(1)_T$ topological symmetries. The refined monopole formula then takes the form:

$$\mathrm{HS}(t) = \sum_{m \in \Gamma_{G^\vee}/\mathcal{W}_{G^\vee}} z^m t^{2\Delta(m)} P_G(m,t) \tag{1.14}$$

The z fugacities are simple root fugacities of the algebra $\mathfrak{g}$ which can be converted to fundamental weight fugacities x using the Cartan matrix of $\mathfrak{g}$. The fugacities x are then used to construct the characters of the irreducible representations. As a result, if the Hilbert series is expanded perturbatively as a Taylor series, the coefficients at each order of t can be grouped together as irreps of G_{global}.

Example: $G = U(2)$ with $N_f = 4$ flavors

Let us study the Coulomb branch Hilbert series of a U(2) gauge group with 4 fundamental flavors. The R-charge is given as the follows:

$$\Delta(m_1, m_2) = -|m_1 - m_2| + \frac{4}{2}(|m_1| + |m_2|) \tag{1.15}$$

where m_1, m_2 are the magnetic charges for U(2). The magnetic lattice $\Gamma_{G^\vee}/\mathcal{W}_{G^\vee}$ is given by m_1 and m_2 taking integer values whilst satisfying $\infty > m_1 \geq m_2 > -\infty$. The Hilbert series computed by the monopole formula gives:

$$\begin{aligned} \mathrm{HS}(t) &= \sum_{\infty > m_1 \geq m_2 > -\infty} t^{2(-|m_1 - m_2| + 2(|m_1| + |m_2|))} P_{U(2)}(m_1, m_2, t) \\ &= \frac{1 + t^2 + 2t^4 + t^6 + t^8}{(1 - t^2)^4 (1 + t^2)^2} \end{aligned} \tag{1.16}$$

This moduli space is known in the mathematics literature as the Slodowy slice $\mathcal{S}_{\mathcal{N},(2^2)} \equiv \mathcal{S}_{(2^2)} \cap \mathcal{N}$. Where $\mathcal{S}_{(2^2)}$ is the Slodowy slice transverse to the nilpotent orbit $\mathcal{O}^{\mathfrak{su}(4)}_{(2^2)}$ and $\mathcal{N}$ is the nilpotent cone of $\mathfrak{su}(4)$.

Nilpotent orbits

Nilpotent orbits are very interesting objects and can be found commonly in algebraic geometry and representation theory literature. However, for this thesis, we will very rarely discuss Slodowy slices and nilpotent orbits. Therefore, for our purposes we will just view them as *labels* to help us identify our moduli spaces. We provide a very brief introduction to nilpotent orbits in Appendix D. For more details on Slodowy slices and nilpotent orbits, we direct the reader to [63].

We do, however, discuss minimal nilpotent orbit closures $\overline{\mathcal{O}}^{\mathfrak{g}}_{\mathrm{min}}$ very often. In physics, these geometric spaces are equivalent to one-$\mathfrak{g}$ instanton moduli spaces.

$G = SU(2)$ **with** $N_f = 4$

The difference between a U(n) and SU(n) gauge theory in the monopole formula is that the magnetic charges for SU(n) satisfies an additional condition that $\sum_{i=1}^{n} m_i = 0$. Such an action is analogous to ridding of a U(1) degree of freedom[5]. The simplest way of executing such an operation is to first compute a quiver with all gauge groups unitary and then introduce an additional term $z_j^{\sum_i^{n_j} m_i^{(j)}}$ to the U(n_j) nodes that you wish to convert to SU(n_j). In our case, we go back to (1.16) and add the addition term $z^{m_1+m_2}$. Now, the operators inside $\mathrm{HS}_{\mathrm{SU}(2)}(t)$ will be the operators in $\mathrm{HS}_{\mathrm{U}(2)}(z,t)$ where $m_1 + m_2 = 0$, which is equivalent to the terms whose coefficient *does not* contain z. Computationally, this is equivalent to taking the residue over z:

$$\begin{aligned} \mathrm{HS}_{\mathrm{SU}(2)}(t) &= \oint \frac{dz}{2\pi i} \mathrm{HS}_{\mathrm{U}(2)}(z,t)(1-t^2) \\ &= \frac{1-t^{12}}{(1-t^4)^2(1-t^6)} \end{aligned} \tag{1.17}$$

where the additional $(1-t^2)$ is required to correct the classical factors by ensuring $\phi^2 + \phi^3 = 0$. As we will see in the next subsection, this procedure can also be interpreted as taking a hyperKähler quotient over the U$(1)_T$ topological symmetry [36]. The Coulomb branch Hilbert series shows the moduli space is $\mathbb{C}^2/\Gamma_{D_4}$ where $\Gamma_{D_4} \cong Dic_4$ is the discrete subgroup of $SU(2)$ that is associated with $D_4 = \mathrm{Lie}(SO(8))$ by the McKay correspondence [64].

In Appendix A, we make some very important comments about computational complexity and the monopole formula.

Coulomb branch global symmetry

In the IR fixed point, the $3d$ $\mathcal{N} = 4$ Coulomb branch global symmetry can be enhanced to some non-Abelian group G_{global} due to bare monopole operators. A powerful set of results in [62] shows that one can immediately read off the algebra of the global symmetry group $\mathfrak{g}_{\mathrm{global}}$

[5]However, one needs to be careful that $U(n)/U(1) \cong SU(n)/\mathbb{Z}_n$ so the difference is not exactly a U(1). In the monopole formula, turning an U(n) to an SU(n) gauge group corresponds to setting $\sum_{i=1}^{n} m_i = 0$ whereas decoupling a U(1) corresponds to setting the last magnetic charge $m_n = 0$. The subtle difference between them is an overall discrete factor $\mathbb{Z}_n$. This is important when dealing with framed vs unframed quivers later on and is source of much confusion in the literature.

by computing the *balance* of gauge groups [6].

A U(k) gauge group is balanced if the flavour from the neighbouring nodes is $N_f = 2k$. The balanced nodes form the Dynkin diagram of $\mathfrak{h}$ which is a subalgebra of $\mathfrak{g}_{\text{global}}$. In most cases where all the gauge nodes are balanced with n nodes overbalanced, one finds that $\mathfrak{g}_{\text{global}} = \prod_i \mathfrak{h}_i \times \mathfrak{u}(1)^n$ which considers all balanced subset of nodes that are connected and form Dynkin diagrams $\mathfrak{h}_i$. If the unitary quiver is unframed/flavorless, then an overall $\mathfrak{u}(1)$ factor needs to be removed from the global symmetry.

The same idea can be carried on for orthosymplectic quivers. In [62], the balance conditions for (special) orthogonal and symplectic gauge groups with N_f fundamental hypermultiplets (i.e. $2N_f$ half-hypermultiplets) are given which we reproduce here:

$$\begin{aligned} \mathrm{SO}(2k) &: N_f = 2k - 1, \\ \mathrm{SO}(2k+1) &: N_f = 2k, \\ \mathrm{USp}(2k) &: N_f = 2k + 1. \end{aligned} \tag{1.18}$$

It has been shown in [62] that a linear chain of n balanced orthosymplectic gauge nodes gives a global symmetry of $\mathfrak{so}(n+1)$. The above is true regardless of the gauge groups being O or SO. A balanced SO(2) gauge group is always assumed to be connected to a USp(0) gauge group which does not affect Coulomb branch computations but is required in order to read off the correct global symmetry. On the other hand USp(0) nodes should not be attached to O(2). For non-linear or non-simply laced orthosymplectic quivers, the global symmetry is different and discussed in detail in Chapter 5.4.1. Furthermore, as will be discussed in Chapter 4, if unframed/flavorless orthosymplectic quivers are discussed, the global symmetry might be further enhanced.

The importance of being able to read off the Coulomb branch global symmetry directly from the quiver cannot be overstated. It serves as a first order check that our monopole formula gives the correct Coulomb branch Hilbert series. Furthermore, if we wish to construct a quiver

[6] One does observe, however, that more complicated quivers such as moduli space of k-instantons [65] and some non-simply laced unitary quivers [7] have factors in $\mathfrak{g}_{\text{global}}$ which cannot be read off from the balance of gauge groups. In such cases, the best way to obtain the global symmetry group is an explicit computation of the Hilbert series to order t^2 which reveals the dimension of the global symmetry group.

with a certain G_{global} in mind, the balance of the gauge node will severely constrain the possible forms the quiver can take. Such constraints often allow us to make classifications of families of quivers.

1.2.2 Higgs branch

The Higgs branch is parameterized by scalar fields with non-zero VEV that lives in the hypermultiplet. For $3d$ $\mathcal{N} = 4$ theory, this is parameterized by the two complex scalars $q, \tilde{q}^\dagger$. This means there are four real scalar fields that parameterizes the moduli space and therefore the manifold is once again hyperKähler. Unlike the Coulomb branch, the Higgs branch in $3d$ is a classical object since it is protected from quantum corrections due to non-renormalization theorems [34]. For Lagrangian theories, the Higgs branch can be straightforwardly studied by taking the hyperKähler quotient.

Free theory

First, consider a theory with 8 free hypermultiplets. Pictorially, one can represent this with the following quiver:

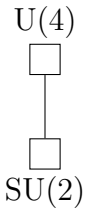

(1.19)

The Higgs branch is then the space of constant scalar fields which in this case is $\mathbb{H}^8$. The Higgs branch Hilbert series is given by the plethystic exponential (PE) of the free fields:

$$\text{HS}(t) = \text{PE}[8t] = \frac{1}{(1-t)^8} \tag{1.20}$$

The Hilbert series only has terms in the denominator, indicating the chiral ring is freely generated, i.e there are 8 generators and no relations between them.

SU(2) with $N_f = 4$

Now, we turn to our canonical example of SU(2) gauge theory with 4 flavors. By gauging the SU(2) in our free theory in (1.19), the scalar potential $V(q, \tilde{q}^\dagger, \phi^{i=1,2,3} = 0, A = 0)$ becomes non-zero in general (as a reminder we are focusing on the Higgs branch where VEV of scalar fields in the vector multiplet are set to zero). To get the vacuum state $V = 0$, one require the F-term and D-term to vanish. The F-term is given by

$$F-\text{term} = \frac{\partial \mathcal{W}}{\partial \Phi} \tag{1.21}$$

where $\mathcal{W}$ is the superpotential. Since we are focusing on the Higgs branch, the non-trivial F-term equations are those where the derivatives are taken with respect to the scalar fields $\Phi = (\phi^2, \phi^3)$ in the 3d $\mathcal{N} = 2$ adjoint chiral multiplet. Thus, the F-term equations only have $q, \tilde{q}^\dagger$ terms. Written in four supercharges, the different 3d $\mathcal{N} = 2$ fields for our quiver are labelled as follows:

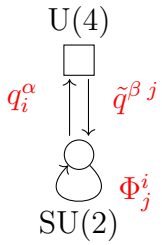

(1.22)

The superpotential is:

$$\mathcal{W} = \text{Tr}(q_i^\alpha \Phi^i_j \tilde{q}^{\beta\, j}) \tag{1.23}$$

where $q_i^\alpha, \tilde{q}^{\beta\, j}$ are the complex scalar fields in the hypermultiplet transforming in the fundamental (anti-fundamental) of SU(2) and anti-fundamental (fundamental) of U(4) with $i, j = 1, 2$ as gauge indices and $\alpha, \beta = 1, \ldots, 4$ as flavour indices. Φ^i_j gives the scalar fields in the adjoint chiral. The superpotential can be read off by following the arrows and taking a full loop from the flavour node and back to itself. Taking the derivative, the non-vanishing F-term that is relevant to us on the Higgs branch is then:

$$q_i^\alpha \tilde{q}^{\beta\, i} = 0 \tag{1.24}$$

Next, we consider only gauge invariant operators. This, along with ensuring the D-terms vanish, translates to quotienting by the complexified gauge group $G^{\mathbb{C}}$. In summary, the Higgs branch of SU(2) with 4 flavors is given by:

$$\text{Higgs branch}_{\text{SU(2)}-[4]} = \frac{\{\text{space of constant scalars } \mathrm{q}_{\mathrm{i}}^{\alpha}, \tilde{\mathrm{q}}^{\beta\,\mathrm{i}} \mid q_i^{\alpha}\tilde{q}^{\beta\,i} = 0\}}{SU(2)_{\mathbb{C}}} \tag{1.25}$$

To define the Higgs branch as an algebraic variety, one can first write down gauge invariant generators in the theory and then use F-terms to impose relations between them. This procedure works well when the quiver is simple, but for more complicated cases it is best to compute the Higgs branch Hilbert series and then extract the generators and relations using plethystics.

The complex dimension of the Higgs branch is given by the number of scalars in the hypers minus the twice dimension of all the gauge groups. For example, an SQCD theory of $SU(N_c)$ with N_f flavors has $2N_cN_f$ complex scalars in the hypers. Imposing F-term equations imposes $N_c^2 - 1$ relations and imposing D-term equations and gauge invariance imposes another $N_c^2 - 1$ relations. Therefore the complex dimension is given by $2N_cN_f - 2(N_c^2 - 1)$. Equivalently, the quaterionic dimension is $N_cN_f - (N_c^2 - 1)$.

The Higgs branch global symmetry is also its flavour symmetry.

Molien-Weyl formula

When computing the Higgs branch Hilbert series, the steps above can be translated into different operations in the Molien-Weyl formula.

1. The first step is to study all possible constant field configurations whilst keeping track of the representations they transform under the gauge group. For our SU(2) with 4 flavors theory, we have:

$$\begin{aligned}
&\mathrm{PE}\Big[(x+\frac{1}{x})(\frac{1}{y_1}+\frac{1}{y_2}+\frac{1}{y_3}+\frac{1}{y_4})t + (x+\frac{1}{x})(y_1+y_2+y_3+y_4)t\Big] \\
&= \frac{1}{(1-\frac{x}{y_1}t)(1-\frac{x}{y_2}t)(1-\frac{x}{y_3}t)(1-\frac{x}{y_4}t)(1-\frac{1}{xy_1}t)(1-\frac{1}{xy_2}t)(1-\frac{1}{xy_3}t)(1-\frac{1}{xy_4}t)} \\
&\times \frac{1}{(1-xy_1t)(1-xy_2t)(1-xy_3t)(1-xy_4t)(1-\frac{y_1}{x}t)(1-\frac{y_2}{x}t)(1-\frac{y_3}{x}t)(1-\frac{y_4}{x}t)}
\end{aligned} \tag{1.26}$$

where x is the fundamental weight fugacity of SU(2) gauge group and y_i are the fugacities of U(4) flavour group. By keeping y_i fugacities, we are computing the refined Higgs branch Hilbert series. One can of course set $y_i = 1$ to compute the unrefined Higgs branch Hilbert series, which is significantly less taxing to compute.

2. The second step is to set the F-term conditions. This is achieved by multiplying the first term with the adjoint representation of the gauge group SU(2):

$$\mathcal{F}(x, y_i, t) = \text{PE}\Big[(x+\frac{1}{x})(\frac{1}{y_1}+\frac{1}{y_2}+\frac{1}{y_3}+\frac{1}{y_4})t+(x+\frac{1}{x})(y_1+y_2+y_3+y_4)t\Big] \times(1-t^2)(1-xt^2)(1-\frac{1}{x}t^2) \tag{1.27}$$

Note that the R-charge of the superpotential is 2 whereas those in the chiral and anti-chiral are 1.

3. Finally, quotienting out $\text{SU}(2)_{\mathbb{C}}$ is given by taking the following residue integral:

$$\text{HS}_{SU(2)-[4]}(y_i, t) = \oint_{SU(2)} d\mu_{SU(2)} \mathcal{F}(x, y_i, t) \tag{1.28}$$

where $d\mu_{SU(2)}$ is the Haar measure. The exact refined Hilbert series is quite a complicated expression, hence we unrefine them by taking $\text{HS}_{SU(2)-[4]}(y_i = 1, t)$ which yields:

$$\text{HS}_{SU(2)-[4]}(y_i = 1, t) = \frac{(1+t^2)(1+17t^2+48t^4+17t^6+t^8)}{(1-t^2)^{10}} \tag{1.29}$$

This is the Hilbert series that describes the space $\overline{\mathcal{O}}_{\text{min}}^{\mathfrak{so}(8)}$ which is the closure of the minimal nilpotent orbit of $\mathfrak{so}(8)$. Equivalently, this is the one-$SO(8)$ instanton moduli space.

1.3 Four-dimension ($4d$ $\mathcal{N} = 2$)

We turn our attention to $4d$ theories. From a historic point of view, the topic of $\mathcal{N} = 2$ is better studied with a plethora of papers in the literature. However, from a gauge theoretic point of view, these theories are often more complicated where the majority of 4d $\mathcal{N} = 2$ superconformal field theories (SCFTs) do not have known Lagrangian descriptions. Once again,

we begin by describing the supermultiplets in this dimension.

R-symmetry

For 4d $\mathcal{N} = 2$ theories, the R-symmetry is $\mathrm{U}(1)_r \times \mathrm{SU}(2)_R$.[7]

Vector multiplet $(A_\mu, \Phi,$ spinors$)$

Contains a gauge field A_μ with $\mu = 0, 1, 2, 3$ [8], one complex scalar field Φ and (Majorana) spinors. The complex scalar field transforms under the $q_{U(1)_r}[0]_{SU(2)_R}$ representation of the R-symmetry group where q is the $U(1)$ charge.

Hypermultiplet $(q, \tilde{q}^\dagger,$ spinors $)$

Contains a complex scalar q and its complex conjugate $\tilde{q}^\dagger$ and (Majorana) spinors. The complex scalars transform under $[0]_{U(1)_r}[1]_{SU(2)_R}$ of the R-symmetry group. In other words, they transform trivially under $\mathrm{U}(1)_r$ and as a doublet under $\mathrm{SU}(2)_R$.

One noticeable feature is that the hypermultiplet content remains the same as in $3d$ $\mathcal{N} = 4$ whilst the vector multiplet is different; it has one fewer real scalar field and the gauge field can no longer be dualized to a scalar. As a result, the Higgs branch remains a hyperKähler manifold whereas the Coulomb branch is a Kähler manifold. In fact, additional structures due to $\mathcal{N} = 2$ SUSY makes the Coulomb branch a (rigid) special Kähler manifold. The complex dimension of the Coulomb branch of a $4d$ $\mathcal{N} = 2$ theory is the sum of the ranks of the gauge groups.

1.3.1 Coulomb branch

Unlike in three dimensions, dressed monopole operators no longer describes the Coulomb branch of 4d theories. Alas, we will use the old ways. To understand the geometry of the Coulomb branch, the traditional approach is to study its metric. The metric can be obtained from the prepotential $\mathcal{F}(a_i)$ where a_i are the entries in the scalar field $\Phi = \mathrm{diag}(a_1, \ldots, a_r)$ for a gauge group of rank r. The prepotential in the UV is a holomorphic function and can be

[7]The best way to arrive at this symmetry group is to dimension reduce from 6d $\mathcal{N} = (1, 0)$ theories. The $\mathrm{SO}(2)_r \cong \mathrm{U}(1)_r$ is the double cover of the rotational group that rotates the two coordinates that are compactified.

[8]The on shell degree of freedom is given by the fundamental representation of the $SO(2)$ little group.

easily determined if the Lagrangian is known. In the IR, however, the prepotential takes a more complicated form:

$$\mathcal{F}(a_i) \sim \tau_{ij}^{UV} a_i a_j + (\text{one} - \text{loop corrections}) + (\text{instanton corrections}) \tag{1.30}$$

where τ^{UV} is the complexified gauge coupling in the UV. The second term is the perturbative one-loop corrections to the metric. The main difficulty in computing the prepotential comes from the final term which are non-perturbative contributions from instantons. Computing the contributions from the instantons was made systematic from the seminal paper of [32, 33] which introduced the concept of Seiberg-Witten curves.

The prepotential can be determined by the IR gauge coupling τ^{IR} through the relation:

$$\tau_{ij}^{\text{IR}} = \frac{\partial^2 \mathcal{F}(a_i)}{\partial a_i \partial a_j} \tag{1.31}$$

The complexified gauge coupling in turn is determined by defining certain 1-cycles (A_i,B_i) on the curve. Using rank 1 theories as an example where $i, j = 1$:

$$\tau^{\text{IR}} = \frac{\partial a_D}{\partial a} \tag{1.32}$$

where

$$a = \frac{1}{2\pi i} \oint_A \lambda \qquad a_D = \frac{1}{2\pi i} \oint_B \lambda \tag{1.33}$$

and λ is some 1-form called the Seiberg-Witten differential. To sum up, once the Seiberg-Witten curve and differential are defined, the gauge coupling can be found using (1.32). Then, integrating twice will return the prepotential which defines the Coulomb branch metric.

To study SCFTs, one can start by finding the SW curve corresponding to the UV Lagrangian and identify neighbourhoods around singular points where the curve exhibits scale invariance. Alternatively, one can immediately write down the SW curve for the IR theory and look for scale invariance to identify non-trivial SCFTs. Such approach has the advantage of identifying 4d $\mathcal{N} = 2$ SCFTs that do not have a known Lagrangian description. Methods like this are instrumental in identifying families of SCFTs such as the list of rank 1 theories in [66]. For more

details on 4d SCFTs and Seiberg-Witten curves, one can look at some excellent reviews [67, 68].

$SU(2)$ with $N_f = 4$

Once again, let us use $SU(2)$ theory with $N_f = 4$ as our example. Since there are twice as many flavors as colours, this theory has vanishing beta function and is superconformal. This is one of the special cases in 4d where the theory is both Lagrangian and an SCFT[9]. This example is explored in the original Seiberg-Witten paper [33][10]. Since the beta function vanishes, we have:

$$\tau^{\text{IR}} = \tau^{\text{UV}} \tag{1.34}$$

The Coulomb branch is defined by a prepotential that is just $\frac{1}{2}\tau^{\text{UV}}a^2$. This may seem uninteresting at first sight but performing S dualities and gaugings on the subgroups of the $SO(8)$ flavour group lead to an incredible zoo of SCFTs that goes under the name class $\mathcal{S}$ theory [70]. Even though we will not discuss this further, we do look at many class $\mathcal{S}$ theories in Chapter 5.

Coulomb branch generating function

In the previous subsection we see the Coulomb branch can be studied by computing its Hilbert series. This counts holomorphic functions on the moduli space, or equivalently, gauge invariant chiral operators in the chiral ring. In general, the Coulomb branch chiral ring for $3d$ $\mathcal{N} = 4$ theories is made of generators which satisfy a certain set of relations. As a result, the Hilbert series is not freely generated (this is indicated by non-trivial terms in the numerator of the Hilbert series). On the other hand, the Coulomb branch chiral ring for $4d$ $\mathcal{N} = 2$ SCFTs are generically freely generated [71]. However, they may not be freely generated when discrete actions are taken into account [72]. For cases studied in this paper, we will only look at freely generated Coulomb branch chiral ring for 4d $\mathcal{N} = 2$ SCFTs where one can define the chiral ring fully by specifying the generators. For instance, the Coulomb branch of the $SU(2)$ with $N_f = 4$ at the superconformal fix point, also known as the D_4 theory, is generated by a single

[9] Another set of Lagrangian theories are those that are free in the UV but has a non-trivial IR fixed point with emergent symmetries.

[10] And also reproduced using instanton counting in [69].

operator with conformal dimension $\Delta = 2$. Here the conformal dimension is given by the $\mathrm{U}(1)_r$ charge. For freely generated theories, the number of $\Delta = 2$ generators also indicates the complex dimension of the Coulomb branch. A single generator means the complex dimension is 1 and equivalently, this means the theory is a rank 1 SCFT.

Such computations make it much easier to analyse the Coulomb branch of 4d theories, especially when the Higgs branch is complicated. Many attempts had been made to extract as much information about the theory as one can just by studying the Coulomb branch. For example, if the spectrum contains non-integer conformal dimension operators, then the theory is an Argyres-Douglas theory [73].

1.3.2 Higgs branch

The hypermultiplet for $3d$ $\mathcal{N} = 4$ and $4d$ $\mathcal{N} = 2$ theories both contain two complex scalars and their Higgs branches are classical and protected from quantum corrections. This is important as the classical Higgs branch remains the same in $d = 3, 4, 5, 6$.[11] As a result, the Higgs branch for this theory is the same as before: $\mathrm{Higgs}^{4d}_{SU(2)-[4]} = \overline{\mathcal{O}}^{\mathfrak{so}(8)}_{\mathrm{min}}$.

In general, most 4d $\mathcal{N} = 2$ SCFTs do not have known Lagrangian description, which makes the hyperKähler quotient construction unfeasible. As a result, we can no longer study the Higgs branch using the Molien-Weyl formula and a new method is needed to systematically extract the Higgs branch. The development of such a method is focus of this thesis and in the context of 4d theories this is explored in section 5.

1.4 Five dimension ($5d$ $\mathcal{N} = 1$)

It was often argued that $5d$ $\mathcal{N} = 1$ gauge theories are non-renormalizable due to the gauge coupling having negative mass dimension. The gauge theories then flow to some free theories and there are no interesting fixed points. This all changed from the seminal paper [74] where non-trivial interacting UV fixed points were found for 5d theories. This lead to a great deal of interest in studying $5d$ SCFTs including many attempts in classifying them

[11] However, we shall see in the next subsection how quantum corrections can arise in the form of massless instantons in $5d$ $\mathcal{N} = 1$ and tensionless strings in $6d$ $\mathcal{N} = (1, 0)$ which corrects the Higgs branch

[75, 76, 77, 78, 79, 80, 81, 82]. Furthermore, new techniques such as brane webs are developed to study them which we will discuss in Section 3.

One particular feature that arise in $5d$ is the existence of a conserved current:

$$j^{(1)} = \mathrm{Tr} * (F \wedge F) \tag{1.35}$$

which gives rise to a $\mathrm{U}(1)_I$ global symmetry. The label I indicates the symmetry is related to the gauge instantons that we are familiar with in 4d by solving self-dual Yang-Mills equations. In 5d, instantons (codimensional 4 objects) are particles and we will name the particles that are charged under this $\mathrm{U}(1)_I$ as *instanton operators*. Crucially, the mass of an instanton operator is inversely proportional to the gauge coupling g:

$$m_I \propto \frac{1}{g^2} \tag{1.36}$$

This means at the UV fixed point where $g \to \infty$, the instantons become massless and contribute to enhance the global symmetry.

R-symmetry

For 5d $\mathcal{N} = 1$ theories, the R-symmetry is $\mathrm{SU}(2)_R$.

Vector multiplet $(A_\mu, \Phi, \text{ spinors})$

Contains a gauge field A_μ with $\mu = 0, 1, 2, 3, 4$, one real scalar field ϕ and (Dirac) spinors. The real scalar field transforms trivially under the R-symmetry.

Hypermultiplet $(q, \tilde{q}^\dagger, \text{spinors})$

Contains the complex scalar q and its complex conjugate $\tilde{q}^\dagger$ and (Dirac) spinors. The complex scalars transform under $\mathrm{SU}(2)_R$ of the R-symmetry group.

1.4.1 Coulomb branch

The Coulomb branch for $5d$ gauge theories is now parameterized by a single real scalar and takes a particularly simple form. For a gauge group G with N_f flavors, the Coulomb branch is:

$$\text{Coulomb}_{(G)-[N_f]} = \frac{\mathbb{R}^r}{\mathcal{W}_G} \tag{1.37}$$

where r is the rank of the gauge group and $\mathcal{W}_G$ is the Weyl group. The manifold is now real and the real dimension of the Coulomb branch is once again the sum of the ranks of the gauge groups. The Coulomb branch metric can again be obtained from the prepotential and thus the effective gauge coupling can be obtained as well. The prepotential can be easily computed by studying brane webs [16, 83].

Now, to say a few words about using the Coulomb branch to classify 5d $\mathcal{N} = 1$ theories with non-trivial superconformal fixed point. This is done by ensuring the effective gauge coupling does not become singular at a finite point in the moduli space which translates to ensuring the Coulomb branch metric is non-negative throughout the Coulomb branch. This condition, in turn, translates to the prepotential being a concave function. Using this as a starting point, attempts were made in [75] to classify 5d SCFTs. A more recent study [76] however shows that such constraints are too strong and a new set of rules were introduced. This includes excluding regions in the Coulomb branch where monopole string tensions are negative. Some of these excluded regions have negative Coulomb branch metric and therefore were previously discarded in [75] but since they are no longer part of the *physical* Coulomb branch, such a theory has a non-trivial UV fixed point. In particular, this result allows quiver gauge theories (with two or more gauge groups) to become SCFTs in the UV.

SU(2) with 4 flavors

Going back to our example, the SU(2) with 4 flavour theory the Coulomb branch is simply $\mathbb{R}/\mathbb{Z}_2 \cong \mathbb{R}^+$ and it can be shown that the Coulomb branch metric is non-negative. There exists a superconformal fixed point.

1.4.2 Higgs branch (Instanton corrections)

The Higgs branch intersects the Coulomb branch along the Weyl chambers of the Coulomb branch where some or all of the VEVs of the real scalar fields are set to zero. As shown previously, the instanton masses are inversely proportional to the gauge coupling squared. Therefore, at the UV fixed point the instantons becomes massless and enhances the Higgs branch. This non-perturbative quantum correction to the Higgs branch distinguishes the $5d$ $\mathcal{N}=1$ theories from $4d$ $\mathcal{N}=2$ and $3d$ $\mathcal{N}=4$ theories where the Higgs branch is always classical. Furthermore, due to these massless instantons, the Higgs branch no longer has a known construction as a hyperKähler quotient. This means our Molien-Weyl formula no longer works and a new method will be needed to systematically extract the Higgs branch. This will form the main content of Section 4.

$SU(2)$ with 4 flavors

Back to our favourite example. The classical Higgs branch of this theory has $\mathrm{SO}(8)\times\mathrm{U}(1)_I$ global symmetry. As shown by the Coulomb branch metric being non-negative, this theory has a UV fixed point. In the fixed point, the instantons becomes massless and this global symmetry is enhanced to $\mathrm{E}_5\cong\mathrm{SO}(10)$. As a result, the Higgs branch is enhanced as well from the classical Higgs branch (which is the same in $4d$ and $3d$) of $\overline{\mathcal{O}}^{\mathfrak{so}(8)}_{\min}$ to:

$$\mathrm{Higgs}^{5d,g_\infty}_{SU(2)-[4]}=\overline{\mathcal{O}}^{\mathfrak{so}(10)}_{\min} \tag{1.38}$$

Stating it in an equivalent way, the one-SO(8) instanton moduli space is enhanced to one-SO(10) instanton moduli space.

1.5 Six dimension ($6d$ $\mathcal{N}=(1,0)$)

To be complete, we will briefly discuss $6d$ $\mathcal{N}=(1,0)$ even though they are not a main focus of this thesis. The novelty that arises in $6d$ is the existence of tensionless BPS-strings.

R-symmetry

For 6d $\mathcal{N} = (1, 0)$ theories, the R-symmetry is $\mathrm{SU}(2)_R$.

Vector multiplet (A_μ, spinors)

Contains a gauge field A_μ with $\mu = 0, 1, 2, 3, 4, 5$ and Weyl spinors. There are no real scalar fields.

Hypermultiplet ($q, \tilde{q}^\dagger$, spinors)

Contains a complex scalar q and its complex conjugate $\tilde{q}^\dagger$ and Weyl spinors. The complex scalars transform under $\mathrm{SU}(2)_R$ of the R-symmetry group.

Tensor multiplet (B, ϕ, spinors)

There is a tensor field B, a real scalar field and (Weyl) spinors. The gauge coupling is inversely proportional to the VEV of this real scalar field (which is also the tension of the BPS-string), thus making it a dynamical object.

Higgs branch and Tensor branch (Tensionless strings)

Due to the absence of scalar fields in the vector multiplet, there are no Coulomb branches in 6*d*. However, the tensor branch of 6d theories are often referred to as the "Coulomb branch" since after dimensional reduction, the tensor multiplet becomes vector multiplets and the tensor branch becomes part of the Coulomb branch of the lower dimensional theories. For 6d theories with several gauge groups, massless degrees of freedom arises from tensionless BPS-strings whenever a gauge coupling is tuned to infinity. This enhances the Higgs branch and when all the gauge couplings are tuned to infinity, we have an 6d SCFT[12].

[12]Of course, like in 5d, an arbitrary gauge theory usually do not have superconformal fixed point. For a classification of 6d SCFTs , see [84].

SU(2) with 4 flavors

For SU(2) with 4 flavors, the moduli space changes at the origin of the tensor branch where the gauge coupling is tuned to infinity. Interestingly, the global symmetry group becomes smaller $\mathrm{SO}(8) \to \mathrm{SO}(7)$ as first predicted in [85]. The moduli space is also shrinks from $\overline{\mathcal{O}}_{\mathrm{min}}^{\mathfrak{so}(8)}$ to $\overline{\mathcal{O}}_{\mathrm{n.min}}^{\mathfrak{so}(7)}$ [86, 87, 88]. This is the result of the identification of a $\mathbb{Z}_2$ symmetry and only operators invariant under this symmetry remains. The Higgs branch dimension remains the same at $\dim_{\mathbb{H}} = 5$.

1.6 Other dimensions

One can go to lower dimensions such as $2d$ $\mathcal{N} = (4, 4)$ theories. Here, the "Coulomb branch" is parameterized by scalars in the vector multiplets which has a generalized Kähler potential that can be studied using non-linear σ models [89]. Similarly, there is a "Higgs branch" parameterized by scalars in the hypermultiplets and is a hyperKähler manifold. For more information, we direct readers to [90] for a review. Although interesting, we will not discuss these and lower dimensional theories in this thesis.

Chapter 2

Magnetic Quivers

With some background and examples covered in the previous chapter, we are now ready to star the main player of this thesis – **Magnetic Quivers**.

2.1 3d mirror symmetry

Before introducing magnetic quivers, we need to cover a crucial phenomenon that appears in $3d$ $\mathcal{N}=4$ theories: three dimensional mirror symmetry. As shown in the previous section, the R-symmetry group in 3d $\mathcal{N}=4$ is $\mathrm{SU}(2)_L \times \mathrm{SU}(2)_R$ with the $\mathrm{SU}(2)_L$ acting on the Coulomb branch and $\mathrm{SU}(2)_R$ acting on the Higgs branch. Furthermore, both moduli spaces are parameterized by four real scalars and are therefore hyperKähler manifolds. This presents a unique opportunity where the two moduli spaces can be put on equal footing. In the pioneering work of [91], a relationship is established between two $3d$ $\mathcal{N}=4$ theories $\mathcal{T}_A$ and $\mathcal{T}_B$ which are said to be 3d mirror pairs if:

$$\begin{aligned} \mathrm{Coulomb}(\mathcal{T}_A) &= \mathrm{Higgs}(\mathcal{T}_B) \\ \mathrm{Higgs}(\mathcal{T}_A) &= \mathrm{Coulomb}(\mathcal{T}_B) \end{aligned} \tag{2.1}$$

Since then, many 3d mirror pairs have been found in the literature. For example, the 3d mirror pair of the following theories are known:

- Quivers taking the form of affine Dynkin diagrams (sunshine quivers) whose Coulomb

branches are G instantons on ALE spaces for classical group G [92].

- Quivers taking the form of finite Dynkin diagrams whose Coulomb branches are slices of the affine Grassmanian. [93]
- $T_\rho^\sigma(G)$ theories (linear quivers) for $G = \mathrm{SU}(n),\ \mathrm{SO}(2n+1),\ \mathrm{USp}(2n),\ \mathrm{USp}(2n)$ [62].
- 4d $\mathcal{N} = 2$ class $\mathcal{S}$ theories compactified on a circle (no quiver description in general) [94].

This list is by no means complete but it does cover quite a significant portion of known 3d mirror pairs in the literature. In fact, we will greatly expand the known 3d mirror pairs in the literature in section [9].

Why is it important?

The motivation to study 3d mirror symmetry is the same as the motivation to study any other dualities in string theory that certain properties are much simpler to compute in the dual theory than in the original. For example, a theory living in a strongly coupled region can be studied by performing S-duality and looking at the weakly coupled region of the dual theory where perturbative computation is applicable. Similarly, 3d mirror symmetry is historically developed to study the Coulomb branches of $3d$ theories. This is because the Coulomb branch is affected by quantum corrections and notoriously difficult to compute. On the other hand, the Higgs branch in 3d is a classical object and can be straightforwardly computed as a hyperKähler quotient. Therefore, the Coulomb branch of theories can be studied by looking at the Higgs branch of the 3d mirror. The process of finding said 3d mirror can be done efficiently using brane systems as we will see in the next chapter.

2.2 Magnetic Quiver

The concept of magnetic quivers is a spiritual extension of the 3d mirror symmetry. Once again, the key is the identification of moduli spaces, in particular a Higgs branch with a Coulomb branch. The main difference is that rather than staying in 3d $\mathcal{N} = 4$, it applies equally well to 4d $\mathcal{N} = 2$, $5d$ $\mathcal{N} = 1$ and $6d$ $\mathcal{N} = (1, 0)$ theories. An issue immediately arises: whilst the Higgs

branch in all these dimensions are parameterized by four real scalars and therefore hyperKähler, the Coulomb branch is drastically different in different dimensions due to the different number of real scalar fields in the vector multiplets. So the idea of a higher d mirror symmetry does not seem to make sense[1]. Indeed, we are only interested in the Higgs branch of theories in $d = 4, 5, 6$, not the Coulomb branch. So what do we compare the Higgs branches of these higher dimensional theories to? These are matched with Coulomb branches of $3d$ $\mathcal{N} = 4$ theories which are also hyperKähler! The 3d theory is called the **magnetic quiver** of the corresponding higher dimensional theory. The definition is as follow:

The magnetic quiver of a d dimensional gauge theory $\mathcal{T}_A$ with 8 supercharges is defined as a $3d$ $\mathcal{N} = 4$ gauge theory that satisfies:

$$\text{Higgs}^{d=3,4,5,6}(\mathcal{T}_A) = \text{Coulomb}^{3d\,\mathcal{N}=4}(\text{Magnetic Quiver}) \tag{2.2}$$

We then refer to $\mathcal{T}_A$ as the *electric quiver*. In some of the chapters when $d = 4, 5, 6$, we also refer to the electric quiver as 'higher dimensional theory' .

As discussed in the previous section, the Higgs branch is protected against quantum corrections and the classical Higgs branch of a gauge theory is the same in $d = 3, 4, 5, 6$. However, the Higgs branch can receive non-perturbative corrections in 5d from massless instantons and 6d from tensionless BPS strings. As a result, the Higgs branches of these theories are no longer hyperKähler quotients and become difficult to study whenever some or all gauge couplings are tuned to infinity. Although such corrections do not exist for the Higgs branch in 4d, the issue there is that the majority of SCFTs do not have Lagrangian descriptions and also lacks an effective description as a quiver gauge theory. Once again, this prevents us from using the hyperKähler quotient as a means to study the Higgs branch.

Solving these difficulties is precisely the purpose of the magnetic quiver. As we shall see in the next chapter, there exists brane constructions for the 5d and 6d gauge theories both at the superconformal fixed point and away from it. From the brane construction, we extract a $3d$ $\mathcal{N} = 4$ theory, which is our magnetic quiver, in a manner very similar to how one extracts

[1]Although some work are done on 4d extension of mirror symmetry [95, 95]. But we will not discuss those further

mirror quivers in 3d. For 4d theories, we can extract the magnetic quiver through a process called *folding* of magnetic quivers of 5d theories.

In the last few years many techniques such as the monopole formula, and as we shall see later on, quiver subtraction which were developed specifically to study the Coulomb branch of 3d $\mathcal{N} = 4$ theories. Now, we can use all of these tools to study the Coulomb branch of the magnetic quiver and hence indirectly study the Higgs branch of the corresponding higher dimensional theory. This is the main purpose of the magnetic quiver.

Role of the monopole formula

In ths author's opinion, it is justifiable to say that the monopole formula makes the 3d Coulomb branch just as easy to study as the Higgs branch. If not, easier. Of course, one can argue that the monopole formula only computes the Hilbert series which does not necessarily uniquely identify the Coulomb branch moduli space. However, from experience, unless one purposely construct a model where this mismatch happens, the Hilbert series we computed were always be able to uniquely identify the Coulomb branch. This extends the Hilbert series from a tool used to study moduli spaces as algebraic varieties to a way of testing newly conjectured 3d mirror pairs or electric-magnetic quiver pairs by matching their Hilbert series. In the past, 3d mirror pairs were conjectured based on counting the dimension of the moduli space, specifying global symmetries and matching mass and FI parameters which are not accurate as there is large degeneracy in theories sharing the same quantities. Computing the Hilbert series, even perturbatively, on the other hand is a significantly more non-trivial check. For example, it is extremely unlikely that two Taylor expanded Hilbert series $\mathrm{HS}_1(t)$, $\mathrm{HS}_2(t)$ that are the same to order t^{20} describe two different moduli spaces.

The invention of magnetic quivers really propels the usefulness and efficiency of the monopole formula beyond 3d $\mathcal{N} = 4$ theories. With these new ideas, we were successful in studying the Higgs branch of various theories in $d = 4, 5, 6$ such as all known rank 1 4d SCFTs, Argyres-Douglas theories, the entirety of 5d SQCD theories with fundamental hypers at UV fixed points, 6d SCFTs corresponding to F theory constructions with -1 curves etc. In the remainder of this thesis, we will first go through how to extract the magnetic quivers from brane

set ups and then study the magnetic quivers of theories in various dimensions case by case.

Union of several hyperKähler cones

As we will see in Chapter 4 and 6, the Higgs branch of electric quivers can be the union of several hyperKähler cones. For such a case, the definition is amended as follows:

The magnetic quiver of a d dimensional gauge theory $\mathcal{T}_A$ with 8 supercharges is defined as a $3d$ $\mathcal{N}=4$ gauge theory that satisfies:

$$\text{Higgs}^{d=3,4,5,6}(\mathcal{T}_A) = \bigcup_i \text{Coulomb}^{3d\,\mathcal{N}=4}(\text{Magnetic Quiver})_i \tag{2.3}$$

where each hyperKähler cone in $\mathcal{T}_A$ corresponds to a single magnetic quiver.

Chapter 3

Brane Dynamics and Magnetic Quivers

Branes form an inseparable part of string theory. Some of the more common branes in the literature include:

- IIA: F1,NS5, $D_{0,2,4,6,8}$
- IIB: F1, NS5 , $D_{1,3,5,7,9}$, (p,q)-5branes, $[p,q]$7-branes
- M-theory: M2, M5, M9, M-wave

where the red coloured branes will play major roles in this thesis. To study low dimensional physics, one usually starts with ten or eleven-dimensional theories and perform specific compatifications. This, however, will not be the route we take. Instead, we will be studying gauge theories by looking at brane systems with different branes ending on each other. Consider a D3-D5-NS5 brane system. Our 3d $\mathcal{N} = 4$ quiver gauge theories will live on the D3 branes which are the dynamical objects. On the other hand, the D5 and NS5 branes are non-dynamical objects whose positions will parameterize various parameters in the gauge theory such as mass parameters, FI parameters and gauge couplings. The branes we look at are 1/2-BPS branes and therefore break half the supersymmetry. However, our brane systems have branes ending on each other in such a way that another half of the supersymmetry is broken, giving us eight supercharges in the end (since we usually work in IIA or IIB).

Orientifold planes

In addition to branes, we will also be including orientifold planes in our brane systems. These are generalizations of orbifolds and are defined by a $\mathbb{Z}_2$ orbifold along with an orientation reversal on the strings in the transverse direction to the plane. The presence of orientifold planes breaks half the supersymmetry. The way we add orientifold planes to our brane systems will *still preserve* eight supercharges in the end. For $d \leq 5$ there exists four types of orientifolds: O_p^+, O_p^-, $\widetilde{O_p^+}$, $\widetilde{O_p^-}$ [39].

O_p^+, O_p^- are planes with positive and negative tensions respectively. Orientifold planes are non-dynamical objects and their presence means we can now have 1/2-D$_p$ and 1/2-NS5 branes. $\widetilde{O_p^+}$, $\widetilde{O_p^-}$ can be viewed as a bound state of O_p^-, O_p^+ and a 1/2-D$_p$ brane stuck on it. From string theory perspective, there is a tight connection between stacks of branes and the gauge group of the gauge theory. For example, a stack of k D$_p$ branes gives a SU(k) SYM living on the worldvolume of the D$_p$ branes. This can be understood as the different ways strings can be stretched from one brane to another which is k^2. This gives a U(k) gauge group but an overall U(1) decouples in order to fix the centre of mass of the brane system, giving an SU(k) and k^2-1 degrees of freedom instead. Similarly, in the presence of orientifold planes, $2k$ stacks of 1/2-D$_p$ branes give rise to a gauge theory with a rank k gauge group. The algebra of the gauge group can be straightforwardly read off which depends on the type of orientifold plane[1]. A summary of the four orientifold planes, their charges and respective algebra are given in Table 3.2.

Table 3.1: *Table detailing the charges of the orientifold planes and their gauge algebra. The third column looks at $2k$ 1/2 D$_p$ branes parallel to the orientifold planes whereas the fourth column looks at $2N$ 1/2 D$_p$ branes perpendicular to the orientifold planes.*

	Charge	Gauge algebra	Flavour algebra (perpendicular)
O_p^-	-2^{p-5}	$\mathfrak{so}(2k)$	$\mathfrak{usp}(2N)$
$\widetilde{O_p^-}$	$\frac{1}{2}-2^{p-5}$	$\mathfrak{so}(2k+1)$	$\mathfrak{usp}(2N)$
O_p^+	2^{p-5}	$\mathfrak{usp}(2k)$	$\mathfrak{so}(2N)$
$\widetilde{O_p^+}$	2^{p-5}	$\mathfrak{usp}(2k)$	$\mathfrak{so}(2N)$

[1]Crucially, the global structure of the group cannot be read off directly. For example, one cannot distinguish between SO and O gauge group from the brane system. Clarifying the difference is a point of active research with several attempts made in the literature. See [52, 56, 72] in the context of quiver gauge theories.

Our strategy

The use of brane systems to find magnetic quivers is as follows:

1. Given the electric quiver, draw the corresponding brane system that describes its Coulomb branch. Such constructions are known in the literature for gauge theories in $d = 3, 4, 5, 6$ with eight supercharges.

2. Since we are only interested in the Higgs branch of these theories, the next step is to transition from the Coulomb branch phase to the Higgs branch phase by setting the masses of the hypermultiplets connected to flavour nodes to be zero.

3. Reading off the magnetic quiver. The degrees of freedom in the Higgs branch phase can be encoded as the degrees of freedom of the Coulomb branch of a $3d$ $\mathcal{N} = 4$ magnetic quiver. The details of this step will be the main focus of this chapter.

3.1 Three-dimension (D3-D5-NS5)

We will start with brane systems for 3d $\mathcal{N} = 4$ quiver gauge theories. The branes that will be involved are D3, D5 and NS5 branes in a Type IIB setting and the span of their spacetime dimensions are given in Table 3.2. Our gauge theory will live on the worldvolume of the D3 branes which has the correct $2 + 1$ spacetime dimension as the D3 branes are always suspended between the five branes.

Table 3.2: *Span of the spacetime dimensions of the different branes and orientifold planes.*

	x^0	x^1	x^2	x^3	x^4	x^5	x^6	x^7	x^8	x^9
D3	×	×	×				×			
D5	×	×	×	×	×	×				
NS5	×	×	×					×	×	×
O3	×	×	×				×			

Coulomb branch

Consider once again U(2) with 4 flavors. The quiver and the corresponding brane system is as follows:

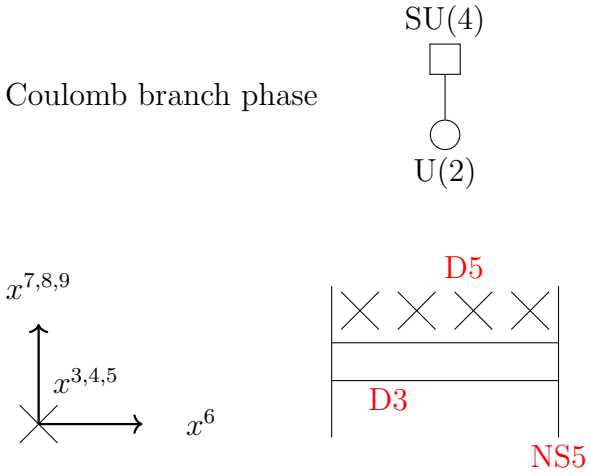

(3.1)

where the spacetime direction of the branes are indicated by the coordinate system. Vertical lines are NS5 branes, crosses (meaning the branes extends into the page) are D5 branes and horizontal lines are D3 branes. All the branes span $x^{0,1,2}$ directions so we did not include them explicitly in the diagram. Let us explain how this brane system corresponds to the quiver. The different supermultiplets in our gauge theory come from F1 strings stretching between the different branes. In particular:

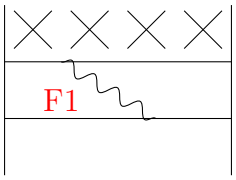

Vector multiplet

(3.2)

where the different ways the F1 string stretches between the same stack of D3 branes give rise to four vector multiplets transforming under the adjoint representation of the U(2) gauge group. When the two D3 branes coincide, the gauge symmetry is enhanced to U(2) and when separated it breaks to $U(1) \times U(1)$. A crucial point here is that the D3 branes are suspended between the NS5 branes and their positions along the NS5 branes parameterizes the VEV of the scalars in the vector multiplet. This is why this brane system represents the Coulomb branch phase. As the D3 branes are free to move along the NS5s, they contribute to dynamical degrees of freedom and hence a gauge group.

Hypermultiplets originate from F1 stretching between the D3 and D5 branes:

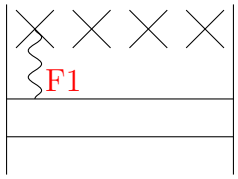

Hypermultiplet (3.3)

The eight hypermultiplets transform under the bifundamental representation of $[1,0,0]_{\mathrm{SU}(4)}[1]_{\mathrm{U}(2)}$. The D5 branes are infinitely more massive than the D3 branes and therefore are non-dynamical objects and contribute as flavour groups. The flavour symmetry is SU(4) when all four D5 branes coincide. Although not necessary, we can perform whats called a Hanany-Witten transition which creates new D3 branes when the D5 branes pass through the NS5s. The moduli spaces always remain the same before and after such transitions [37]. We often conduct such a manoeuvre as it makes it easier for us to read off the 3d mirror. Pulling the D5 branes out of the NS5 branes brings us to the following set up:

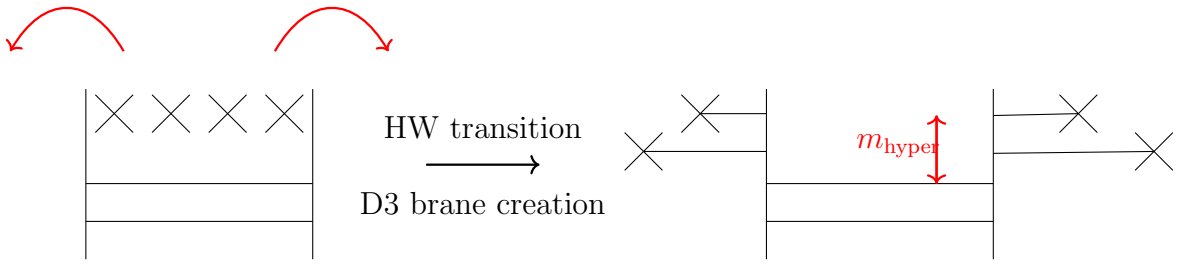

(3.4)

In the centre we see freely moving D3 branes and on the sides we have non-dynamical (frozen) D3 branes because they are suspended between a D5 and NS5 brane which extends in perpendicular directions. As a result, we have hypers connecting a gauge group and a flavour group. Furthermore, the vertical distance (in $x^{7,8,9}$) from the D3 branes suspended between the NS5s to the D3 branes suspended between the NS5 and D5 parameterizes the (bare) mass parameters of the hypermultiplets m_i where $i = 1, \ldots, 8$. This is important later on when we move to the Higgs branch.

Higgs branch

Now that we have a brane system that describes the Coulomb branch of U(2) with 4 flavors, we would like to move to the Higgs branch phase. The first step is to set the hypermultiplet mass parameters m_i to zero . This is achieved by putting them at the same height as the D3 branes suspended between the NS5s:

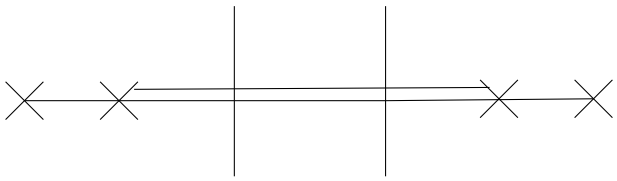

Higgs branch phase (3.5)

Despite the spacings in the drawing, this is how we will draw coincidence branes. In this phase, the D3 branes can actually be suspended between the D5 branes which extends into the page. The positions of D3 branes along D5 branes parameterizes the VEV of the scalars in the hypermultiplet. Therefore their positions parameterizes the Higgs branch! To make this picture more obvious, we can rotate the image at some angle and see the position of the D3 branes at a generic position in the brane set up.

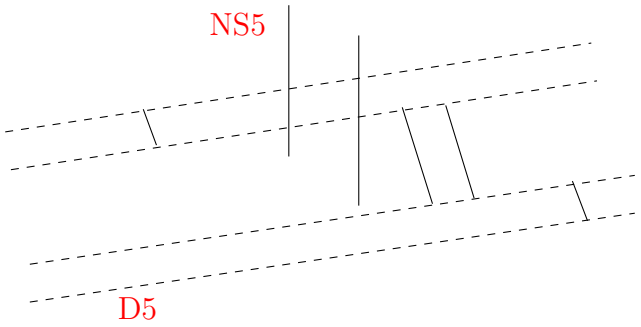

Higgs phase (3.6)

where the dotted lines are D5 and the vertical lines are NS5. Now that we brought the brane system to the Higgs branch phase, we can proceed to find the 3d mirror pair.

3.1.1 3d mirror

3d mirror symmetry was first demonstrated using brane systems in [37]. Starting with the Higgs branch phase, we first take the S-dual:

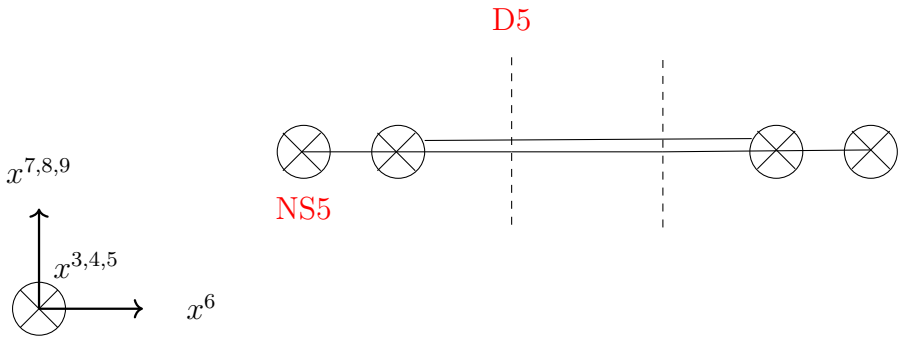

(3.7)

using the fact that NS5 and D5 branes are exchanged under S-duality whereas D3 branes are invariant. We use a circle and a cross on the NS5 branes just to differentiate the notation from D5 branes but they both extends into the paper. The final step is to reorient the diagram to get our familiar Coulomb branch phase brane set up, but this time for the Coulomb branch of the 3d mirror:

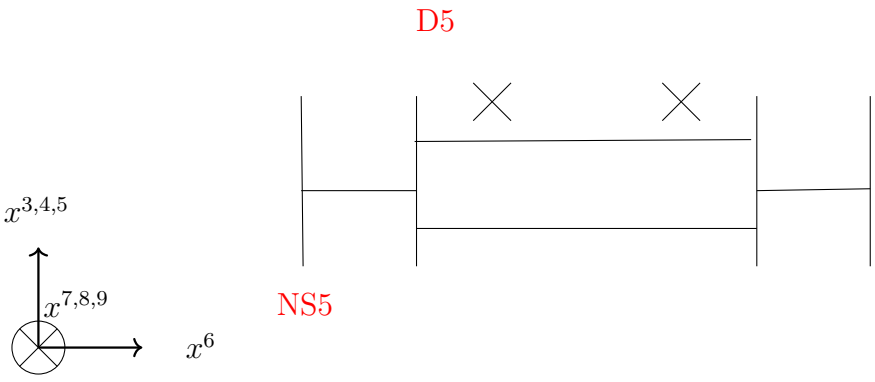

(3.8)

From the Coulomb branch phase, we can straightforwardly read off the 3d mirror quiver and it is:

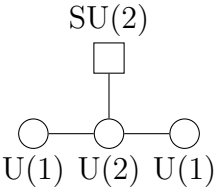

(3.9)

which is the correct 3d mirror pair of U(2) with 4 flavors. The quickest and best way to check that these two theories are indeed 3d mirror pairs is to compute the Coulomb branch and Higgs branch Hilbert series on both sides and compare them. One important thing to note is that after we arrived at the Higgs branch phase, the process of doing S-duality and changing the orientation of the coordinates is a fairly trivial process. In the sense that from (3.5) we can straightforwardly read off the 3d mirror. This is important later on because magnetic quivers of higher dimensional theories are not obtained by doing any S-dualities but instead they are directly read off from the Higgs branch phase.

For 3d $\mathcal{N} = 4$ theories, the brane set up allows us to construct quivers with unitary gauge groups but not special unitary gauge groups. This remains quite a mystery and its resolution is discussed in chapter 6.

3.1.2 Inserting O3 planes

Now we would like to insert some O_p orientifold planes. For 3d gauge theories we will be using O3 planes which were studied in great detail in [40] and later on extended in [62]. One important feature about O_p planes is that they change from one form to the other when passing through NS5 and D_p branes. For O3 planes, we give the details in Table 3.3 as well as our convention in drawing them in brane systems [40].

Table 3.3: *O3 planes as they passes through D5 and NS5 branes. S-dual of the O3 planes. We also write down the convention for writing the O3 planes in our brane set up.*

	Passing NS5	Passing D5	S-dual	Convention
$O3^-$	$O3^+$	$\widetilde{O3^-}$	$O3^-$	(No line)
$\widetilde{O3^-}$	$\widetilde{O3^+}$	$O3^-$	$O3^+$	—— (Solid line)
$O3^+$	$O3^-$	$\widetilde{O3^+}$	$\widetilde{O3^-}$	····· (Dotted line)
$\widetilde{O3^+}$	$\widetilde{O3^-}$	$O3^-$	$\widetilde{O3^+}$	- - - - - (Dashed line)

Let's turn to our canonical example of SU(2) $\cong$ USp(2) gauge theory with 4 full hypers (or

8 half-hypers). The brane set up for the Coulomb branch takes the following form:

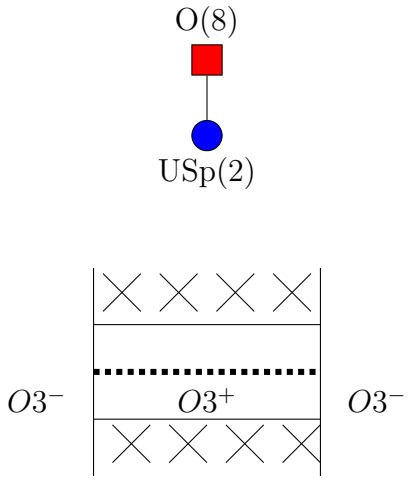

Coulomb branch phase (3.10)

Remember that the O3 plane comes with a $\mathbb{Z}_2$ orbifold action on the transverse direction to the brane. Therefore, everything above the brane is reflected below it. As a result, the horizontal line now represents a 1/2-D3 brane whereas the crosses represents 1/2-D5 brane. Eight 1/2-D5 branes then contributes to eight half-hypers or equivalently four full hypers as required.

Higgs branch phase

Following the same procedure as before we arrive at the following Higgs branch phase:

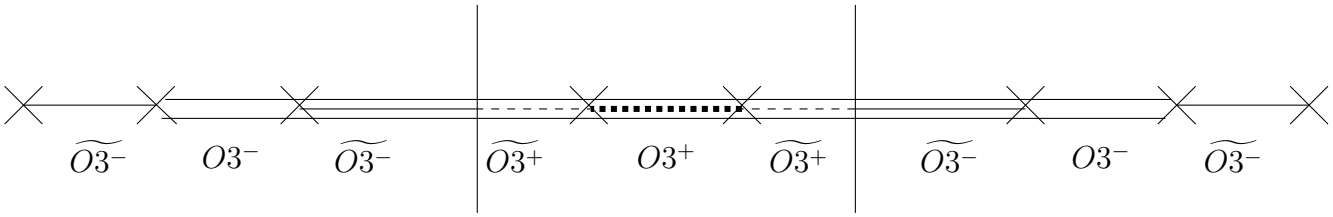

Higgs branch phase (3.11)

Here, we moved the eight 1/2-D5 branes towards the O3 plane where they recombine and then splitted again into half branes moving parallel along the O3 plane. We then moved them out of the NS5 branes resulting in D3 branes being created whilst being careful on how the O3 planes changes type as they passes through the D5 branes. We didn't move the last two 1/2-D5 branes

out because in this configuration it is easier to read off the 3d mirror after taking the S-dual. Furthermore, the process of brane creation in the presence of O3 planes is non-trivial as one needs to make sure the resulting configuration remains supersymmetric. This is done by making sure the linking numbers are invariant and this is outlined in detail in [40].

3d mirror

Taking the 3d mirror and using the S-duals of O3 planes listed in Table 3.3, we arrive at the following brane set up (where we also oriented the coordinates as before):

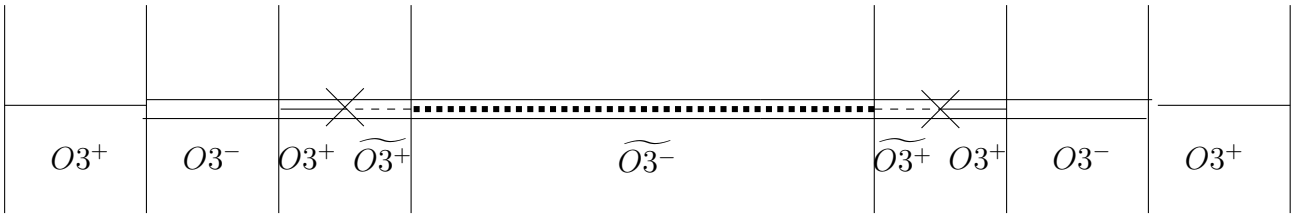

Coulomb branch phase

(3.12)

Reading off the 3d mirror gives:

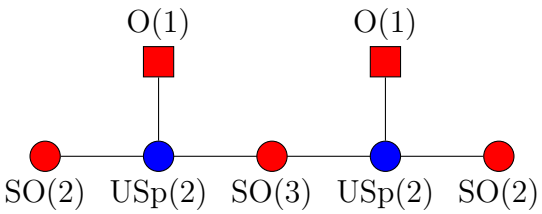

(3.13)

where the 1/2-D3 branes between the 1/2-D5 and 1/2-NS5 on the left/right side of the diagram are stuck and hence contribute flavour degrees of freedom. As a reminder, the brane system can only tell us the algebra of the gauge groups so here we computed the Coulomb branch Hilbert series (which are sensitive to discrete factors such as O vs SO) in order to identify the global structure of the gauge groups [96, 56]. We see that even though the strategy in finding the 3d mirror is the same, orthosymplectic quivers whose brane systems require orientifold planes are more difficult to deal with.

3.2 Four-dimension (D4-D6-NS5)

Extending the brane systems to $4d\ \mathcal{N}=2$, one should expect D4 branes being the dynamical object suspending between D6 branes and NS5 branes in a Type IIA setting. Such brane systems were constructed in [97] and used to describe SQCD theories in 4d. The spacetime span of the different branes are given in Table 3.4.

Table 3.4: *Span of the spacetime dimensions of the different branes.*

	x^0	x^1	x^2	x^3	x^4	x^5	x^6	x^7	x^8	x^9
D4	×	×	×	×			×			
D6	×	×	×	×	×	×		×		
NS5	×	×	×	×					×	×

One feature that arises when D4 branes ends on NS5 branes is that due to quantum effects (i.e when the gauge coupling is non-zero), the NS5 branes are not fixed at a particular value of x^6. In fact, the end point of the D4 brane behaves like a charge and creates a dimple that bends the NS5 brane logarithmically according to:

$$x^6 = l_s g_s \log(|v-a|) \tag{3.14}$$

where v is the complex coordinate $x^8 + ix^9$ and a is the coordinate of the D4 brane [97]. l_s and g_s are the string length and string coupling respectively. Such complications are not surprising which capture the intricate nature of the Coulomb branch of $4d\ \mathcal{N}=2$ theories. Logarithmic bending makes it tricky to draw the brane system and go to the Higgs branch phase. Furthermore, since we know that the Higgs branch of $4d\ \mathcal{N}=2$ gauge theories are the same as that of a $3d\ \mathcal{N}=4$ theory with the same gauge theoretic content, it is not necessary to go through the trouble of constructing a D4-D6-NS5 system when we can get the same result from a D3-D5-NS5 system. Ultimately, many SCFTs in 4d do not have a Lagrangian description which prevents us from drawing such a brane set up. For such cases, alternative descriptions such as compatifications from 6d $\mathcal{N}=(2,0)$ theories in class $\mathcal{S}$ constructions or compatifications from $5d\ \mathcal{N}=1$ theories which do have brane set ups will be more helpful. Nevertheless, the 4d brane system does reveal an important feature: the logarithmic bending means an overall

U(1) degree of freedom of the gauge group is frozen. Therefore, instead of getting U(n) gauge groups in the 4d brane system, we will be getting only SU(n) gauge groups. We shall see that this feature carries to 5d brane systems as well.

3.3 Five dimension (Brane webs)

In this thesis, much of the topics revolve around $5d$ $\mathcal{N} = 1$ gauge theories. These are theories living on the worldvolume of 5-branes in Type IIB where both D5 and NS5 branes are now dynamical objects. Previously, we saw when a D4 brane ends on an NS5 brane, the end point acts like a charged object causing the NS5 brane to bend logarithmically. Now, we have a D5 brane ending on an NS5 brane, which are equally massive, where the end point leads to a linear Coulomb like interaction and the NS5 brane bends linearly. In fact, the bent brane can be interpreted as a bound state denoted as a $(1, 1)$ 5-brane:

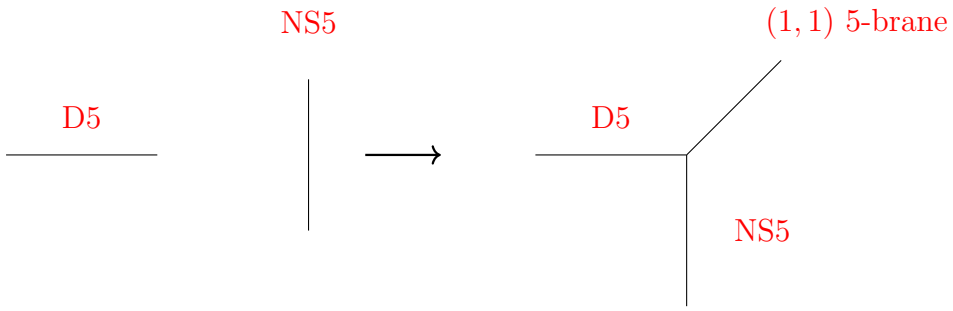

(3.15)

The position x^6 is given by:

$$x^6 = \frac{g_s}{2}(|x^5 - a| + x^5) \tag{3.16}$$

where a is the x^5 location of the D5 brane ending from the left. This was first observed in the seminal paper [16]. As a result, the Coulomb branch phase of the brane set up consists of a web-like brane system which is denoted appropriately as *brane webs*. Brane web prove to be an invaluable tool in studying 5d gauge theories. Using the convention that the complex coupling (or axiodilaton) is $\tau = i$, we have the $(1, 1)$ 5-brane bending at an 45 degree angle, consistent with the conventions used in [16] and the papers that followed. Continuing the idea of constructing a $\mathrm{D}_p - \mathrm{D}_{p+2} - \mathrm{NS5}$ brane system, we will now include D7 branes. Under the

SL$(2,\mathbb{Z})$ S-duality, one can rotate the D7 brane to the bound state $[p,q]$ 7-brane where a $[0,1]$ 7-brane is often called a NS7 brane. They are not really required when studying the Coulomb branch of 5d theories but are absolutely essential when describing the Higgs branch. These 7-branes and their spacetime span are detailed in Table 3.5.

Table 3.5: *Span of the spacetime dimensions of the different branes. A (p,q) 5-brane is a line of slope $\tan(\alpha) = q\tau_2/(p+q\tau_1)$ in the $x^{5,6}$ plane where the axiodilaton is $\tau = \tau_1 + \tau_2$. In the following, the brane webs are drawn with $\tau = i$ so that $\tan(\alpha) = q/p$ as consistent with the convention in [16].*

	x^0	x^1	x^2	x^3	x^4	x^5	x^6	x^7	x^8	x^9
D5	×	×	×	×	×		×			
NS5	×	×	×	×	×	×				
(p,q) 5-brane	×	×	×	×	×	α				
$[p,q]$ 7-brane	×	×	×	×	×			×	×	×
O5	×	×	×	×	×	×				

Coulomb branch

Now, we look at our favourite example of SU(2) with 4 flavors. The brane system for the Coulomb branch phase takes the following form:

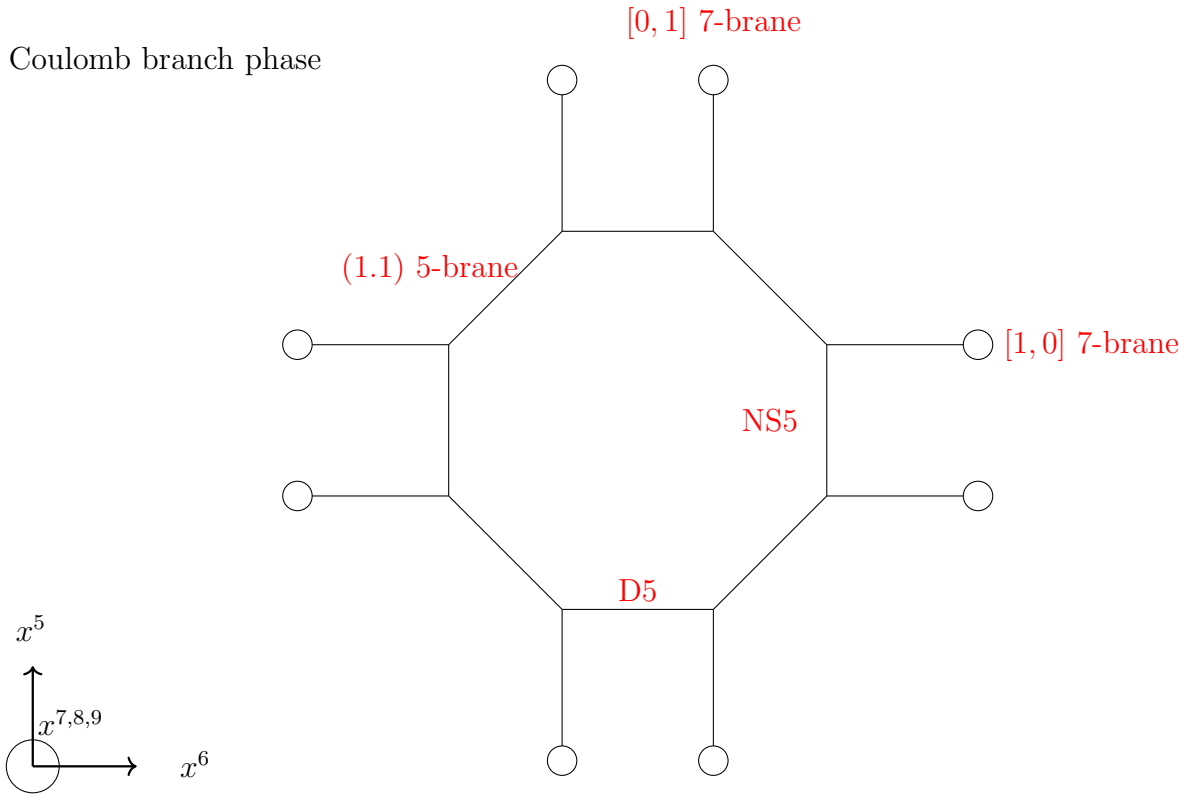

(3.17)

where the circles represents $[p, q]$ 7-branes and extend into the paper. We choose this convention rather than crosses or circle with crosses to distinguish from the NS5 and D5 branes in 3d brane systems. They should also not be confused with gauge nodes[2]. The Coulomb branch is parameterized by a single real scalar field the vector multiplet and has real dimension 1. In 3d case, we see that the position of D3 branes moving along the NS5 branes as parameterizing the VEV of the scalar field and thus the Coulomb branch. Here, when we move the D5 branes along the NS5 branes, it also locally deforms the web whilst keeping the asymptotic external legs the same. Pictorially, we have:

Coulomb branch phase

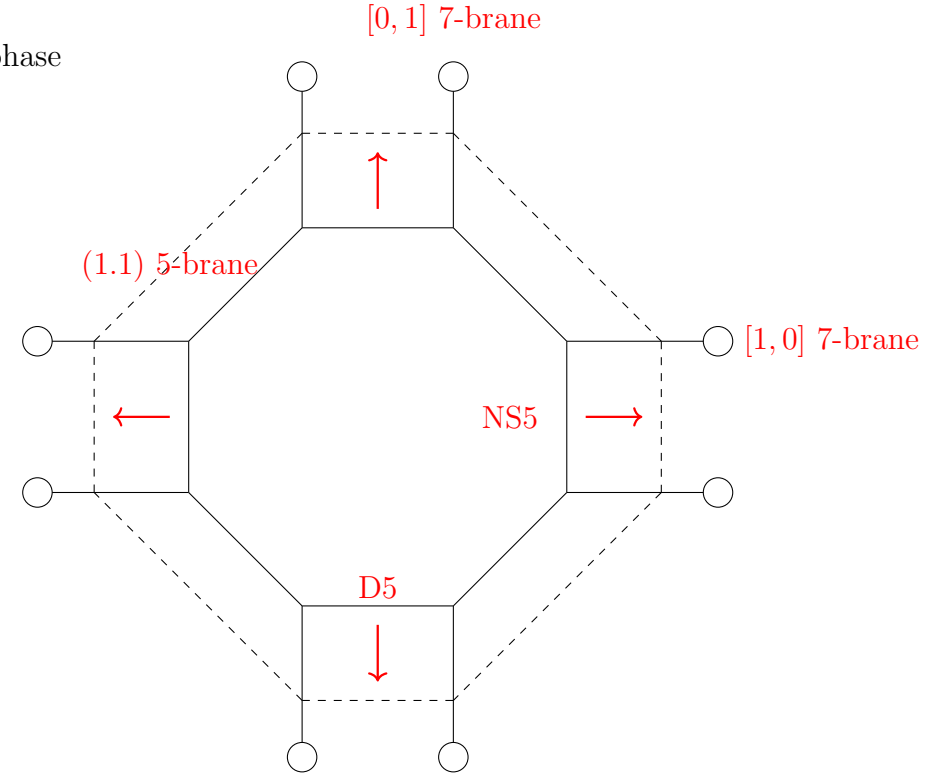

(3.18)

The Coulomb branch degree of freedom is now the shrinking and embiggening of the polygon/faces in the middle. When there are more gauge groups, the counting of the number of polygon/faces determines the real Coulomb branch dimension. Just like the 4d case, the freezing of the external leg means that an overall U(1) degree of freedom is frozen and the gauge group is SU(2) rather than U(2). This means that using brane web constructions, we only know how to build 5d electric quivers with special unitary gauge groups. Whats powerful about the brane web set up

[2]One must admit that this choice of convention in the literature was a poor one.

is that the relative distance between the branes also parameterizes many important parameters in the theory:

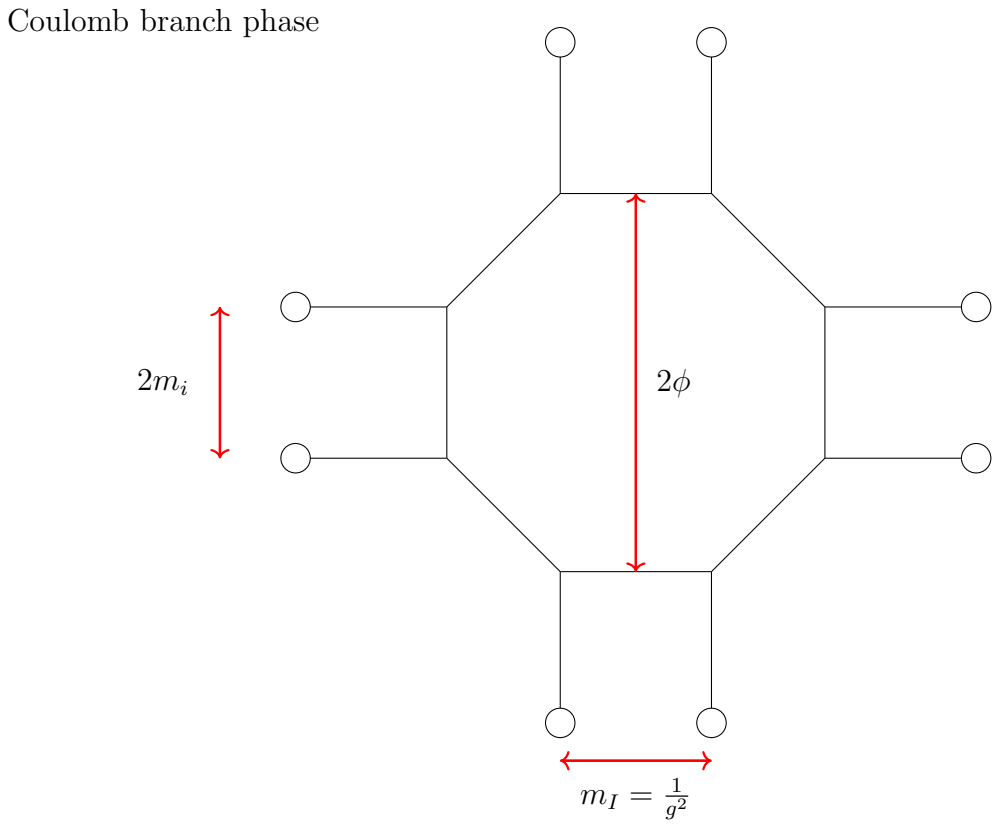

(3.19)

where ϕ is the VEV of the real scalar field that parameterizes the Coulomb branch, m_I is the bare mass of the instantons, g is the gauge coupling, m_i is the bare mass of the hypers. Under certain normalization, ϕ can also be thought of as the mass of the W-boson of the SQCD theory obtained from stretching a fundamental string between the two D5 in the polygon. The gauge instanton originates from fundamental strings stretched between the vertical NS5 branes. The area of the polygon is the tension of the monopole string. These important information can be used to directly compute the prepotential for the Coulomb branch of the theory, making the process as easy as drawing the brane web and measuring lengths/areas. This idea is extended to whats called the "complete prepotential" which includes not just the usual perturbative effects in [75] but non-perturbative contributions (massless instantons) as well as shown in [83]. Furthermore, studying the Coulomb branch using brane webs can help in the classification of 5d gauge theories with superconformal fixed points [76]. Even though there are a lot of interesting

features in the Coulomb branch phase, we will return our attention to the Higgs branch.

3.3.1 Higgs branch

To enter the Higgs branch we once again set the masses of the hypers to be zero. Now, the importance of the 7-branes comes in as the various 5-branes will now be suspended between the 7-branes which extends in $x^{7,8,9}$:

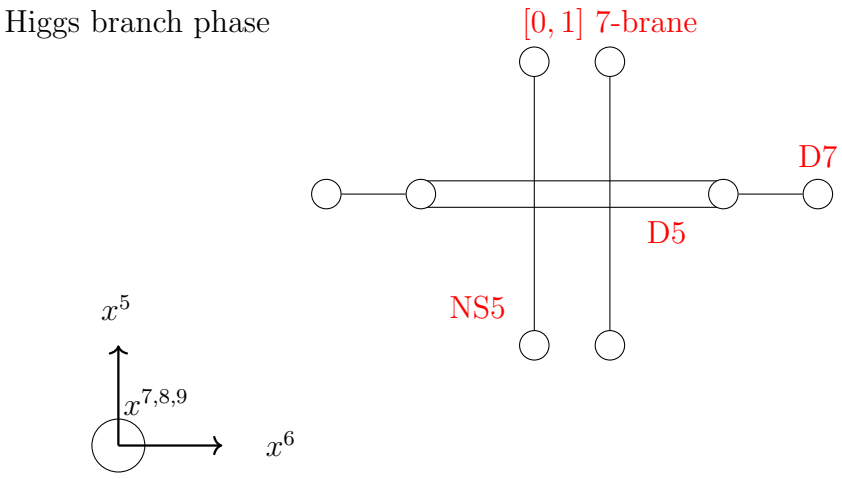

(3.20)

The 5-branes (in this case they are just D5 and NS5 but in general it can be (p, q) 5-branes stretching between the 7-branes) moving along the 7-branes gives VEV to the scalar fields in the hypers, hence parameterizing the Higgs branch. Remember the Higgs branch in 5d $\mathcal{N} = 1$ is also parameterized by 4 real scalar fields and manifold is hyperKähler just like in $3d$ $\mathcal{N} = 4$. Now that we see the similarities with 3d, one might wonder if other properties such as 3d mirror symmetry can be applied here. Note that in the previous section on $3d$ theories, we mentioned briefly that once we arrived at the Higgs branch phase we can straightforwardly read off the 3d mirror. Of course, physically we still do an S-dual and reorientation but with practice, one can skip that step on pen and paper. This convenience in calculation turns into something more physical now that we are in $5d$. First of all, it is not clear what will happen when one takes the S-dual especially in the presence of all the bound states. The fact that the web diagram is now 2-dimensional also complicates matters and even if the result is the Coulomb branch of some 5d gauge theory, it is not what we desire as the moduli space is not hyperKähler and hence cant be used to describe the Higgs branch of the original theory. Instead, what we do is something

much simpler. We look at the Higgs branch phase and conjecture a $3d$ $\mathcal{N} = 4$ magnetic quiver whose Coulomb branch is the same as the Higgs branch of the 5d theory. The first step of determining the gauge groups of the magnetic quiver is easy as they can be read off from the stacks of 5-branes. In our example, we have two separate D5 branes, a stack of two coincident D5 branes and two separate NS5 branes which contributes $\mathrm{U}(1)^2 \times \mathrm{U}(2) \times \mathrm{U}(1)^2$ gauge groups respectively. However, in more complicated examples we will have generic (p, q) 5-branes and one need to maximally divide the brane web into *subwebs* which are free to move along the 7-branes a single piece. Each such subweb corresponds to a U(1) degree of freedom whilst a k identical subwebs stacked together will give $\mathrm{U}(k)$ degree of freedom. To obtain the edges that connects the different gauge groups in the quiver, we have to compute something called *intersection number*[3]. In 3d brane system with D3-D5-NS5 branes, the object that stretches between the D-branes are F1 strings which give rise to hypermultiplets. Doing some S and T dualities, one can envision that in the brane web set up, the objects are D3 branes which are stretched between the various 5-branes. However, due to bound states of (p, q) 5-branes, there can be multiple intersection points between 5-branes which requires one D3 brane stretched between each point. The stable intersection between (p, q) and (p', q') 5-branes is given by the absolute value of the determinant:

$$\text{Stab Intersection} = \text{Abs} \begin{vmatrix} p & q \\ p' & q' \end{vmatrix} \tag{3.21}$$

On top of what was mentioned, when two subwebs intersect, there can be multiple stable intersection points, all of which are needed to be summed up. The resulting value is the multiplicity of edges between the two gauge groups. So far we have only seem edges with multiplicity 1, hence they are given by a single line. When 7-branes are present, the edge multiplicity formula is amended so that two subwebs ending on the same 7-brane on opposite

[3]The idea originates from tropical geometry. By viewing the subwebs as tropical curves, the stable intersection between different tropical curves is then our intersection number.

(same) sides contributes $+1(-1)$ to the multiplicity:

$$\text{Edge Multiplicity} = \text{Stab Intersection} + \sum_i X_i - \sum_i Y_i \tag{3.22}$$

where X_i and Y_i are the combinations of two 5-branes in different subwebs ending on a 7-brane on opposite and same side respectively. Applying this rule to our current example, the stable intersection between the single D5 and stack of two D5 branes on the left side of the brane system is 0 but they end on the D7 on opposite side and thus have edge multiplicity 1. Similarly for the stack of two D5s and the single D5 on the right side. The stable intersection between the NS5 and stack of two D5s is 1 as well, hence there is an edge with multiplicity 1 connecting them. Overall, the magnetic quiver is:

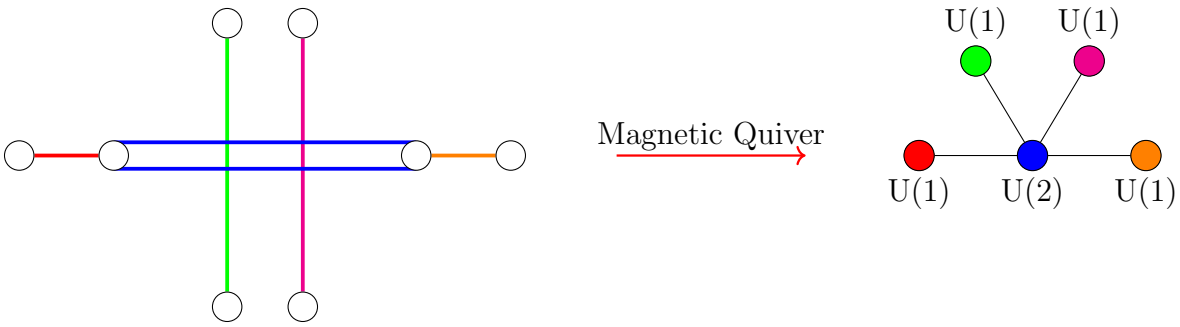

(3.23)

where we color coded the different subwebs on the left and their corresponding gauge groups on the right (the color is just to distinguish the nodes, all gauge groups here are unitary). The resulting magnetic quiver is also known as the affine Dynkin quiver of D_4 whose Coulomb branch is the expected one-$SO(8)$ instanton moduli space (or equivalently, the minimal nilpotent orbit closure $\overline{\mathcal{O}}_{\text{min}}^{\mathfrak{so}(8)}$). The algorithm of reading off the magnetic quivers from 5d brane webs discussed above is given in [25] where more examples and detailed explanations can be found.

Commented on unframed/flavorless unitary magnetic quivers

Here, we make a comment on the magnetic quiver we found. Contrary to previous examples, this unitary quiver (quiver with only unitary gauge groups) does not have any explicit flavor group. If we were to compute the Coulomb branch Hilbert series of this quiver as it is, we will

find that the result diverges. This is because, a quiver with only unitary gauge groups does not have its center of mass fixed, resulting in infinite configurations with the same $\Delta(m)$. This can be seen from the Higgs branch phase of the brane web where the center of mass of the subwebs moving along the 7-branes are not fixed. In the previous set ups of D3-D5-NS5 systems, the center masses are fixed in the Higgs branch phase due to the infinitely more massive NS5 branes which acts as flavor groups in the 3d mirror quiver. In the 5d brane system, we do not have such analogue (it would correspond to the appearance of 7-branes that are not connected to any of the 5-branes). To fix this U(1) center of mass in the magnetic quiver, all we have to do is quotient out a diagonal U(1) subgroup. The simplest way to do so is just turn one of the U(1) gauge group into a flavor group:

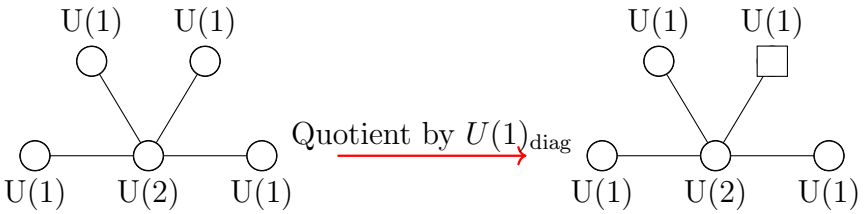

(3.24)

This can be done in any of the U(1) gauge groups[4]. It can also be done on the U(2), which we label as a 'squircle' and will be useful later on when dealing with unframed/flavorless magnetic quivers where there are no U(1) gauge groups.

3.3.2 Infinite coupling limit

So far we study the low energy effective theory at some finite gauge coupling. This can be seen from the brane webs where there is a finite horizontal distance between the NS5s. This distance is identified with the mass of the instantons and inversly proportional to the gauge coupling squared. Thus, to go to the infinite coupling limit (UV superconformal fixed point),

[4]This seem trivial in this example due to the symmetry of the quiver. However, it works even when ungauging different U(1) gauge groups results in inequivalent quivers and the Coulomb branch will still be the same. One can even consider an equivalence class of such quivers. However, other quantities such as one-form symmetries can vary depending on which gauge node the U(1) is ungauged [4]

we need to collide the two NS5 branes:

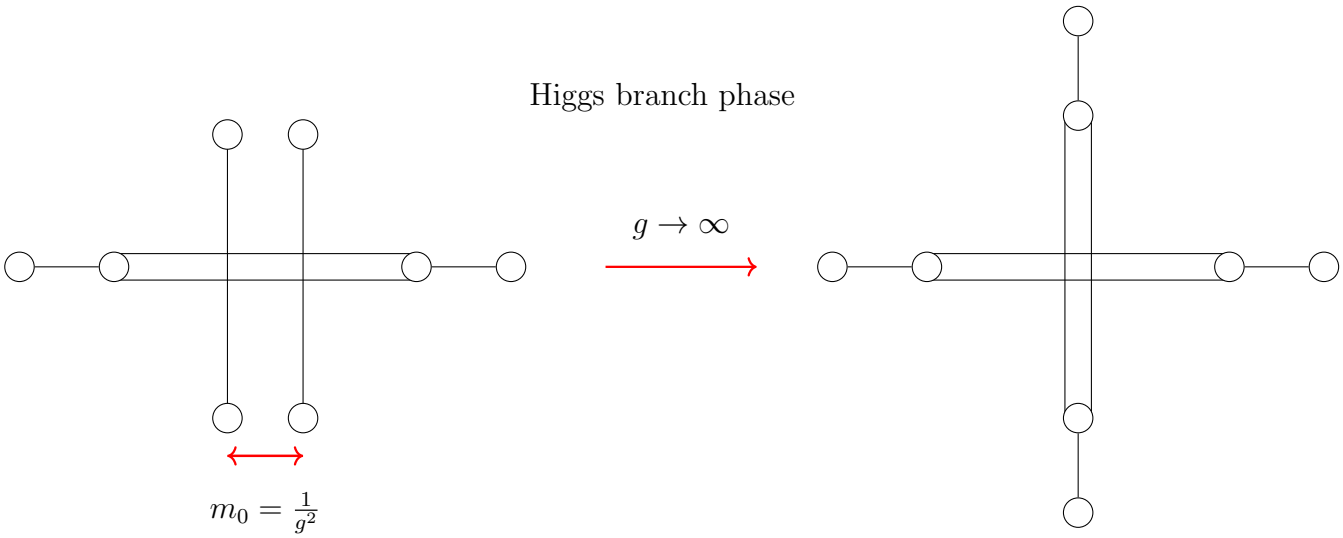

(3.25)

In this limit, the instantons become massless and contribute to the Higgs branch. The global symmetry is now enhanced from SO(8) to SO(10). The magnetic quiver obtained from this new configuration is:

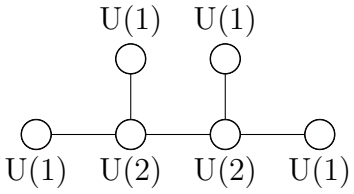

(3.26)

This 3d $\mathcal{N} = 4$ magnetic quiver is also known as the affine Dynkin quiver of D_5 and whose Coulomb branch is the one-$SO(10)$ instanton moduli space (or equivalently the minimal nilpotent orbit closure $\overline{\mathcal{O}}_{\text{min}}^{\mathfrak{so}(10)}$). This is consistent with the Higgs branch prediction in [74] and we fulfilled the magnetic quiver definition that:

$$\text{Higgs}^{5d,g_\infty}_{SU(2)-[4]} = \text{Coulomb}^{3d}(3.26) \tag{3.27}$$

Chern-Simons levels

The classical Higgs branches are not affected by Chern-Simons (CS) level of the gauge group, which we show explicitly in [11]. However, at infinite coupling limit, the CS level is important and need to be specified, in particular not all CS levels give UV fixed point. For

our case of SU(2) with 4 flavors, the CS levels is $k = 0$. For general SQCD theories with only fundamental matter fields and have non-trival UV fixed points, the theories and their CS levels and corresponding magnetic quivers are all detailed in [25]. When additional matterfields such as those transforming in the anti-symmetric representation of the gauge group are included, their magnetic quivers are given in [98].

Comment on magnetic quiver and compatification

One common question about the magnetic quiver program is whether the procedure is the same as doing compatification of the 5d theory to 3d and then finding the 3d mirror. The answer is no. The reasoning is that the magnetic quiver is obtained directly from the Higgs branch phase of the higher dimensional theory and compatification is not involved in any of the steps. Furthermore, we make no comment on whether the *Coulomb branch* of the 5d theory compactified to 3d will be the same as the *Higgs branch* of the magnetic quiver in order to satisfy the 3d mirror relation. There are examples, which we shall see later on, that this is indeed true. But in general, we will not make such a statement nor will we explicitly perform any compatification to 3d. Another point is that the Higgs branch of many higher dimensional theories at superconformal fixed points is the union of several hyperKähler cones. On the otherhand, the Coulomb branch of any $3d$ $\mathcal{N} = 4$ gauge theory is conjectured to be only a single hyperKähler cone [99]. So it is not clear how to make a one-to-one correspondence in the case of 3d mirror symmetry.

Comment on finite coupling limit

In the previous section, we are actually studing the classical Higgs branch rather than the Higgs branch at finite gauge coupling. The crucial difference is the existence of a gaugino bilinear (this is a glueball superfield which is a chiral superfield biliniear in the gaugino superfield) [100]. This contributes a discrete sector $\mathbb{Z}_2$ (fat points in the language of algebraic geometry) to the Higgs branch. Unfortunately, such phenomenons are not sensitive from the brane set up but do affect the chiral ring by adding new singlet generator S that squares to zero. For example, the classical Higgs branch of SU(2) with N_f flavors is given by the one-SO($2N_f$) instanton

moduli space. But at finite gauge coupling, the inclusion of the gaugino bilinear makes the moduli space one-$\mathrm{SO}(2N_f)$ instanton $\cup\,\mathbb{Z}_2$. In terms of the Hilbert series, the difference is just $\mathrm{HS}_{\text{finite}} = \mathrm{HS}_{\text{classical}} + t^2$. This phenomenon is studied in early works such as [101] and in the current context in [100]. For the purpose of the thesis, we ignore the contribution of the gaugino bilinear when discussing the Higgs branch at finite coupling so the object we are really talking about is the classical Higgs branch.

3.3.3 Inserting O5 planes

The results from this subsection comes from our paper [3]. After obtaining the magnetic quivers from brane webs in the previous section, the next question is what happens when we add orientifold planes. We wish to explore 5d theories that give rise to orthosymplectic magnetic quivers, therefore the orientifold planes to add are O5 planes. The spacetime span of the O5 planes are detailed in Table 3.5. Like the addition of O3 planes in 3d, the addition of O5 planes come with many subtleties. Using the same example but exploting the fact that $\mathrm{SU}(2) \cong \mathrm{Sp}(1)$, we look at the brane web of Sp(1) with 8 half-hypers:

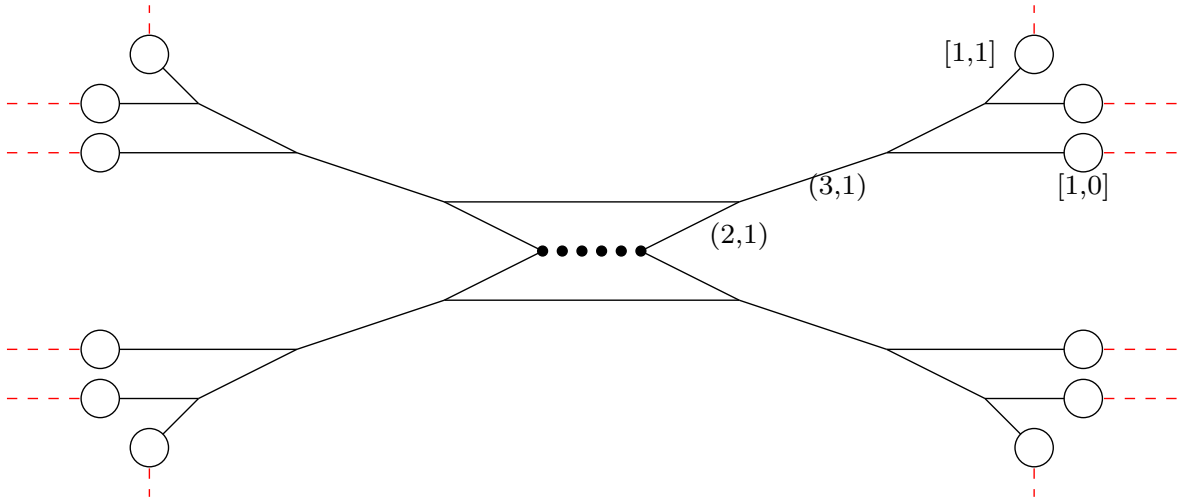

(3.28)

where all the 5-branes and 7-branes are now 1/2 5-branes and 1/2 7-branes due to the presence of the oreintifold planes. We use the same convention for drawing O5 planes as in Table 3.3. The bending of branes in 5d brane webs is necessary due to charge conservation. Since O5 planes also carry charges as shown in Table 3.2, their presence will casuse the branes to bend

accordingly as well.

Monodromy lines

Whenever there are 7-branes present, there are also monodromy cuts generated by them. We indicate this as red dotted lines coming out of the 7-branes. For a $[p, q]$ 7-brane, the associated monodromy matrix is:

$$M_{[p,q]} = \begin{pmatrix} 1 - pq & p^2 \\ -q^2 & 1 + pq \end{pmatrix} \tag{3.29}$$

The importance of these monodromy cuts occurs when 5-branes passes through them. Given a $(a, b,)$5-brane, the action of the monodromy matrix changes it to a (a', b') 5-brane:

$$\begin{pmatrix} a' \\ b' \end{pmatrix} = \begin{pmatrix} 1 - pq & p^2 \\ -q^2 & 1 + pq \end{pmatrix} \begin{pmatrix} a \\ b \end{pmatrix} \tag{3.30}$$

This can happen often as we go from finite coupling to infinite coupling in the Higgs phase. Its presence in the Coulomb branch phase also generate interesting phenomenons such as tha Tao diagrams in [18] that describes 5d theories with 6d UV fixed points. In the example of the previous section, we did not label the monodromy cuts as they do not interfere with our results, although for more complicated 5d SQCD theories, one needs to pay attention to their presence. For the monodromy cuts originating from the 7-branes, we always have the freedom to rotate them in any direction we want. Normally, they are rotated to not intersect with 5-branes or other monodromy cuts. For 5d theories with O5 planes, another complication arises. In [102] it was argued on the grounds of charge conservation that an $\widetilde{O5}$ plane must always be accompanied by an *half-monodromy line*, which we indicate by red dotted lines along the O5 planes. For more details on this feature we refer readers to [102, 103, 3]

Higgs branch phase

Now, we enter the Higgs phase. As we set the masses of the hypers to zero, various 1/2 5-branes and their reflections across the O5 plane will now coincide and then split along the orientifold planes. This procedure is the same as for O3 planes. Taking care of the monodromy cuts, the various possible splitting for the different types of O5 planes are given in [104]. The resulting Higgs branch brane set up gives:

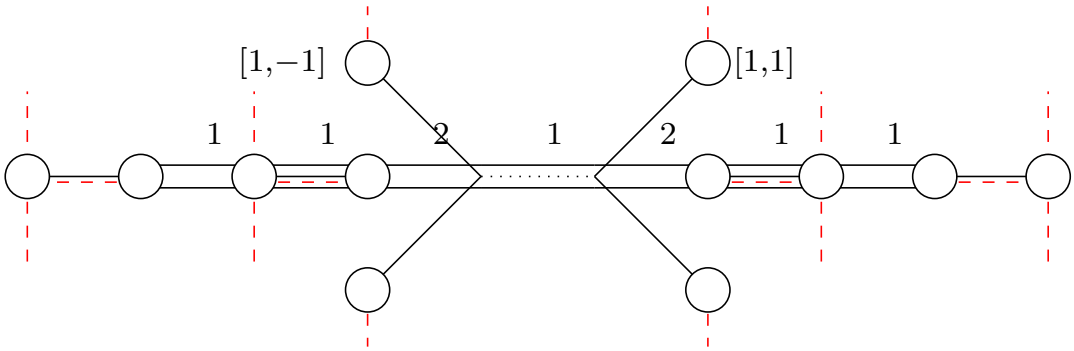

(3.31)

where we labeled the multiplicity of the 1/2 D5 branes. To make the appearance of the magnetic quiver clearer, we move the two bended $(1,1)$5-branes outwards across the 7-branes until they reach a configuration where they are connected to D7 branes and are no longer dynamical:

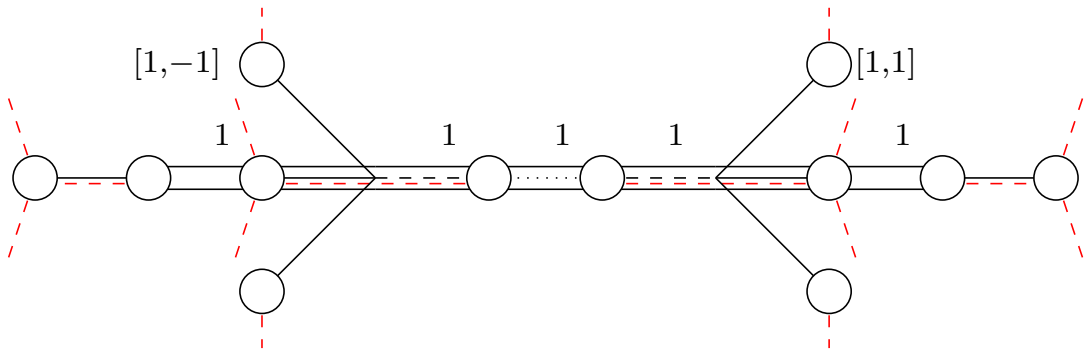

(3.32)

The non-dynamical $(1,1)$ 5-branes on the left and right will now each contribute a half-hypermultiplet to the magnetic quiver. Following the same procedure as above such as computing

the stable intersection number, we arrive at the following orthosymplectic magnetic quiver:

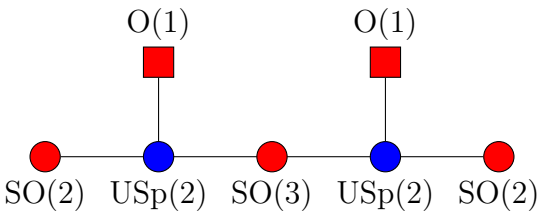

(3.33)

which is the same as in (3.13). This is a consistency check as the classical Higgs branch should be the same in 3d and in 5d.

Infinite coupling limit

Once again, we now go towards the infinite coupling limit. The gauge coupling is given by the horizontal distance between the two $(1,1)$ 5-branes, pushing them together gives us:

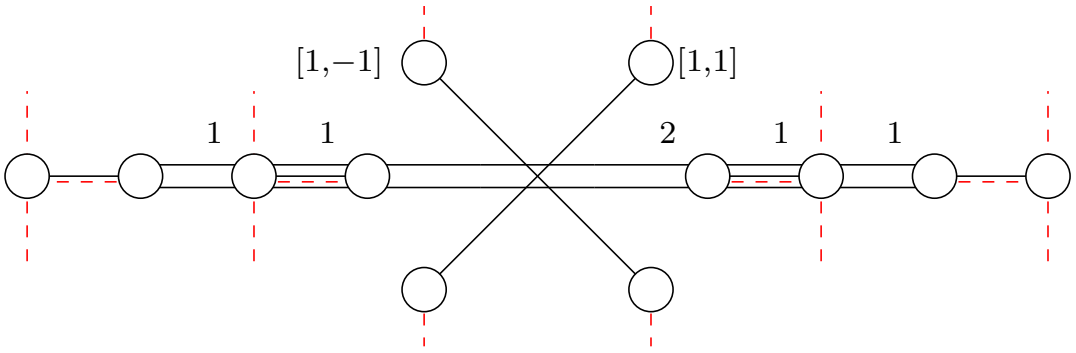

(3.34)

The 'cross' in the middle now form a subweb that is free to move along the 7-branes. Most of the brane set up is easy to identify with gauge nodes in the magnetic quiver. However, the 'cross' in the middle requires some conjecturing. We know the algebra of the gauge group associated with branes stretching parallel and perpendicular of the orientifold plane as shown in Table 3.2. However, here we have branes that are at a 45 degree angle to the orientifold! Through some trials and errors, we were able to identify and further conjecture that 5-branes that are neither parallel nor perpendicular but at an angle to the O5 plane will contribute to a U(1) gauge node

in the magnetic quiver. The resulting magnetic quiver is then:

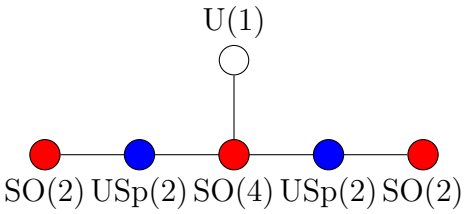

(3.35)

This *unitary-orthosymplectic* magnetic quiver made its first appearence in our paper [3] and it turns out they occur ubiquitously as magnetic quivers of 5d SCFTs as shown in [3] as well as subsequent works [105, 106, 8, 5, 107].

Unitary quivers and orthosymplectic counterparts

Now we have the magnetic quivers at finite coupling both as unitary quiver (3.23) and orthosymplectic quiver (3.33). We also have magnetic quivers at infinite coupling both as unitary quiver (3.26) and unitary-orthosymplectic quiver (3.35). One may wonder just how similar these two theories are. It turns out, they not only have the same Coulomb branches but the same Higgs branches as well. Furthermore, the superconformal index (which contains field theoretic information beyond moduli spaces) and other properties are computed as well and shown to be the same [4]. These provide evidences that these theories might be dual to each other. We will explore this in more detail in chapter 4.

3.4 Six dimension (D6-D8-NS5)

For completeness, let us discuss 6d gauge theories that lives on the D6 branes of a D6-D8-NS5 brane system in IIA. However, we will rarely look at these theories in this thesis. The spacetime span of the branes is given Table 3.6.

Higgs and Tensor branch

Note that in Table 3.6 all the spacetime span of the NS5 brane is already included in the span of the D6 branes. This means there is no sense for the D6 branes to 'move along' the NS5

Table 3.6: *Span of the spacetime dimensions of the different branes.*

	x^0	x^1	x^2	x^3	x^4	x^5	x^6	x^7	x^8	x^9
D6	×	×	×	×	×	×				
NS5	×	×	×	×	×					
O6	×	×	×	×	×					
D8	×	×	×	×	×			×	×	×

branes, hence showing there is no Coulomb branch as expected. There is, however, a tensor branch. The scalar in the tensor multiplet is parameterized by a scalar field that is inversly proportional to the gauge coupling. The gauge coupling is again the horizontal distance between the two NS5 branes and hence when the spacing becomes zero, we reach the origin of the tensor branch. The scalar field VEV is also proportional to the tension of the BPS string, hence at the origin they become tensionless and new massless states can arise. When there are multiple gauge groups, one can study the Higgs branch at different phases of the tensor branch where some or all of the BPS string becomes tensionless. Such investigation is the focus of [108, 109]. The steps in extracting unitary magnetic quivers for 6d theories are given in [108].

SU(2) with 4 flavors

Let us construct the theory of SU(2) with 4 flavors:

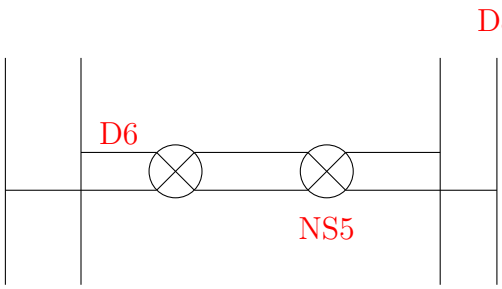

(3.36)

where now the horizontal D6 brane and NS5 branes are the dynamical objects. To enter the Higgs branch, we break the D6 branes along the D8 branes and lift the NS5 branes out:

Higgs branch phase (infinite coupling)

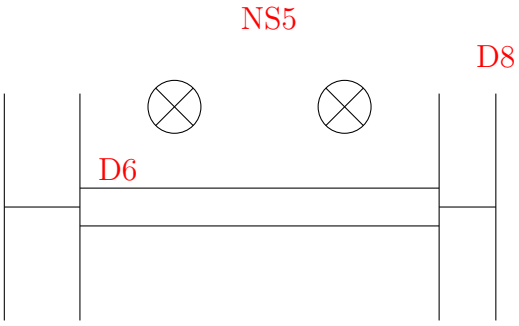

Magnetic quiver

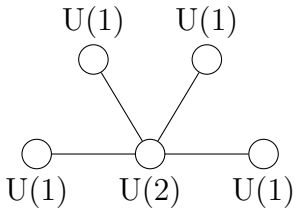

(3.37)

The D6 branes moving along the D8 branes (vertical) thus parametrizes the Higgs branch of the 6d theory. When reading off the magnetic quiver, we treat both D6 and NS5 branes as dynamical objects and we get the expected affine D_4 Dynkin quiver.

Going to infinite gauge coupling

To go to the infinite coupling limit, we once again pull the two NS5 branes together.

Higgs branch phase (infinite coupling)

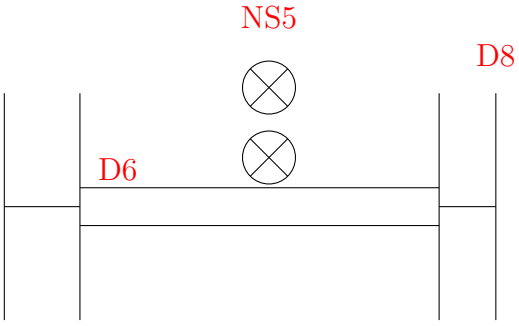

Magnetic quiver

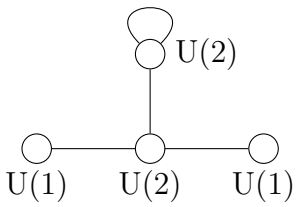

(3.38)

The resulting NS5 branes are on top of each other which we treate as a U(2) with matter fields in the adjoint representation (loop) in the magnetic quiver [88]. The coincident NS5 branes means there is a gauging of the $\mathbb{Z}_2$ discrete symmetry of the two NS5 when they are separate [86]. As a result of the $\mathbb{Z}_2$ projection, the Higgs branch moduli space actually shrinks from $\overline{\mathcal{O}}^{\mathfrak{so}(8)}_{\text{min}}$ to $\overline{\mathcal{O}}^{\mathfrak{so}(7)}_{\text{n.min}}$ which is the next to minimal nilpotent orbit of $\mathfrak{so}(7)$. For this case, there are no new tensionless strings that contributes to enhancing the Higgs branch. The Higgs branch

dimension remains the same.

3.4.1 O6 planes

The theory of SU(2) with 4 flavors in the F-theory construction is a theory on -2 self-intersection curves. Such construction comes from D6-D8-NS5 systems without orientifolds. To include orientifolds, we need to look at theories on -1 self-intersection curves. The steps in extracting orthosymplectic magnetic quivers for 6d theories are given in [109]. The simplest theory that is non-trivial in the finite coupling limit is Sp(1) with 10 flavors (or 20 half-hypers). The brane system takes the following form:

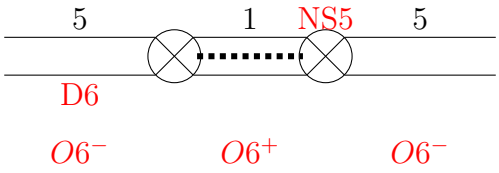

(3.39)

We also use the same convention for the O6 planes as before and detailed in Table 3.3. The x label means there are x full D6 branes or equivalently $2x$ 1/2 D6 branes due to the presence of the orientifold plane. The D6 branes on the two sides are semi-infinite and hence can be viewed as flavors, giving us 20 half-hypers in total. We didn't add the D8 branes in this diagram to avoid cluttering the brane set up.

In order to enter the Higgs branch phase, we need to attach all the 20 semi-infinite 1/2 D6 branes with 20 1/2 D8 branes (analagous to the 7-branes in 5d system and 5-branes in 3d system). After setting the masses of the hypers to be zero, we obtain the following brane system:

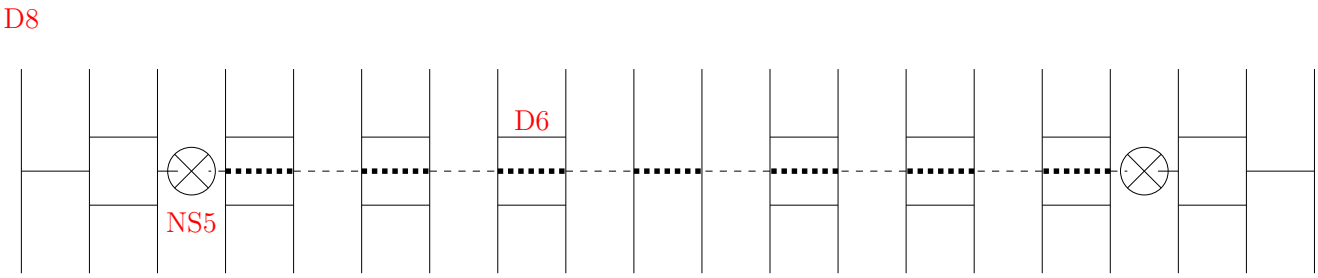

(3.40)

The magnetic quiver reads:

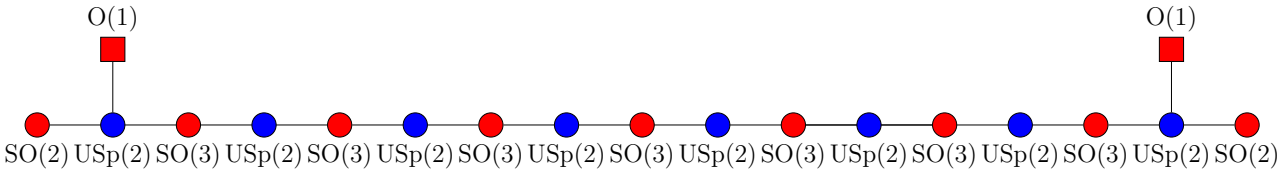

(3.41)

Since the gauge coupling is finite, we are dealing with the classical Higgs branch and therefore the magnetic quiver is the same for the Higgs branch of Sp(1) with 10 flavors in $d = 3, 4, 5, 6$. The moduli space is the one-SO(20) instanton moduli space. The 1/2 NS5 branes at the two ends are connected to the D8 branes through a D6 brane and hence frozen in place and contribute as flavor charges rather than dynamical degrees of freedom. The algebra of the gauge groups are identified by the brane system and the global structure is obtained through explicit checks using the Coulomb branch Hilbert series. The global structure of the flavor group of O(1) is written because $SO(1)$ is trivial, and not because our computation are sensitive to the global structure of the flavour groups.

Infinite coupling

Now we go to the infinite coupling limit by once again coinciding the NS5 branes. The NS5 branes stuck on the O6 plane will coincide and move out of the orientifold:

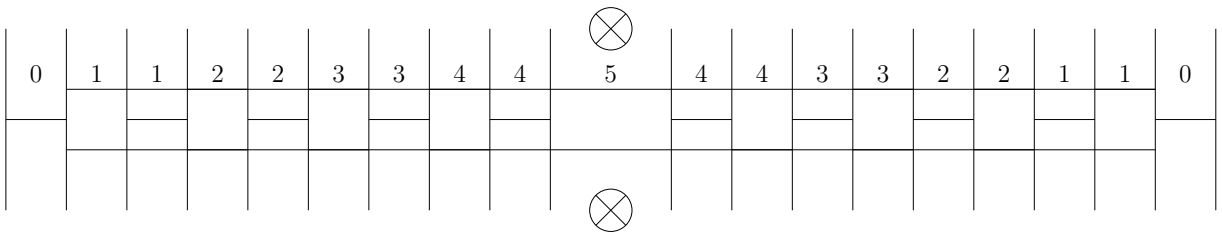

(3.42)

The magnetic quiver will now have gauge groups of higher ranks since pulling the NS5 branes inwards causes D6 brane creation:

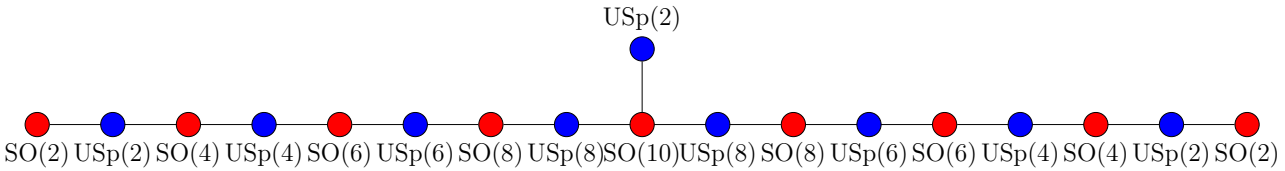

(3.43)

The Coulomb branch of this magnetic quiver does not have a simple analogue in the maths literature.

Chapter 4

Five dimensional SUSY gauge theories

In this chapter we delve into 5d $\mathcal{N} = 1$ gauge theories, with the focus on SQCD theories (i.e a single gauge group G with fundamental flavors). In particular, we look at $G = SU(N_c)$ and $G = Sp(N_c)$.

4.1 $SU(N_c)$ SQCD Quivers

Based on our paper [1]

We start with $5d$ $\mathcal{N} = 1$ SQCD theories with $G = SU(N_c)$, N_f flavors and κ (Chern-Simons) levels. We will call this 5d quiver gauge theory the *electric quiver*. Our focus will be on the Higgs branch of the electric quiver at infinite gauge coupling $\mathcal{H}_\infty^{5d}$ which is often the union of several hyperKähler cones. Each cone has the description as the Coulomb branch of a $3d$ $\mathcal{N} = 4$ magnetic quiver. We can equivalently view the cone as the moduli space of dressed monopole operators [25]. Therefore, to analyse $\mathcal{H}_\infty$ of the electric quiver, we compute the Coulomb branch Hilbert series (or equivalently, enumerate dressed monopole operators and grade them by their quantum numbers) of the corresponding magnetic quivers using the monopole formula.

Chern-Simons level

A brief comment on the Chern-Simons level. The prepotential that defines the 5d Coulomb branch contains a classical Chern-Simons level κ. Due to gauge invariance, the Chern-Simons level is quantized to be integer or half-integer and as shown in [75, 76]. The Coulomb branch

therefore differs depending on the Chern-Simons level and only some of them have UV fixed points as classified in [76] for SQCD theories of classical gauge group. Therefore, for our SQCD theories, we require three parameters (N_c, N_f, κ) to define the theory. The classical Chern-Simons level is associated with third order Casimir factors in the prepotential which is absent for $G = Sp(N_c)$, so there is no need to specify κ in those cases.

The magnetic quivers were already obtained in [25]. The new results we present here are the explicit derivations of the refined Coulomb branch Hilbert series (in the form of a highest weight generating functions (HWG) for these theories. The computations are based on an unpublished work [1] although some of the results were subsequently published in our other works [11, 3].

It has been conjectured in [110] that $5d$ $\mathcal{N} = 1$ SQCD theories obeying the bound $|\kappa| \leq N_c - \frac{N_f}{2} + 2$ have UV fix points for generic N_c. In [25], this bound is further divided into four regions[1]:

$$\textbf{1)}\ |\kappa| < N_c - \tfrac{N_f}{2}$$

$$\textbf{2)}\ |\kappa| = N_c - \tfrac{N_f}{2}$$

$$\textbf{3)}\ |\kappa| = N_c - \tfrac{N_f}{2} + 1$$

$$\textbf{4)}\ |\kappa| = N_c - \tfrac{N_f}{2} + 2$$

In this section, we will focus on the corresponding magnetic quivers and their HWG in regions **1**,**2**,**3** and **4**.

General procedure

We are interested in computing the HWG for these Coulomb branches because they are a simple generating function that captures the exact Coulomb branch Hilbert series refined by representations of the global symmetry group. Furthermore, a given family of theories often

[1]For small N_c, there can be more regions such as $|\kappa| = N_c - \frac{N_f}{2} + 3$ and $N_c = 3$ [76, 77]. The magnetic quivers in this region are well known and the Coulomb branch are two E_{N_f} instanton moduli spaces as explained in [25].

have very similar HWGs that can be generalized into one general expression. The steps in finding the HWGs are as follows:

1. Compute the refined Hilbert series $\mathrm{HS}(z_i, t)$ using the monopole formula. The refinement is achieved by including fugacities z_i with $i = 1, \ldots, r$ which are simple root fugacities of the global symmetry group G_F of rank r.

2. Use a fugacity map to map the simple root fugacities z_i to fundamental weight fugacities y_i. The latter can then be readily converted to Dynkin labels $[\ldots]_{G_F}$ and then to highest weight fugacities μ_i. The computations done so far will likely be perturbative. Rewrite the perturbative Hilbert series using μ_i to obtain $\mathrm{HWG}_{\mathrm{pert}}(\mu_i, t)$.

3. Take the plethystic logarithm (PL) of $\mathrm{HWG}_{\mathrm{pert}}(\mu_i, t)$. If the PL terminates, take the plethystic exponential (PE) of the result. This will be the $\mathrm{HWG}_{\mathrm{exact}}(\mu_i, t)$ in a rational form which contains all the information of the refined Hilbert series and hence the chiral ring.

Edge multiplicity

One of the novelties of $5d$ $\mathcal{N} = 1$ SQCD theories is that they are defined by three terms: N_f, N_c and κ. Therefore, it is natural that some of the families of magnetic quivers require three parameters to define them as well. It turns out a new feature of these magnetic quivers is *edge multiplicities*[2]. These are multiplicities on the edge that connects the gauge nodes. For example:

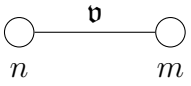

(4.1)

where two gauges nodes $U(n)$ and $U(m)$ are connected with an edge of multiplicity $\mathfrak{v}$ (representing $\mathfrak{v}nm$ hypermultiplets transforming in the bifundamental representation of the neighbouring gauge groups).

In terms of Coulomb branch Hilbert series, edge multiplicities only change the conformal dimension Δ in the monopole formula. Furthermore, since the multiplicities are on the edges,

[2]We differentiate this with the term "bonds" which we usually use to refer to non-simply laced quiver diagrams with a direction on it, see [65].

only contributions from the hypermultiplets Δ_{hypers} are changed. For the quiver in (4.1), Δ_{hypers} is given as:

$$\Delta_{\text{hypers}}(\boldsymbol{n}, \boldsymbol{m}) = +\frac{\mathfrak{v}}{2} \sum_{i}^{n} \sum_{j}^{m} |n_i - m_j| \tag{4.2}$$

In the following sections, we first look at regions **1**, **2** and **3** where the magnetic quivers all have SU global symmetries. We categorize the new[3] magnetic quivers with multiplicities into two families: Trapezium family and Pyramid family due to their resemblance. In region **4**, the global symmetry is SO and the new magnetic quivers with multiplicities can be categorized into two new families: Truck family and Kite family.

The remaining magnetic quivers are well known. Their Coulomb branch are either closures of nilpotent orbits, product of closures of nilpotent orbits and $\mathbb{C}^2/\mathbb{Z}_2$ or those already computed in [111].

4.1.1 Trapezium Family

The Trapezium family in Figure 4.1 is parameterized by three parameters and covers all the new magnetic quivers with edge multiplicities found in region **1** and **3**.

This family of quivers is parameterized by $\mathfrak{v}$ which is the multiplicity of edges between the two unbalanced $U(1)$ nodes (cyan), n which is the rank of the repeated unitary gauge groups in the middle and $N_f - 1$ which is the length of the base of the quiver. In regions **1** and **3**, these three parameters are all functions of N_c, N_f and κ.

Let us compute the refined Hilbert series $\text{HS}(z_i, t)$ where z_i are simple root fugacities of G_F. We can determine G_F by looking at the subsets of balanced[4] nodes corresponding to a Dynkin diagram. The first step is to decouple an overall $U(1)$ gauge group[5] which (for simplicity) we choose to be one of the two unbalanced $U(1)$ gauge groups connected by $\mathfrak{v}$ edges. This gives

[3]New in the sense that they first appear in [25]

[4]See section 1.2 for a reminder on the definition of balanced and unbalanced.

[5]For a quiver with only unitary gauge nodes, we have an infinite number of solutions to the conformal dimension $\Delta = 0$ hence the Hilbert series will be divergent. Decoupling an overall $U(1)$ is equivalent to 'fixing a centre of mass' in the perspective of brane configurations.

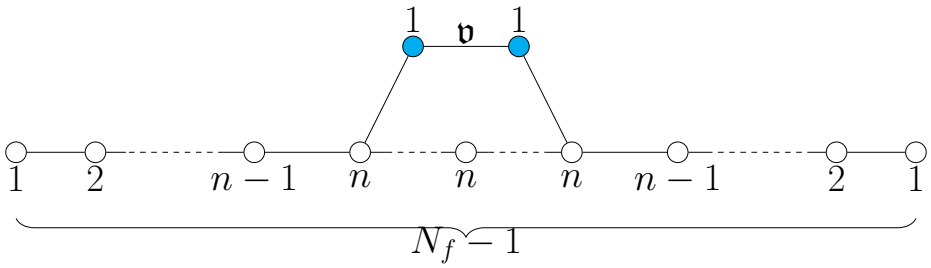

Figure 4.1: *Trapezium family of quivers. The base of the quiver have $N_f - 1$ balanced gauge nodes. There are two unbalanced $U(1)$ gauge node (cyan) with $\mathfrak{v}$ edges between them. The global symmetry is $SU(N_f) \times U(1)$.*

us the resulting quiver in Figure 4.2. Here, we used the fact that $\mathfrak{v}$ edges to a $U(1)$ flavour node is equivalent to a single edge to a $U(\mathfrak{v})$ flavour node. As a result, the $N_f - 1$ balanced unitary gauge groups correspond to the Dynkin diagram of A_{N_f-1}. The remaining $U(1)$, which is unbalanced, just contributes $U(1)$ to the global symmetry. Hence, the global symmetry is $SU(N_f) \times U(1)$.[6]

Now that we have the global symmetry group, we need to map the simple root fugacities of the global symmetry group to the fundamental weight fugacities so that we can express the latter in terms of Dynkin labels. We assign the simple root fugacities $z_1, z_2, ..., z_{N_f-1}$ to the gauge nodes that make up the Dynkin diagram of A_{N_f-1}. Our ordering starts by assigning z_1 to the left most node all the way to z_{N_f-1} at the rightmost node. We then assign h to be the fugacity of $U(1)$. We assign $y_1, y_2, ..., y_{N_f-1}$ to be the fundamental weight fugacities for $SU(N_f)$ and q for $U(1)$. The fugacity mapping is a non-trivial task as we cannot simply apply the Cartan matrix due to the extra $U(1)$ factor in the global symmetry. Using the Cartan matrix *and* ensuring the fugacities form characters of irreducible representations of the global symmetry group, we find the following fugacity map:

$$z_1 = \frac{y_1^2}{y_2}, \quad z_2 = \frac{y_2^2}{y_1 y_3}, \quad ...z_{N_f-1} = \frac{y_{N_f-1}^2}{y_{N_f-2}}, \quad h = \frac{y_n}{q} \, . \tag{4.3}$$

Once we obtained the Taylor expanded Hilbert series in terms of fundamental weight fugacities, it is a trivial task to repackage them in terms of highest weight fugacities μ_i for

[6]Alternatively, we can look at the balanced/unbalanced gauge nodes in the quiver before ungauging and in the end take out a $U(1)$ factor to remove the centre of mass giving: $(SU(N_f) \times U(1) \times U(1))/U(1)$. Which is equivalent to the expression above.

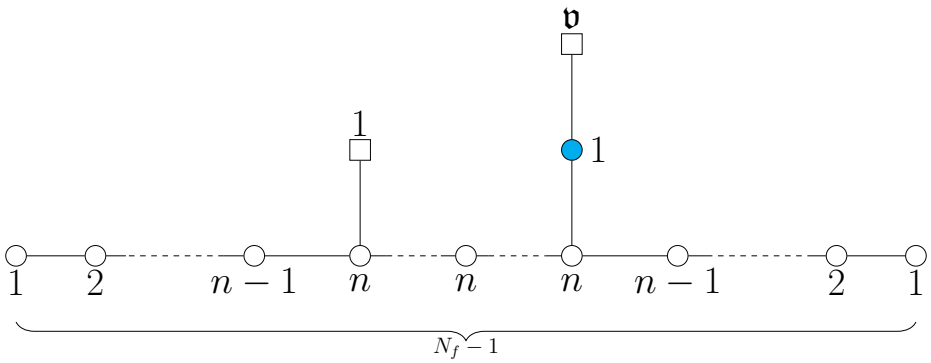

Figure 4.2: *Trapezium family of quivers but with an overall $U(1)$ ungauged. There is one unbalanced $U(1)$ gauge node (cyan).*

$SU(N_f)$ and q for $U(1)$. At each order of t, the coefficients are now expressed as irreducible representations of G_F in terms of highest weight fugacities.

In order to get the generating function, we need to compute the plethystic logarithm (PL) of the above Taylor series. Note, this is the PL of the HWG, and not of the Hilbert series. If the PL terminates, we simply translate the result to a HWG where the positive terms in the PL contributes to the denominator and negative terms to the numerator of the HWG. All the quiver families in this paper have terminating PLs for the HWG[7]. We list several quivers in this family along with their HWG in Appendix B.

Using these results, we find the general form of the HWG for the Trapezium quiver family to be:

$$\mathrm{HWG}(\mu_i, q, t) = \frac{1 - \mu_n \mu_{N_f-n}\, t^{2(n+\mathfrak{v})}}{(1-t^2)(1-\mu_n q\, t^{n+\mathfrak{v}})(1-\dfrac{\mu_{N_f-n}}{q}\, t^{n+\mathfrak{v}}) \prod_{i=1}^{n}(1-\mu_i \mu_{N_f-i} t^{2i})} \tag{4.4}$$

If we start from the HWG, it is trivial to obtain the unrefined Hilbert series in a Taylor expanded form. However, finding the exact unrefined Hilbert series is highly non-trivial, especially when G_F is large. Therefore, for several members of the Trapezium quiver family, we compute the exact unrefined Hilbert series in Table Tables B.1 to B.17 of Appendix B.

Even though the unrefined Hilbert series contains less information than the refined Hilbert series, it is still a very useful object. Usually, by showing that the exact (as a rational function)

[7]This is the same analysis for when dealing with quivers whose moduli space is a complete intersection (i.e the PL of the Hilbert series terminates). For PL of HWG, we can think of this as the *HWG variety* having a complete intersection.

unrefined Coulomb branch Hilbert series of two quivers are the same is enough to show they have the same Coulomb branch. If two Coulomb branches differ by a discrete group, we can also divide the volumes of the two Coulomb branches (defined to be the residues of the unrefined Hilbert series at the pole $t = 1$) to obtain the order of the discrete group.

4.1.2 Pyramid Quiver Family

The next family of quivers with multiplicities is the Pyramid quiver family as shown in Figure 4.3. Just like the Trapezium family, this quiver family is parameterized by N_f, n and $\mathfrak{v}$. Magnetic quivers with multiplicities found in region **2** are all members of this family.

Before looking at the global symmetry group, we once again ungauge one of the two unbalanced $U(1)$ gauge groups (cyan) giving Figure 4.4. The $N_f - 1$ balanced unitary gauge nodes on the base of the pyramid quiver form a balanced subset which resembles the Dynkin diagram of A_{N_f-1}. Therefore, a subgroup of the global symmetry group is $SU(N_f)$. Unlike the Trapezium quivers, the Pyramid quivers also have a balanced $U(1)$ gauge node on top of the pyramid. This corresponds to the Dynkin diagram of A_1, and therefore contributes a $SU(2)$ factor to the global symmetry. Upon ungauging, the final contribution to the global symmetry group is the $U(1)$ unbalanced gauge node (cyan) which contributes a $U(1)$ global symmetry. Therefore, the overall global symmetry is $G_F = SU(N_f) \times SU(2) \times U(1)$.

As before, the next step is to compute the refined Hilbert series. We assigned the fugacities $z_1, z_2, ..., z_{N_f-1}$ to the $N_f - 1$ balanced gauge nodes at the base of the pyramid (starting from the left most node to the right most node), h for the fugacity of unbalanced $U(1)$ gauge node (cyan) and w for the balanced $U(1)$ gauge node on top of the pyramid. These are the simple root fugacities for G_F. We need to find the fugacity map to $y_1, y_2, ..., y_{N_f-1}, x, q$, the fundamental weight fugacities of G_F where y_i are the fugacities for $SU(N_f)$, x for $SU(2)$ and q for $U(1)$.

The fugacity map is given by:

$$z_1 = \frac{y_1^2}{y_2}, \quad z_2 = \frac{y_2^2}{y_1 y_3}, \quad ..., \; z_{N_f-1} = \frac{y_{N_f-1}^2}{y_{N_f-2}}, \quad w = x^2, \quad h = \frac{q}{x y_{N_f-1}} \; . \tag{4.5}$$

Once we get the refined Hilbert series (in a Taylor expanded form) in terms of fundamental

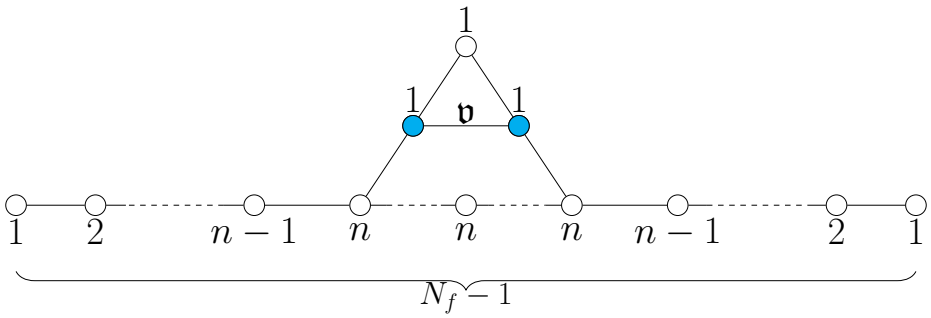

Figure 4.3: *Pyramid quiver family. There are $N_f - 1$ balanced gauge nodes at the base of the pyramid. There are $\mathfrak{v}$ edges between the two unbalanced $U(1)$ gauge nodes (cyan) in the middle. The overall global symmetry is $SU(N_f) \times SU(2) \times U(1)$.*

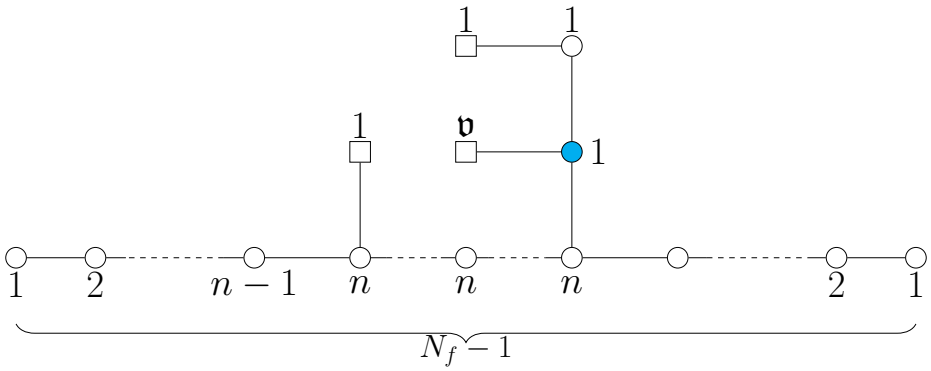

Figure 4.4: *Pyramid family of quivers with an overall $U(1)$ ungauged. There is one unbalanced $U(1)$ gauge node (cyan).*

weight fugacities of G_F, we can obtain the HWG by computing its PL. The resulting HWG for the Pyramid quiver family is:

$$\mathrm{HWG}(\mu_i, \nu, q, t) = \frac{1 - \nu^2 \mu_n \mu_{N_f - n}\, t^{2(1+n+\mathfrak{v})}}{(1-t^2)(1-\nu^2 t^2)(1-\nu \mu_n q\, t^{1+n+\mathfrak{v}})(1 - \frac{\nu \mu_{N_f-n}}{q}\, t^{1+n+\mathfrak{v}}) \prod_{i=1}^{n} (1 - \mu_i \mu_{N_f - i} t^{2i})} \tag{4.6}$$

As with the Trapezium family, we listed several members of the Pyramid quiver family along with their HWG, unrefined Hilbert series in the appendix.

With the Trapezium quiver family and Pyramid quiver family, we can now write down the HWG for all the magnetic quivers in region **1**, **2** and **3**.

4.1.3 Kite family

In region **4**, the magnetic quivers have balanced subset of nodes with a D-Type Dynkin diagram instead of A-type. The first new family of quivers is the Kite family shown in Figure

4.5.

When dealing with the Trapezium and Pyramid family of quivers we defined the 'length' of the quiver as the number of nodes at its base. This is because their base forms a Dynkin diagram for A_{N_f-1}. For the Kite (and later on the Truck) family of quivers, we look for subset of nodes that form a D-type Dynkin diagram which is non-linear. Therefore, we will not define the notion of a 'length' in these two families.

The quiver family is determined by the parameters n and $\mathfrak{v}$. To determine the global symmetry, and subsequently compute the Hilbert series, we ungauge one of the unbalanced $U(1)$ gauge nodes (cyan) located at the 'top' of the kite. The resulting quiver is in Figure 4.6. Now, we see clearly the Dynkin diagram of D_{2n} and an unbalanced $U(1)$ gauge node attached to one of its two legs. The global symmetry is therefore $G_F = SO(4n) \times U(1)$.

As usual, we proceed to compute the refined Hilbert series by first assigning the simple root fugacities to the gauge nodes. We assign $z_1, .., z_{2n}$ for the gauge nodes that form the D_{2n} Dynkin diagram starting with z_1 on the left most node. For the two spinor nodes, we assign z_{2n-1} to the $U(n-1)$ node and z_{2n} to the $U(n)$ node and h for the unbalanced $U(1)$ gauge node. The fugacity map to the fundamental weights y_i is given as:

$$z_1 = \frac{y_1^2}{y_2}, \quad z_2 = \frac{y_2^2}{y_1 y_3}, \quad ... \quad z_{2n-2} = \frac{y_{2n-2}^2}{y_{2n-3} y_{2n-1} y_{2n}} \quad z_{2n-1} = \frac{y_{2n-1}^2}{y_{2n-2}} \quad z_{2n} = \frac{y_{2n}^2}{y_{2n-2}}, \quad h = \frac{q}{y_{2n}} \,. \tag{4.7}$$

The fugacity map allows us to write the refined Hilbert series in terms of highest weight fugacities. Following the same procedure as above, we obtain the HWG for the Kite quiver family:

$$HWG(\mu_i, t) = \frac{1 - \mu_{2n}^2 \, t^{2n+2\mathfrak{v}}}{(1-t^2)(1-\mu_{2n}^2 \, t^{2n})(1-\mu_{2n} q \, t^{n+\mathfrak{v}})(1-\frac{\mu_{2n}}{q} \, t^{n+\mathfrak{v}}) \prod_{i=1}^{n-1}(1-\mu_{2i} t^{2i})} \tag{4.8}$$

4.1.4 Truck quiver family

The fourth and last new family of magnetic quivers with multiplicities is the Truck quiver family shown in Figure 4.7. Members of this family of quivers can once again be found in region **4**.

The Truck quivers are parameterized by $\mathfrak{v}$ which is the multiplicity of edges between the

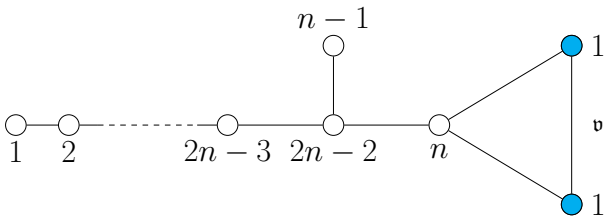

Figure 4.5: *Kite family of quivers where* $\mathfrak{v}$ *is the multiplicity of edges between the two unbalanced* $U(1)$ *gauge nodes (cyan).*

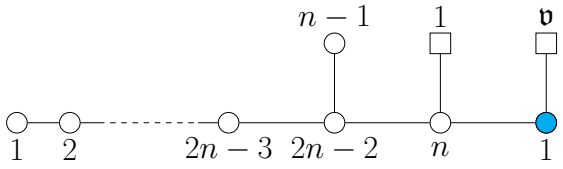

Figure 4.6: *Kite quiver family with an overall* $U(1)$ *ungauged. There is one unbalanced* $U(1)$ *gauge node (cyan).*

two unbalanced $U(1)$ gauge nodes (cyan) and n. We ungauge one of the unbalanced $U(1)$ nodes giving us the quiver in Figure 4.8. We can now identify the subset of balanced gauge nodes with the Dynkin diagram of D_{2n+1}.

The balanced D_{2n+1} Dynkin diagram shows the subgroup of the global symmetry is $SO(4n+2)$. The remaining component is the unbalanced $U(1)$ gauge group which contributes $U(1)$ to the global symmetry. Therefore, $G_f = SO(4n+2) \times U(1)$.

To compute the refined Hilbert series, we assign the fugacities $z_1, ..., z_{2n}, z_{2n+1}$ for the balanced gauge nodes that form the Dynkin diagram for D_{2n+1}. We assign z_{2n} to the n gauge node connected to a $U(1)$ flavor node and z_{2n+1} to the gauge node that is connected to the unbalanced $U(1)$ gauge node. We assign h to the fugacity of the unbalanced $U(1)$ gauge node. We perform the fugacity mapping to $y_1, ..., y_{2n+1}$ which are the fundamental weight fugacities of $SO(4n+2)$ and q the fundamental weight fugacity map of $U(1)$. The fugacity map is:

$$z_1 = \frac{y_1^2}{y_2}, \quad z_2 = \frac{y_2^2}{y_1 y_3}, \quad ... \quad z_{2n-1} = \frac{y_{2n-1}^2}{y_{2n-2} y_{2n} y_{2n+1}} \quad z_{2n} = \frac{y_{2n}^2}{y_{2n-1}} \quad z_{2n+1} = \frac{y_{2n+1}^2}{y_{2n-1}}, \quad h = \frac{q}{y_{2n+1}} \,. \tag{4.9}$$

Now that we have the refined Hilbert series we can follow the same procedure as the

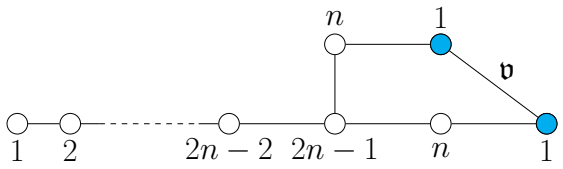

Figure 4.7: *Truck quiver family where $\mathfrak{v}$ is the multiplicity of edges between the two unbalanced $U(1)$ gauge nodes (cyan).*

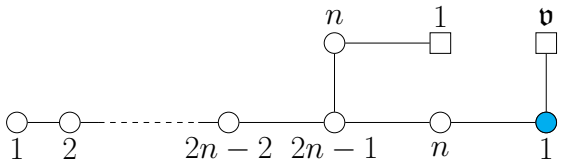

Figure 4.8: *Truck quiver family with an overall $U(1)$ ungauged. There is one unbalanced $U(1)$ gauge node (cyan).*

previous quiver families. We obtain the HWG for the Truck family:

$$\frac{1-\mu_{2n}\mu_{2n+1}\,t^{2n+2\mathfrak{v}}}{(1-t^2)(1-\mu_{2n}\mu_{2n+1}\,t^{2n})(1-\mu_{2n}q\,t^{n+\mathfrak{v}})(1-\frac{\mu_{2n+1}}{q}\,t^{n+\mathfrak{v}})\prod_{i=1}^{n-1}\mu_{2i}t^{2i}} \tag{4.10}$$

With the HWG of the Kite quiver family and Truck quiver family, we can now write down the HWG for all the magnetic quivers in region **4**.

4.2 Magnetic quivers for different regions

4.2.1 First region: $|\kappa| < N_c - \frac{N_f}{2}$

In the following sections, we take the magnetic quivers outlined in [25] and write down their respective HWG (Highest weight generating function).

For $\kappa \geq 0$, there are several components for the Higgs branch I, II, III (here we adopt the same notation as in [25]). The first component is present for cases where $|\kappa| \leq \frac{N_f}{2}$ and the magnetic quiver is given in the first line of Table 4.1. These are exactly members of the Trapezium family of quivers we outlined in Section 4.1.1.

Component II is present for $N_f \geq N_c$ and $\kappa \geq 0$. It also belongs to the Trapezium quiver family but with $\mathfrak{v}$ and n taking different values compared to component I. The length of the quiver remains the same as $N_f - 1$. This component is now parameterized only by N_f and

N_c and therefore independent of the Chern-Simons level κ. The global symmetry group is $SU(N_f) \times U(1)$.

The highest weight generating function for component I and II are given in (4.4) but with n and $\mathfrak{v}$ defined as functions of N_f, N_c and κ.

The quivers for component III is present only when $|\kappa| > 1/2$. Furthermore, the quivers differ depending on whether N_f is odd or even. In both cases, their Coulomb branches are closures of nilpotent orbits of A_{N_f-1} with height two. This is obvious once we ungauge the unbalanced $U(1)$ node on the upper part of the two diagrams. The general HWG for this class of quivers is very straightforward and given in [112] as:

$$\text{HWG}_{\text{Height 2}} = \prod_{i=1}^{n} \frac{1}{(1-\mu_i \mu_{N_f-i} t^{2i})} \tag{4.11}$$

where n is the rank of the repeated gauge nodes towards the centre of the quiver.

For N_f even, the partition [8] for the nilpotent orbit is $[2,2,2...,2] = [2^{N_f/2}]$ where we used the exponent form for the partition. The HWG is:

$$\text{HWG}_{[2^{N_f/2}]} = \prod_{i=1}^{N_f/2} \frac{1}{(1-\mu_i \mu_{N_f-i} t^{2i})} \tag{4.12}$$

For N_f odd, the partition would be $[2,2,2...,2,1] = [2^{(N_f-1)/2}, 1]$ and the HWG is

$$\text{HWG}_{[2^{(N_f-1)/2},1]} = \prod_{i=1}^{(N_f-1)/2} \frac{1}{(1-\mu_i \mu_{N_f-i} t^{2i})} \tag{4.13}$$

If we wish to compare our Hilbert series with the Higgs branch of the original $5d$ electric SQCD quiver, we need to take the union of all the cones (components). In terms of Hilbert series (and HWG), we do this by adding the Hilbert series (and HWG) of the respective cones and subtracting the intersections between them. The intersections between the different components can be represented as quivers and are given in Table 4.2. We note that the Coulomb branch of the intersections are all closures of nilpotent orbits of height 2. We will see that this pattern

[8] The entries in the partition are the sizes of Jordan blocks when representing the nilpotent matrix in Jordan normal form.

persists in other regions as well where the intersections are nilpotent orbits (or the product of nilpotent orbits with $\mathbb{C}^2/\mathbb{Z}_2$).

Table 4.1: *Different phases of 3d Coulomb branch quivers that correspond to the 5d Higgs branch at infinite coupling. The SQCD theories subject to the condition $|\kappa| \leq N_c - \frac{N_f}{2}$. Phase I exists for $\frac{N_f}{2} \geq |\kappa|$. Phase II exists for $N_f \geq N_c$. The third component exists for $N_f \geq 2$ and $|\kappa| > \frac{1}{2}$.For all the quivers, the length (the base of the quiver) is $N_f - 1$. The global symmetry and the plethystic logarithm of the Highest Weight Generating function (HWG) is given.*

Phase	Quiver			Global Symmetry	$PL[HWG(\mu_i, t)]$
	$\kappa > \frac{1}{2}$	$\kappa = \frac{1}{2}$	$\kappa = 0$		
I	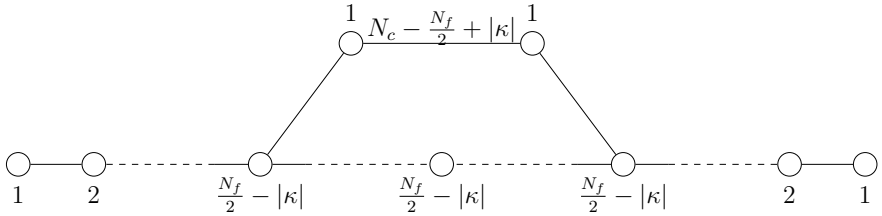			$SU(N_f) \times U(1)$	$\sum_{i=1}^{N_f/2-\lvert\kappa\rvert} \mu_i \mu_{N_f-i} t^{2i} + t^2 + \mu_{N_f/2-\lvert\kappa\rvert} q t^{N_c} + \mu_{\lvert\kappa\rvert - N_f/2}/q t^{N_c} - \mu_{\lvert\kappa\rvert - N_f/2} \mu_{\lvert\kappa\rvert - N_f/2} t^{2N_c}$
II	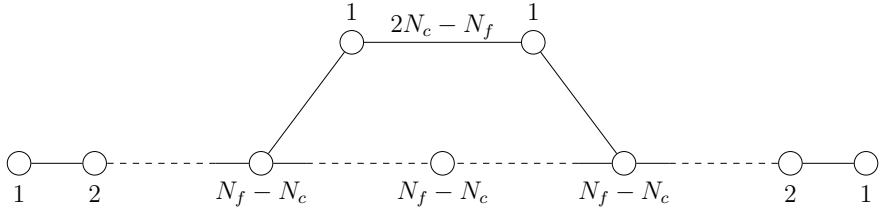			$SU(N_f) \times U(1)$	$\sum_{i=1}^{N_c - N_f} \mu_i \mu_{N_f-i} t^{2i} + t^2 + \mu_{N_f - N_c} q t^{N_c} + \mu_{N_c}/q t^{N_c} - \mu_{N_f - N_c} \mu_{N_c} t^{2N_c}$
III (N_f even)	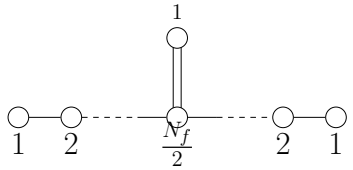			$SU(N_f)$	$\sum_{i=1}^{N_f/2} \mu_i \mu_{N_f-i} t^{2i}$
III (N_f odd)	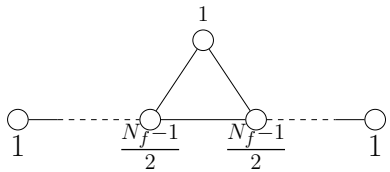			$SU(N_f)$	$\sum_{i=1}^{(N_f-1)/2} \mu_i \mu_{N_f-i} t^{2i}$

Table 4.2: *The quivers in this table are the intersection between the different components in region I. The global symmetry group G_F and the plethystic logarithm of the Highest weight generating function HWG are given in each case.*

Phase		$\kappa > \frac{1}{2}$	$\kappa = \frac{1}{2}$	$\kappa = 0$
I ∩ II	Quiver	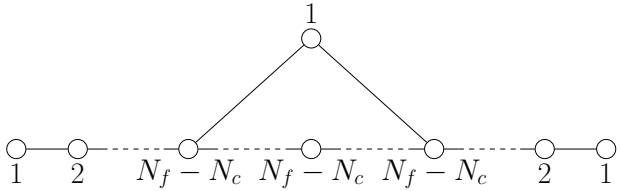		
	G_F	$SU(N_f)$		
	PL[HWG]	$\sum_{i=1}^{N_f - N_c} \mu_i \mu_{N_f - i} t^{2i}$		
I ∩ III	Quiver	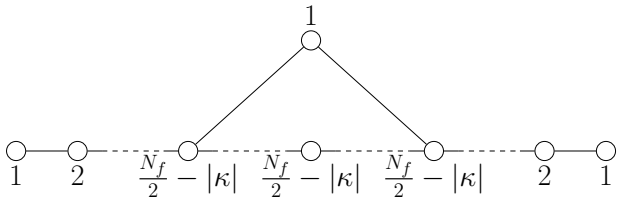	-	
	G_F	$SU(N_f)$	-	
	PL[HWG]	$\sum_{i=1}^{N_f/2 - \lvert\kappa\rvert} \mu_i \mu_{N_f - i} t^{2i}$	-	
II ∩ III, I ∩ II ∩ III	Quiver	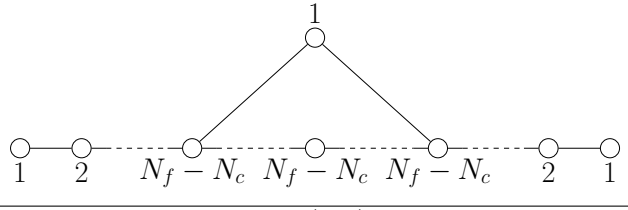	-	
	G_F	$SU(N_f)$	-	
	PL[HWG]	$\sum_{i=1}^{N_f - N_c} \mu_i \mu_{N_f - N_c - i} t^{2i}$	-	

4.2.2 Second region: $|\kappa| = N_c - \frac{N_f}{2}$

The equation that defines the second region means we can define all the quivers with just two variables (such as N_f and κ). The magnetic quivers that correspond to different components of the Higgs branch of $5d$ electric quiver at different κ is given in Table 4.3. We also present their global symmetries and HWG (Highest weight generating function). At any value of N_f, there are only two components I and III.

Component I is defined for $|\kappa| \leq \frac{N_f}{2}$. When $|\kappa| > 1$, the magnetic quivers belongs to the Pyramid family of quivers defined in section 4.1.2 with $G_F = SU(N_f) \times SU(2) \times U(1)$. The HWG is exactly that of equation 4.6. When $\kappa = 0$, the brane webs tells us the magnetic quiver looks different with a global symmetry enhanced to $G_F = SU(N_f) \times SU(2) \times SU(2)$ instead [25]. The HWG of this quiver is given in [22].

The other component is III. When N_f is even and greater than zero and $|\kappa| > 1$, the Coulomb branch of the quivers in III are the closure of the $[2^{N_f/2}]$ nilpotent orbit of A_{N_f-1} times $\mathbb{C}^2/\mathbb{Z}_2$. This is made clear once we ungauge the unbalanced $U(1)$ gauge node. This effectively breaks it into two quivers as can be seen in Figure 4.9.

As a result, the moduli space is the product of the two moduli spaces and the Hilbert series is:

$$\text{HWG}_{[2^{N_f/2}]\times\mathbb{C}^2/\mathbb{Z}_2} = \prod_{i=1}^{N_f/2} \frac{1}{(1-\mu_i\mu_{N_f-i}t^{2i})} \times \frac{1}{1-\nu^2t^2} \tag{4.14}$$

where we denote the highest weight fugacity ν for $SU(2)$ and μ_i for $SU(N_f)$.

At $\kappa = 1$, the Coulomb branch of the magnetic quiver is just the closure of the nilpotent orbit $[2^{N_f/2}]$. And this component does not exist for $\kappa < 1$[9]

When N_f odd and greater than zero, the process is very similar. For $|\kappa| > \frac{1}{2}$ the Coulomb branch is the closure of the $[2^{(N_f-1)/2}, 1]$ nilpotent orbit of A_{N_f-1} times $\mathbb{C}^2/\mathbb{Z}_2$. We can once again see this by ungauging the unbalanced $U(1)$ gauge node (cyan) in Figure 4.10.

[9]Here we used a simple property of HWG. Consider the product of two moduli spaces $\mathcal{M}_A$ and $\mathcal{M}_B$. Now, for the HWG of $\mathcal{M}_A$, with global symmetry G_A, we assign the highest weight fugacities μ_i. Similarly, for $\mathcal{M}_B$, with global symmetry G_B, we assign ν_i. It then follows that the HWG of the product moduli space is $\text{HWG}_{\mathcal{M}_A\times\mathcal{M}_B}(\mu,\nu,t) = \text{HWG}_{\mathcal{M}_A}(\mu,t) \times \text{HWG}_{\mathcal{M}_B}(\nu,t)$. This is because we kept the fugacities of the two individual factors in the total global symmetry group $G_F = G_A \times G_B$ separate. The same applies for the product of any number of moduli spaces. Note, the resulting Hilbert series will be incorrect if we use the same fugacity. Therefore, we always assign a different highest weight fugacity for each contributing factor in the global symmetry group.

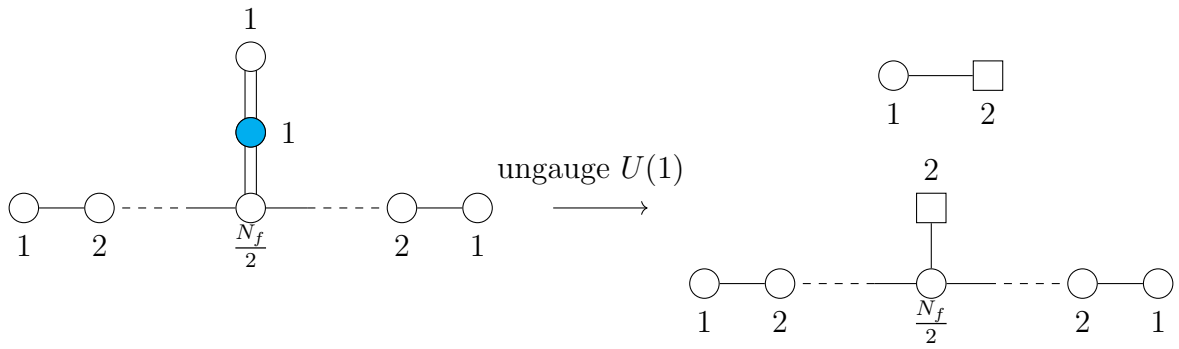

Figure 4.9: *We ungauge the unbalanced $U(1)$ gauge node (cyan) in the quiver on the left, effectively breaking it into a quiver whose Coulomb branch is the closure of the nilpotent orbit of $[2^{N_f/2}]$ and a quiver whose Coulomb branch is $\mathbb{C}^2/\mathbb{Z}_2$. The moduli space of the quiver on the left is therefore the product $\overline{\mathcal{O}}_{[2^{N_f/2}]} \times \mathbb{C}^2/\mathbb{Z}_2$.*

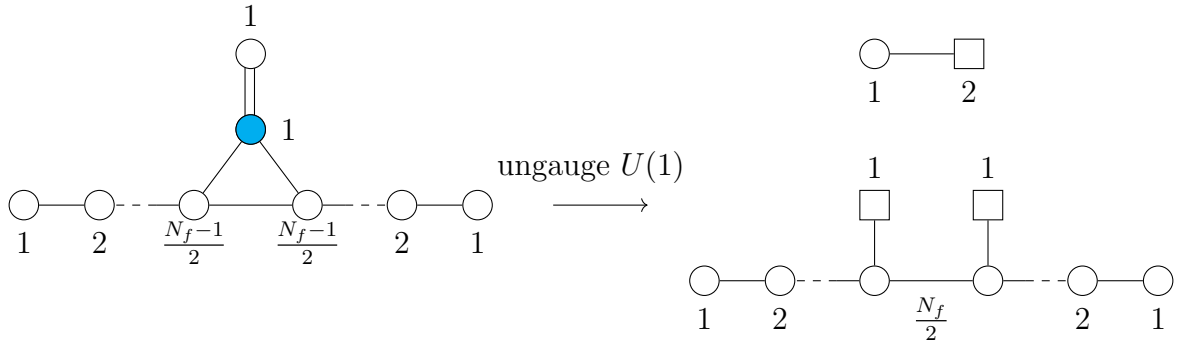

Figure 4.10: *We ungauge the unbalanced $U(1)$ gauge node (cyan) on the left, effectively breaking the quiver into a quiver whose Coulomb branch is the closure of the nilpotent orbit of $[2^{(N_f-1)/2}, 1]$ and a quiver whose Coulomb branch is $\mathbb{C}^2/\mathbb{Z}_2$. The Coulomb branch of the quiver on the left is therefore the product $\overline{\mathcal{O}}_{[2^{(N_f-1)/2},1]} \times \mathbb{C}^2/\mathbb{Z}_2$*

The HWG is:

$$\text{HWG}_{[2^{(N_f-1)/2},1]\times\mathbb{C}^2/\mathbb{Z}_2} = \prod_{i=1}^{(N_f-1)/2} \frac{1}{(1-\mu_i\mu_{N_f-i}t^{2i})} \times \frac{1}{1-\nu^2t^2} \tag{4.15}$$

For $\kappa = 1$, the Coulomb branch of the magnetic quivers is just the closure of the nilpotent orbit of $[2^{(N_f-1)/2}, 1]$. This component does not exist for $|\kappa| < 1$.

The intersections are given in Table 4.4 and since there are only two components for $|\kappa| \geq 1$, there is only one intersection to consider: between I and III. For N_f even, the Coulomb branch of the intersection at $|\kappa| > 1$ is the product of the closure of the nilpotent orbit $[2^{N_f/2-|\kappa|}, 1^{2|\kappa|}]$ of A_{N_f-1} and $\mathbb{C}^2/\mathbb{Z}_2$. For $|\kappa| = 1$, we no longer have the balanced $U(1)$ gauge node on top of the quiver, and the Coulomb branch is simply the closure of $[2^{N_f/2-|\kappa|}, 1^{2|\kappa|}]$ orbit of A_{N_f-1}.

Similarly, for N_f odd, the Coulomb branch is the product of the closure of the nilpotent orbit $[2^{(N_f-1)/2-|\kappa|}, 1^{2|\kappa|+1}]$ of A_{N_f-1} and $\mathbb{C}^2/\mathbb{Z}_2$. And $[2^{(N_f-1)/2-|\kappa|}, 1^{2|\kappa|+1}]$ for $|\kappa| = 1$.

Component III does not exist for $|\kappa| < 1$, and hence the intersection is trivial.

Table 4.3: *5d SQCD theories subject to the condition $|\kappa| = N_c - \frac{N_f}{2}$. Phase I exists for $\frac{N_f}{2} \geq |\kappa|$. Phase III exists for $N_f \geq 1$ and $|\kappa| \geq \frac{1}{2}$. For all the quivers, the length (the base of the quiver) is $N_f - 1$. The global symmetry and the plethystic logarithm of the Highest Weight Generating function (HWG) is given.*

Phase		$\kappa > 1$	$\kappa = 1$	$\kappa = \frac{1}{2}$	$\kappa = 0$
I	Quiver	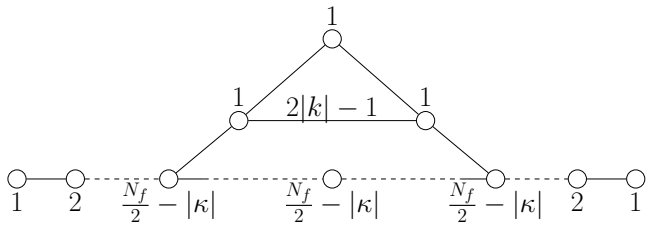			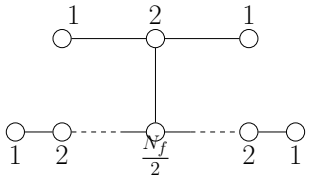
	G_F	$SU(N_f) \times SU(2) \times U(1)$			$SU(N_f) \times SU(2) \times SU(2)$
	PL[HWG]	$\sum_{i=1}^{N_f/2-\|\kappa\|} \mu_i \mu_{N_f-i} t^{2i} + t^2 + \nu^2 t^2 + \nu \mu_{N_f/2-\|\kappa\|} q t^{N_f/2+\|\kappa\|} + \nu \mu_{\|\kappa\|-N_f/2} / q t^{N_f/2+\|\kappa\|} - \nu^2 \mu_{N_f/2-\|\kappa\|} \mu_{\|\kappa\|-N_f/2} t^{2(N_f/2+\|\kappa\|)}$			$\sum_{i=1}^{N_f/2} \mu_i \mu_{N_f-i} t^{2i} + t^4 + \nu_1^2 t^2 + \nu_2^2 t^2 + \nu_1 \nu_2 \mu_{N_f/2} t^{N_f/2} + \nu_1 \nu_2 \mu_{N_f/2} t^{N_f/2+2} - \nu_1^2 \nu_2^2 \mu_{N_f/2}^2 t^{N_f+4}$
III(even)	Quiver	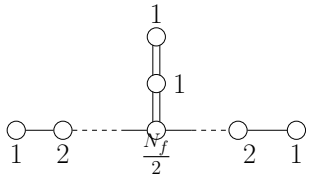	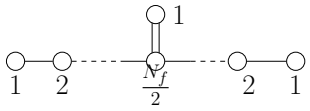		None
	G_F	$SU(N_f) \times SU(2)$	$SU(N_f)$		-
	PL[HWG]	$\sum_{i=1}^{N_f/2} \mu_i \mu_{N_f-i} t^{2i} + \nu^2 t^2$	$\sum_{i=1}^{N_f/2} \mu_i \mu_{N_f-i} t^{2i}$		-
III(odd)	Quiver	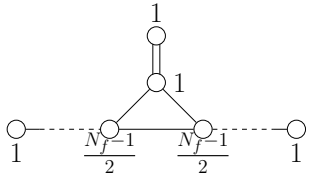	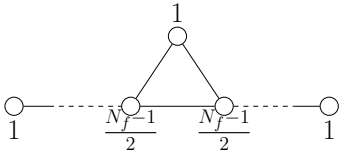		None
	G_F	$SU(N_f) \times SU(2)$	$SU(N_f)$		-
	PL[HWG]	$\sum_{i=1}^{(N_f-1)/2} \mu_i \mu_{N_f-i} t^{2i} + \nu^2 t^2$	$\sum_{i=1}^{(N_f-1)/2} \mu_i \mu_{N_f-i} t^{2i}$		-

Table 4.4: *The quivers in this table are the intersection between the different components in region one. The intersection for $\kappa \leq \frac{1}{2}$ are trivial. The global symmetry group G_F and the plethystic logarithm of the Highest weight generating function HWG are given in each case.*

Phase		$\kappa > 1$	$\kappa > \frac{1}{2}$	$\kappa = \frac{1}{2}$ | $\kappa = 0$
I $\cap$ III	Quiver	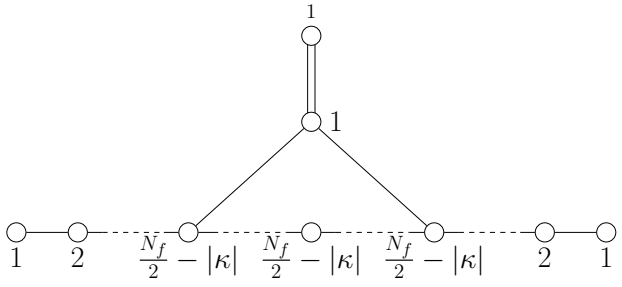	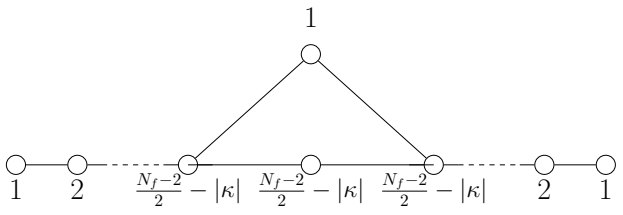	-
	G_F	$SU(N_f) \times SU(2)$	$SU(N_f)$	-
	PL[HWG]	$\sum_{i=1}^{N_f/2-\lvert\kappa\rvert} \mu_i \mu_{N_f-i} t^{2i} + \nu^2 t^2$	$\sum_{i=1}^{(N_f-2)/2-\lvert\kappa\rvert} \mu_i \mu_{N_f-i} t^{2i}$	-

4.2.3 Third region: $|\kappa| = N_c - \frac{N_f}{2} + 1$

The magnetic quivers in the third region shows a strong resemblance to those in the first region. However, there are only up to two components rather than three. The quivers are given in Table 4.5 along with their global symmetry and HWG.

Component I exists for $|\kappa| \leq \frac{N_f}{2} + 1$. For $|\kappa| \geq 1$, the quivers belong to the Trapezium quiver family. The key difference with region **1** is that the quivers all have lengths N_f (counting the number of nodes at the base of the quiver) rather than $N_f - 1$. Hence, the subset of balanced nodes gives the Dynkin Diagram for A_{N_f}. The global symmetry is therefore $SU(N_f + 1) \times U(1)$ (since we still have the unbalanced $U(1)$ gauge node).

For $|\kappa| = \frac{1}{2}$, the global symmetry is enhanced to $SU(N_f + 1) \times SU(2)$. For $|\kappa| = 0$ the global symmetry is enhanced to $SU(N_f + 2)$. The HWG for these two quivers are given in [22] which we reproduced in Table 4.5.

Component III exists for $N_f \geq 1$ and $|\kappa| > \frac{3}{2}$. The shape of magnetic quivers depends on whether N_f is even or odd. They all have length N_f, giving a global symmetry of $SU(N_f + 1)$. For N_f even, the Coulomb branch is the closure of the nilpotent orbit $[2^{N_f/2}, 1]$ of A_{N_f}. For N_f odd, the Coulomb branch is the closure of the nilpotent orbit of $[2^{(N_f-1)/2}, 1]$. For $|\kappa| \leq \frac{3}{2}$, component III does not exist.

For $|\kappa| > \frac{3}{2}$, the Coulomb branch of the intersection between I and III is the closure of the nilpotent orbit $[2^{N_f/2-|\kappa|+1}, 1^{2|\kappa|-2}]$ for N_f even and $[2^{(N_f-1)/2-|\kappa|+1}, 1^{2|\kappa|-1}]$ for N_f odd. For $|\kappa| \leq \frac{3}{2}$, the intersection is trivial as component III is absent.

Table 4.5: *5d SQCD theories subject to the condition $|\kappa| \leq N_c - \frac{N_f}{2} + 1$. Phase I exists for $\frac{N_f}{2} \geq |\kappa| - 1$. The component III exists for $N_f \geq 1$ and $|\kappa| > \frac{3}{2}$.For all the quivers, the length (the base of the quiver) is $N_f - 1$. The global symmetry and the plethystic logarithm of the Highest Weight Generating function (HWG) is given.*

Phase		$\kappa > \frac{3}{2}$	$\kappa = \frac{3}{2}$	$\kappa = 1$	$\kappa = \frac{1}{2}$	$\kappa = 0$
I	Quiver	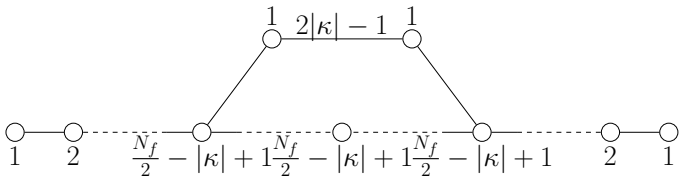			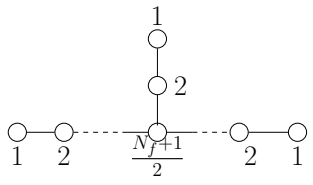	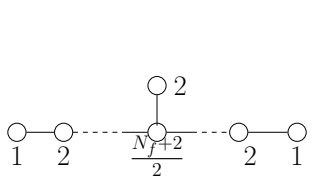
	G_F	$SU(N_f+1) \times U(1)$			$SU(N_f+1) \times SU(2)$	$SU(N_f+2)$
	PL[HWG]	$\sum_{i=1}^{N_f/2-\|\kappa\|+1} \mu_i \mu_{N_f-i} t^{2i} + t^2 + \mu_{N_f-\|\kappa\|+1} q t^{N_f+\|\kappa\|} + \mu_{\|\kappa\|-1}/q t^{N_f+\|\kappa\|} - \mu_{\|\kappa\|-1}\mu_{N_f-\|\kappa\|+1} t^{2(N_f+\|\kappa\|)}$			$\sum_{i=1}^{(N_f+1)/2} \mu_i \mu_{N_f+1-i} t^{2i} + t^4 + \nu^2 t^2 + \nu \mu_{(N_f+1)/2} t^{(N_f+1)/2} + \nu \mu_{(N_f+1)/2} t^{(N_f+5)/2} - \nu^2 \mu^2_{(N_f+1)/2} t^{N_f+3}$	$\sum_{i=1}^{(N_f)/2} \mu_i \mu_{N_f+2-i} t^{2i} + t^4 + \mu_{(N_f+2)/2} t^{(N_f-2)/2} + \mu_{(N_f+2)/2} t^{(N_f+2)/2}$
III(even)	Quiver	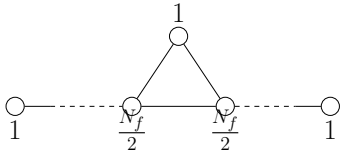	None			
	G_F	$SU(N_f+1)$	-			
	PL[HWG]	$\sum_{i=1}^{N_f/2} \mu_i \mu_{N_f-i} t^{2i}$	-			
III(odd)	Quiver	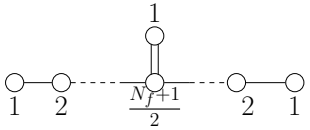	None			
	G_F	$SU(N_f+1)$	-			
	PL[HWG]	$\sum_{i=1}^{(N_f+1)/2} \mu_i \mu_{N_f-i} t^{2i}$	-			

Table 4.6: *The quivers in this table are the intersection between the different components in region one. The intersection for $\kappa \leq \frac{3}{2}$ are trivial. The global symmetry group G_F and the plethystic logarithm of the Highest weight generating function HWG are given in each case.*

Phase		$\kappa > \frac{3}{2}$	$\kappa = \frac{3}{2}$	$\kappa = 1$	$\kappa = \frac{1}{2}$	$\kappa = 0$
I $\cap$ III	Quiver		-			
	G_F	$SU(N_f + 1)$	-			
	PL[HWG]	$\sum_{i=1}^{N_f/2-\lvert\kappa\rvert+1} \mu_i \mu_{N_f-i} t^{2i}$	-			

4.2.4 Fourth region: $|\kappa| = N_c - \frac{N_f}{2} + 2$

Region **4** can have up to two components depending on κ. The different components are given in Table 4.7 along with their respective global symmetry and HWG. Unlike the previous three regions, the magnetic quivers here have a SO subgroup in the global symmetry.

Component IV [10] exists when N_f is even and $\kappa > 2$. There is an edge of multiplicity two between the $\frac{N_f}{2}$ node and the $U(1)$ node and upon ungauging the $U(1)$ node, we obtain a $SU(2)$ flavor node and the remaining quiver is balanced. The balanced quiver has the shape of the Dynkin diagram of D_{N_f}. In fact, this is one of the two components of the very even nilpotent orbit $[2^{N_f}]$, and the other component is given by the flavor node attached to the other spinor node (after balancing). The HWG is given in [112]. For $\kappa \leq 2$, this component does not exist.

Component V takes a different form depending on whether N_f is odd or even. For even N_f and $\kappa > 1$, the quiver belongs to the kite family outlined in Section 4.1.3 where $n = N_f/2$ and $\mathfrak{v} = N_c - N_f/2$. For $\kappa = 1$, the $U(1)$ subgroup in the global symmetry is enhanced to a $SU(2)$. The HWG is given in [111].

For N_f is odd and $\kappa > 1$, the quiver belongs to the Truck family in section 4.1.4 where $n = N_f/2$ and $\mathfrak{v} = N_c - (N_f - 1)/2$. Since the quiver only exists for N_f odd, it does not appear at $\kappa = 1$. For $\kappa = \frac{1}{2}$, the global symmetry is enhanced to $SO(2N_f + 2)$ and the corresponding HWG is given in [111].

For $\kappa = 0$, the theory has a 6d fix point [25].

Since component IV is only defined for $\kappa > 2$, this is the only region where the intersection is non-trivial. The intersections are given in Table 4.8. The intersection IV $\cap$ V is the affine Dynkin diagram of D_{N_f} (which becomes the Dynkin diagram when we ungauge the $U(1)$ attached to the $N_f - 2$ node). The Coulomb branch is the closure of the $[2^{(N_f-2)}, 1^4]$ orbit of $SO(2N_f)$. The intersection for $\kappa < 2$ is trivial.

[10] We use this label to be consistent with [25].

Table 4.7: *5d SQCD theories subject to the condition $|\kappa| = N_c - \frac{N_f}{2} + 2$. Phase IV exists for $N_f \geq 2$ and $|\kappa| > 2$. Phase V(even) exists for $N_f \geq 0$ when κ is ven and $N_f \geq 2$ when κ is odd. And $N_f \geq 1$ for V(odd). The global symmetry and the plethystic logarithm of the Highest Weight Generating function (HWG) is given.*

Phase		$\kappa > 2$	$\kappa = 2$ | $\kappa = \frac{3}{2}$	$\kappa = 1$	$\kappa = \frac{1}{2}$
IV (N_f even)	Quiver	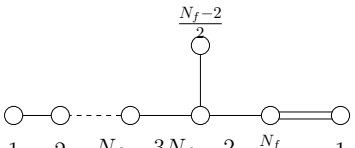	None		
	G_F	$SO(2N_f)$	-		
	PL[HWG]	$\sum_{i=1}^{N_f/2-1} \mu_{2i}t^{2i} + \mu_{N_f}^2 t^{N_f}$	-		
V(even)	Quiver	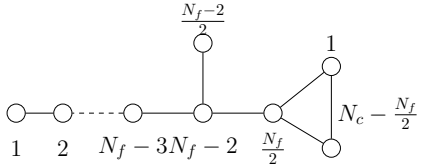		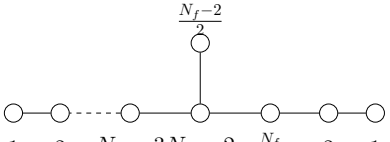	None
	G_F	$SO(2N_f) \times U(1)$		$SO(2N_f) \times SU(2)$	-
	PL[HWG]	$\sum_{i=1}^{N_f/2-1} \mu_{2i}t^{2i} + t^2 + \mu_{N_f}^2 t^{N_f} + \mu_{N_f} q\ t^{N_c} + \mu_{N_f}/q t^{N_c} - \mu_{N_f}^2 t^{2N_c}$		$\sum_{i=1}^{N_f/2-1} \mu_{2i}t^{2i} + t^4 + \nu^2 t^2 + \nu\mu_{N_f}(t^{\frac{N_f}{2}-1} + t^{\frac{N_f}{2}+1}) + \mu_{N_f}^2 t^{N_f} - \nu^2\mu_{N_f}^2 t^{N_f+2}$	-
V(odd)	Quiver	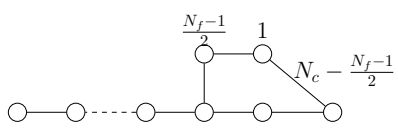		None	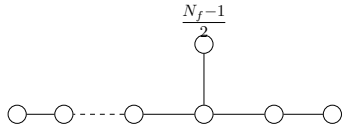
	G_F	$SO(2N_f) \times U(1)$		-	$SO(2N_f+2)$
	PL[HWG]	$\sum_{i=1}^{N_f/2-1} \mu_{2i}t^{2i} + t^2 + \mu_{N_f}\mu_{N_f-1}t^{N_f-1} + \mu_{N_f-1} q\ t^{N_c} + \mu_{N_f}/q t^{N_c} - \mu_{N_f}\mu_{N_f-1}t^{2N_c}$		-	$\sum_{i=1}^{N_f/2-1/2} \mu_{2i}t^{2i} + t^4 + \mu_{N_f+1}(t^{\frac{N_f-3}{2}} + t^{\frac{N_f+1}{2}})$

Table 4.8: *The quivers in this table are the intersection between the different components in region I.For $\kappa > 2$, the Coulomb branch is the closure of the nilpotent orbit $\mathcal{O}_{[2^{(N_f-2)},1^4]}$ The intersection is trivial for $\kappa \leq 2$.The global symmetry group G_F and the plethystic logarithm of the Highest weight generating function HWG are given in each case.*

Phase		$\kappa > 2$	$\kappa \leq 2$
IV ∩ V	Quiver		-
	G_F	$SO(2N_f)$	-
	PL[HWG]	$\sum_{i=1}^{(N_f-2)/2} \mu_{2i} t^{2i}$	-

Closing remarks

The purpose of the magnetic quiver is to understand the Higgs branch moduli space of the parent theory. One significant way of doing that is to study its chiral ring through computing the Hilbert series. What we did in this section is the first step. The next step will be to use the refined Hilbert series to explicitly write down the generators and relations that define the Coulomb branch chiral ring of the magnetic quiver and hence the Higgs branch chiral ring of the 5d theory. In terms of the Higgs branch chiral ring, one can go a step further to define it by the matrices of the mesons, instantons and gaugino bilinears of the theory as achieved for $N_c = 2$ theories in [100]. However, even without doing so, the work here has already proven useful as the Hilbert series is a unique signature that identifies the moduli space of the magnetic quiver. So if we find a completely different magnetic quiver with the same Hilbert series, then we know the 3d Coulomb branch of these two theories, and hence the Higgs branch of their parent theories, are identical. This is discussed in the next section where magnetic quivers in the fourth region have the same Coulomb branch as certain orthosymplectic quivers.

4.3 $Sp(N_c)$ SQCD theories

Now we turn our attention to $5d$ $\mathcal{N} = 1$ theories with an $Sp(N_c)$ gauge group and N_f fundamental flavors. The main focus will therefore be magnetic quivers that are unitary-orthosymplectic (made of $U(1)$, SO(even) and USp(even)).

4.3.1 Bottom-Up approach

Here, we discuss two approaches we take to obtain magnetic quivers. The first is a Top-Down approach where we start by drawing the brane system of the 5d theory and then move to the Higgs branch phase and read off the magnetic quivers as we did in the previous chapter. This approach was used in [25] to obtain the magnetic quivers in the previous section. The second is a Bottom-Up approach which we now introduce:

1. List all the properties of the 5d parent theory's Higgs branch that you can find such as global symmetry, dimension etc.

2. Use these partial data to determine what the structure of the magnetic quiver should look like. For example, the Higgs branch global symmetry G_F of the parent theory translates to G_F Coulomb branch global symmetry of the magnetic quiver which is determined by the set of balanced nodes [62]. The Higgs branch dimension of the parent theory is the Coulomb branch dimension of the magnetic quiver which is the sum of the ranks of the gauge groups in the magnetic quiver. Such properties are often quite constraining, and for simple theories they often give accurate conjectures.

3. Once a magnetic quiver is conjectured, compute the Coulomb branch Hilbert series with the monopole formula and see if it gives the expected moduli space.

In the last step, one may wonder: how do we know if the Hilbert series is correct since studying this unknown moduli space is the whole point of developing magnetic quivers? The process seems circular. As a result, this Bottom-Up approach is really only useful when we are dealing with an infinite family of magnetic quivers such as the trapezium, pyramid, kite and truck families in the previous section where the moduli space is known for the smallest member of each family. For example, for $SU(2)$ with N_f flavors with $N_f \leq 7$, we know that at the 5d UV fixed point, the Higgs branch is the one-E_{N_f+1} instanton moduli space. For each N_f we can then generate an infinite family which we call E_n families where $1 \leq n \leq 8$ which is the UV fixed point of $Sp(N_c)$ with $N_f = N_c + n - 2$ flavors. Therefore, for a given E_n family, we can conjecture an infinite family of magnetic quivers parametrized by N_c. For SQCD theories, it seems the moduli spaces are surprisingly simple enough that an obvious pattern arises for general N_c [11]. If the global symmetry and dimension of all the members of the family are consistent with what to expect and if the 3d Coulomb branch of the $N_c = 1$ case match the expected one-E_{N_f+1} instanton moduli space then we have high confidence that the resulting family of magnetic quivers is correct for all N_c.

[11] We apply the same tricks for 4d SCFTs later on where a similar analysis can get the desired set of families of magnetic quivers

Orthosymplectic quivers and one-E_n instanton

Let us take the one-E_n instantons as an example. Coulomb branches of unitary quivers that describes these moduli spaces are well known [35] and takes the form of affine E_n Dynkin diagrams.

For orthosymplectic quivers, this is less studied. The quivers are known for $E_{6,7,8}$. In particular:

- E_8: A three-legged quiver [113] that is the 3d mirror to a class $\mathcal{S}$ theory with three D_4 untwisted punctures [114]
- E_7: A three-legged quiver that is the 3d mirror to a $\mathcal{S}$ theory with three untwisted D_3 untwisted punctures [115]. This case is the same as three untwisted A_3 punctures due to the isomorphism of $SU(4) \cong SO(6)$.
- E_6: A three-legged quiver that is the 3d mirror to a $\mathcal{S}$ theory with two twisted A_3 punctures and one untwisted A_3 puncture [20]

In general, the procedure in obtaining the 3d mirrors of class $\mathcal{S}$ theories compactified on a circle is given in [113]. However, for $n \leq 5$, the orthosymplectic quivers are not known. Using a hybrid of both the Top-Down approach of brane systems and the Bottom-Up approach, we were able to find the corresponding quivers which contain new features that were not present in the literature.

$E_5 \cong D_5$ **and** $E_4 \cong A_4$

We start with the one-E_5 instanton moduli space which is the same as the one-$SO(10)$ instanton. The Hilbert series is well known for this moduli space which allows us to quickly test any conjectured magnetic quiver using the monopole formula. By studying the brane system of $SU(2)$ with 4 flavors at infinite coupling, we can guess most of the structure of the magnetic

quiver:

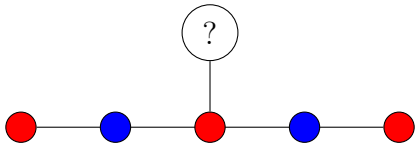

SO(2) USp(2) SO(4) USp(2) SO(2)

$E_5 \cong D_5$ magnetic quiver (4.16)

We recall the brane set up in (3.34) contains two $(1,1)$ 5-branes that are at an 45 degree angle to the O5 plane and at the time we did not know the gauge group it corresponds to in the magnetic quiver (question mark). The linear chain of nodes tells me the global symmetry is $SO(8)$ whereas we should expect $SO(10)$ Coulomb branch symmetry. Hence, the final node must enhance the symmetry somehow. From dimensional analysis, the remaining gauge group must be a rank 1 gauge group, it can be $U(1) \cong SO(2)$, $Sp(1)$ or $SO(3)$ and other groups that differ by a discrete subgroup (e.g $O(2)$). The natural choice was an $Sp(1)$ gauge group since we expected an orthosymplectic quiver where the gauge groups are supposed to alternate between symplectic and (special) orthogonal gauge groups to prevent bad quivers from forming [62]. Unfortunately, the $Sp(1)$ gauge group has negative balance, a signature that the node and hence the quiver is bad and the Hilbert series will diverge.

Using the computationally efficient monopole formula, we quickly exhausted all these possibilities and found that the right choice is a $U(1)$ gauge group connected to the central $SO(4)$ gauge group.

The question now is how do we interpret this in the monopole formula since it is first time such a feature appeared[12]. The vector multiplet contribution to the conformal dimension and lattice of magnetic charges for the $U(1)$ gauge group is the same as before and given in [36]. The only question is how to interpret the hypermultiplets between the $U(1)$ and $SO(4)$. In the end, we find the correct description is to keep the hypermultiplet as if between an $Sp(1)$ and $SO(4)$ but then only *gauge* the $U(1) \subset Sp(1)$. In other words the hypermultiplet contribution to the conformal dimension remains as $\Delta_{Sp(1)-SO(4)}$ but the vector multiplet contribution and

[12]Unitary-orthosymplectic quivers did exist in [62] but the unitary gauge groups are connected to symplectic gauge group. This is the first occurrence when the unitary gauge group connects to an (special) orthogonal gauge group

magnetic lattice is that of an $U(1)$. Therefore, the magnetic quiver takes the form:

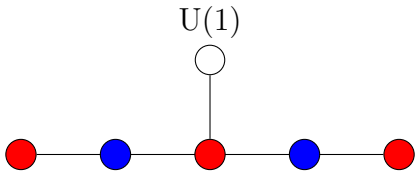

$$\mathrm{SO}(2)\,\mathrm{USp}(2)\,\mathrm{SO}(4)\,\mathrm{USp}(2)\,\mathrm{SO}(2)$$

$E_5 \cong D_5$ magnetic quiver (4.17)

The Coulomb branch Hilbert series shows that this is indeed the one-$SO(10)$ instanton moduli space. And with this example, we started allowing the possibility of magnetic quivers being unitary-orthosymplectic quivers.

Next, we can study the case of $E_4 \cong A_4$. The expected moduli space is one-$SU(5)$ instanton moduli space, whose Hilbert series is also well known. From the brane system we expect the following structure:

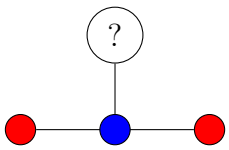

$$\mathrm{SO}(2)\,\mathrm{USp}(2)\,\mathrm{SO}(2)$$

$E_4 \cong A_4$ magnetic quiver (4.18)

The missing gauge group is another rank 1 theory. This time, we tried replacing it with $U(1)$ but the resulting moduli space is still incorrect as checked by the monopole formula. The correct answer in the end turns out to be a $U(1)$ gauge group connected with a *charge 2 hypermultiplet*[13]:

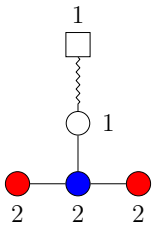

(4.19)

This marks the first appearance of a charge 2 hypermultiplet in study of orthosymplectic quivers.

[13]It is still up to debate whether it is actually a charge 2 hyper. Since a $U(1)$ gauge group with matter field transforming in the symmetric representation will give the same result. So far our tests are indifferent to either of these so we will stick with charge 2 hypers for the rest of the thesis.

There is an inherent difference between a charge 2 hyper and two charge one hypers even though they contribute the same in the conformal dimension of the monopole formula. This is because by choosing a charge 2 hyper, there is an overall $\mathbb{Z}_2$ diagonal subgroup that we can decouple from the quiver. We will now discuss in detail the importance of this discrete symmetry for orthosymplectic quivers.

4.4 Diagonal $\mathbb{Z}_2$ symmetry

Based on our paper [2].

If one directly applies the monopole formula to compute the Coulomb branch of unframed/flavorless orthosymplectic quivers such as any of the E_n quivers, one will find that the Hilbert series does not match the one-E_n instanton moduli space. In fact, the mismatch already occurs at the first order which means the dimensional of the global symmetry group predicted by the HS is already incorrect. This mismatch does not mean a limitation of the monopole formula but rather our incorrect identification of the gauge groups. Take (4.17) for example, whenever we label a gauge group we don't just identify the algebra but the global structure as well. However, if the quiver is made of only $U(n)$, $SO(2n)$, $USp(2n)$ gauge groups, there is actually a $(\mathbb{Z}_2)_{\text{diag}}$ that acts trivially on the matter content of the theory. This is identical to the common centre of the gauge groups. Whenever this happens, we can choose whether or not to ungauge this $\mathbb{Z}_2$. This action will affect the magnetic lattices in the monopole formula from which we sum over the magnetic charges [61]. In [2], we denote the choice of whether to ungauge as the choice of choosing $H = \{1\}$ (not to ungauge) or $H = \mathbb{Z}_2$ (ungauge). This H is also the zero-form symmetry associated with the quiver [116]. Such phenomenon were studied in early works in the context of standard model gauge theory and spectrum of line operators [117]. In our case, $H = \{1\}$ means there are no zero-form symmetry but there is a $\mathbb{Z}_2$ one-form symmetry where the line operators can be charged under [116]. On the other hand, if we *gauge*[14] this

[14]Here we need to be careful what we call gauging and ungauging. Throughout this thesis, and in [2], we refer to ungauging as quotienting out or decoupling a subgroup H from the gauge group G. On the other hand, one-form symmetry groups are global symmetries, so if H is trivial then there is a non-trivial group H that is the one-form symmetry.Then, *gauging* it will be the equivalent action of decoupling the subgroup H from the gauge group G.

one-form symmetry, we will have a non-trivial zero form symmetry $H = \mathbb{Z}_2$ instead, which will be the case for all our unframed/flavorless magnetic orthosymplectic quivers.

4.4.1 Magnetic lattice

We now present some more detailed analysis around this discrete subgroup.

A quiver Q can be seen as a way of encoding a representation $\phi : G \to GL(V)$ of a group G into a finite dimensional vector space V. We follow standard conventions, associating a *group* to each vertex of the quiver, and a bifundamental representation to a link between two vertices. Importantly, it is not enough to specify a Lie algebra at each vertex of the quiver; in general several groups correspond to the same algebra, and give distinct gauge theories. Other kinds of representations, beyond bifundamentals, are also allowed. For a given quiver Q with gauge group G and symmetry group $\ker\phi$, there is a choice which 3d $\mathcal{N} = 4$ gauge theory one likes to consider. For any normal subgroup $H \trianglelefteq \ker\phi$, there exists a theory defined by a Lagrangian with matter content represented by V and with a gauge group G_H, where

$$\boxed{\frac{G}{\ker\phi} \subseteq G_H \coloneqq \frac{G}{H} \subseteq G}\,, \tag{4.20}$$

as well as interactions dictated by supersymmetry. Given a quiver Q and the choice of H, we define the *Coulomb branch* of the pair (Q, H), denoted $\mathcal{C}_H(\mathsf{Q})$ as being the Coulomb branch of the 3d $\mathcal{N} = 4$ gauge theory defined in the previous sentence. It is important to notice that this is a definition of what we mean by the Coulomb branch of a quiver with a choice of group H. Furthermore, the different choices of subgroups of $\ker\phi$ lead to an orbifold relation among the Coulomb branches:

$$\mathcal{C}_{\{1\}}(\mathsf{Q}) = \frac{\mathcal{C}_H(\mathsf{Q})}{H} \qquad \text{for any} \quad H \trianglelefteq \ker\phi\,. \tag{4.21a}$$

Alternatively, using the quotient $N_H = \frac{\ker\phi}{H}$, one arrives at

$$\mathcal{C}_H(\mathsf{Q}) = \frac{\mathcal{C}_{\ker\phi}(\mathsf{Q})}{N_H}\,. \tag{4.21b}$$

Given a unitary quiver with nodes $\mathrm{U}(k)$, for instance, then each node has a subgroup $\mathbb{Z}_k$ which

one can choose to ungauge or not. Hence, there exists multitude of *different* orbifold moduli spaces that one can construct from a single quiver simply by choosing different nodes to ungauge a discrete group.

Unframed orthosymplectic quivers – $\ker\phi = \mathbb{Z}_2$

The Coulomb branch Hilbert series of orthosymplectic quivers had previously been studied and computed in [118, 96, 56, 57, 119], where most of the Coulomb branches are either closures of nilpotent orbits or their intersections with Slodowy slices. A ubiquitous feature of these quivers is that they all contain flavor nodes[15]. On the other hand, when we are dealing with unframed/flavorless orthosymplectic quivers, G is a product of special orthogonal and symplectic groups, and the representation ϕ is a direct sum of bifundamental representations. As a consequence, we distinguish two situations:

- If there is at least one $\mathrm{SO}(2r+1)$ node in the quiver, then $\ker\phi$ is trivial and $G_H = G$.
- If there is no node of type $\mathrm{SO}(2r+1)$ in the quiver, then $\ker\phi = \mathbb{Z}_2^{\mathrm{diag}}$, and we have two choices for the gauge group. $G_{\{1\}} = G$, which is the product of orthosymplectic gauge groups, and $G_{\mathbb{Z}_2} = G/\mathbb{Z}_2^{\mathrm{diag}}$, which is the product of orthosymplectic groups divided by $\mathbb{Z}_2^{\mathrm{diag}}$.

To see the effect on magnetic lattices, consider a product of two groups, $\mathrm{SO}(2r)$ and $\mathrm{USp}(2k)$. The magnetic lattice for the product $G = \mathrm{SO}(2r) \times \mathrm{USp}(2k)$ is $\mathbb{Z}^r \oplus \mathbb{Z}^k$. For $\mathrm{SO}(2r)/\mathbb{Z}_2 \times \mathrm{USp}(2k)/\mathbb{Z}_2$ the magnetic lattice is

$$\left[\mathbb{Z}^r \cup \left(\mathbb{Z} + \frac{1}{2}\right)^r\right] \oplus \left[\mathbb{Z}^k \cup \left(\mathbb{Z} + \frac{1}{2}\right)^k\right] . \tag{4.22}$$

Finally, for $(\mathrm{SO}(2r) \times \mathrm{USp}(2k))/\mathbb{Z}_2^{\mathrm{diag}}$ where we quotient by a diagonal $\mathbb{Z}_2^{\mathrm{diag}}$ subgroup, we obtain

[15] We note that correct Coulomb branch Hilbert series computations of flavorless orthosymplectic quivers had been given in [118]. However, the approach used the Hall-Littlewood formula [120] rather than the monopole formula. As a result, it does not use the explicit magnetic lattice of the gauge groups (aside from the central node of the three-legged theories).

the magnetic lattice

$$\left[\mathbb{Z}^r \oplus \mathbb{Z}^k\right] \cup \left[\left(\mathbb{Z}+\frac{1}{2}\right)^r \oplus \left(\mathbb{Z}+\frac{1}{2}\right)^k\right] = \mathbb{Z}^{r+k} \cup \left(\mathbb{Z}+\frac{1}{2}\right)^{r+k} . \tag{4.23}$$

An interesting feature that arises is that we now also include integer-plus-half terms in the magnetic lattice.

As an illustration, we consider the simplest orthosymplectic quiver:

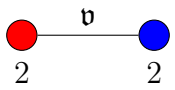

(4.24)

For $\mathfrak{v} \geq 3$, the USp(2) node is not bad in the sense of [62] and hence the Coulomb branch Hilbert series does not diverge. The presence of bad gauge nodes occurs frequently in constructing orthosymplectic quivers which limits our ability to study its Coulomb branch.

We can now present the different choices of discrete quotients in terms of Hilbert series:

$$\begin{aligned}
\mathrm{HS}\Big(\mathrm{SO}(2) \times \mathrm{USp}(2)\Big) &= \mathrm{HS}_{\mathbb{Z}^2} && \text{(4.25a)}\\
\mathrm{HS}\left(\frac{\mathrm{SO}(2)}{\mathbb{Z}_2} \times \mathrm{USp}(2)\right) &= \mathrm{HS}_{\mathbb{Z}^2} + \mathrm{HS}_{(\mathbb{Z}+\frac{1}{2})\oplus\mathbb{Z}} && \text{(4.25b)}\\
\mathrm{HS}\left(\mathrm{SO}(2) \times \frac{\mathrm{USp}(2)}{\mathbb{Z}_2}\right) &= \mathrm{HS}_{\mathbb{Z}^2} + \mathrm{HS}_{\mathbb{Z}\oplus(\mathbb{Z}+\frac{1}{2})} && \text{(4.25c)}\\
\mathrm{HS}\left(\frac{\mathrm{SO}(2)}{\mathbb{Z}_2} \times \frac{\mathrm{USp}(2)}{\mathbb{Z}_2}\right) &= \mathrm{HS}_{\mathbb{Z}^2} + \mathrm{HS}_{\mathbb{Z}\oplus(\mathbb{Z}+\frac{1}{2})} && \\
& \quad + \mathrm{HS}_{\mathbb{Z}\oplus(\mathbb{Z}+\frac{1}{2})} + \mathrm{HS}_{(\mathbb{Z}+\frac{1}{2})^2} && \text{(4.25d)}\\
\mathrm{HS}\left(\frac{\mathrm{SO}(2) \times \mathrm{USp}(2)}{\mathbb{Z}_2^{\mathrm{diag}}}\right) &= \mathrm{HS}_{\mathbb{Z}^2} + \mathrm{HS}_{(\mathbb{Z}+\frac{1}{2})^2} && \text{(4.25e)}
\end{aligned}$$

where the Hilbert series subscripts $\Lambda_w^{\mathrm{SO}(2)^\vee} \oplus \Lambda_w^{\mathrm{USp}(2)^\vee}$ explicitly denotes the lattice of the magnetic charges of SO(2) and USp(2) respectively[16]. The Hilbert series takes the form above because, for example, if m takes all integers and n takes all positive integers and integers-plus-half, we can decompose them into two separate Hilbert series. For the quiver (4.24) the gauge group is

[16]Note, this is the only time we explicitly label the Hilbert series with their respective magnetic charges. For the rest of the chapter, we continue to use the notation $\mathrm{HS}_{\mathbb{Z}}$ to denote the Hilbert series where all charges are integer values and $\mathrm{HS}_{\mathbb{Z}+\frac{1}{2}}$ for half-plus-integer value charges and $\mathrm{HS}_{\mathbb{Z}\,\cup\,\mathbb{Z}+\frac{1}{2}}$ for their sum.

the quotient $G_{\mathbb{Z}_2} = \frac{\mathrm{SO}(2)\times\mathrm{USp}(2)}{\mathbb{Z}_2^{\mathrm{diag}}}$ of $G = \mathrm{SO}(2) \times \mathrm{USp}(2)$ by the kernel $\mathbb{Z}_2^{\mathrm{diag}}$. This means that the Coulomb branch Hilbert series of (4.24) is given by (4.25e). Note that the GNO dual of $G_{\mathbb{Z}_2}$ is not a product of classical groups. The electric and magnetic lattices for the five cases of equations (4.25) are represented in Figure 4.11.

Unframed unitary orthosymplectic quivers – $\ker\phi = \mathbb{Z}_2$

Finally, we can consider quivers which contain both orthosymplectic gauge nodes and unitary nodes, with or without charge 2 hypermultiplets. When this is the case, the same analysis is valid, with $\ker\phi = \mathbb{Z}_2^{\mathrm{diag}}$, and the magnetic lattice is a direct sum of a $\mathbb{Z}^r$ component and a $\left(\mathbb{Z} + \frac{1}{2}\right)^r$ component. A myriad of examples is given in the remaining of this chapter.

Notation. The lattice (4.23), or its generalizations to arbitrary unframed orthosymplectic or unitary orthosymplectic quivers, are relevant for the Coulomb branch Hilbert series computations for the choice $H = \ker\phi$. To lighten the notation, the following convention is adopted. For the choice $H = \ker\phi$, the Hilbert series $\mathrm{HS}(t)$ can be decomposed as a sum of two pieces, which are symbolically called $\mathrm{HS}_{\mathbb{Z}}(t)$ and $\mathrm{HS}_{\mathbb{Z}+\frac{1}{2}}(t)$. For the choice $H = \{1\}$, the total Hilbert series is just $\mathrm{HS}_{\mathbb{Z}}(t)$.

4.4.2 Sums over magnetic sublattices

Above, we see how the magnetic lattice of $G_{\mathbb{Z}_2}$ can be split into the lattice containing integer magnetic charges $\mathbb{Z}$ and the lattice containing magnetic charges shifted by a half, $\mathbb{Z} + \frac{1}{2}$. This can be generalized to $G_{\mathbb{Z}_k}$ for some k where the lattice is the sum $\bigcup_{i=0}^{k-1}(\mathbb{Z} + \frac{i}{k})$. The Hilbert series can therefore be decomposed as:

$$\mathrm{HS}(t) = \sum_{i=0}^{k-1} \mathrm{HS}_{\mathbb{Z}+\frac{i}{k}}(t) \tag{4.26}$$

where $\mathrm{HS}_{\mathbb{Z}+\frac{i}{k}}(t)$ is the Hilbert series obtained by summing magnetic lattices with $\mathbb{Z}+\frac{i}{k}$ magnetic charges.

It is currently unknown how to compute the refined Hilbert series for orthosymplectic

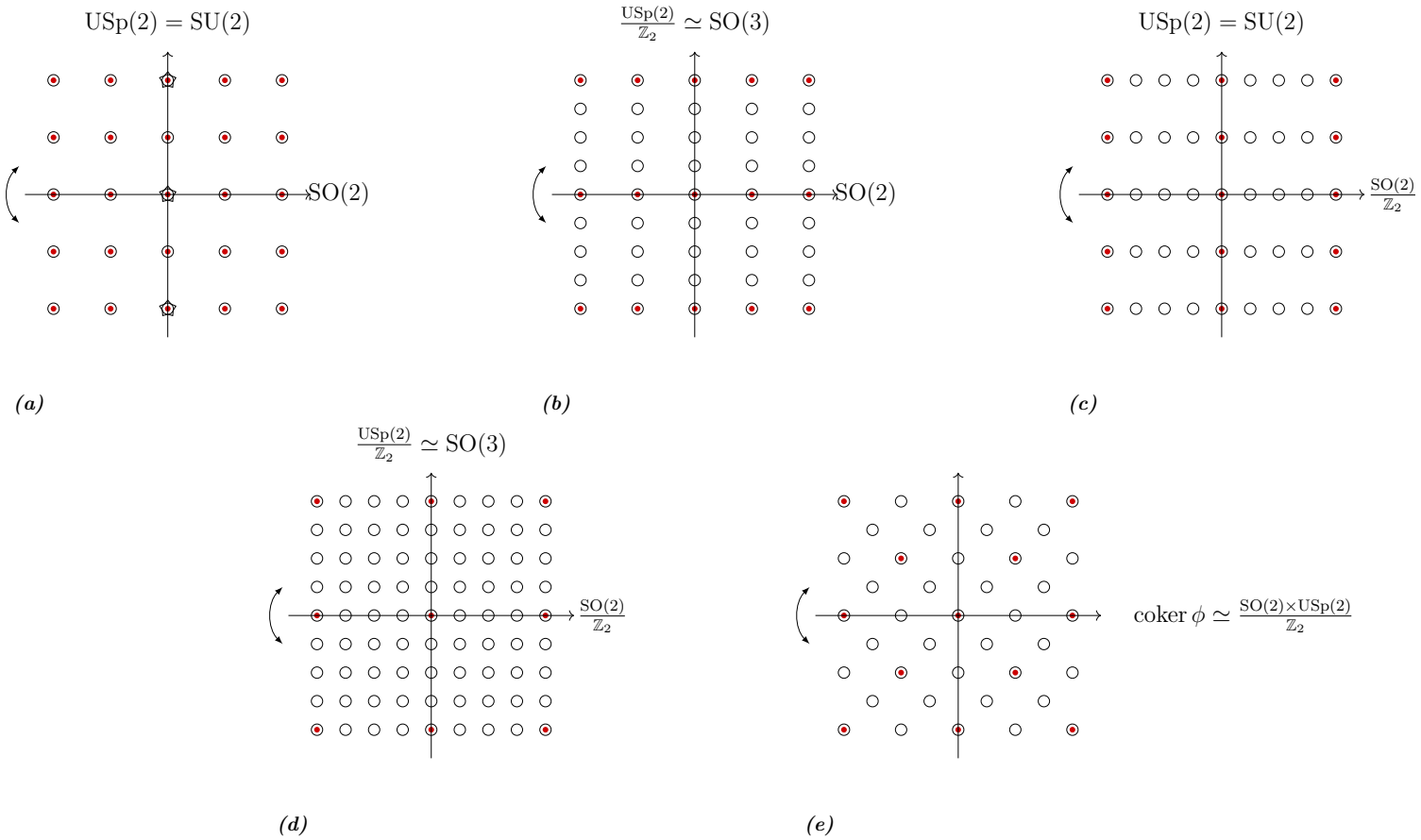

Figure 4.11: *In all the diagrams, the red dots show the weight lattice, and the black circles show the dual lattice, which is the magnetic lattice involved in the monopole formula. The arrow denotes the action of the Weyl group. a: The stars show the root lattice of* $\mathrm{USp}(2)$*. This notion does not extend to the full group* $\mathrm{SO}(2) \times \mathrm{USp}(2)$ *because of the Abelian factor. We do not show the roots on the other diagrams. b:* $\mathrm{USp}(2)$ *is replaced by* $\mathrm{SO}(3)$*. c:* $\mathrm{SO}(2)$ *is replaced by* $\mathrm{SO}(2)/\mathbb{Z}_2 \simeq \mathrm{SO}(2)$*, which rescales the weights. d: Combinations of the two* $\mathbb{Z}_2$ *modifications of b and c. The weight lattice has index* 4 *compared to a. e: Finally this is the weight and coweight lattices for the quiver group.*

quivers using the monopole formula. However, the refined Hilbert series can in some cases be inferred from a unitary quiver counterpart, or alternatively, in many cases (including star shaped orthosymplectic quivers), be computed using the Hall-Littlewood method [120]. An exact refined Hilbert series can be concisely encapsulated in the form of a highest weight generating function (HWG) [50]. The expression of the HWG follows the same decomposition as (4.26):

$$\mathrm{HWG}(\mu_i, t) = \sum_{i=0}^{k-1} \mathrm{HWG}_{\mathbb{Z}+\frac{i}{k}}(\mu_i, t) \tag{4.27}$$

Unframed unitary quivers – $\ker\phi = \mathrm{U}(1)$

Notice that our analysis can be equally well applied for an unframed quiver with only unitary gauge groups. The common centre is $H = U(1)$ and hence the diagonal subgroup to decouple is a $U(1)_{\text{diag}}$. When computing the monopole formula, this ungauging action can be achieved in these three equivalent ways:

- If there are $U(1)$ gauge groups, turn them into $U(1)$ flavor groups.
- Take a non-Abelian $U(k)$ with magnetic charges $(m_1, \ldots, m_k)$ and set the last charge to zero: $(m_1, \ldots, m_k = 0)$
- Since a $U(k)/U(1) = SU(k)/\mathbb{Z}_k$, we first turn an $U(k)$ gauge group into $SU(k)$, then take a $\mathbb{Z}_k$ diagonal quotient over *all* the gauge groups.

However, unlike the orthosymplectic cases, we cannot choose $H = \{1\}$ since then the centre of mass will not be fixed and the Hilbert series will diverge. $H = \{1\}$ is possible in the orthosymplectic case because in the brane system the orientifold plane already fixed the centre of mass of the system and the Hilbert series will not diverge.

SCFTs and $(\mathbb{Z}_2)_{\text{diag}}$

An interesting observation is that whenever we are looking at magnetic quivers of SCFTs, such as 5d SQCD theories, 6d theories on -1 curves, 4d class $\mathcal{S}$ theories etc, they are almost always unframed/flavorless. Furthermore, it is only when we ungauge this $(\mathbb{Z}_2)_{\text{diag}}$ one-form symmetry that we obtain the correct Coulomb branch that describes the Higgs branch of these SCFTs (this is true for all examples we have investigated). It remains interesting as to why this must be the case and how does it tie to the story about higher-form symmetries and SCFTs.

4.5 Orthosymplectic magnetic quivers

Based on our paper [2].

In this section we present the main results of our 5d magnetic quivers. They are obtained using an hybrid of the Top-Down approach (extraction from brane webs) as well as Bottom-Up approach (using partial data to constrain the form of the magnetic quiver).

Discrete θ angles

Unlike the $SU(N_c)$ case, we don't have to worry about Chern-Simons levels for Sp gauge groups. However, when there are no matter fields, there is a $\pi_4(Sp(N_c)) = \mathbb{Z}_2$ discrete θ angle one can choose [75]. For $N_c = 1$, this is important for differentiating E_1 and $\widetilde{E_1}$ theories. This can be extended to two infinite families for general N_c. However, when there are fundamental flavors, $\pi_4(Sp(N_c))$ is trivial and we don't need to worry about discrete theta angles.

Even number of hypers

A related concept is the 5th homotopy group $\pi_5(Sp(N_c)) = \mathbb{Z}_2$. This has the consequence that $Sp(N_c)$ with an odd number of half-hypers has a global anomaly that renders the theory inconsistent. This is why our theories always have even number of half-hypers [75, 121]. This is true not only in 5d but in other dimensions as well.

4.5.1 Rank 1 E_n theories

We start off with $SU(2)$ with $N_f = n - 1, \ldots, 7$ whose Higgs branch at the UV fixed point is one-E_n instanton moduli space. The Coulomb branch of these magnetic quivers give the correct moduli space when $H = \mathbb{Z}_2$. However, it is also important to provide the moduli space when the choice is $H = \{1\}$. The result will be a $\mathbb{Z}_2$ orbifold of the instanton moduli space and we provide their Hilbert series as well. The Hilbert series are given both unrefined as well as refined by representations of the global symmetry group (in the form of a highest weight generating function).

E_8 quiver

We start with the orthosymplectic quiver whose Coulomb branch is the closure of the E_8 minimal nilpotent orbit $\overline{\mathcal{O}}^{\mathfrak{e}_8}_{\text{min}}$.

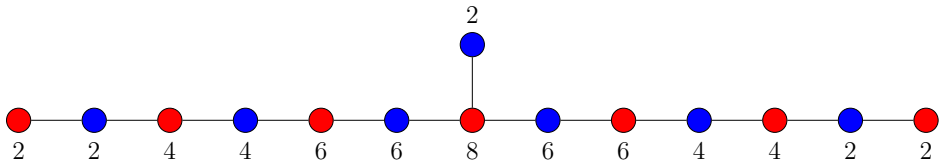

(4.28)

The Coulomb branch Hilbert series is given in Figure 4.12 which matches the computation of the one E_8 instanton in [122]. In addition to the unrefined Hilbert series, the exact refined Hilbert series is also given in the form of a highest weight generating function (HWG) [50].

In Figure 4.12, the first line shows the Hilbert series obtained by summing over the integer lattice $\text{HS}_{\mathbb{Z}}(t)$. The resulting Hilbert series is that of a symplectic singularity with global symmetry PSO(16). Note that the global symmetry is a strict subalgebra of the exceptional $\mathfrak{e}_8$, which is reflected in the decomposition of the 248 dimensional adjoint representation of $\mathfrak{e}_8$ into the 120 dimensional adjoint and the 128 dimensional spinor of $\mathfrak{so}(16)$. The integers-plus-half lattice $\text{HS}_{\mathbb{Z}+\frac{1}{2}}(t)$ adds precisely the missing $\mathfrak{so}(16)$ spinor at order t^2 in the Hilbert series, so that the full result displays $\mathfrak{e}_8$ global symmetry. These facts can be deduced directly from the HWGs, where μ_2 stands for the $\mathfrak{so}(16)$ adjoint and μ_8 for the spinor.

As can be read from the table, the HWG of the minimal $\mathfrak{e}_8$ nilpotent orbit, which is $\text{PE}[\mu_7 t^2]$ in terms of $\mathfrak{e}_8$ fugacities, reads $\text{PE}[(\mu_2+\mu_8)t^2+(1+\mu_4+\mu_8)t^4+\mu_6 t^6]$ in terms of $\mathfrak{so}(16)$ fugacities. A $\mathbb{Z}_2^{\text{diag}}$ quotient can be performed, in which the $\mathbb{Z}_2^{\text{diag}}$ acts non-trivially on the spinor terms $\mu_8 t^2$ and $\mu_8 t^4$. As explained in [86], this is accounted for by replacing $\mu_8 t^2+\mu_8 t^4$ by $\mu_8^2 t^4+\mu_8^2 t^6+\mu_8^2 t^8-\mu_8^4 t^{12}$, which gives exactly the HWG for the PSO(16) space from the integer lattice.

In the following subsections, similar comments and observations can be made.

	Hilbert Series	HWG
$\mathrm{HS}_{\mathbb{Z}}(t)$	$\frac{\mathcal{P}_{116}(t)}{(1-t^2)^{29}(1-t^4)^{29}}$ $= 1 + 120t^2 + 13560t^4 + 881205t^6$ $+39574360t^8 + 1321374912t^{10} + O\left(t^{12}\right)$	$\mathrm{PE}\big[\mu_2 t^2 + (1+\mu_4+\mu_8^2)t^4$ $+(\mu_6+\mu_8^2)t^6 + \mu_8^2 t^8$ $-\mu_8^4 t^{12}\big]$
$\mathrm{HS}_{\mathbb{Z}+\frac{1}{2}}(t)$	$\frac{128t^2\,\mathcal{P}_{112}(t)}{(1-t^2)^{29}(1-t^4)^{29}}$ $= 128t^2 + 13440t^4 + 881920t^6$ $+39568640t^8 + 1321402368t^{10} + O\left(t^{12}\right)$	$\mu_8 t^2\ \mathrm{PE}\big[t^2 + \mu_2 t^2 + (\mu_4+\mu_8^2)t^4$ $+\mu_6 t^6 + \mu_8^2 t^8\big]$
$\mathrm{HS}(t)$	$\frac{(1+t^2)\,\mathcal{P}_{56}(t)}{(1-t^2)^{58}}$ $= 1 + 248t^2 + 27000t^4 + 1763125t^6$ $+79143000t^8 + 2642777280t^{10} + O\left(t^{12}\right)$	$\mathrm{PE}\big[(\mu_2+\mu_8)t^2$ $+(1+\mu_4+\mu_8)t^4$ $+\mu_6 t^6\big]$

Figure 4.12: *Hilbert series for the E_8 magnetic quiver (4.28). The first line of the table provides the Hilbert series when the GNO magnetic lattice is integer $\mathrm{HS}_{\mathbb{Z}}(t)$, the second line shows the sum over the integers-plus-half lattice $\mathrm{HS}_{\mathbb{Z}+\frac{1}{2}}(t)$ and the last line is their sum $\mathrm{HS}(t)$. The palindromic numerator terms $\mathcal{P}_k(t)$ are very long expressions and given in Appendix E in [2]. In the third column, we show the HWG in terms of fugacities for $\mathfrak{so}(16)$ (denoted $\mu_1, \ldots, \mu_8$). Note that we pick the branching of $\mathfrak{e}_8 \to \mathfrak{so}(16)$ where $(\mu_7)_{\mathfrak{e}_8} \mapsto (\mu_2+\mu_8)_{\mathfrak{so}(16)}$.*

E_7 quiver

We move on to the unitary-orthosymplectic quiver whose Coulomb branch is the closure of the E_7 minimal nilpotent orbit $\overline{\mathcal{O}}^{\mathfrak{e}_7}_{\text{min}}$.

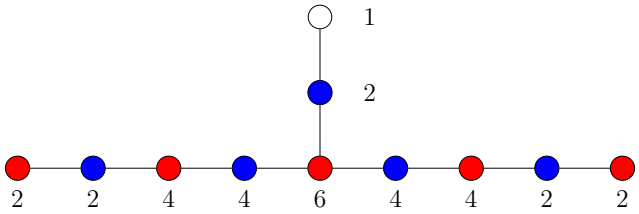

(4.29)

where the white node represents a U(1) gauge group. As discussed earlier in the chapter, under the diagonal $\mathbb{Z}_2^{\text{diag}}$ quotient, we take integer and integers-plus-half magnetic charges for the unitary gauge groups as well.

The U(1) gauge node can equivalently be expressed as an SO(2) gauge node and this quiver thereby acts as a bridge between different families of quivers. As an SO(2), it comes more naturally from D-type punctures of 4d $\mathcal{N}=2$ class $\mathcal{S}$ theories. As U(1) it comes more naturally from a brane construction with O5 planes [3]. The Coulomb branch Hilbert series is given in

Figure 4.13, which matches the computation of the one E_7 instanton in [122], alongside with the Hilbert series for the orbifold moduli space with global symmetry PSO(12) × PSU(2).

E_6 quiver

The unitary-orthosymplectic quiver whose Coulomb branch is the closure of the E_6 minimal nilpotent orbit $\overline{\mathcal{O}}_{\text{min}}^{\mathfrak{e}_6}$ takes the following form:

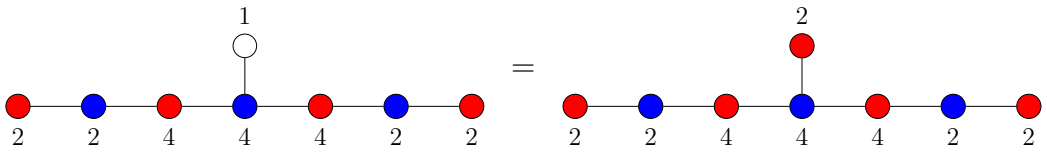

(4.30)

Again, the U(1) gauge node can equivalently be expressed as an SO(2) gauge node. The Coulomb branch Hilbert series is given in Figure 4.14 which matches the computation of the one E_6 instanton in [122], along side with the Hilbert series for the orbifold moduli space with global symmetry SO(10) × U(1) .

E_5 quiver

Using the isomorphism $\mathfrak{e}_5 \cong \mathfrak{so}(10)$, the unitary-orthosymplectic quiver whose Coulomb branch is the closure of the $\mathfrak{so}(10)$ minimal nilpotent orbit $\overline{\mathcal{O}}_{\text{min}}^{\mathfrak{so}(10)}$ takes the following form:

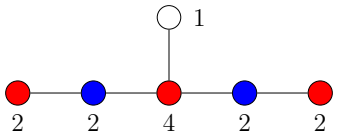

(4.31)

In this case, as opposed to equation (B.6), the U(1) node can not be replaced by an SO(2) node, as the central node of the quiver is already of orthogonal type. Instead, one may view the U(1) as gauging a subgroup of a USp(2) flavour symmetry. The Hilbert series is given in Figure 4.15 and matches the moduli space of $\overline{\mathcal{O}}_{\text{min}}^{\mathfrak{so}(10)}$ [56], along side with the Hilbert series for the orbifold moduli space with global symmetry PSO(8) × U(1) .

	Hilbert Series	HWG
$\mathrm{HS}_{\mathbb{Z}}(t)$	$\frac{\mathcal{P}_{68}(t)}{(1-t^2)^{17}(1-t^4)^{17}}$ $= 1 + 69t^2 + 3723t^4 + 119434t^6$ $+2625390t^8 + 42857892t^{10} + O\left(t^{12}\right)$	$\mathrm{PE}\big[(\mu_2+\nu^2)t^2$ $+(1+\mu_4+\nu^2\mu_6^2)t^4$ $+(\mu_6^2+\nu^2\mu_6^2)t^6$ $-\nu^4\mu_6^4t^{12}\big]$
$\mathrm{HS}_{\mathbb{Z}+\frac{1}{2}}(t)$	$\frac{64t^2\,\mathcal{P}_{64}(t)}{(1-t^2)^{17}(1-t^4)^{17}}$ $= 64t^2 + 3648t^4 + 119168t^6$ $+2623360t^8 + 42852096t^{10} + O\left(t^{12}\right)$	$\mu_6\nu t^2\,\mathrm{PE}\big[t^2+\nu^2t^2+\mu_2t^2$ $\mu_4t^4+\mu_6^2t^6+\nu^2\mu_6^2t^4\big]$
$\mathrm{HS}(t)$	$\frac{(1+t^2)\,\mathcal{P}_{32}(t)}{(1-t^2)^{34}}$ $= 1 + 133t^2 + 7371t^4 + 238602t^6$ $+5248750t^8 + 85709988t^{10} + O\left(t^{12}\right)$	$\mathrm{PE}\big[(\mu_2+\nu^2+\nu\mu_6)t^2$ $+(1+\mu_4+\nu\mu_6)t^4$ $+\mu_6^2t^6-\nu^2\mu_6^2t^8\big]$

Figure 4.13: *Hilbert series for the E_7 magnetic quiver (4.29). The first line of the table provides the Hilbert series when the GNO magnetic lattice is integer $\mathrm{HS}_{\mathbb{Z}}(t)$, the second line shows the sum over the integers-plus-half lattice $\mathrm{HS}_{\mathbb{Z}+\frac{1}{2}}(t)$ and the last line is their sum $\mathrm{HS}(t)$. The palindromic numerator terms $\mathcal{P}_k(t)$ are given in Appendix E of [2]. In the third column, we show the HWG in terms of fugacities for $\mathfrak{su}(2)$ and $\mathfrak{so}(12)$ (denoted ν and $\mu_1,\ldots,\mu_6$ respectively). Note that we pick the branching of $\mathfrak{e}_7 \to \mathfrak{su}(2)\times\mathfrak{so}(12)$ where $(\mu_1)_{\mathfrak{e}_7} \mapsto (\nu\mu_6+\nu^2+\mu_2)_{\mathfrak{su}(2)\times\mathfrak{so}(12)}$.*

	Hilbert Series	HWG
$\mathrm{HS}_{\mathbb{Z}}(t)$	$\frac{\mathcal{P}_{44}(t)}{(1-t^2)^{11}(1-t^4)^{11}}$ $= 1 + 46t^2 + 1278t^4 + 22254t^6$ $+270798t^8 + 2491731t^{10} + O\left(t^{12}\right)$	$\mathrm{PE}\big[\mu_2t^2+t^2$ $+(\mu_4^2q^6+\mu_5^2q^{-6}+\mu_4\mu_5)t^4$ $-\mu_4^2\mu_5^2t^8\big]$
$\mathrm{HS}_{\mathbb{Z}+\frac{1}{2}}(t)$	$\frac{32t^2\,\mathcal{P}_{40}(t)}{(1-t^2)^{11}(1-t^4)^{11}}$ $= 32t^2 + 1152t^4 + 21504t^6$ $+267168t^8 + 2477376t^{10} + O\left(t^{12}\right)$	$(\mu_4q^3+\frac{\mu_5}{q^3})t^2\,\mathrm{PE}\big[t^2+\mu_2t^2+\mu_4^2q^6t^4+\frac{\mu_5^2}{q^6}t^4\big]$
$\mathrm{HS}(t)$	$\frac{(1+t^2)\,\mathcal{P}_{20}(t)}{(1-t^2)^{22}}$ $= 1 + 78t^2 + 2430t^4 + 43758t^6$ $+537966t^8 + 4969107t^{10} + O\left(t^{12}\right)$	$\mathrm{PE}\big[\mu_2t^2+t^2$ $+(\mu_4q^3+\mu_5q^{-3})t^2\big]$

Figure 4.14: *Hilbert series for the E_6 magnetic quiver (B.6). The first line of the table provides the Hilbert series when the GNO magnetic lattice is integer $\mathrm{HS}_{\mathbb{Z}}(t)$, the second line shows the sum over the integers-plus-half lattice $\mathrm{HS}_{\mathbb{Z}+\frac{1}{2}}(t)$ and the last line is their sum $\mathrm{HS}(t)$. The palindromic numerator terms $\mathcal{P}_k(t)$ are given in Appendix E of [2]. In the third column, we show the HWGs in terms of fugacities for $\mathfrak{so}(10)$ (denoted $\mu_1,\ldots,\mu_5$) and $\mathfrak{u}(1)$ (denoted q). Note that the q-charge is normalized, such that the branching of $\mathfrak{e}_6 \to \mathfrak{so}(10)\times\mathfrak{u}(1)$ is $(\mu_6)_{\mathfrak{e}_6} \mapsto q^{+2}(\mu_1)_{\mathfrak{so}(10)} + q^{-1}(\mu_4)_{\mathfrak{so}(10)} + q^{-4}$.*

	Hilbert Series	HWG
$\mathrm{HS}_{\mathbb{Z}}(t)$	$\frac{\left(\begin{array}{c}1+22t^2+245t^4+1442t^6+5355t^8+12978t^{10}\\+21919t^{12}+25900t^{14}+\ldots\,\text{palindrome}\,\ldots+t^{28}\end{array}\right)}{(1-t^2)^7(1-t^4)^7}$ $= 1 + 29t^2 + 434t^4 + 4060t^6 + 27384t^8 + 144312t^{10} + O\left(t^{12}\right)$	$\mathrm{PE}\big[\mu_2 t^2 + t^2 + (\mu_4^2 q^4 + \mu_4^2 q^{-4})t^4 + \mu_4^2 t^4 - \mu_4^4 t^8\big]$
$\mathrm{HS}_{\mathbb{Z}+\frac{1}{2}}(t)$	$\frac{16t^2\left(\begin{array}{c}1+14t^2+91t^4+336t^6+819t^8+1362t^{10}\\+1618t^{12}+\ldots\,\text{palindrome}\,\ldots+t^{24}\end{array}\right)}{(1-t^2)^7(1-t^4)^7}$ $= 16t^2 + 336t^4 + 3584t^6 + 25536t^8 + 138432t^{10} + O\left(t^{12}\right)$	$\mu_4(q^2+\frac{1}{q^2})t^2\,\mathrm{PE}\big[t^2 + \mu_2 t^2 + \frac{\mu_4^2}{q^2}t^4 + \mu_4^2 q^4 t^4\big]$
$\mathrm{HS}(t)$	$\frac{\left(\begin{array}{c}1+30t^2+201t^4+394t^6+201t^8+30t^{10}+t^{12}\end{array}\right)}{(1-t^2)^{14}(1+t^2)^{-1}}$ $= 1 + 45t^2 + 770t^4 + 7644t^6 + 52920t^8 + 282744t^{10} + O\left(t^{12}\right)$	$\mathrm{PE}\big[\mu_2 t^2 + t^2 + (\mu_4 q^2 + \mu_4 q^{-2})t^2\big]$

Figure 4.15: *Hilbert series for the E_5 magnetic quiver (4.31). The first line of the table provides the Hilbert series when the GNO magnetic lattice is integer $\mathrm{HS}_{\mathbb{Z}}(t)$, the second line shows the sum over the integers-plus-half lattice $\mathrm{HS}_{\mathbb{Z}+\frac{1}{2}}(t)$ and the last line is their sum $\mathrm{HS}(t)$. In the third column, we show the HWG in terms of fugacities for $\mathfrak{so}(8)$ (denoted $\mu_1,\ldots,\mu_4$) and $\mathfrak{u}(1)$ (denoted q). Note that the q-charge is normalized, such that the branching of $\mathfrak{so}(10)\to\mathfrak{so}(8)\times\mathfrak{u}(1)$ is $(\mu_5)_{\mathfrak{so}(10)}\mapsto q^{+1}(\mu_1)_{\mathfrak{so}(8)}+q^{-1}(\mu_3)_{\mathfrak{so}(8)}$.*

E_4 quiver

For the exceptional theory of E_4, the algebra has the isomorphism $\mathfrak{e}_4\cong\mathfrak{su}(5)$. Hence, we expect to find a quiver whose Coulomb branch is the closure of the $\mathfrak{su}(5)$ minimal nilpotent orbit $\overline{\mathcal{O}}_{\text{min}}^{\mathfrak{su}(5)}$. Here, there is another novel feature in the quiver, the existence of a charge 2 hypermultiplet between the U(1) gauge group and the U(1) flavor group. The quiver takes the form:

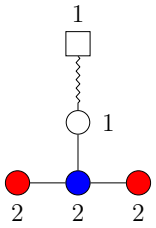

(4.32)

where the wiggly line represents the charge 2 hypermultiplet. The Hilbert series is given in Figure 4.16 and matches the moduli space of $\overline{\mathcal{O}}_{\text{min}}^{\mathfrak{su}(5)}$, along side with the Hilbert series for the orbifold moduli space with global symmetry SO(6) × U(1) .

	Hilbert Series	HWG
$\mathrm{HS}_{\mathbb{Z}}(t)$	$\frac{1+12t^2+58t^4+124t^6+170t^8+\ldots\text{palindrome}\ldots t^{16}}{(1-t^2)^4(1-t^4)^4}$ $= 1+16t^2+120t^4+560t^6+1995t^8+5824t^{10}+O\left(t^{12}\right)$	$\mathrm{PE}\big[\mu_1\mu_3t^2+t^2$ $+(\mu_1^2q^{10}+\frac{\mu_3^2}{q^{10}})t^4-\mu_1^2\mu_3^2t^8\big]$
$\mathrm{HS}_{\mathbb{Z}+\frac{1}{2}}(t)$	$\frac{8t^2(1+6t^2+17t^4+22t^6+17t^8+6t^{10}+t^{12})}{(1-t^2)^4(1-t^4)^4}$ $=8t^2+80t^4+440t^6+1680t^8+5152t^{10}+O\left(t^{12}\right)$	$(\mu_1q^5+\frac{\mu_3}{q^5})\,\mathrm{PE}\big[\mu_1\mu_3t^2+t^2$ $+\mu_1^2q^{10}t^4+\frac{\mu_3^2}{q^{10}}t^4\big]$
$\mathrm{HS}(t)$	$\frac{1+16t^2+36t^4+16t^6+t^8}{(1-t^2)^8}$ $= 1+24t^2+200t^4+1000t^6+3675t^8+10976t^{10}+O\left(t^{12}\right)$	$\mathrm{PE}\big[\mu_1\mu_3t^2+t^2$ $+(\mu_1q^5+\frac{\mu_3}{q^5})t^2-\mu_1\mu_3t^4\big]$

Figure 4.16: *Hilbert series for the E_4 magnetic quiver (4.32). The first line of the table provides the Hilbert series when the GNO magnetic lattice is integer $\mathrm{HS}_{\mathbb{Z}}(t)$, the second line shows the sum over the integers-plus-half lattice $\mathrm{HS}_{\mathbb{Z}+\frac{1}{2}}(t)$ and the last line is their sum $\mathrm{HS}(t)$. In the third column, we show the HWG in terms of fugacities for $\mathfrak{su}(4)$ (denoted $\mu_1,\ldots,\mu_3$) and $\mathfrak{u}(1)$ (denoted q). Note that the q-charge is normalized, such that the branching of $\mathfrak{su}(5)\to\mathfrak{su}(4)\times\mathfrak{u}(1)$ is $(\mu_1)_{\mathfrak{su}(5)}\mapsto q^{+1}(\mu_1)_{\mathfrak{su}(4)}+q^{-4}$.*

E_3 quiver

For the exceptional theory of E_3, the algebra has the isomorphism $\mathfrak{e}_3\cong\mathfrak{su}(3)\times\mathfrak{su}(2)$. The moduli space is a union of two hyper-Kähler cones, the closure of the $\mathfrak{su}(3)$ minimal nilpotent orbit $\overline{\mathcal{O}}_{\text{min}}^{\mathfrak{su}(3)}$ and the closure of the $\mathfrak{su}(2)$ orbit $\overline{\mathcal{O}}_{\text{min}}^{\mathfrak{su}(2)}$. We therefore expect two unitary-orthosymplectic quivers whose Coulomb branches are the two cones. The quiver for $\overline{\mathcal{O}}_{\text{min}}^{\mathfrak{su}(3)}$ cone is:

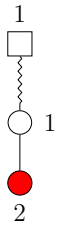

(4.33)

where the wiggly line is a charge 2 hypermultiplet and the $\overline{\mathcal{O}}_{\text{min}}^{\mathfrak{su}(2)}$ cone is the Coulomb branch of an SO(2) gauge theory with 1 flavor[17]. The Hilbert series is given in Figure 4.17 and matches the moduli space of $\overline{\mathcal{O}}_{\text{min}}^{\mathfrak{su}(3)}$, along side with the Hilbert series for the orbifold moduli space with global symmetry $\mathrm{Spin}(3)\times\mathrm{U}(1)$.

As discussed in Section 4.6, the exceptional theories can arise as the infinite coupling limit of the Higgs branch of certain 5d $\mathcal{N}=1$ theories. For the E_3 quiver, this is the Higgs branch

[17]For this quiver, the flavor is a usual charge 1 hypermultiplet and therefore one does not need to ungauge an overall $\mathbb{Z}_2$. Only the integer lattice needs to be summed.

of USp(2) gauge theory with 2 flavors at infinite coupling. At finite coupling, the two cones are the same and the moduli space is their union $\overline{\mathcal{O}}^{\mathfrak{so}(4)}_{[2,2]} \cong \overline{\mathcal{O}}^{\mathfrak{su}(2)}_{\text{min}} \cup \overline{\mathcal{O}}^{\mathfrak{su}(2)}_{\text{min}}$, where we recall that $\overline{\mathcal{O}}^{\mathfrak{su}(2)}_{\text{min}} \cong \mathbb{C}^2/\mathbb{Z}_2$. At infinite coupling, one of the two cones is enhanced to $\overline{\mathcal{O}}^{\mathfrak{su}(3)}_{\text{min}}$ whereas the other cone remains as $\overline{\mathcal{O}}^{\mathfrak{su}(2)}_{\text{min}}$.

E_2 and E_1 quivers

For the E_2 theory, the moduli space is $\overline{\mathcal{O}}^{\mathfrak{su}(2)}_{\text{min}} \cup \{\bullet\bullet\} \cong \mathbb{C}^2/\mathbb{Z}_2 \cup \{\bullet\bullet\}$ [100]. The discrete moduli space $\{\bullet\bullet\}$ is generated by the gaugino bilinear S and our quivers, which ultimately arise from brane configurations, are insensitive to it. The moduli space for E_1 is simply $\overline{\mathcal{O}}^{\mathfrak{su}(2)}_{\text{min}} \cong \mathbb{C}^2/\mathbb{Z}_2$. Therefore, for both E_2 and E_1 theories, we find a unitary-orthosymplectic quiver that has the moduli space $\mathbb{C}^2/\mathbb{Z}_2$:

(4.34)

where the wiggly line is a charge 2 hypermultiplet. The Hilbert series is given in Figure 4.18 alongside with the Hilbert series for the orbifold moduli space $\mathbb{C}^2/\mathbb{Z}_4$ with global symmetry U(1).

$\tilde{E}_1$ and E_0 quivers

In [100], we note two more members of the exceptional family: $\tilde{E}_1$ and E_0. The moduli space for $\tilde{E}_1$ is $\{\bullet\bullet\}$ and is generated by nilpotent elements that our quivers are not sensitive to. For E_0 the moduli space is trivial.

4.6 5d E_n families

Based on our paper [2].

Next, the general exceptional sequences E_n for $-\infty < n \leq 8$ are analysed. Here the negative label n may come as a surprise, but it comes as a natural extension when one studies

	Hilbert Series	HWG
$\mathrm{HS}_{\mathbb{Z}}(t)$	$\frac{1+2t^2+6t^4+2t^6+t^8}{(1-t^2)^4(1+t^2)^2}$ $= 1+4t^2+15t^4+32t^6+65t^8+108t^{10}+O\left(t^{12}\right)$	$\mathrm{PE}\left[\mu^2t^2+t^2 + \mu^2(q^6+\frac{1}{q^6})t^4-\mu^4t^8\right]$
$\mathrm{HS}_{\mathbb{Z}+\frac{1}{2}}(t)$	$\frac{4t^2(1-t+t^2)(1+t+t^2)}{(1-t^2)^4(1+t^2)^2}$ $= 4t^2+12t^4+32t^6+60t^8+108t^{10}+O\left(t^{12}\right)$	$\mu(q^3+\frac{1}{q^3})t^2\ \mathrm{PE}\left[\mu^2t^2+t^2 +\mu^2(q^6+\frac{1}{q^6})t^4-\mu^2t^4\right]$
$\mathrm{HS}(t)$	$\frac{1+4t^2+t^4}{(1-t^2)^4}$ $= 1+8t^2+27t^4+64t^6+125t^8+216t^{10}+O\left(t^{12}\right)$	$\mathrm{PE}\left[\mu^2t^2+t^2 + \mu(q^3+\frac{1}{q^3})t^2-\mu^2t^4\right]$

Figure 4.17: *Hilbert series for the E_3 magnetic quiver (4.33), representing the $\overline{\mathcal{O}}_{min}^{\mathfrak{su}(3)}$ cone in $\overline{\mathcal{O}}_{min}^{\mathfrak{e}_3}$. The first line of the table provides the Hilbert series when the GNO magnetic lattice is integer $\mathrm{HS}_{\mathbb{Z}}(t)$, the second line shows the sum over the integers-plus-half lattice $\mathrm{HS}_{\mathbb{Z}+\frac{1}{2}}(t)$ and the last line is their sum $\mathrm{HS}(t)$. In the third column, we show the HWG in terms of fugacities for $\mathfrak{su}(2)$ (denoted μ) and $\mathfrak{u}(1)$ (denoted q). Note that the q-charge is normalized, such that the branching of $\mathfrak{su}(3)\to\mathfrak{su}(2)\times\mathfrak{u}(1)$ is $(\mu_1)_{\mathfrak{su}(3)}\mapsto q^{+1}(\mu)_{\mathfrak{su}(2)}+q^{-2}$.*

USp($2k$) gauge theories with N_f fundamental flavours[18]. The relation is $n=N_f-2k+3$. The index n labels the moduli space global symmetry for $k=1$ and is then used to denote the entire sequence. Within each fixed n sequence, the members are distinguished by the rank k of the 5d $\mathcal{N}=1$ electric gauge group together with the restriction $N_f\leq 2k+5$ for the existence of a 5d fixed point [123].

4.6.1 E_n sequences of 5d $\mathcal{N}=1$ theories ($H=\ker\phi=\mathbb{Z}_2^{\mathrm{diag}}$)

The 3d $\mathcal{N}=4$ Coulomb branch of the E_n unitary-orthosymplectic quivers (with $H=\mathbb{Z}_2^{\mathrm{diag}}$) is the 5d $\mathcal{N}=1$ Higgs branch of USp($2k$) gauge theory with N_f flavors at infinite gauge coupling :

$$\mathcal{H}_{\infty}^{5d}\left(\begin{array}{c}\text{  }\\ \text{}\end{array}\right)=\mathcal{C}^{3d}\left(\begin{array}{c}E_n\text{ unitary-}\\ \text{orthosymplectic}\\ \text{quivers}\end{array}\right), \tag{4.35}$$

for $n=N_f-2k+3$. The respective magnetic quivers are shown in Figure 4.19. For the E_n sequences with $n\leq 4$, we observe charge two hypermultiplets transforming under the bifundamental of a U(1) gauge group and a U($l+1$) flavor group, with $l=k-\lfloor\frac{N_f}{2}\rfloor$. In fact, for $n\leq 4$ one can divide the exceptional E_n families into two groups, one for n even such that the

[18]The notation here is that $k=N_c$.

	Hilbert Series	HWG
$\mathrm{HS}_{\mathbb{Z}}(t)$	$\frac{(1+t^4)}{(1-t^2)^2(1+t^2)}$ $= 1+t^2+3t^4+3t^6+5t^8+5t^{10}+O\left(t^{12}\right)$	$\mathrm{PE}\left[t^2+(q^4+\frac{1}{q^4})t^4-t^8\right]$
$\mathrm{HS}_{\mathbb{Z}+\frac{1}{2}}(t)$	$\frac{2t^2}{(1-t^2)^2(1+t^2)}$ $= 2t^2+2t^4+4t^6+4t^8+6t^{10}+O\left(t^{12}\right)$	$(q^2+\frac{1}{q^2})t^2\ \mathrm{PE}\left[t^2+(q^4+\frac{1}{q^4})t^4-t^4\right]$
$\mathrm{HS}(t)$	$\frac{\left(\ 1+t^2\ \right)}{(1-t^2)^2}$ $= 1+3t^2+5t^4+7t^6+9t^8+11t^{10}+O\left(t^{12}\right)$	$\mathrm{PE}\left[t^2+(q^2+\frac{1}{q^2})t^2-t^4\right]$

Figure 4.18: *Hilbert series for the E_2 magnetic quiver (4.34). The first line of the table provides the Hilbert series when the GNO magnetic lattice is integer $\mathrm{HS}_{\mathbb{Z}}(t)$, the second line shows the sum over the integers-plus-half lattice $\mathrm{HS}_{\mathbb{Z}+\frac{1}{2}}(t)$ and the last line is their sum $\mathrm{HS}(t)$. In the third column, we show the HWG in terms of fugacities for $\mathfrak{u}(1)$ (denoted q). Note that the q-charge is normalized such that the branching of $\mathfrak{su}(2)\to\mathfrak{u}(1)$ is $(\mu)_{\mathfrak{su}(2)}\mapsto q^{+1}+q^{-1}$.*

moduli space is a single cone and one for n odd where the moduli space is a union of two cones.

E_{4-2l} family. For n even, the families are E_4, E_2, E_0, E_{-2}, E_{-4}, ... The parameter l, introduced above, characterizes the group E_{4-2l}, where $l+1$ is the number of charge 2 hypermultiplets.

E_{3-2l} family. Similarly, the group where n is odd consists of E_3, E_1, E_{-1}, E_{-3}, ... and we can characterize them by E_{3-2l}. Again, the number of charge 2 hypermultiplets equals $l+1$. The Higgs branch of USp($2k$) gauge group with $2k-2l$ flavors at finite gauge coupling is $\overline{\mathcal{O}}^{\mathfrak{so}(4k-4l)}_{[2^{2k-2l}]}$. This is known in the literature as *very even* D-type orbits and the space is the union of two identical hyper-Kähler cones. Each cone is given by the Coulomb branch of the flavoured orthosymplectic quiver in Figure 4.20. The intersection between both cones is non-trivial and equals a nilpotent orbit of type $\overline{\mathcal{O}}^{\mathfrak{so}(4k-4l)}_{[2^{2k-2l-2},1^4]}$. In the infinite coupling limit, one of the two cones gets enhanced and is given by the Coulomb branch of the unitary-orthosymplectic quiver listed in the last row of Figure 4.19. Importantly, the intersection between the two cones at infinite coupling is the same as the intersection at finite coupling.

4.6.2 Rank 0 limit

When $k=1$, the quiver families return the E_n theories. If we go further down to $k=0$, the resulting theories become free. This is clear from the electric quiver where the Higgs branch

at infinite gauge coupling consists of free hypermultiplets. We tabulate all the non-trivial $k = 0$ cases in Figure 4.21. Due to the fact that the moduli space is $\mathbb{H}^l$, for some l, the global symmetry is enhanced to USp($2l$). The branching rule of the enhanced global symmetry is also tabulated. These can be viewed as $5d$ rank zero theories.

4.6.3 Global symmetry

By studying the different highest weight fugacities that appear in the HWG, we can determine exactly the global symmetry group and not just its algebra by looking at the HWG. These are provided in Figure 4.19 and 4.22.

4.6.4 Dimension of 3d $\mathcal{N} = 4$ Higgs branch

We now turn our attention to the *Higgs branch* of the families of 3d $\mathcal{N} = 4$ unitary-orthosymplectic magnetic quivers in Figure 4.19. The quaterionic dimension of the Higgs branch of *all* the quivers in the families is k. This is not surprising, as they are magnetic quivers for a 5d theory with rank k gauge group. This offers another non-trivial check for the existence of charge 2 hypermultiplets in E_{4-2l} and E_{3-2l} which gives the correct Higgs branch dimension.

4.6.5 E_n sequences of 5d $\mathcal{N} = 1$ theories ($H = \{1\}$)

Now, we can investigate the orthosymplectic quivers of the E_n sequences where the discrete group is $H = \{1\}$. The Coulomb branches here are $\mathbb{Z}_2$ orbifolds of those in Figure 4.19. The $\text{HWG}_{\mathbb{Z}}$ of the orbifolds are easily obtained with the $\mathbb{Z}_2$ action -1 on the spinors. The results are tabulated in Figure 4.22.

Orthosymplectic Quiver	Global Symmetry	PL[HWG]
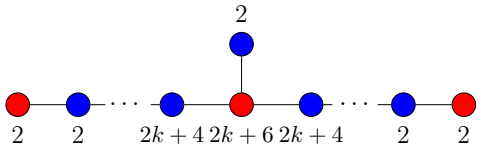	$E_8 \quad (k=1)$ $\mathrm{Ss}(4k+12) \quad (k>1)$	$\sum_{i=1}^{k+2} \mu_{2i} t^{2i} + t^4 + \mu_{2k+6}\left(t^{k+1}+t^{k+3}\right)$
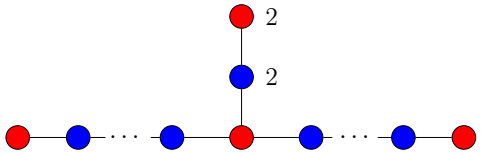	$E_7/\mathbb{Z}_2 \quad (k=1)$ $(\mathrm{Ss}(4k+8)\times \mathrm{Spin}(3))/\mathbb{Z}_2 \quad (k>1)$	$\sum_{i=1}^{k+1} \mu_{2i} t^{2i} + \nu^2 t^2 + t^4 + \nu\mu_{2k+4}\left(t^{k+1}+t^{k+3}\right) + \mu_{2k+4}^2 t^{2k+4} - \nu^2\mu_{2k+4}^2 t^{2k+6}$
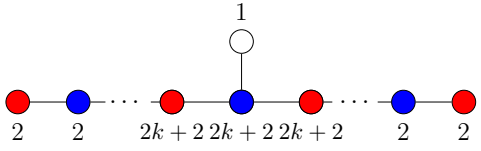	$E_6/\mathbb{Z}_3 \quad (k=1)$ $\mathrm{Spin}(4k+6)\times \mathrm{U}(1) \quad (k>1)$	$\sum_{i=1}^{k} \mu_{2i} t^{2i} + t^2 + \left(\mu_{2k+2} q + \mu_{2k+3}\frac{1}{q}\right) t^{k+1}$
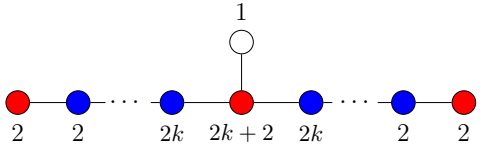	$E_5/\mathbb{Z}_4 \cong \mathrm{Spin}(10)/\mathbb{Z}_4 \quad (k=1)$ $\mathrm{Ss}(4k+4)\times \mathrm{U}(1) \quad (k>1)$	$\sum_{i=1}^{k} \mu_{2i} t^{2i} + t^2 + \mu_{2k+2}\left(q+\frac{1}{q}\right) t^{k+1}$
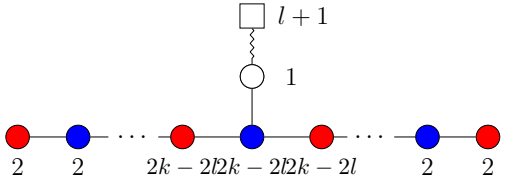	$E_4/\mathbb{Z}_5 \cong \mathrm{PSU}(5) \quad (k=1 \,\&\, l=0)$ $\mathrm{SU}(2)\subset E_2 \quad (k=l=1)$ $\mathrm{U}(1) \quad (k=l\neq 1)$ $\mathrm{Spin}(4k-4l+2)\times \mathrm{U}(1) \quad \text{otherwise}$	$\sum_{i=1}^{k-l-1} \mu_{2i} t^{2i} + t^2 + \mu_{2k-2l}\mu_{2k-2l+1} t^{2k-2l} - \mu_{2k-2l}\mu_{2k-2l+1} t^{2k+2} + \left(\mu_{2k-2l} q + \mu_{2k-2l+1}\frac{1}{q}\right) t^{k+1}$
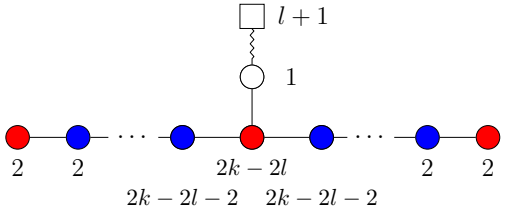	$\mathrm{SU}(3)\subset E_3 \quad (k=1 \,\&\, l=0)$ $E_1 \cong \mathrm{SU}(2) \quad (k=l=1)$ $\mathrm{U}(1) \quad (k=l\neq 1)$ $\mathrm{Ss}(4k-4l)\times \mathrm{U}(1) \quad \text{otherwise}$	$\sum_{i=1}^{k-l-1} \mu_{2i} t^{2i} + t^2 + \mu_{2k-2l}^2 t^{2k-2l} - \mu_{2k-2l}^2 t^{2k+2} + \mu_{2k-2l}\left(q+\frac{1}{q}\right) t^{k+1}$

Figure 4.19: *The unitary-orthosymplectic E_n families. The discrete group here is chosen to be $H = \ker\phi = \mathbb{Z}_2^{\mathrm{diag}}$. We also provide the Hilbert series in the form of Highest Weight Generating (HWG) functions where μ_i, ν and q are the Dynkin fugacities of the (non-exceptional) global symmetry. In the second row, the $\mathbb{Z}_2$ acts as -1 simultaneously on ν and μ_{2k+4}. The wiggly line represents a hypermultiplet of charge 2. The last two rows are the E_{4-2l} and E_{3-2l}(larger cone) families.*

Family	Orthosymplectic Quiver	Global Symmetry	PL[HWG]
E_{3-2l} (smaller cone)	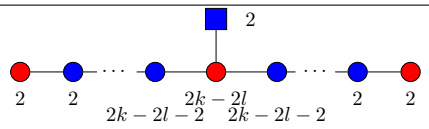	SO(4k − 4l)	$\sum_{i=1}^{k-l-1} \mu_{2i} t^{2i} + \mu_{2k-2l-1}^2 t^{2k-2l}$

Figure 4.20: *The smaller cone of the E_{3-2l} family along with the global symmetry and HWG. The HWG contains the spinor fugacity $\mu_{2k-2l-1}$ because the larger cone in Figure 4.19 contains the other spinor fugacity μ_{2k-2l}. This originates from the finite coupling case where the two cones are the same, but the HWG for each of them carries one of the two spinor fugacities. Their union then contains both spinors fugacities and the intersection contains neither spinors.*

Family	$k=0$ Orthosymplectic Quiver	Global Symmetry	Hilbert Series	Branching rules
E_8	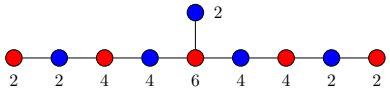	USp(32)	$\frac{1}{(1-t)^{32}}$	$[1,0,\ldots,0]_{\mathfrak{usp}(32)} \to$ $[0,0,0,0,0,1]_{\mathfrak{so}(12)}$
E_7	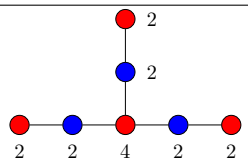	USp(16)	$\frac{1}{(1-t)^{16}}$	$[1,0,\ldots,0]_{\mathfrak{usp}(16)} \to$ $[0,0,0,1;1]_{\mathfrak{so}(8)\times\mathfrak{su}(2)}$
E_6	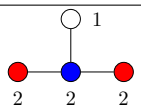	USp(8)	$\frac{1}{(1-t)^{8}}$	$[1,0,0,0]_{\mathfrak{usp}(8)} \to$ $(q[0,1,0]+\frac{1}{q}[0,0,1])_{\mathfrak{so}(6)\times\mathfrak{u}(1)}$
E_5		USp(4)	$\frac{1}{(1-t)^{4}}$	$[1,0]_{\mathfrak{usp}(4)} \to$ $(q+\frac{1}{q})[1]_{\mathfrak{su}(2)\times\mathfrak{u}(1)}$
E_4		USp(2)	$\frac{1}{(1-t)^{2}}$	Trivial
E_3		USp(2)	$\frac{1}{(1-t)^{2}}$	Trivial

Figure 4.21: *The $k=0$ limit of the family of E_n quivers in Figure 4.19. The choice of discrete group is $H=\mathbb{Z}_2$. For $n<3$, the $k=0$ limit is trivial. The last column lists the branching rules for the fundamental representation of the* USp *global symmetry group of the free theory to the global symmetry group in the $k=0$ limit of Figure 4.19. Note the nice pattern of power of 2.*

Orthosymplectic Quiver	Global Symmetry	PL[HWG]
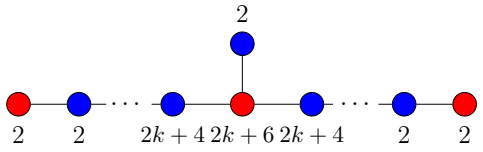	$\mathrm{PSO}(4k+12) \quad (k \geq 1)$	$\sum_{i=1}^{k+2} \mu_{2i} t^{2i} + t^4 + \mu_{2k+6}^2 \left(t^{2k+2} + t^{2k+4} + t^{2k+6}\right) - \mu_{2k+6}^4 t^{4k+8}$
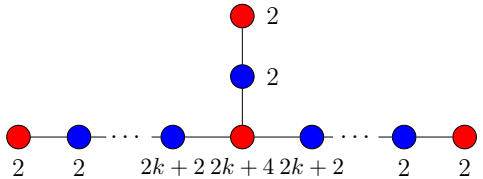	$\mathrm{PSO}(4k+8) \times \mathrm{PSU}(2) \quad (k \geq 1)$	$\sum_{i=1}^{k+1} \mu_{2i} t^{2i} + \nu^2 t^2 + t^4 + \nu^2 \mu_{2k+4}^2 \left(t^{2k+2} + t^{2k+4}\right) + \mu_{2k+4}^2 t^{2k+4} - \nu^4 \mu_{2k+4}^4 t^{4k+8}$
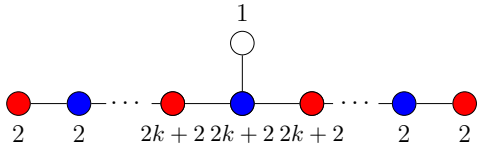	$\mathrm{SO}(4k+6) \times \mathrm{U}(1) \quad (k \geq 1)$	$\sum_{i=1}^{k} \mu_{2i} t^{2i} + t^2 + \left(\mu_{2k+2}^2 q^2 + \mu_{2k+2}\mu_{2k+3} + \mu_{2k+3}^2 \frac{1}{q^2}\right) t^{2k+2} - \mu_{2k+2}^2 \mu_{2k+3}^2 t^{4k+4}$
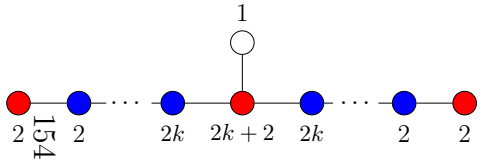	$\mathrm{PSO}(4k+4) \times \mathrm{U}(1) \quad (k \geq 1)$	$\sum_{i=1}^{k} \mu_{2i} t^{2i} + t^2 + \mu_{2k+2}^2 \left(q^2 + 1 + \frac{1}{q^2}\right) t^{2k+2} - \mu_{2k+2}^4 t^{4k+4}$
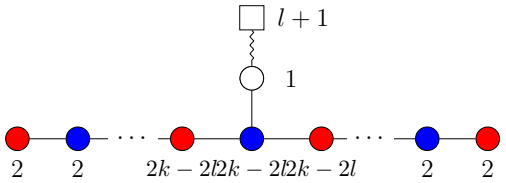	$\mathrm{U}(1) \quad (k = l)$ $\mathrm{SO}(4k-4l+2) \times \mathrm{U}(1) \quad \text{otherwise}$	$\sum_{i=1}^{k-l-1} \mu_{2i} t^{2i} + t^2 + \mu_{2k-2l}\mu_{2k-2l+1} t^{2k-2l} - \mu_{2k-2l}\mu_{2k-2l+1} t^{2k+2} + \left(\mu_{2k-2l}^2 q^2 + \mu_{2k-2l+1}^2 \frac{1}{q^2}\right) t^{2k+2} - \mu_{2k-2l}\mu_{2k-2l+1} t^{4k+4}$
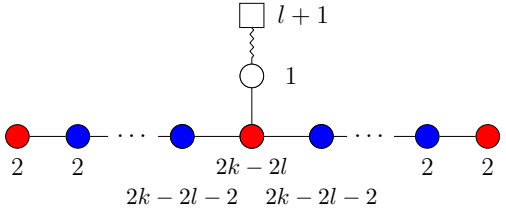	$\mathrm{U}(1) \quad (k = l)$ $\mathrm{PSO}(4k-4l) \times \mathrm{U}(1) \quad \text{otherwise}$	$\sum_{i=1}^{k-l-1} \mu_{2i} t^{2i} + t^2 + \mu_{2k-2l}^2 t^{2k-2l} - \mu_{2k-2l}^2 t^{2k+2} + \mu_{2k-2l}^2 \left(q^2 + \frac{1}{q^2}\right) t^{2k+2} - \mu_{2k-2l}^4 t^{4k+4}$

Figure 4.22: *The unitary-orthosymplectic E_n families. The discrete group here is chosen to be $H = \{1\}$. The Coulomb branches are $\mathbb{Z}_2$ orbifolds of those in Figure 4.19. We also provide the Hilbert series in the form of Highest Weight Generating (HWG) functions where μ_i, ν and q are the Dynkin fugacities of the (non-exceptional) global symmetry. The wiggly line represents a hypermultiplet of charge 2. The last two rows are the E_{4-2l} and E_{3-2l}(larger cone) families.*

Duality between unitary and unitary-orthosymplectic magnetic quivers

Based on our work in [4]

For SQCD theories with $Sp(N_c)$ gauge group and non-trivial 5d fixed point, they each have two equivalent choices of magnetic quivers: an unitary quiver and an unitary-orthosymplectic quiver. The unitary quivers coincide with those in the fourth region in section 4.1 with $|\kappa| = N_c - \frac{N_f}{2} + 2$ and are listed in Table 4.7. The unitary-orthosymplectic quivers are those we just covered in the E_n families. This phenomenon occurs due to a duality between $SU(N_c + 1)$ theory with N_f flavors and $\kappa = N_c + 3 - N_f/2$ and $Sp(N_c)$ theory with N_f flavors at the 5d UV fixed point [17]. In terms of brane systems, the unitary quivers can be obtained using O7 planes as outlined in [3] and orthosymplectic quivers obtained using O5 planes as previously demonstrated in section 3.3.3. As a result, the Higgs branches of the two theories at the fixed point, and subsequently the Coulomb branch of the magnetic quivers, are the same. The two sets of magnetic quivers are given in Table 4.9.

Surprisingly, we found in [4] that the two sets of magnetic quivers agree more than just their $3d$ $\mathcal{N} = 4$ Coulomb branch. In fact, the $3d$ $\mathcal{N} = 4$ Higgs branch are the same as well. For example, both the unitary and the orthosymplectic Higgs branch of the E_8 quiver are $\mathbb{C}^2/\Gamma_{E_8}$. Also, the superconformal indices which we computed for $N_c = 1$ cases are shown to match as well (perturbatively up to the order we were able to compute). The details are in Appendix B.

In addition, we also computed expectation values of extended objects such as Wilson lines using the topologically twisted indices. To be exact, these are twisted partition functions on $S^1 \times S^2$ with a topological twist along the S^2. A topological twist with the Cartan subgroup of $SU(2)_R$ leads to an A-twisted index whereas a twist in the Cartan subgroup of $SU(2)_L$ leads to the B-twisted index. As a reminder, these are subgroups of our $3d$ $\mathcal{N} = 4$ R-symmetry group $SU(2)_L \times SU(2)_R$. It was conjectured in [124] that the A twisted index and B-twisted index computes the $3d$ $\mathcal{N} = 4$ Coulomb branch Hilbert series and Higgs branch Hilbert series respectively. For A-twisted index, one can employ techniques such as Bethe Ansatz summation [125, 124], which we show to be consistent with computation from the monopole formula for some SQED theories in [4]. For B-twisted index, the general formula applies to twisted functions for $S^1 \times \Sigma$ for some 2d Riemann surface, whereas the case of $\Sigma = S^2$, the twisted index is

identical to our Molien-Weyl formula.

With the B-twisted index, we can also compute expectation value of the Wilson lines. The B-twisted index with inclusion of Wilson lines is given as:

$$\mathbb{I}^B(t) = \oint_{\text{JK}} \prod_{\text{gauge}} \frac{1}{|W_G|} \left[\frac{dz}{2\pi i z}\right] Z^B_{\text{vec}}(z) \prod_{\text{matter}} Z^B_{\text{chiral}}(z)\, \mathcal{W}(z)\,, \tag{4.36}$$

where the contributions from a vector multiplet and a chiral multiplet are

$$Z^B_{\text{vec}}(z) = \left(t - t^{-1}\right)^{\text{rk}(G)} \prod_{\alpha\in\Delta} \left(1 - z^\alpha\right)\left(t - z^\alpha t^{-1}\right)\,, \tag{4.37a}$$

$$Z^B_{\text{chiral}}(z) = \prod_{w\in R} \frac{z^{\frac{w}{2}} t^{\frac{1}{2}}}{1 - z^w t}\,. \tag{4.37b}$$

We were able to find a non-trivial matching between the Wilson lines on the unitary quiver and their unitary-orthosymplectic counterparts. The results of the matching and the twisted indices are given in [4]. Another interesting detail is that when $H = \{1\}$ for unframed/flavorless orthosymplectic quivers, we find that the expectation value of Wilson lines vanishes. This is consistent with known results that the presence of a $\mathbb{Z}_2$ one-form symmetry means Wilson lines in the fundamental representation will vanish. This shows the $\mathbb{Z}_2$ subgroup we quotient from the orthosymplectic quivers is indeed the one-form symmetry. This is an interesting find since the Higgs branch Hilbert series is insensitive to the $(\mathbb{Z}_2)_{\text{diag}}$ subgroup and will return the same Hilbert series whether or not it is quotiented out. On the other hand, the B-twisted index for Wilson lines are sensitive to this discrete group. This adds to our arsenal of tools that will help us explore how discrete subgroups in gauge/global symmetries affect the moduli spaces of gauge theories.

This duality offers a rich connection between unitary and orthosymplectic quivers. For example, certain computations are much simpler when performed on orthosymplectic quivers than their unitary counterparts. On the other hand Hilbert series refinement, which is notoriously difficult for orthosymplectic quivers, is straightforward for unitary ones. One possible extension in the future is to see if certain properties that are hidden in the unitary quiver of well known theories (such as the E_n Dynkin quivers) can be made apparent from their orthosymplectic

counterparts. For instance, there is always a $\mathbb{Z}_2$ outer automorphism for the E_n orthosymplectic quivers but not present in the unitary ones. This useful property will make an appearance in a later section.

4.7 Product theories and Forked quivers ($Sp(N_c)$ SQCD theories)^2

Based on our paper [5]

Another interesting phenomenon that arises for orthosymplectic quivers is that the Coulomb branch of a single quiver can be the product of two moduli spaces. This multiplicity was first observed in class $\mathcal{S}$ theories in [114] and further studied in [126, 127, 128]. In the context of magnetic quivers of 5d theories, this was later studied in [106]. Following these results, we discovered in [5] that a unique feature of orthosymplectic quivers that exhibits such products is a balanced subset of nodes that forms a *fork*.

In a *forked quiver*[19], the set of gauge nodes are arranged in the shape of a D-type Dynkin diagram. Forked quivers are non-linear quivers in the sense that the gauge groups are not arranged in a single line. This is in contrast to the ABC-type orthosymplectic quivers, which are a linear chain of gauge nodes. The Coulomb branch global symmetry of forked orthosymplectic quivers has been conjectured in [62, Sec. 7.4]: For a balanced fork composed of m gauge nodes (i.e. *all* gauge nodes are balanced)

$$G_{\text{global}} = \text{SO}(m) \times \text{SO}(m) \qquad (4.38)$$

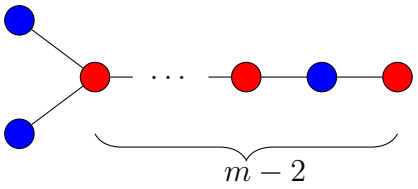

the global symmetry is a product. If there is a balanced $SO(2)$ gauge node, then the global symmetry is enhanced to $\text{SO}(m+1) \times \text{SO}(m+1)$. This is verified through explicit Hilbert series computations for multiple examples, and the rule (4.38) remains the same regardless of the rank of the gauge groups as long as they are balanced. Even if the tail begins with Sp gauge

[19]This term is first used in [129].

group or if the two bifurcated nodes are SO gauge groups, the global symmetry remains the same. Furthermore, for unframed forked quivers, the integer-plus-half contributions can further enhance the global symmetry such as to exceptional symmetries as we will see.

In order for the Coulomb branch of a quiver to be a product of Coulomb branches of two theories, the global symmetry must be the product of (at least) two non-Abelian groups. This allows to argue that quivers with such a feature are natural candidates for product theories.

$E_n \times E_n$ family

In [5], we list all possible orthosymplectic quivers with a balanced fork that satisfies a set of conditions. Amongst them, are magnetic quivers of products of 5d SCFTs which we will now discuss.

Product of rank 1 theories. The $E_n \times E_n$ orthosymplectic quivers whose Coulomb branches are the product of two minimal nilpotent orbit closures of $\mathfrak{e}_n$ are displayed in Table 4.10. For these quivers, integer-plus-half contributions enhances the Coulomb branch global symmetry. When this enhancement happens, (4.38) no longer predicts the correct global symmetry and explicit Hilbert series computations are required. For $4 \leq n \leq 8$, the Coulomb branch Hilbert series are computed and, upon taking the square root, are compared with the known Hilbert series of $\overline{\mathcal{O}}_{\text{min}}^{\mathfrak{e}_n}$. Details are provided in Table B.36.

For the $n = 6, 7, 8$ cases of Table 4.10, the orthosymplectic quivers can be understood as class $\mathcal{S}$ theories with untwisted D_4, D_5, and D_7 punctures, respectively. For $n = 6$, the $E_6 \times E_6$ orthosymplectic quiver already appeared in [19]. For $n = 7$, the orthosymplectic quiver is derived in [106] using brane webs and O5 planes.

General product families. In the previous section, the E_n orthosymplectic quivers have been extended to infinite families for each n. The orthosymplectic quivers in Table 4.10 can be extended in a similar fashion to the infinite families shown in Table 4.11. These magnetic quivers describe the Higgs branches of two copies of 5d $\mathcal{N} = 1$ Sp(k) SQCD theories at the UV fix point, see Section 4.7. For $n < 8$ and small k, Coulomb branch Hilbert series have been computed, see Table B.36, and compared against the results (after taking their products) in

[2]. Also, the Coulomb branch dimension, computed directly from the quiver, is compared and agreement is found for all the infinite sequences.

The dashed line here represents fundamental-fundamental hypermultiplets which have been introduced in [105]. The appearing 5d $\mathcal{N} = 1$ SQCD theories exhaust *all* Sp(m) gauge theories with the allowed range $0 \leq N_f \leq 2m + 5$ of fundamental flavours, with $m \geq 1$.

5 branes with O5-O7-ON planes

One can also construct the brane systems for these 5d product theories. It has been shown in [62] that for 3d gauge theories, an intersection of O3 and O5 plane will also generate an ON plane [39] (which is the S-dual of an O5 plane). We can apply the same idea to 5d brane webs where the orientifolds are now an O5 and O7 plane with an ON at the intersection. The results are detailed in [5] and from the brane webs one can straight away read off the forked orthosymplectic magnetic quivers. There, we also discussed how the product structure arises in the brane webs.

Table 4.9: *Magnetic quivers at infinite coupling. The $5d$ $\mathcal{N}=1$ duality between "Theory SU" and "Theory Sp" has been observed in [17], also [18]. The wiggly link denotes a charge 2 hypermultiplet. The "Magnetic quiver OSp" and "Magnetic Quiver U" are obtained in [3]. For $k=0$, the moduli spaces are free hypermultiplets transforming as spinors of the global symmetry. The "Magnetic quiver OSp" for $E_{8,7,6}$ can be obtained from class S [19, 20].*

Family	Theory SU	Theory Sp	Magnetic quiver U	Magnetic quiver OSp
E_8	$2k+5$  $\mathrm{SU}(k+1)_{\pm\frac{1}{2}}$	D_{2k+5}  $\mathrm{Sp}(k)$	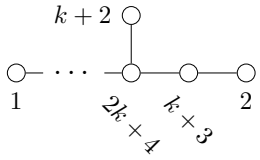	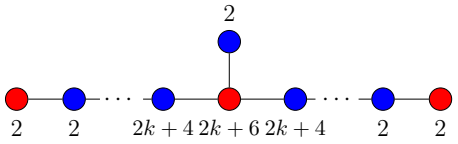
E_7	$2k+4$  $\mathrm{SU}(k+1)_{\pm 1}$	D_{2k+4}  $\mathrm{Sp}(k)$	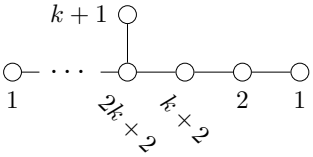	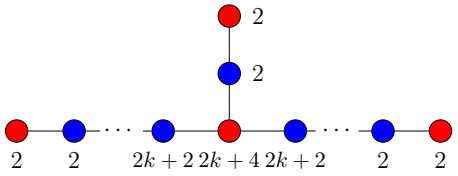
E_6	$2k+3$  $\mathrm{SU}(k+1)_{\pm\frac{3}{2}}$	D_{2k+3}  $\mathrm{Sp}(k)$	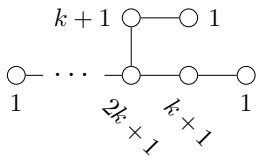	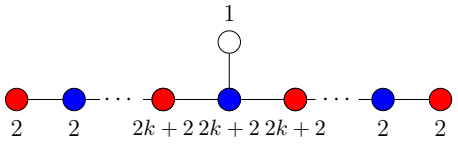
E_5	$2k+2$  $\mathrm{SU}(k+1)_{\pm 2}$	D_{2k+2}  $\mathrm{Sp}(k)$	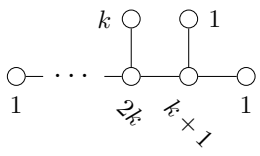	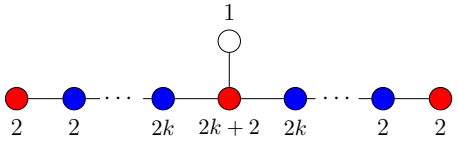
E_{4-2l} $k\geq l\geq 0$	$2k-2l+1$  $\mathrm{SU}(k+1)_{\pm(\frac{5}{2}+l)}$	$D_{2k-2l+1}$  $\mathrm{Sp}(k)$	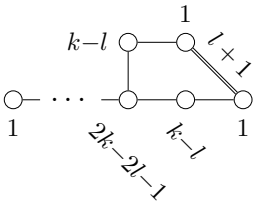	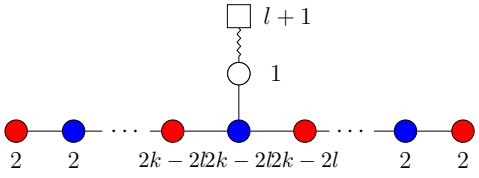
E_{3-2l} $k\geq l\geq 0$	$2k-2l$  $\mathrm{SU}(k+1)_{\pm(3+l)}$	D_{2k-2l}  $\mathrm{Sp}(k)$	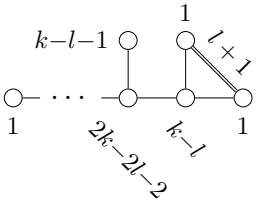 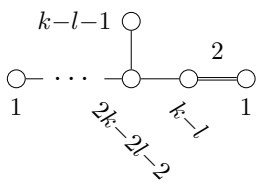	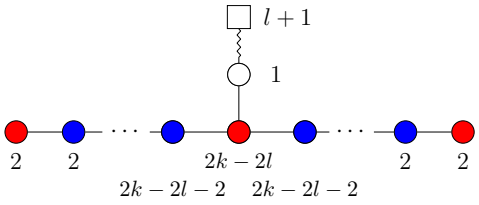 Cannot be read from brane diagram

Table 4.10: *The Coulomb branches of orthosymplectic quivers are products of two copies of the minimal nilpotent orbits closures of exceptional algebras $\mathfrak{e}_n$ for $n = 4, \ldots, 8$. The numbers coloured in red represent gauge nodes that are overbalanced.*

Orthosymplectic quiver	Coulomb branch
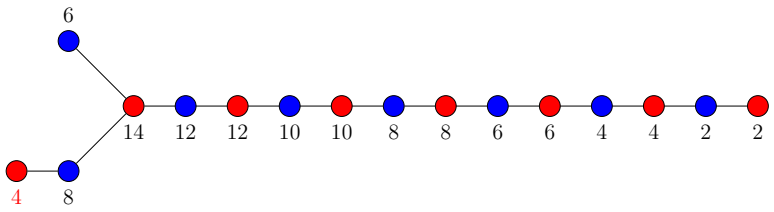	$\overline{\mathcal{O}}^{\mathfrak{e}_8}_{\text{min}} \times \overline{\mathcal{O}}^{\mathfrak{e}_8}_{\text{min}}$
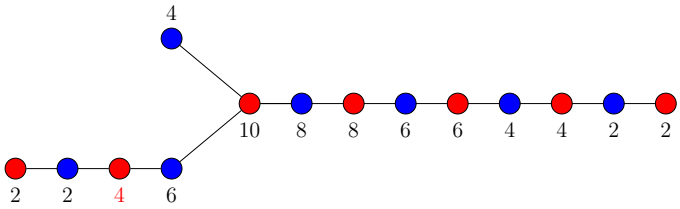	$\overline{\mathcal{O}}^{\mathfrak{e}_7}_{\text{min}} \times \overline{\mathcal{O}}^{\mathfrak{e}_7}_{\text{min}}$
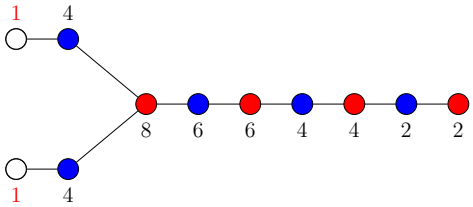	$\overline{\mathcal{O}}^{\mathfrak{e}_6}_{\text{min}} \times \overline{\mathcal{O}}^{\mathfrak{e}_6}_{\text{min}}$
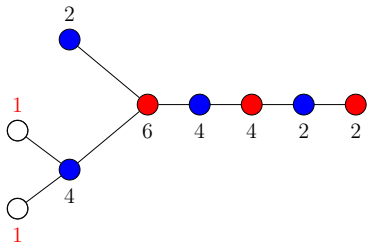	$\overline{\mathcal{O}}^{\mathfrak{so}(10)}_{\text{min}} \times \overline{\mathcal{O}}^{\mathfrak{so}(10)}_{\text{min}}$
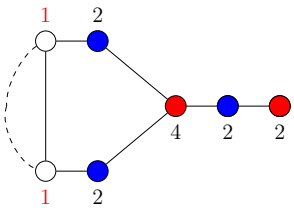	$\overline{\mathcal{O}}^{\mathfrak{su}(5)}_{\text{min}} \times \overline{\mathcal{O}}^{\mathfrak{su}(5)}_{\text{min}}$

Table 4.11: *The extended infinite families of the orthosymplectic quivers in Table 4.10. The Coulomb branch of the forked orthosymplectic quivers on the left are the same as the Coulomb branch of product theories on the right. The numbers coloured in red represent gauge nodes that are overbalanced.*

Family	Orthosymplectic quiver	Products
$(E_8)^2$	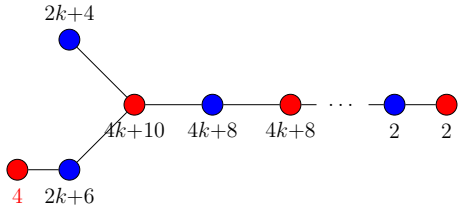	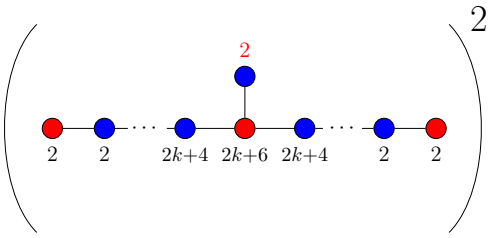
$(E_7)^2$	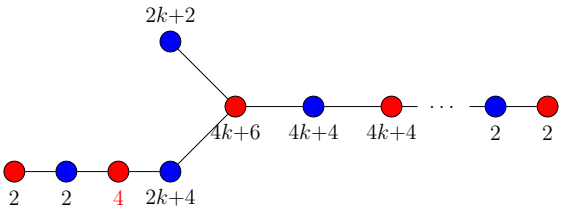	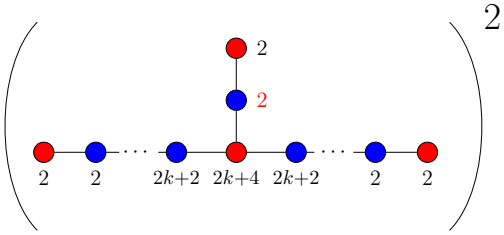
$(E_6)^2$	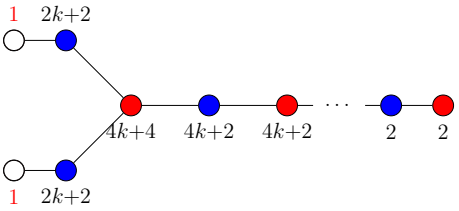	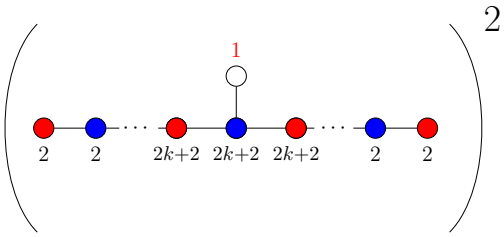
$(E_5)^2$	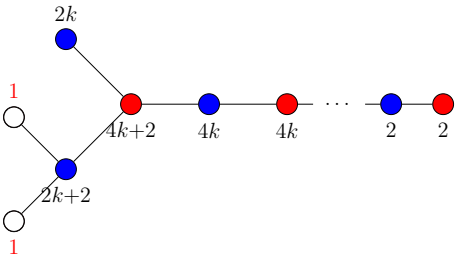	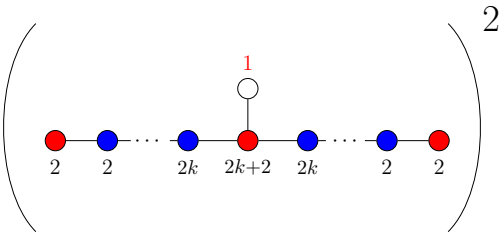
$(E_{4-2l})^2$	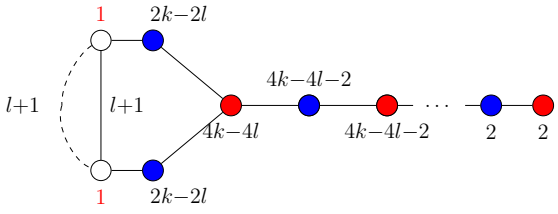	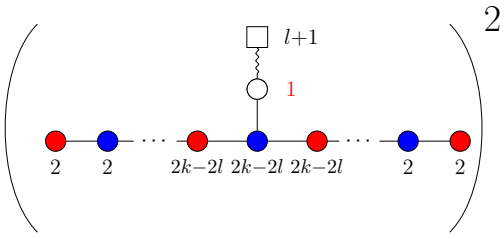
$(E_{3-2l})^2$	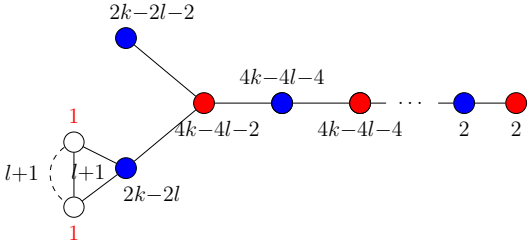	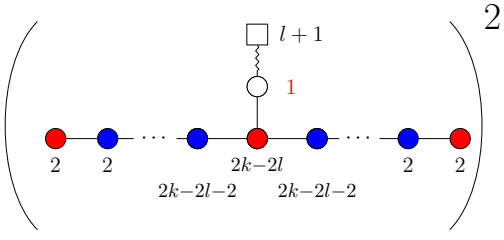

Chapter 5

Four dimensional gauge theories

In this chapter we look at $4d$ $\mathcal{N} = 2$ gauge theories, with a particular focus on SCFTs. Since we are living in a four dimensional universe, 4d gauge theories had always received more attention than theories in other dimensions. The usual approach to these theories is to study the Lagrangian in the UV and flow to a strongly coupled fixed point in the IR. However, *most* 4d theories at the superconformal fixed point do not have Lagrangian descriptions and they often lack a weakly coupled description as well. In this section, we will see examples of such theories and outline how we can nevertheless extract the corresponding magnetic quivers.

The simplest 4d $\mathcal{N} = 2$ SCFTs are $SU(N_c)$ gauge theories with $N_f = 2N_c$. Here, the beta function vanishes and we have a superconformal fix point. The theory has a Lagrangian description and their Higgs branches are hyperKähler quotients. The geometry of the Higgs branches are known as height two nilpotent orbit closures of $\mathfrak{su}(2N_c)$. However, unlike in $d = 3, 5, 6$, many of the known 4d SCFTs are non-Lagrangian and do not have a known effective quiver description. Examples include Argyres-Douglas theories, class $\mathcal{S}$ theories, $\mathcal{S}$-folds etc. [1] On the other hand, the lack of Lagrangian descriptions did not deter the progress in understanding these SCFTs. Many powerful tools were developed to analyse these theories including studying the Coulomb branch using Seiberg-Witten curves and counting the spectrum of operators according to their scaling dimension. Another powerful tool is the superconformal

[1] Of course, some of these theories do have Lagrangian descriptions. In particular, some families of Argyres-Douglas theories were shown to be described by quiver gauge theories with mixed unitary and special unitary gauge groups.

index which is a trace over the states in an SCFT in radial quantization. Furthermore, special limits to the superconformal index such as the Macdonald index, Hall-Littlewood index and Schur index are important on their own right, each computing a different spectrum of operators. In particular, the Schur index allows one to study the vertex operator algebra (VOA) associated with the SCFT. And, in some special cases such as class $\mathcal{S}$ theories with zero genus, the Hall-Littlewood index also returns the Higgs branch Hilbert series which allows one to study the chiral ring. These are of course only some of the tools used to study these theories, others include compactification from 5d and 6d theories that we have more control over (for example whats known in the literature as geometric engineering). Furthermore, one can compute and match anomaly polynomials associated with the t'Hooft and Weyl anomalies in the theory that are invariant under RG flows.

Over the decades, there were many papers written on the Coulomb branch of 4d SCFTs whilst their Higgs branches were less frequented. This is unfortunate since the Higgs branch is a very interesting object and has a rich structure as well (arguably much richer since the geometry is hyperKähler and their chiral ring are almost never freely generated). The lack of study can be attributed to the absence of a hyperKähler quotient construction since most of the theories are non-Lagrangian. This again demonstrates the importance of the magnetic quiver as they will help us crack open the Higgs branch of these SCFTs. The obvious question is then: how do we construct such magnetic quivers?

This chapter is broken into two parts. The first part concerns magnetic quivers of rank one 4d SCFTs that were obtained through a) Bottom-Up approach as described in the previous chapter and b) from *folding* magnetic quivers of 5d SCFTs. These magnetic quivers are then generalized to infinite families. The second part focuses on the magnetic quiver of $\mathcal{S}$-fold theories.

5.1 Rank one 4d $\mathcal{N} = 2$ SCFTs

Based on our paper [6]

It had been conjectured that rank zero 4d $\mathcal{N} = 2$ SCFTs do not exist [66], so the simplest

theories we will start with are rank one SCFTs. Rank one here meaning the 4d Coulomb branch has one complex dimension. Recently, there has been attempts [66, 130, 131, 132] to classify all possible 4d rank one SCFTs. Some on the list are theories we are already familiar with such as $SU(2)$ with 4 flavors and $E_{6,7,8}$ Minahan-Nemeschansky theories [133]. The Higgs branches of these theories are well known and the corresponding magnetic quivers are D_4, $E_{6,7,8}$ affine Dynkin quivers with unitary gauge nodes respectively. There are also the rank one Argyres-Douglas theories labelled by the global symmetry A_0, A_1, A_2 [73] whose 3d mirrors can be constructed using class $\mathcal{S}$ techniques [134]. Others on the list are less familiar and are labelled by the Higgs branch global symmetry G_F. A brief introduction to these theories is given in Appendix C.

The classification gives a list of 17 rank 1 $\mathcal{N} = 2$ SCFTs (not counting IR-free theories). The list of 17 SCFTs is presented in the right part of Table 5.1. Alternatively, the theories can be obtained from $\mathbb{Z}_k$ $\mathcal{N} = 2$ S-fold constructions [135], from the compactification of $(1, 0)$ $6d$ SCFTs with non-trivial global symmetry background [136], or from $\mathbb{Z}_k$ twisted compactification from 5d $\mathcal{N} = 1$ SCFTs, as explained in more detail in Section 5.13.

5.1.1 Magnetic quivers

In this section, the magnetic quivers Q of the $4d$ $\mathcal{N} = 2$ rank 1 SCFTs are presented. The $3d$ $\mathcal{N} = 4$ Coulomb branches of the magnetic quivers are equal to the Higgs branches of the rank 1 SCFTs. Out of the 17 rank one theories, the magnetic quivers for 11 of them are already known in the literature. This section serves to present the magnetic quivers for the remaining 6 as given in Table 5.8. These magnetic quivers are all unframed/flavorless non-simply laced unitary quivers. Being unframed/flavorless means an overall $U(1)$ gauge group needs to be decoupled from the magnetic quiver as usual. However, since the theory is non-simply laced, the resulting Coulomb branch will actually be different depending on whether we ungauge the $U(1)$ on a long node or short node (in the sense of long and short roots in Lie algebra). Long nodes are the ones on the side where the non-simply laced edge points away from and short nodes are the ones pointed towards at. For non-simply laced unitary quivers, we will always ungauge on a long node. Ungauging on the short node does not give the right answer and one

Table 5.1: *`Left:` List of the seven singular Coulomb branch geometries at rank 1. These are freely generated, and $[u]$ is the scaling dimension of the generator.* *`Right:` List of 4d $\mathcal{N}=2$ rank 1 SCFTs (IR-free theories are omitted). Each entry represents one theory, labeled by its flavor symmetry. In the rest of the paper, for conciseness we ignore the discrete $\mathbb{Z}_2$ in the naming of the theories. The symbol χ_δ signals the existence of a chiral deformation parameter of scaling dimension δ. The magnetic quivers for the theories of the $\mathbb{Z}_k$ column involve k-laced edges. The theory in blue is $\mathcal{N}=4$ SYM with gauge group $SU(2)$. Theories in green are $\mathcal{N}=3$ S-fold theories [21].*

Geometry K	$[u]$	$\mathbb{Z}_1$	$\mathbb{Z}_2$	$\mathbb{Z}_3$	$\mathbb{Z}_4$	$\mathbb{Z}_6$
II^*	6	E_8	C_5	$A_3 \rtimes \mathbb{Z}_2$	$A_2 \rtimes \mathbb{Z}_2$	
III^*	4	E_7	C_3A_1	$A_1U_1 \rtimes \mathbb{Z}_2$	$U_1 \rtimes \mathbb{Z}_2$	
IV^*	3	E_6	C_2U_1	U_1	$\emptyset$	
I_0^*	2	$D_4\chi_0$	$C_1\chi_0$			
IV	$\frac{3}{2}$	$A_2\chi_{\frac{1}{2}}$				
III	$\frac{4}{3}$	$A_1\chi_{\frac{2}{3}}$				
II	$\frac{6}{5}$	$\chi_{\frac{4}{5}}$				

can even argue whether it makes sense[2]. The gauge node we choose to ungauge is indicated by a *squircle* (which is a gauge node inside a box). We indicate these features on the magnetic quiver of the rank one C_5 theory:

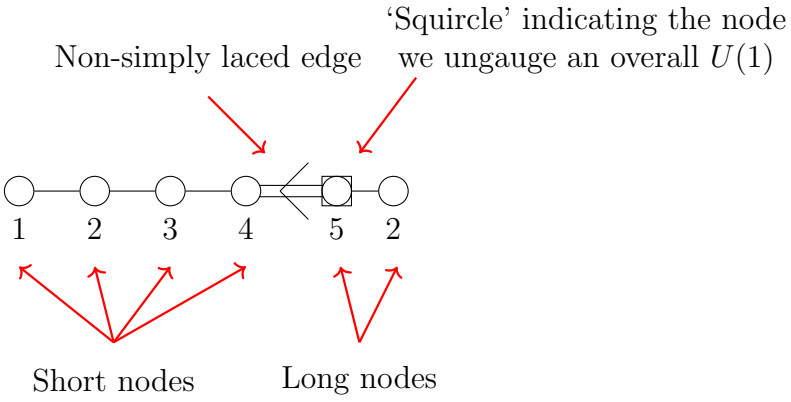

(5.1)

As shown in [137], ungauging on any long node will give the same Coulomb branch. Since we always ungauge on a long node and those ungaugings always give the same result, later on in the chapter we will drop the squircle notation with the ungauging implied.

[2]This was investigated in great detail in [137]. There is an exception of ungauging the $U(1)$ gauge node on the short side, thus turning it into a flavor node. Such an operation gives reasonable Coulomb branches because this phenomenon can be equivalently obtained from ungauging a long $U(1)$ node of a different quiver. This is explored in Section 5.2.2. However, it is not clear if ungauging the $U(1)$ on a non-Abelian node on the short side makes sense.

Bottom-Up approach

As discussed in the last chapter, the Bottom-Up approach is a very useful technique in obtaining magnetic quivers. It basically use properties that you know from the parent theory to constrain the structure of the magnetic quiver. For instance, a C_n Higgs branch global symmetry of the 4d SCFT means the magnetic quiver needs to have a balanced subquiver with a non-simply laced edge of multiplicity two so that it takes the form of a C-type Dynkin diagram. For A_n global symmetry one can either look at simply-laced quivers that take the shape of A-type Dynkin diagram, or at non-simply laced quivers which takes the form of twisted A-type Dynkin diagrams. As it turns out, twisted A-type and D-type Dynkin diagrams make a prominent appearance as subdiagrams of the magnetic quivers of 4d SCFTs. At first sight, the inclusion of twisted Dynkin quivers might make things more complicated as it increases the possible structures that the magnetic quiver can have. However, as all the rank one theories can be obtained using $\mathbb{Z}_k$ $\mathcal{S}$ fold constructions, we already know that these magnetic quivers contain at least one non-simply laced edge with $\mathbb{Z}_k$ multiplicity. The discrete group $\mathbb{Z}_k$ associated with each theory is given in Table 5.8. This puts a severe constraint on the shape of our magnetic quiver.

On top of that, the Higgs branch dimension of the 4d SCFTs were already known in [131], allowing for a restriction on possible ranks of the gauge groups in the magnetic quiver. Once a candidate has been conjectured, we can quickly compute the Coulomb branch Hilbert series and determine the set of generators of the chiral ring. This can then be compared with [136] where the scaling dimension of the Higgs branch chiral ring generators of some of the 4d SCFTs are listed. As it turns out, applying all the constraints above allows us to uniquely identify the magnetic quivers for the rank one 4d SCFTs.

In addition to the Bottom-Up approach above, the magnetic quivers of the $4d$ $\mathcal{N}=2$ theories in question can also be obtained from magnetic quivers of $5d$ $\mathcal{N}=1$ theories compactified with a $\mathbb{Z}_k$ twist. In this case one starts with the magnetic quiver Q' of the 5d theory, which contains k identical simply-laced legs, and obtains the magnetic quiver Q of the $4d$ $\mathcal{N}=2$ theory by folding the k legs of Q':

$$\mathcal{F}_k : Q' \mapsto Q \tag{5.2}$$

Table 5.2: *The magnetic quivers of 4d $\mathcal{N}=2$ rank 1 theories with enhanced Coulomb branches (labeled by their global symmetry).*

Rank 1 SCFT	Magnetic quiver
C_5	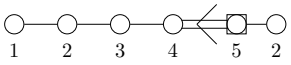
$C_3 \times A_1$	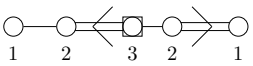
$C_2 \times U_1$	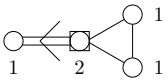
A_3	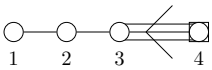
$A_1 \times U_1$	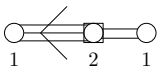
A_2	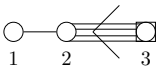

where $\mathcal{F}_k$ is the action of folding k identical legs. Remarkably, most of the $5d$ theories in question are all well known, simple theories. In some cases, the 5d origin of the 4d theories are already known [138]. However, this is not known for all the rank one theories. Therefore, we still need to rely on the bottom-up approach to fill in the blanks. Once the magnetic quivers that satisfy all the constraints are constructed, one can then 'unfold' them to see which magnetic quiver of 5d theories do they originate from.

Hilbert series and chiral ring. The Coulomb branch Hilbert series and refined plethystic logarithm (PL) of Q are given in Table 5.3. The refined PL encodes information on the generators of the chiral ring and their relations [51]. The first few positive terms are representations of the generators whereas the first few negative terms are the representations of the relations. Higher order terms are often higher syzygies. The terms at order t^2 transform in the adjoint representations of the global symmetry group [139].

The C_5, $C_3 \times A_1$, and $C_2 \times U_1$ magnetic quivers can be derived from $5d$ $\mathcal{N}=1$ SQCD magnetic quivers Q' through folding [22], as detailed in Section 5.13 below. Therefore, one can expect that the highest order relations exist at order $t^{4\Delta_B}$ where $\Delta_B = 3/2$ is the conformal dimension of the baryonic/instanton generators, see for example [22, Sec. 2.2]. As a result, there should be no relations beyond t^6. This is consistent with the fact that there are no negative

Table 5.3: *Higgs branch Hilbert series of the 4d $\mathcal{N}=2$ SCFTs (labeled by their global symmetry) as well as the refined plethystic logarithm (PL).*

Rank 1 SCFT	Hilbert series	Refined PL[HS]
C_5	$\frac{\left(\begin{smallmatrix} 1+2t+40t^2+194t^3+1007t^4+4704t^5+18683t^6+67030t^7+220700t^8+657352t^9+1796735t^{10} \\ +4540442t^{11}+10610604t^{12}+23011366t^{13}+46535540t^{14}+87887734t^{15}+155277056t^{16} \\ +257288236t^{17}+400453203t^{18}+585971786t^{19}+807195575t^{20}+1047954388t^{21} \\ +1282842123t^{22}+1481462886t^{23}+1615002952t^{24}+1662191888t^{25}+\cdots\text{palindrome}\cdots+t^{50} \end{smallmatrix}\right)}{(-1+t)^{32}(1+t)^{18}(1+t+t^2)^{16}}$	$t^2:[20000]$ $t^3:[00001]$ $t^4:-[01000]$ $t^5:-[10010]$ $t^6:-[00200]-[20000]+[01000]$
$C_3\times A_1$	$\frac{\left(\begin{smallmatrix} 1+2t+17t^2+66t^3+205t^4+572t^5+1415t^6+2914t^7+5368t^8+8874t^9+12992t^{10} \\ +16856t^{11}+19865t^{12}+21032t^{13}+19865t^{14}+16856t^{15}+12992t^{16}+8874t^{17}+5368t^{18} \\ +2914t^{19}+1415t^{20}+572t^{21}+205t^{22}+66t^{23}+17t^{24}+2t^{25}+t^{26} \end{smallmatrix}\right)}{(-1+t)^{16}(1+t)^{10}(1+t+t^2)^8}$	$t^2:[000;2]+[200;0]$ $t^3:[001;2]$ $t^4:-[000;0]-[010;0]$ $t^5:-[001;2]-[001;0]-[110;2]$ $t^6:-[000;2]-[002;0]-[020;2]$ $-[200;4]-[200;0]+[010;0]$
$C_2\times U_1$	$\frac{\left(\begin{smallmatrix} 1+2t+8t^2+20t^3+41t^4+62t^5+87t^6+96t^7+87t^8+62t^9+41t^{10}+20t^{11}+8t^{12}+2t^{13}+t^{14} \end{smallmatrix}\right)}{(-1+t)^8(1+t)^6(1+t+t^2)^4}$	$t^2:[00]+[20]$ $t^3:(1/q+q)[01]$ $t^4:-[00]-[01]$ $t^5:-(q+1/q)([01]+[20])$ $t^6:-(1+q^2+1/q^2)[00]+[01]$ $-[02]-[20]$
A_3	$\frac{\left(\begin{smallmatrix} 1-t+10t^2+23t^3+67t^4+190t^5+525t^6+1053t^7+2292t^8+4167t^9+7299t^{10} \\ +11494t^{11}+17114t^{12}+23080t^{13}+29925t^{14}+35107t^{15} \\ +39221t^{16}+40320t^{17}+\cdots\text{palindrome}+\cdots+t^{34} \end{smallmatrix}\right)}{(-1+t)^{18}(1+t)^{10}(1+t^2)^5(1+t+t^2)^7}$	$t^2:[101]$ $t^3:[003]+[300]$ $t^4:[030]$ $t^5:-[011]-[110]$ $t^6:-[000]-[022]-[101]-[111]-[202]$ $-[220]$ $t^7:[001]-[003]+[100]-[112]-[122]$ $-[211]-[221]-[300]$ $t^8:-[000]+[002]+[012]-[020]+[022]$ $-[040]+2[101]+[103]+2[111]+[200]$ $+[210]+[220]-[222]+[301]$
$A_1\times U_1$	$\frac{(1-t+t^2)(1+2t^2+4t^3+4t^4+4t^5+2t^6+t^8)}{(-1+t)^6(1+t)^2(1+t^2)(1+t+t^2)^3}$	$t^2:[2]+[0]$ $t^3:(q+1/q)[3]$ $t^4:(q^2+1/q^2)[0]$ $t^5:-(q+1/q)[1]$ $t^6:-[0]-(1+1/q+q)[2]-[4]$ $t^7:-(q+\frac{1}{q})[3]$ $t^8:-[0]+(2+q^2+\frac{1}{q^2})[2]+[4]$
A_2	$\frac{\left(\begin{smallmatrix} 1+3t^2+31t^4+55t^6+156t^8+132t^{10}+156t^{12}+55t^{14}+31t^{16}+3t^{18}+t^{20} \end{smallmatrix}\right)}{(-1+t)^{10}(1+t)^{10}(1+t^2)^5}$	$t^2:[11]$ $t^4:[04]+[40]$ $t^6:-[12]-[21]$ $t^8:-[00]+[01]-[04]+[10]-[11]$ $-[22]-[24]-[33]-[40]-[42]$

terms in the PL at order t^7 and t^8. At higher orders, negative terms re-emerge in the form of higher syzygies, i.e. relations between relations [51]. As a result, for these three families, all the generators and relations can be seen in Table 5.3.

In contrast, the A_3, $A_1\times U_1$, and A_2 rank 1 SCFTs originate from folding more complicated magnetic quivers. For example, the A_3 magnetic quiver comes from the folding of the T_4 theory which has a diverse set of chiral ring relations [140]. Therefore, only some of the relations (up to t^8) are listed in Table 5.3.

5.1.2 C_5 rank 1 SCFT

The global symmetry for this theory is C_5, the dimension of the Higgs branch is 16, and there is a generator of the chiral ring at $[00001]_{C_5}$ and scaling dimension 3/2. These facts lead to a guess for a magnetic quiver among the minimally unbalanced quivers of [141], where the unbalanced node is attached to the last node. We recall that for a (not necessarily simply laced) unitary quiver, the imbalance e of a given node is defined as the number of hypers attached to that node, minus twice the rank of the gauge group. In case that the gauge node is on the long side of a non simply laced edge, the number of hypers for that edge is counted with multiplicity. Nodes with $e = 0$ are said to be balanced.

Luckily, the dimension of this moduli space is indeed 16 and the imbalance indeed leads to a scaling dimension 3/2. As a general rule [22], a node with imbalance e gives rise to an operator with $\mathrm{SU}(2)_R$ spin $1 + \frac{e}{2}$ which transforms in a representation of the global symmetry given by the balanced node to which it is attached (the balanced nodes forming the Dynkin diagram of the non-Abelian part of the global symmetry). This corresponds to an operator of conformal dimension $2 + e$ in 4d. The Hilbert series for the C_5 theory, see Table 5.3, is consistent with the prediction in [136, Sec. 2.1] obtained by compactifying on a torus with a non-trivial flavour background of the $6d$ $\mathcal{N} = (1, 0)$ SCFT, which is the UV completion of an SU(2) gauge theory with 10 flavours.

5.1.3 $C_3 \times A_1$ rank 1 SCFT

The computation in Table 5.3 agrees with the Hilbert series computation in [138, Eq. (40)]. The approach is as follows: The Higgs branches of the $5d$ $\mathcal{N} = 1$ theories T_2 and T_3 have a $\mathbb{Z}_2$ symmetry that we can twist by. Both of the resulting Higgs branches, $T_2^{\mathbb{Z}_2^{\text{twisted}}}$ and $T_3^{\mathbb{Z}_2^{\text{twisted}}}$, have an $SU(2)$ isometry subgroup. Hence, the diagonal $SU(2)$ can be gauged such that the resulting Higgs branch, $T_2^{\mathbb{Z}_2^{\text{twisted}}} \times_{SU(2)} T_3^{\mathbb{Z}_2^{\text{twisted}}}$, becomes the Higgs branch of the $C_3 \times A_1$ rank 1 SCFT. Consequently, the Higgs branch is given by the hyper-Kähler quotient

$$\mathcal{H}\left(C_3 \times A_1 \text{ SCFT}\right) = \left(\mathcal{H}\left(T_2^{\mathbb{Z}_2^{\text{twisted}}}\right) \times \mathcal{H}\left(T_3^{\mathbb{Z}_2^{\text{twisted}}}\right)\right) /\!/\!/ SU(2)\,. \tag{5.3}$$

One can equivalently perform this gauging process from the point of view of magnetic quivers. The $\mathcal{F}_2$ folding of the magnetic quivers for the $5d$ $\mathcal{N}=1$ theories T_2 and T_3 proceeds as follows:

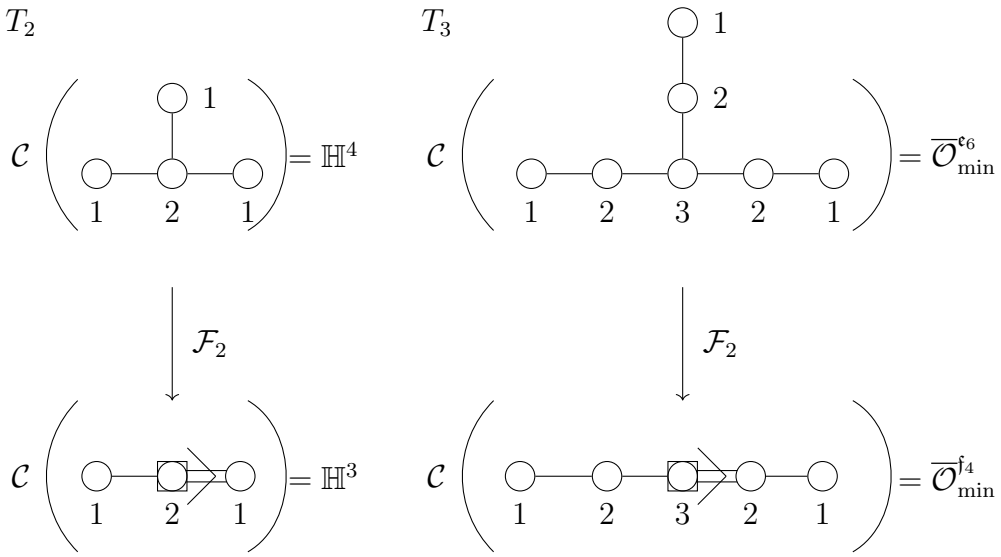

(5.4)

The folded theories, with the $U(1)$ ungauged on a long node, have Coulomb branches $\mathbb{H}^3$ with $Sp(3)$ global symmetry and the closure of the minimal nilpotent orbit of F_4 respectively. Following the prescription in [86], the gauging of an $SU(2)$ subgroup of the Coulomb branch global symmetry of the two magnetic quivers is performed as follows:

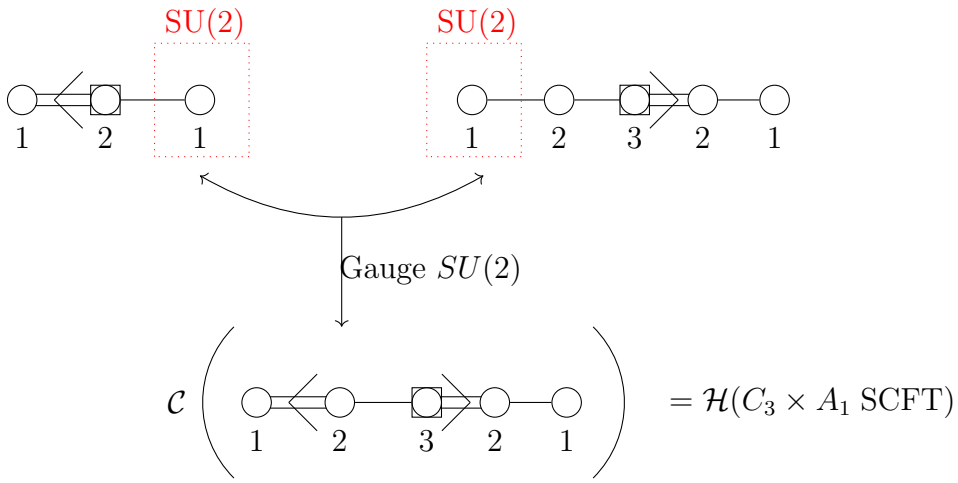

(5.5)

which provides the magnetic quiver of the $C_3 \times A_1$ theory.

In the magnetic quiver of the $C_3 \times A_1$ theory, the U(2) node on the long side is the only one which is not balanced. The imbalance is $e=1$, corresponding to an operator at $\text{SU}(2)_R$ spin 3/2 transforming in the adjoint of A_1 and in the representation [001] of C_3. This operator

can be read in the HWG given in Table 5.5. It is straightforward to make similar comments for all the other quivers appearing in the next subsections.

5.1.4 $C_2 \times U_1$ rank 1 SCFT

For this case we note that the global symmetry is $C_2 \times U_1$ and there is a simple way of getting the magnetic quiver by attaching two nodes of $U(1)$ to the C_2 quiver as in Table 5.8. Nicely enough this guess verifies that the dimension is 4 and the two generators in the chiral ring are in $[01]_{C_2}$ with scaling dimension 3/2 and $U(1)$ charges ± 1, respectively. The Hilbert series results of Table 5.3 agree with [142, Sec. 3.3] which obtain the rank 1 theory as the class $\mathcal{S}$ theory of a sphere with a minimal untwisted A_2 puncture and two maximal twisted A_2 punctures connected with a cylinder with a $\mathbb{Z}_2$ twist line.

5.1.5 A_3 rank 1 SCFT

For this case, the global symmetry and the Z_3 twist lead to a very natural guess of folding a theory that has an $SU(4)^3$ global symmetry. There is a very natural candidate for such a theory. The so called T_4 theory. This leads to the guess as in Table 5.8. This guess is verified by a set of consistency checks like the dimension of the Higgs branch, the generators in the chiral ring, etc. The Hilbert series in Table 5.3 is consistent with the prediction of [143, Eq. 5.7] obtained by a class $\mathcal{S}$ construction of compactifying a $\mathbb{Z}_3$ twisted D_4 theory. Moreover, the result also agrees with the prediction in [136, Sec. 2.2] obtained by compactifying on a torus with a non-trivial flavour background of the $6d$ $\mathcal{N} = (1, 0)$ SCFT, which is the UV completion of an SU(3) gauge theory with 12 flavours.

5.1.6 $A_1 \times U_1$ rank 1 SCFT

The global symmetry of the Coulomb branch of a quiver can be read from the balance of its nodes. The low rank of the global symmetry for this SCFT places a very strong restriction on the form of the quiver. The twist is $\mathbb{Z}_3$, implying that there should be a triply-laced edge. These conditions make the magnetic quiver in Table 5.8 a very natural guess.

In addition, we also conjecture an explicit construction of the Higgs branch using a hyper-Kähler quotient. We check that these two independent descriptions of the Higgs branch are consistent, by computing the Hilbert series in both cases and find perfect agreement.

The Higgs branch of the $A_1 \times U_1$ SCFT is conjectured to be given by the hyper-Kähler quotient:

$$\mathcal{H}\left(A_1 \times U_1 \text{ SCFT}\right) = \left(\overline{\mathcal{O}}_{G_2}^{\min} \times \mathbb{H}^2 \times \mathbb{C}^2/\mathbb{Z}_2\right) /// SU(2)\,. \tag{5.6}$$

Explicitly, we first take the refined Hilbert series $\text{HS}_{\overline{\mathcal{O}}_{G_2}^{\min}}(x_1, x_2, t)$, where x_1, x_2 are the fundamental weight fugacities of G_2 and decompose it with respect to the branching $G_2 \to SU(2) \times SU(2)$. The resulting Hilbert series is $\text{HS}_{\overline{\mathcal{O}}_{G_2}^{\min}}(y, z, t)$ where y and z are the weight fugacities of $SU(2) \times SU(2)$ and is given in [144, Tab. 10]. The $\mathbb{H}^2$ theory can be described by the Higgs branch of $[SU(2)] - [O2]$ with Hilbert series $\text{HS}_{\mathbb{H}^2}(z, q, t)$, where z is the fugacity for $SU(2)$ and q is the fugacity for $O(2)$. The hyper-Kähler quotient then takes the form:

$$\begin{aligned}\text{HS}_{A_1\times U_1}(y, q, t) = \oint_{\text{SU(2)}} d\mu_{\text{SU(2)}} \text{HS}_{\overline{\mathcal{O}}_{G_2}^{\min}}(y, z, t)\text{HS}_{\mathbb{H}^2}(z, q, t)\text{HS}_{\mathbb{C}^2/\mathbb{Z}_2}(z, t) \\ \cdot (1 - z^2t^2)\left(1 - \frac{1}{z^2}t^2\right)(1 - t^2)\end{aligned} \tag{5.7}$$

which is consistent with the result in Table 5.3. Following an analogous gluing process in (5.5), one would expect:

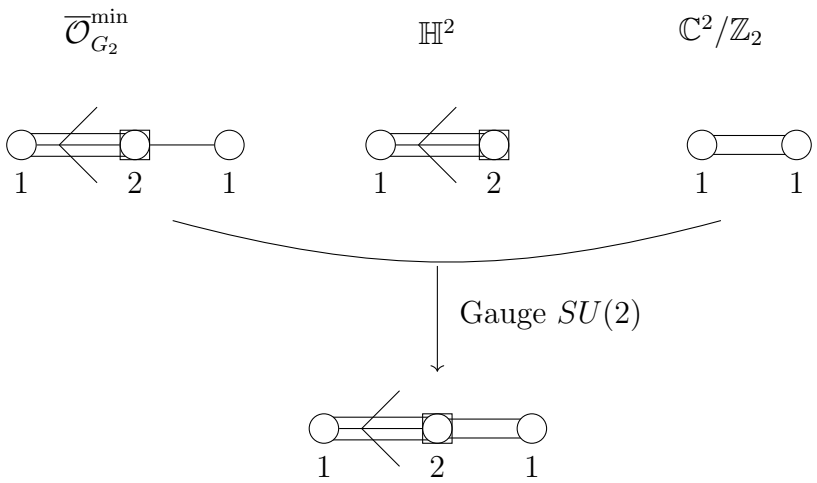

(5.8)

Although exactly how to do this gluing process as an action on magnetic quivers is unclear.

5.1.7 A_2 rank 1 SCFT

For this case we repeat the guess which is made for the A_3 theory, with adaptation of the details. The twist is $\mathbb{Z}_4$, implying that there should be 4 identical legs, each with an $SU(3)$ global symmetry. Folding this quiver leads to the magnetic quiver in Table 5.8. The Hilbert series results of Table 5.3 are consistent with the prediction in [136, Sec. 2.3] obtained by compactifying on a torus with a non-trivial flavor background of the $6d$ $\mathcal{N} = (1, 0)$ SCFT, which is the UV completion of an SU(4) gauge theory with 12 flavours in the fundamental representation and one flavour in the antisymmetric representation.

5.1.8 $\mathbb{H}/\mathbb{Z}_k$ rank 1 SCFTs

For completeness, consider four more rank 1 theories whose Higgs branches are $\mathbb{H}/\mathbb{Z}_k$ orbifolds with $k = 2, 3, 4, 6$. These give the blue and green theories in Table 5.1. The magnetic quivers take the unified form:

(5.9)

where k denotes the multiplicity of hypermultiplets. The Hilbert series is well known, see for instance [36]:

$$\text{HS}(5.9) = \frac{1 - t^{2k}}{(1 - t^2)(1 - t^k q)(1 - t^k/q)} \ . \tag{5.10}$$

The Coulomb branch global symmetry is SU(2) for $k = 2$ where the generators are all at order t^2 transforming as $[2]_{A_1}$ and a singlet relation at order t^4. The Coulomb branch global symmetry is $U(1)$ for $k > 2$, with a singlet generator at order t^2, and $q + \frac{1}{q}$ generators at order t^k satisfying a singlet relation at order t^{2k}. These are consistent with the results in Table 5.1. The $U(1)$ global symmetry is a remnant of the accidental enhanced supersymmetry. The moduli space consists of 3 complex scalars, with a starting $SO(6)$ global symmetry. These are the 6 transverse scalars to a D3 brane probe. Complexification breaks the symmetry to $U(3)$, out of which $SU(3)$ is an R symmetry. We are left with a $U(1)$ which is the symmetry that is observed for the orbifold cases $k = 3, 4, 6$. The extra enhancement of symmetry for the case of $k = 2$ is a signal of the additional enhancement of supersymmetry to 16 supercharges.

Closing remarks

In this section, we looked at magnetic quivers of rank 1 SCFTs which were fully classified in the literature. In some sense (such as the complexity of the Coulomb branch), these are the simplest 4d SCFTs. The 4d Coulomb branches of these theories were well studied such as the specturm of Coulomb branch operators and computing the Seiberg-Witten curves. Now, we are able to fully describe their Higgs branch chiral ring as well by finding the corresponding magnetic quivers. The explicit computation of the refined Hilbert series is a first and essential step to fully defining the chiral ring in terms of generators and relations, which we will leave for the future.

5.2 Higher rank magnetic quivers

Based on our paper [6] and [7]

Now that we have the magnetic quivers of the rank one theories, we can describe some advantage of studying magnetic quivers. The 4d SCFTs by themselves lack a Lagrangian description, making it difficult to draw a quiver for them. On the other hand, the corresponding magnetic quivers are indeed Lagrangian theories. This means one can study their structure and seek to generalize them into infinite families. These infinite families, we will argue, are magnetic quivers of higher rank 4d SCFTs. In this section, we will generalize the rank one theories in two direction.

- The first generalization work by *unfolding* the non-simply laced magnetic quivers and see whether the resulting simply-laced quivers are known magnetic quivers of 5d SCFTs. Magnetic quivers of 5d theories often form part of an infinite family. We then take the infinite family and fold it back to an infinite family of non-simply laced magnetic quivers where the $n = 1$ case is our rank one theories. As a result, the infinite family will have different number of gauge nodes and the rank of the global symmetry group increases linearly in n.

- The second generalization is to view the rank one SCFTs as $\mathcal{S}$-fold constructions. The

generalized $\mathcal{S}$-fold families will have a fixed number of gauge nodes and the global symmetry (except for lower rank cases) will be the same for the infinite family.

5.2.1 Compactification from 5d

The magnetic quivers for rank 1 theories can be derived by taking magnetic quivers of $5d$ $\mathcal{N} = 1$ theories and folding them. The relevant $5d$ theories are summarized in Table 5.4 with each of them extended to a general family. The folding of k legs of the magnetic quivers of the $5d$ theories is directly related to the compatification of these $5d$ theories with a $\mathbb{Z}_k$ twist discussed in [138, 136]. The folded theories are listed in Table 5.5. We also provide the Higgs branch dimension of the magnetic quivers and, where possible, the refined Hilbert series expressed as a highest weight generating function (HWG)[3][145]. For a given family the parametrisation is chosen such that *after folding*:

- $n = 0$ one obtains a magnetic quiver for flat space $\mathbb{H}^l$ for some l. The folded quivers are given in Table 5.6.
- $n = 1$ one obtains a magnetic quiver for a rank 1 theory without enhanced Coulomb branch, they are closures of minimal nilpotent orbits of some algebra. The folded quivers are given in Table 5.6.
- $n = 2$ one obtains a magnetic quiver for a rank 1 theory with enhanced Coulomb branch, which partially Higgses to the theory with the $n = 1$ magnetic quiver. These are the quivers of main interest in this paper and are given in Table 5.8.
- $n > 2$ one obtains a magnetic quiver for a higher rank theory, which can be Higgsed to the $n = 2$ and $n = 1$ case, and possibly other theories. These are tabulated in Table 5.5.

Before folding, all but one family of magnetic quivers are either star shaped quivers, such as T_N, or those found in [25]. These are given in Table 5.4 and summarized as:

[3]The HWG here are expressed as a plethystic logarithm (PL) which allows one to express the rational function in an elegant polynomial form. This PL of the HWG is not to be confused with the PL of the Hilbert series where the positive and negative terms encode the generators and relations in the chiral ring.

- The C_{n+3} family ($n = 2$ case gives the C_5 rank 1 SCFT) comes from folding the E_7 family, which are the magnetic quiver of $5d$ $\mathcal{N} = 1$ $SU(n+1)_0$ SQCD with $2n+4$ flavours. The magnetic quivers here describe the Higgs branch of the $4d$ SCFTs generated by compactifying the $5d$ SCFT lifts of these $\mathcal{N} = 1$ SQCD theories to $4d$ with a $\mathbb{Z}_2$ twist. An alternative construction is as the compactification of the $6d$ $\mathcal{N} = (1,0)$ SCFT completion of the USp$(2n-2)$ gauge theory with $2n+6$ flavours on a torus with a non-trivial flavour background. For n odd, these can be identified as class $\mathcal{S}$ theories associated with the compactification of the $D_{\frac{n+5}{2}}$ $(2,0)$ theory on a sphere with two twisted maximal punctures and one untwisted minimal puncture [136]. For n even, these can also be identified with class $\mathcal{S}$ theories, though the identification is slightly more involved, see [136, Sec. 3.1.2].

- The $C_{n+1} \times A_1$ family ($n = 2$ case gives the $C_3 \times A_1$ rank 1 SCFT) comes from folding the two long tails and two short tails of the magnetic quiver for $5d$ $\mathcal{N} = 1$ $SU(n+1)_0$ SQCD with $2n+2$ flavours. The magnetic quivers here describe the Higgs branch of the $4d$ SCFTs generated by compactifying the $5d$ SCFT lifts of these $\mathcal{N} = 1$ SQCD theories to $4d$ with a $\mathbb{Z}_2$ twist. For n odd, these can be identified as class $\mathcal{S}$ theories associated with the compactification of the $D_{\frac{n+3}{2}}$ $(2,0)$ theory on a sphere with two twisted maximal punctures and one untwisted puncture of type $[n, 1^3]$ [138]. For $n = 4$ the theory seems to match [146, p. 53, #15] up to free hypermultiplets.

- The $C_n \times U_1$ family ($n = 2$ case gives the $C_2 \times U_1$ rank 1 SCFT) comes from folding (the two long tails) of the magnetic quiver of one of the two cones of the $5d$ $\mathcal{N} = 1$ $SU(n+1)_0$ SQCD theory with $2n$ flavours. The magnetic quivers here describe the Higgs branch of the $4d$ SCFTs generated by compactifying the $5d$ SCFT lifts of these $\mathcal{N} = 1$ SQCD theories to $4d$ with a $\mathbb{Z}_2$ twist. For n even, these can be identified as class $\mathcal{S}$ theories named $R_{2,n}$ that were introduced in [142]. These can be constructed by the compactification of the A_n $(2,0)$ theory on a sphere with two twisted maximal punctures and one untwisted minimal puncture. Alternatively, they can also be constructed by the compactification of the A_{2n} $(2,0)$ theory on a sphere with one twisted maximal puncture and one twisted irregular puncture [147, 148].

- The A_{n+1} family ($n = 2$ case gives the A_3 rank 1 SCFT) comes from folding the three legs of a T_{n+2} theory. The magnetic quivers here describe the Higgs branch of the $4d$ SCFTs generated by compactifying the $5d$ T_{n+2} theories to $4d$ with a $\mathbb{Z}_3$ twist. There is also an alternative construction involving the compactification of a family of $6d$ $\mathcal{N} = (1, 0)$ SCFTs on a torus with a non-trivial flavour background. The exact description of these SCFTs, in terms of, for instance, the low-energy gauge theory on the tensor branch, is quite involved and can be found in [136, Sec. 3.2.2].

- The $A_{n-1} \times U_1$ family ($n = 2$ case gives the $A_1 \times U_1$ rank 1 SCFT) comes from taking the extension of the magnetic quiver of the T_n theory with a $U(1)$ connected by a multiplicity 2 edge to the central $U(n)$ node and folding the three long legs. The magnetic quivers here describe the Higgs branch of the $4d$ SCFTs generated by compactifying particular $5d$ SCFTs to $4d$ with a $\mathbb{Z}_3$ twist. The $5d$ SCFTs in question can be conveniently described as the result of a $\mathbb{Z}_3$ symmetric mass deformation of the $5d$ T_{n+2} SCFTs.

- The $A_n{}'$ family ($n = 2$ case gives the A_2 rank 1 SCFT) comes from folding all four legs of the magnetic quiver for the Higgs branch of a class $\mathcal{S}$ theory defined by a sphere with four maximal punctures. The magnetic quivers here describe the Higgs branch of the $4d$ SCFTs generated by compactifying particular $5d$ SCFTs to $4d$ with a $\mathbb{Z}_4$ twist. The $5d$ SCFTs in question are the UV completions of the $5d$ gauge theories made from a linear quiver of n $SU(n + 1)$ groups, connected via bifundamental hypers, without Chern-Simons terms and with $n + 1$ fundamental hypers for both edge groups. These $5d$ SCFTs can be engineered in string theory through the intersection of $n + 1$ D5-branes and $n + 1$ NS5-branes. In order to read the magnetic quiver associated to this brane web, one should impose the $\mathbb{Z}_4$ invariance when decomposing the web into subwebs.

The Higgs branch dimension of the magnetic quivers $\dim_{\mathbb{H}}(\mathcal{H}(Q'))$ listed in Table 5.4 gives indication of the complexity of the moduli space. For dimensions linear in n, the HWG of the Coulomb branch has a simple expression. For those quadratic in n, the HWG is complicated. This is also reflected in the simplicity of the Hasse diagrams as we will discuss in Chapter 7.

Orbifolds $\mathbb{H}/\mathbb{Z}_k$ for $k = 2, 3, 4, 6$. Another pattern that emerges is the relation between magnetic quivers before folding and $5d$ $\mathcal{N} = 1$ SQCD theories of $SU(n+1)_0$ with N_f flavours. In the $\mathbb{Z}_2$ column in Table 5.8, we start with the C_5 theory with $N_f = 2n + 4$ and the flavor reduces by 2 when we go to the next row for $C_3 \times A_1$ and another 2 for $C_2 \times U_1$. Following this, the $C_1 \times \chi_0$ (which is the $\mathbb{H}/\mathbb{Z}_2$ orbifold) family should come as the magnetic quiver of the $n = 1$ member of the family $SU(n+1)_0$ with $2n - 2$ flavours. The magnetic quiver of the $5d$ $\mathcal{N} = 1$ theory takes the form:

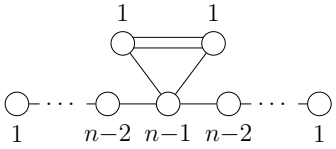

(5.11)

The HWG reads

$$\text{HWG}(\mu_i, t) = \text{PE}\left[\sum_{i=1}^{n+1} \mu_i \mu_{2n-2-i} t^{2i} + t^2 + \mu_{n-1}\left(q + \frac{1}{q}\right) t^{n+1} - \mu_{n-1}^2 t^{2n+2}\right] \tag{5.12}$$

and

$$\dim_{\mathbb{H}} \mathcal{H}(5.11) = n - 1\,. \tag{5.13}$$

Folding the quiver (5.11) yields the general family of the $\mathbb{H}/\mathbb{Z}_2$ rank 1 theories is tabulated in Table 5.7. Since the orbifold itself is a minimal nilpotent orbit, the $n = 1$ case gives our desired $\mathbb{H}/\mathbb{Z}_2$ theory. For the remaining orbifolds $\mathbb{H}/\mathbb{Z}_k$ with $k = 2, 3, 4, 6$, the general family of quiver before folding will be (5.11) but with k multiplicity of hypermultiplets between the two $U(1)$ nodes and k long legs from 1 to $n - 1$. The folded quivers are listed in Table 5.7. The $n = 1$ cases reduces to the $\mathbb{H}/\mathbb{Z}_k$ orbifolds.

5.2.2 $\mathcal{S}$-fold construction

The $\mathcal{S}$-fold constructions we are interested in are worldvolume theories on D3 branes probing Type IIB background called $\mathcal{S}$-folds. This is a generalization of orientifolds from $\mathbb{Z}_2$ projection to $\mathbb{Z}_\ell$ projection which also acts on the axio-dilaton by fixing it to a specific value. Our construction also requires 7-branes to be present in the background. The 7-branes creates a deficit angle Δ_7 and gauge algebra G as follows:

G	$\emptyset$	A_1	A_2	D_4	E_6	E_7	E_8
Δ_7	$\frac{6}{5}$	$\frac{4}{3}$	$\frac{3}{2}$	2	3	4	6

The idea is to consider a $\mathbb{Z}_\ell$ quotient of the Kodaira singularity (see Appendix C) which describes the 7-branes in F-theory. In Type IIB this is implemented by performing a $\mathbb{Z}_\ell$ quotient of the plane transverse to the 7-branes, accompanied by a $\mathbb{Z}_{\ell\Delta_7} \subset SL(2,\mathbb{Z})$ quotient to preserve supersymmetry. Furthermore, we take a $\mathbb{Z}_\ell$ quotient of the $\mathbb{C}^2$ along the 7-branes world-volume but transverse to the D3 branes. The construction can be thought of as a generalization of the $\mathcal{N}=3$ $\mathcal{S}$-fold since it precisely reduces to the more supersymmetric background in the absence of 7-branes (namely $\Delta_7 = 1$).

Requiring $\mathbb{Z}_{\ell\Delta_7}$ to be a subgroup of $SL(2,\mathbb{Z})$, we find that

$$\ell\Delta_7 = 1, 2, 3, 4 \text{ or } 6 \tag{5.14}$$

and we should further impose the compatibility between the 7-branes (which freezes the axio-dilaton at a specific value) and the $\mathbb{Z}_{\ell\Delta_7}$ quotient. We then easily conclude that[4]

- For $\ell = 2$ the allowed solutions are $\Delta_7 = \frac{3}{2}$, 2, and 3.
- For $\ell = 3$ we can have $\Delta_7 = \frac{4}{3}$ and 2.
- For $\ell = 4$ only the 7-branes of type A_2, namely $\Delta_7 = \frac{3}{2}$ is allowed.

The models with $\ell = 2, 3, 4$ come in two variants, depending on whether we include discrete flux for the B-field in Type IIB or not. The models with discrete flux, the $\mathcal{S}^{(r)}_{G,\ell}$ theories, have been constructed in [135]. The rank of the theory is r, the number of probe D3 branes, and for $r = 1$ they coincide with the rank-1 theories we just studied. This is the infinite family we will focus on in this section.

$\mathcal{S}$-fold magnetic quivers

The $\mathcal{S}^{(r)}_{G,\ell}$ magnetic quivers were obtained using two inequivalent ways:

- A Bottom-Up approach by constraining the magnetic quiver using the global symmetry, dimension of moduli space and multiplicity ℓ of the non-simply laced edge which is

[4] In principle also $\ell = 5, 6$ could be considered but we concentrate on the $\ell \leq 4$ case in this thesis.

determined by the $\mathbb{Z}_\ell$ folds.

- Starting from 6d $\mathcal{N} = (1, 0)$ SCFTs, one compactify on a S^1 and perform mass deformations to get to a 5d SCFT. A further compactification on a S^1 with $\mathbb{Z}_\ell$ twist gives the 4d $\mathcal{S}$-fold theory. On the magnetic quiver side, the mass deformation becomes FI deformations (rules on how to perform FI deformation on magnetic quivers is introduced in [7]) and the twisted compactification is done by folding ℓ identical legs into a non-simply laced leg with multiplicity ℓ.

The magnetic quivers for of $\mathcal{S}^{(r)}_{G,\ell}$ are given in Table 5.8 and for rank $r = 2$ cases, the unrefined Hilbert series and refined plethsytic logarithms are given in Table 5.9 and Table 5.10.

Discretely gauged theories

The $\mathcal{S}^{(r)}_{G,\ell}$ theories above has a discrete $\mathbb{Z}_\ell$ global symmetry which one can consider gauging to give a different SCFT. We will call this discretely gauged version $\mathring{\mathcal{S}}^{(r)}_{G,\ell}$. We conjecture that this can be understood at the level of magnetic quivers by changing where you ungauge the overall $U(1)$. It was conjectured in [137] that for a multiplicity ℓ non-simply laced edge, moving from ungauging a $U(1)$ on a long node to the short node results in a $\mathbb{Z}_\ell$ orbifold in the moduli space. For the $\mathcal{S}$-fold theories, the choice of ungauging on the $U(1)$ short node, gives us $\mathring{\mathcal{S}}^{(r)}_{G,\ell}$. Note that the magnetic quivers of $\mathcal{S}^{(r)}_{G,\ell}$ always has a $U(1)$ gauge group on the short side which we can turn into a flavor node. To be consistent with our notation of only presenting unframed quivers where a long node is ungauged, a $U(1)$ flavor node on the short side of the quiver is equivalent to replacing the original $U(1)$ short node with a multiplicity ℓ non-simply laced edge

pointing towards the rest of the quiver. For example, the $\mathcal{S}^{(r)}_{E_6,2}$ and its discrete quotient $\mathring{\mathcal{S}}^{(r)}_{E_6,2}$:

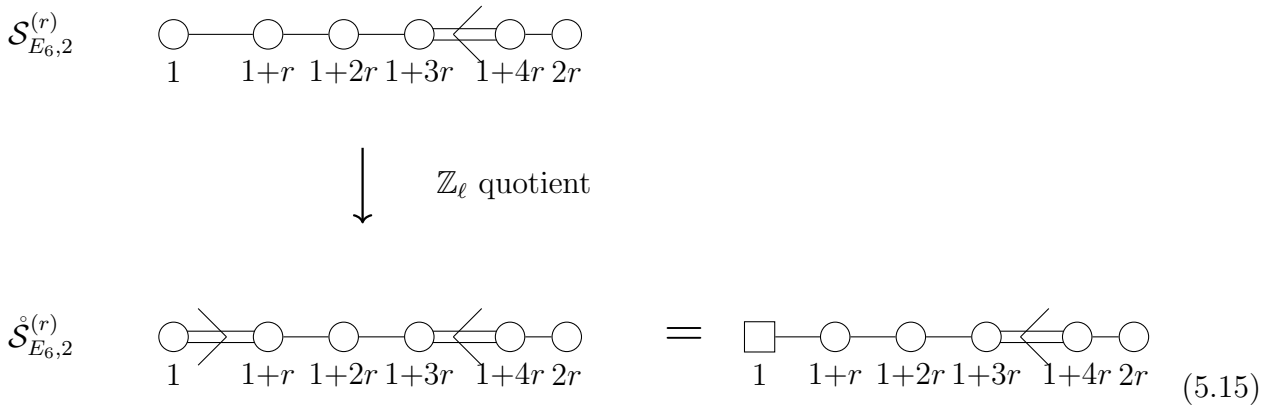

(5.15)

where the Coulomb branch of the bottom left quiver with ungauging on any one of the long nodes is equivalent to the Coulomb branch on the right. The magnetic quivers after discrete gauging $\mathring{\mathcal{S}}^{(r)}_{G,\ell}$ are given in Table 5.11.

New rank one SCFTs?

If $\mathring{\mathcal{S}}^{(r)}_{G,\ell}$ is indeed a new set of 4d SCFTs then implications can be quite interesting. This means that for $r = 1$, we have new rank one SCFTs that are beyond the classifications of [131] [5]. More arguments for the resulting theories being SCFTs are given in [7] from F-theory constructions and by viewing $\mathcal{S}$-fold theories as moduli space of r G instantons on $\mathbb{C}^2/\mathbb{Z}_\ell$.

[5]However, this might be expected as the authors of [137] told us their classification does not include discrete quotients of the theories.

Table 5.4: *Magnetic quivers of 5d $\mathcal{N}=1$ theories. In the case of $n=2$, folding these theories reproduces the magnetic quivers of 4d $\mathcal{N}=2$ theories of Table 5.8. We provide the dimension of both the Higgs branch $\mathcal{H}(Q')$ and the Coulomb branch $\mathcal{C}(Q')$ of the unfolded magnetic quivers. The HWGs are given in [22, 1]. The prime in the label of the last family is to distinguish it from the fourth family.*

Family	Unfolded Magnetic quiver Q'	$\dim_{\mathbb{H}}(\mathcal{H}(Q'))$	$\dim_{\mathbb{H}}(\mathcal{C}(Q'))$	PL(HWG($\mathcal{C}(Q')$))
C_{n+3}	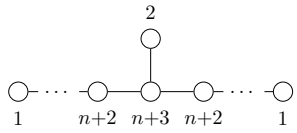	n	$n^2+6n+10$	$\sum_{i=1}^{n+2}\mu_i\mu_{2n+6-i}t^{2i}+t^4$ $+\mu_{2n+6}(t^{n+1}+t^{n+3})$
$C_{n+1}\times A_1$	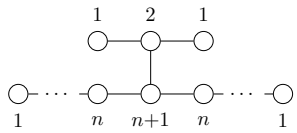	n	$n(n+2)+4$	$\sum_{i=1}^{n+1}\mu_i\mu_{2n+2-i}t^{2i}+(\nu_1^2+\nu_2^2)t^2$ $+t^4+\nu_1\nu_2\mu_{2n+2}(t^{n+1}+t^{n+3})$ $-\nu_1^2\nu_2^2\mu_{n+1}^2t^{2n+6}$
$C_n\times U_1$	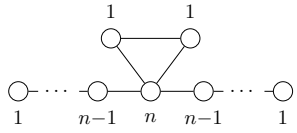	n	n^2+1	$\sum_{i=1}^{n}\mu_i\mu_{2n-i}t^{2i}+t^2+\mu_n(q$ $+\frac{1}{q})t^{n+1}-\mu_n^2t^{2(n+1)}$
A_{n+1}	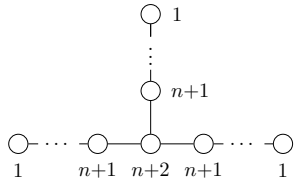	$\frac{n(n+1)}{2}$	$\frac{1}{2}(1+n)(8+3n)$	Complicated
$A_{n-1}\times U_1$	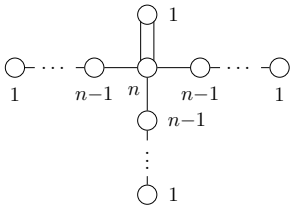	$\frac{n(n+1)}{2}$	$\frac{n(3n-1)}{2}$	Complicated
$A_n{}'$	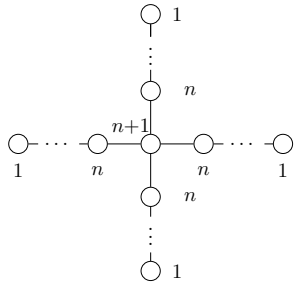	n^2	$n(2n+3)$	Complicated

Table 5.5: *General quiver families obtained by folding the legs in the magnetic quivers Q' in Table 5.4. In the case of $n = 2$ these families correspond to the magnetic quivers of 4d $\mathcal{N} = 2$ rank 1 theories with enhanced Coulomb branch. For $n > 1$ the families are labelled by their global symmetry. For $n = 1$ the magnetic quivers describe rank 1 theories without enhanced Coulomb branch, and for $n = 0$ each of the moduli spaces is some $\mathbb{H}^l$ for a suitable l. The dimensions and the HWGs of the Coulomb branches of the magnetic quivers $\mathcal{C}(Q)$ are provided.*

Family	Magnetic quiver Q	$\dim_{\mathbb{H}}(\mathcal{C}(Q))$	PL(HWG($\mathcal{C}(Q)$))
C_{n+3}	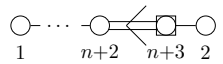	$\frac{(n+3)(n+4)}{2}+1$	$\sum_{i=1}^{n+2}\mu_i^2t^{2i}+t^4+\mu_{n+3}(t^{n+1}+t^{n+3})$
$C_{n+1}\times A_1$	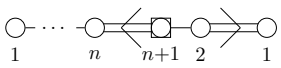	$\frac{(n+1)(n+2)}{2}+2$	$\sum_{i=1}^{n+1}\mu_i^2t^{2i}+\nu^2t^2+t^4+\nu^2\mu_{n+1}(t^{n+1}+t^{n+3})-\nu^4\mu_{n+1}^2t^{2n+6}$
$C_n\times U_1$	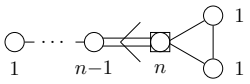	$\frac{n(n+1)}{2}+1$	$\sum_{i=1}^{n}\mu_i^2t^{2i}+t^2+\mu_n(q+\frac{1}{q})t^{n+1}-\mu_n^2t^{2(n+1)}$
A_{n+1}	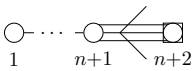	$\frac{(n+2)(n+3)}{2}-1$	Complicated
$A_{n-1}\times U_1$	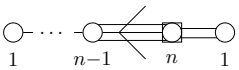	$\frac{n(n+1)}{2}$	Complicated
$A_n{}'$	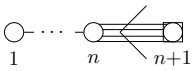	$\frac{(n+1)(n+2)}{2}-1$	Complicated

Table 5.6: *The $n = 1$ and $n = 0$ members of the general Families of Table 5.5, where the Coulomb branches are closures of minimal nilpotent orbits and freely generated theories respectively. The $n = 1$ cases correspond to rank 1 theories without enhanced Coulomb branch. Notice that the global symmetry here does not match the labelling of the family.*

Family	Case $n = 1$		Case $n = 0$	
	Magnetic quiver	Moduli space	Magnetic quiver	Moduli space
C_{n+3}	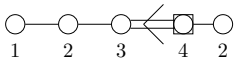	$\overline{\mathcal{O}}_{E_6}^{\min}$	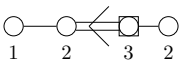	$\mathbb{H}^7$
$C_{n+1}\times A_1$	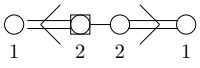	$\overline{\mathcal{O}}_{D_4}^{\min}$	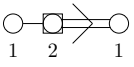	$\mathbb{H}^3$
$C_n\times U_1$		$\overline{\mathcal{O}}_{A_2}^{\min}$		$\mathbb{H}$
A_{n+1}	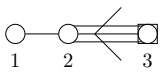	$\overline{\mathcal{O}}_{D_4}^{\min}$	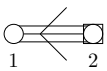	$\mathbb{H}^2$
$A_{n-1}\times U_1$		$\overline{\mathcal{O}}_{A_1}^{\min}$		Trivial
$A_n{}'$	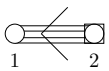	$\overline{\mathcal{O}}_{A_2}^{\min}$		Trivial

Table 5.7: *The $n = 1$ case of these families correspond to the magnetic quivers of 4d $\mathcal{N} = 2$ rank 1 theories whose Higgs branch are $\mathbb{H}/\mathbb{Z}_k$ orbifolds for $k = 2, 3, 4, 6$.*

Family	Magnetic quiver	G_{global}	PL(HWG)
$\mathbb{H}/\mathbb{Z}_2$	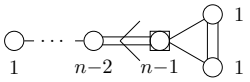	$C_{n-1} \times U_1$	$\sum_{i=1}^{n-1} \mu_i^2 t^{2i} + t^2 + \mu_{n-1}(q + \frac{1}{q}) t^{n+1} - \mu_{n-1}^2 t^{2n+2}$
$\mathbb{H}/\mathbb{Z}_3$	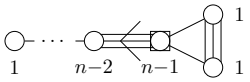	$A_{n-2} \times U_1$	Complicated
$\mathbb{H}/\mathbb{Z}_4$	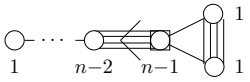	$A_{n-2} \times U_1$	Complicated
$\mathbb{H}/\mathbb{Z}_6$	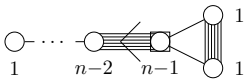	$A_{n-2} \times U_1$	Complicated

Table 5.8: *The magnetic quivers of 4d $\mathcal{N} = 2$ rank r $\mathcal{S}$-fold theories. The Higgs branch dimension of $\mathcal{S}^{(r)}_{G,\ell}$ is $(6r + \ell)(\Delta_7 - 1)$, which matches the Coulomb branch dimension of the magnetic quiver. The folding parameter ℓ also indicates the multiplicity of the non-simply laced edge. The global symmetry of the magnetic quiver displays the expected enhancement for $r = 1$ [23]. Recall that a* U(1) *is ungauged on a long node for all the quivers.*

SCFT	Magnetic quiver	Global Symmetry $r > 1$	Global Symmetry $r = 1$	(ℓ, Δ_7)	Dimension
$\mathcal{S}^{(r)}_{E_6,2}$	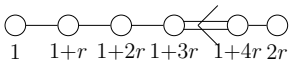	$C_4 A_1$	C_5	$(2, 3)$	$12r + 4$
$\mathcal{S}^{(r)}_{D_4,2}$	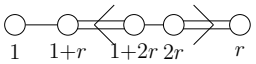	$C_2 A_1 A_1$	$C_3 A_1$	$(2, 2)$	$6r + 2$
$\mathcal{S}^{(r)}_{A_2,2}$	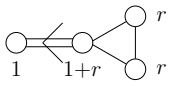	$C_1 A_1 U_1$	$C_2 U_1$	$(2, \frac{3}{2})$	$3r + 1$
$\mathcal{S}^{(r)}_{D_4,3}$	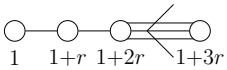	$A_2 U_1$	A_3	$(3, 2)$	$6r + 3$
$\mathcal{S}^{(r)}_{A_1,3}$	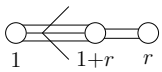	$U_1 U_1$	$A_1 U_1$	$(3, \frac{4}{3})$	$2r + 1$
$\mathcal{S}^{(r)}_{A_2,4}$	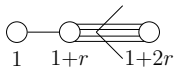	$A_1 U_1$	A_2	$(4, \frac{3}{2})$	$3r + 2$

Table 5.9: *Coulomb branch Hilbert series and plethystic logarithm for the magnetic quivers of $\mathcal{S}^{(r=2)}_{G,\ell}$ theories in Table 5.8. The unrefined monopole formula can be evaluated exactly for all but two cases. The unrefined PL confirms the dimension of the global symmetry.*

SCFT	Hilbert Series	PL[HS]
$\mathcal{S}^{(2)}_{E_6,2}$	$1+39t^2+108t^3+989t^4+4540t^5+O(t^6)$	$39t^2+108t^3+209t^4+328t^5+O[t^6]$
$\mathcal{S}^{(2)}_{D_4,2}$	$\frac{\left(\begin{array}{c}1+t+11t^2+42t^3+159t^4+551t^5+1829t^6+5584t^7+16155t^8+43955t^9+113250t^{10}\\+276689t^{11}+643191t^{12}+1424394t^{13}+3012854t^{14}+6095898t^{15}+11818736t^{16}\\+21987612t^{17}+39306452t^{18}+67596644t^{19}+111957432t^{20}+178757670t^{21}+275393063t^{22}\\+409695251t^{23}+588987515t^{24}+818774420t^{25}+1101255657t^{26}+1433825259t^{27}\\+1807938114t^{28}+2208595573t^{29}+2614801861t^{30}+3001022474t^{31}+3339685060t^{32}\\+3604301588t^{33}+3772852500t^{34}+3830735670t^{35}+\ldots\,\text{palindrome}+\cdots+t^{70}\end{array}\right)}{(1-t)^{-1}(1-t^2)^6(1-t^3)^{11}(1-t^4)^6(1-t^5)^6}$	$16t^2+42t^3+68t^4+88t^5-58t^6-692t^7$ $-2429t^8-4572t^9-204t^{10}+O\left(t^{11}\right)$
$\mathcal{S}^{(2)}_{A_2,2}$	$\frac{\left(\begin{array}{c}1+2t+6t^2+19t^3+55t^4+133t^5+303t^6+637t^7+1258t^8+2312t^9+3986t^{10}\\+6422t^{11}+9754t^{12}+13947t^{13}+18841t^{14}+24047t^{15}+29059t^{16}+33215t^{17}+35995t^{18}+36958t^{19}\\+\ldots\,\text{palindrome}+\cdots+t^{38}\end{array}\right)}{(1-t)^{-2}(1-t^2)^4(1-t^3)^5(1-t^4)^4(1-t^5)^3}$	$7t^2+14t^3+21t^4+18t^5-14t^6-88t^7$ $-211t^8-236t^9+157t^{10}+O\left(t^{11}\right)$
$\mathcal{S}^{(2)}_{D_4,3}$	$1+9t^2+28t^3+92t^4+338t^5+O(t^6)$	$9t^2+28t^3+47t^4+86t^5+O\left(t^6\right)$
$\mathcal{S}^{(2)}_{A_1,3}$	$\frac{\left(\begin{array}{c}1-t+2t^2+t^3+6t^4+6t^5+13t^6+18t^7+32t^8+39t^9+59t^{10}+70t^{11}\\+93t^{12}+101t^{13}+120t^{14}+120t^{15}+133t^{16}+120t^{17}+120t^{18}+101t^{19}\\+93t^{20}+70t^{21}+59t^{22}+39t^{23}+32t^{24}+18t^{25}+13t^{26}+6t^{27}+6t^{28}+t^{29}+2t^{30}-t^{31}+t^{32}\end{array}\right)}{(1-t)(1-t^3)^3(1-t^4)^2(1-t^5)(1-t^6)^2(1-t^7)}$	$2t^2+6t^3+8t^4+10t^5+8t^6+2t^7$ $-17t^8-42t^9-72t^{10}+O\left(t^{11}\right)$
$\mathcal{S}^{(2)}_{A_2,4}$	$\frac{\left(\begin{array}{c}1-2t+2t^2+11t^4-12t^5+30t^6-10t^7+94t^8-30t^9+210t^{10}-8t^{11}\\+493t^{12}+16t^{13}+908t^{14}+166t^{15}+1633t^{16}+356t^{17}+2507t^{18}+714t^{19}+3579t^{20}\\+1074t^{21}+4520t^{22}+1422t^{23}+5293t^{24}+1626t^{25}+5486t^{26}+\ldots\,\text{palindrome}+\cdots+t^{52}\end{array}\right)}{(1-t)^2(1-t^2)^3(1-t^3)^2(1-t^4)^3(1-t^6)^3(1-t^8)^3}$	$4t^2+4t^3+16t^4+12t^5+30t^6+24t^7$ $+22t^8-16t^9-138t^{10}+O\left(t^{11}\right)$

Table 5.10: *Refined plethystic logarithm of the Hilbert series for the magnetic quivers of the $\mathcal{S}^{(r=2)}_{G,\ell}$ theories in Table 5.8. In abuse of notation, $[\ldots]_G$ denotes the G-character of a representation with Dynkin labels $[\ldots]$. Moreover, q and b label $\mathrm{U}(1)$ charges.*

SCFT	Refined PL[HS]
$\mathcal{S}^{(2)}_{E_6,2}$	$t^2:[2]_{A_1}[0000]_{C_4}+[0]_{A_1}[2000]_{C_4}$ $t^3:[1]_{A_1}[0001]_{C_4}+[2]_{A_1}[1000]_{C_4}$ $t^4:[4]_{A_1}[0000]_{C_4}+[1]_{A_1}[0010]_{C_4}+[2]_{A_1}[2000]_{C_4}$
$\mathcal{S}^{(2)}_{D_4,2}$	$t^2:[2]_{A_1}[0]_{A_1}[00]_{C_2}+[0]_{A_1}[2]_{A_1}[00]_{C_2}+[0]_{A_1}[0]_{A_1}[20]_{C_2}$ $t^3:[1]_{A_1}[2]_{A_1}[01]_{C_2}+[2]_{A_1}[0]_{A_1}[10]_{C_2}$ $t^4:[4]_{A_1}[0]_{A_1}[00]_{C_2}+[2]_{A_1}[2]_{A_1}[00]_{C_2}+[4]_{A_1}[0]_{A_1}[00]_{C_2}+[2]_{A_1}[2]_{A_1}[10]_{C_2}+[2]_{A_1}[0]_{A_1}[20]_{C_2}$
$\mathcal{S}^{(2)}_{A_2,2}$	$t^2:[2]_{A_1}[0]_{C_1}+[0]_{A_1}[2]_{C_1}+[0]_{A_1}[0]_{C_1}$ $t^3:(q+1/q)[1]_{A_1}[1]_{C_1}+[2]_{A_1}[1]_{C_1}$ $t^4:(q+1/q)[1]_{A_1}[0]_{C_1}+[2]_{A_1}[0]_{C_1}+[4]_{A_1}[0]_{C_1}+[2]_{A_1}[2]_{C_1}$
$\mathcal{S}^{(2)}_{D_4,3}$	$t^2:[00]_{A_2}+[11]_{A_2}$ $t^3:q^9[00]_{A_2}+q^7[01]_{A_2}+q^3[03]_{A_2}+q^{-3}[30]_{A_2}+q^{-7}[10]_{A_2}+q^{-9}[00]_{A_2}$ $t^4:q^6[30]_{A_2}+q^4[20]_{A_2}+q^2[10]_{A_2}+[00]_{A_2}+[11]_{A_2}+q^{-2}[01]_{A_2}+q^{-4}[02]_{A_2}+q^{-6}[03]_{A_2}$
$\mathcal{S}^{(2)}_{A_1,3}$	$t^2:2$ $t^3:b^2q+\frac{1}{b^2q}+\frac{b}{q}+\frac{q}{b}+q+\frac{1}{q}$ $t^4:b^3+\frac{1}{b^3}+b^2+\frac{1}{b^2}+b+\frac{1}{b}+2$
$\mathcal{S}^{(2)}_{A_2,4}$	$t^2:[0]_{A_1}+[2]_{A_1}$ $t^3:(q^5+q^{-5})[1]_{A_1}$ $t^4:(1+q^8+q^{-8})[0]_{A_1}+[2]_{A_1}+(q^4+q^{-4})[4]_{A_1}$

Table 5.11: *The $\mathring{\mathcal{S}}^{(r)}_{G,\ell}$ theories with their magnetic quivers. The global symmetry is independent of r. The dimension of the Higgs branch of $\mathring{\mathcal{S}}^{(r)}_{G,\ell}$ is equal to the dimension of the Higgs branch of $\mathcal{S}^{(r)}_{G,\ell}$. Recall that a* U(1) *is ungauged on a long node of all the quivers.*

SCFT	Magnetic quiver	Global Symmetry	Dimension
$\mathring{\mathcal{S}}^{(r)}_{E_6,2}$	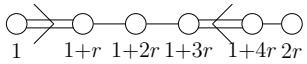	C_4A_1	$12r+4$
$\mathring{\mathcal{S}}^{(r)}_{D_4,2}$	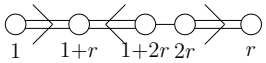	$C_2A_1A_1$	$6r+2$
$\mathring{\mathcal{S}}^{(r)}_{A_2,2}$	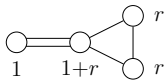	$C_1A_1U_1$	$3r+1$
$\mathring{\mathcal{S}}^{(r)}_{D_4,3}$	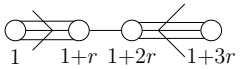	A_2U_1	$6r+3$
$\mathring{\mathcal{S}}^{(r)}_{A_1,3}$	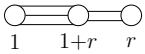	U_1U_1	$2r+1$
$\mathring{\mathcal{S}}^{(r)}_{A_2,4}$	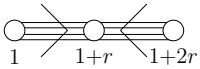	A_1U_1	$3r+2$

5.3 Folding orthosymplectic quivers

Based on our paper [8]

In the previous section, we looked at the presence of non-simply laced quivers which are magnetic quivers of 4d SCFTs. In the literature, non-simply laced quivers were restricted to theories with unitary gauge groups. Our paper [8] marks the first time *non-simply laced orthosymplectic quivers* are investigated. These theories are obtained by folding simply-laced orthosymplectic quivers with two or more identical legs to form a non-simply laced edge. The resulting Coulomb branches are well defined and in many times give us surprising results. Some of these quivers are also magnetic quivers of $4d$ SCFTs.

5.3.1 Monopole formula for non-simply laced orthosymplectic quivers

We first discuss how to compute the monopole formula for a non-simply laced orthosymplectic quiver. For the conformal dimension $\Delta(m)$ of the monopole formula, the additional contribution coming from the multiplicity l non-simply laced edge is treated in the same way as the the non-simply laced edge in the unitary quiver as described in [65]. Basically, the magnetic charge from the long node has a l multiplicity factor in front of them in the conformal dimension. The details are given in Appendix A.

For unframed non-simply laced orthosymplectic quivers, one needs to take into consideration both changes to the conformal dimension as well as changes to the magnetic lattice due to the choice of H (the zero-form symmetry we saw in previous chapter). Once again, we divide the nodes of the non-simply laced quivers into long and short nodes. Denote by Λ_L the magnetic lattice of the long nodes/gauge groups and by Λ_S the magnetic lattice of the short nodes/gauge groups. A vector of magnetic charges $m \in \Lambda$ is represented as a pair $m \in (m_L, m_S) \in \Lambda_L \times \Lambda_S$. Let r_L denote the sum of the ranks of all long nodes and r_S the sum of the ranks of all short nodes. If the non-simply laced edge is even (i.e. with double, quadruple bond etc.), then the magnetic lattice to be summed over is as follows:

$$\mathbb{Z}^{r_S+r_L} \oplus ((\mathbb{Z}+\tfrac{1}{2})^{r_L} \times \mathbb{Z}^{r_S}) \tag{5.16}$$

In contrast, if the non-simply laced edge is odd (i.e. with triple, quintuple bond etc.), then the magnetic lattice is:

$$\mathbb{Z}^{r_S+r_L} \oplus (\mathbb{Z}+\tfrac{1}{2})^{r_S+r_L} \tag{5.17}$$

If the non-simply laced orthosymplectic quiver is framed, then the Hilbert series sum is evaluated only over the integer-valued magnetic charges, because the discrete group H is trivial, see [2].

Global symmetry

Building on the investigation of non-simply laced orthosymplectic quivers, the following subsets of balanced nodes:

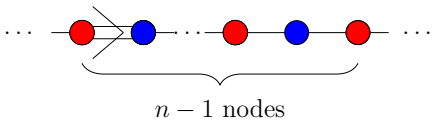

(5.18)

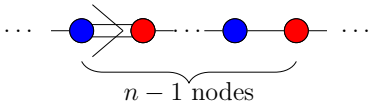

(5.19)

both contribute an $\mathfrak{sl}(n)$ factor to the global symmetry. When is a balanced $SO(2)$ node, this is enhanced to $\mathfrak{sl}(n+1)$. For unframed quivers, the contribution from half-plus-integer lattice can further enhance this symmetry, such as to exceptional global symmetries as will see.

5.3.2 T_4 example

Since this is the first time such computation is made, we should find a set of examples where we know what to expect from the Coulomb branch of the non-simply laced quiver.

The theory known as T_4 is constructed by gluing together quivers whose Coulomb branches are closures of maximal nilpotent orbits of $\mathfrak{sl}(4)$. Due to the isomorphism $\mathfrak{sl}(4) \cong \mathfrak{so}(6)$, the

following quivers have equivalent moduli spaces:

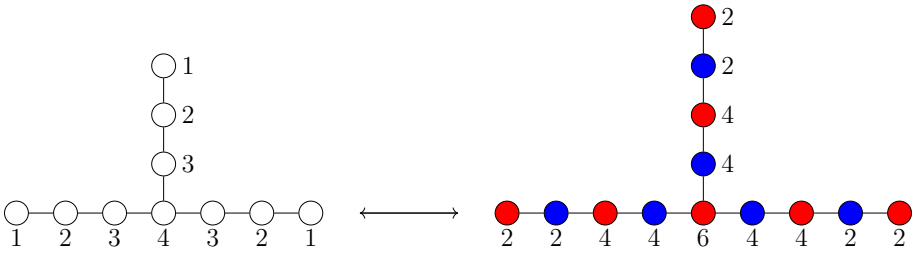

(5.20)

Computation of the Coulomb branch Hilbert series of the orthosymplectic quiver is given in [2, Fig.39] and is consistent with the unitary counterpart.

As a first step, one can fold two of the quiver legs which yields:

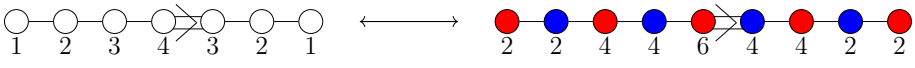

(5.21)

Computation of the Coulomb branch Hilbert series of both quivers yields:

$$\mathrm{HS}_{\mathrm{U}}(t)=\mathrm{HS}_{\mathrm{OSp}}(t)=\frac{\left(\begin{array}{c}1+21t^2+68t^3+341t^4+1300t^5+4936t^6+15988t^7\\+50242t^8+142812t^9+384411t^{10}+960772t^{11}+2270650t^{12}\\+5038840t^{13}+10601001t^{14}+21083004t^{15}+39862377t^{16}\\+71590384t^{17}+122553812t^{18}+199944220t^{19}+311642452t^{20}\\+464078612t^{21}+661421665t^{22}+902317920t^{23}+1179751147t^{24}\\+1478423752t^{25}+1777451140t^{26}+2050065624t^{27}\\+2269933494t^{28}+2412458048t^{29}+2462182956t^{30}\\+\text{palindromic}+\cdots+21t^{58}+t^{60}\end{array}\right)}{(1-t^2)^9\,(1-t^3)^{12}\,(1-t^4)^9} \tag{5.22}$$

As a next step, one folds all three identical legs which yields

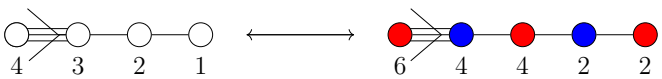

(5.23)

The unitary quiver in (5.23) is a known member of the generalized rank 1 4d $\mathcal{N}=2$ sequence studied earlier in the chapter. An explicit computation of the Coulomb branch Hilbert series of

the both quivers in (5.23) yields

$$\mathrm{HS}_{\mathrm{U}}(t) = \mathrm{HS}_{\mathrm{OSp}}(t) = \frac{\left(\begin{array}{c} 1 - t + 10t^2 + 23t^3 + 67t^4 + 190t^5 + 525t^6 + 1053t^7 \\ +2292t^8 + 4167t^9 + 7299t^{10} + 11494t^{11} + 17114t^{12} + 23080t^{13} \\ +29925t^{14} + 35107t^{15} + 39221t^{16} + 40320t^{17} \\ +\text{palindromic} + \cdots + 10t^{32} - t^{33} + t^{34} \end{array}\right)}{(1-t)(1-t^2)^5(1-t^3)^7(1-t^4)^5} . \quad (5.24)$$

The above examples reinforce the conjecture that folding orthosymplectic quivers yields valid results, so one may proceed to fold quivers where the resulting Coulomb branches cannot easily be determined from accidental isomorphisms.

5.3.3 Folding of E_n theories

Previously we looked at the E_n theories (theories whose Coulomb branch are one-E_n instanton moduli space), where the unitary quivers take the form of affine E_n Dynkin diagrams and the orthosymplectic quivers are given in Table 4.9. One interesting feature this set of orthosymplectic quivers is that they all have a $\mathbb{Z}_2$ symmetry, making them ideal candidates to be folded into a non-simply laced quiver. Such symmetry is not always present in the unitary counterpart.

Upon folding their identical legs, one obtains the following key results:

- First, folding orthosymplectic quivers, whose Coulomb branches are closures of E_n minimal nilpotent orbits for $4 \leq n \leq 8$, leads to non-simply laced orthosymplectic quivers, whose Coulomb branches are also closures of minimal nilpotent orbits. Folding the E_8, E_7, E_6, $E_5 \cong D_5$, $E_4 \cong A_4$ quivers, leads to non-simply laced orthosymplectic quivers, whose Coulomb branches are closures of minimal orbits of E_7, E_6, D_5, D_4, D_3 respectively. This can be depicted as follows:

$$\begin{array}{ccccccccccc} E_8 & \longrightarrow & E_7 & \longrightarrow & E_6 & \longrightarrow & D_5 & \longrightarrow & A_4 & \longrightarrow & \cdots \\ & \searrow & & \searrow & & \searrow & & \searrow & & \searrow & \\ & & E_7 & \longrightarrow & E_6 & \longrightarrow & D_5 & \longrightarrow & D_4 & \longrightarrow & A_3 & \longrightarrow & \cdots \end{array} \quad (5.25)$$

The red arrows denote orthosymplectic folding. Note that the top line corresponds to the

standard exceptional sequence while the bottom line corresponds to a chain of inclusions of associated affine Weyl groups studied in [149, 150]. The results for the rank 1 E_n theories are given in Table 5.12.

- Second, each member of the E_n family of orthosymplectic quivers can be generalized to an infinite sequence of quivers, as shown in [2]. These quivers are magnetic quivers for 5d $\mathcal{N} = 1$ SQCD theories. Each of these families of quivers can be folded, producing infinite sequences of non-simply laced orthosymplectic quivers. Some of these families are magnetic quivers for 4d $\mathcal{N} = 2$ theories.

Table 5.12: *The orthosymplectic quivers on the left have Coulomb branches that are closures of exceptional algebras E_n for $n = 8, 7, 6, 5, 4$. Red nodes with an index k denote $\mathrm{SO}(k)$ groups while blue nodes with index $2k$ denote $\mathrm{USp}(2k)$ groups. Folding these quivers along the identical legs gives the non-simply laced orthosymplectic quivers on the right. The Coulomb branches of these theories are given as well. In all the quivers here, there is an overall $\mathbb{Z}_2$ which is ungauged, see [2] for more details.*

Before folding		After folding	
Orthosymplectic quiver	Coulomb branch	Orthosymplectic quiver	Coulomb branch
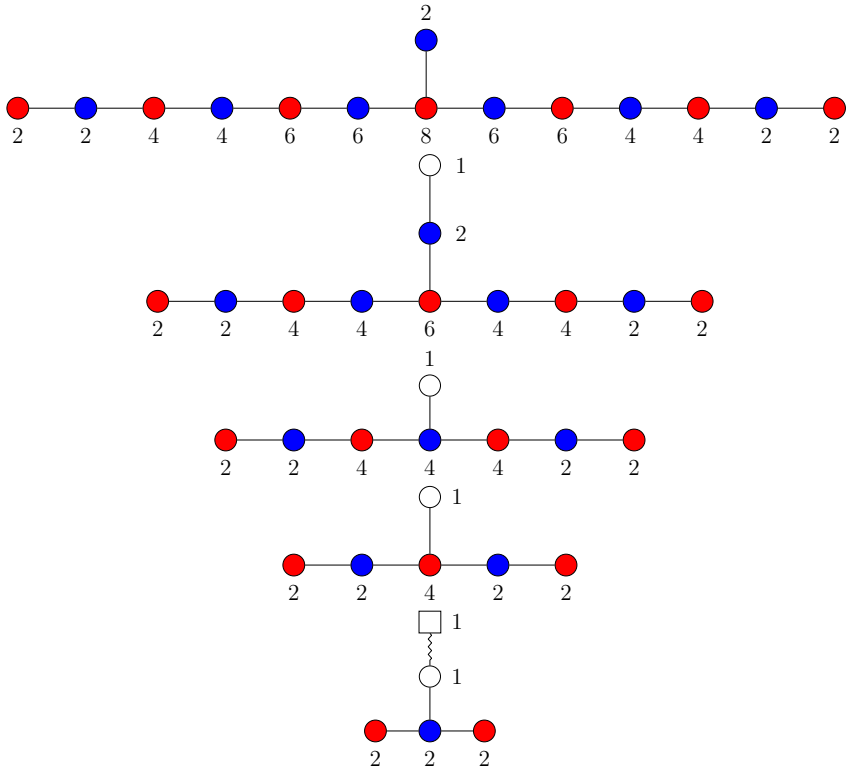	$\overline{\mathcal{O}}^{\mathfrak{e}_8}_{\min} = e_8$	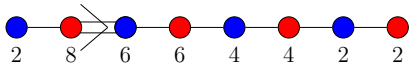	$\overline{\mathcal{O}}^{\mathfrak{e}_7}_{\min} = e_7$
	$\overline{\mathcal{O}}^{\mathfrak{e}_7}_{\min} = e_7$	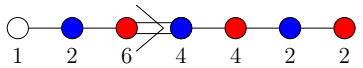	$\overline{\mathcal{O}}^{\mathfrak{e}_6}_{\min} = e_6$
	$\overline{\mathcal{O}}^{\mathfrak{e}_6}_{\min} = e_6$	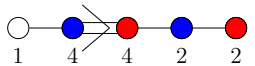	$\overline{\mathcal{O}}^{\mathfrak{so}(10)}_{\min} = d_5$
	$\overline{\mathcal{O}}^{\mathfrak{so}(10)}_{\min} = d_5$	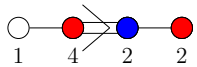	$\overline{\mathcal{O}}^{\mathfrak{so}(8)}_{\min} = d_4$
	$\overline{\mathcal{O}}^{\mathfrak{sl}(5)}_{\min} = a_4$	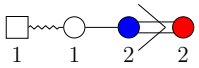	$\overline{\mathcal{O}}^{\mathfrak{sl}(4)}_{\min} = a_3$

We will now discuss these cases in more detail.

5.3.4 E_n orbits

To begin with, consider the folding of orthosymplectic quivers whose Coulomb branches are closures of E_n minimal nilpotent orbits: $\overline{\mathcal{O}}_{\text{min}}^{\mathfrak{e}_n}$ for $n = 4, 5, 6, 7, 8$. Since the quivers are all unframed, there is a non-trivial choice of the discrete group $H \subset \mathbb{Z}_2$ that one can ungauge. For all the quivers in this section, the Coulomb branches are defined by the choice $H = \mathbb{Z}_2$, see [2] for more details. The results are summarized in Table 5.12 along with the identification of the Coulomb branch. Below, some observations for the individual cases are discussed in turn and how they are compared with folding their unitary quiver counterparts.

E_8 orbit. The unitary quiver whose Coulomb branch is the closure of the minimal E_8 orbit takes the form of the affine Dynkin diagram of E_8. The unitary quiver does not have any identical legs and, therefore, cannot be folded. In contrast, the orthosymplectic quiver with the same Coulomb branch is given in the first row of Table 5.12 and has two identical legs that one can fold. Folding these identical legs gives a non-simply laced quiver, see Table 5.12, whose Coulomb branch is the closure of the minimal E_7 orbit $\overline{\mathcal{O}}_{\text{min}}^{\mathfrak{e}_7}$.

E_7 orbit. The unitary quiver whose Coulomb branch is the closure of the minimal E_7 orbit takes the form of the affine Dynkin diagram of E_7 and, hence, has two identical legs one can fold. Folding them yields the non-simply laced unitary quiver whose Coulomb branch is $\overline{\mathcal{O}}_{\text{min}}^{\mathfrak{e}_6}$. The orthosymplectic quiver of E_7 is provided in the second row of Table 5.12 and has two identical legs. Folding these two legs also gives the non-simply laced orthosymplectic quiver whose Coulomb branch is $\overline{\mathcal{O}}_{\text{min}}^{\mathfrak{e}_6}$.

E_6 orbit. The unitary quiver is the affine E_6 Dynkin diagram which has three identical legs. When two of the legs are folded, the resulting Coulomb branch is $\overline{\mathcal{O}}_{\text{min}}^{\mathfrak{f}_4}$ [137].[6] The orthosymplectic quiver of E_6 is listed in the third row of Table 5.12 and has only two identical legs. Folding them results in the non-simply laced quiver whose Coulomb branch is $\overline{\mathcal{O}}_{\text{min}}^{\mathfrak{e}_5} \cong \overline{\mathcal{O}}_{\text{min}}^{\mathfrak{so}(10)}$.

[6] Folding all three identical legs gives the minimal nilpotent orbit of $\mathfrak{so}(8)$ [6].

The discrepancy is not necessarily a surprise since there are several different embeddings of $\mathbb{Z}_2$ in E_6.

To summarize, one reaches the surprising statement that folding orthosymplectic quivers whose Coulomb branch are closures of the minimal E_8, E_7, E_6 nilpotent orbits gives non-simply laced quivers whose Coulomb branches are closures of the $E_7, E_6, E_5 \cong D_5$ orbits respectively.

E_5 orbit. The unitary quiver is the affine D_5 Dynkin diagram. Folding the pairs of identical nodes on the two sides of the diagram produces a quiver with two non-simply laced edges

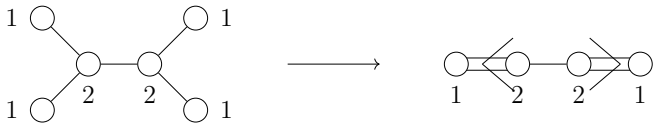

(5.26)

The Coulomb branches of the quivers on the right are the minimal orbits of $\overline{\mathcal{O}}_{\text{min}}^{\mathfrak{so}(8)}$ [6]. The orthosymplectic quiver of D_5 is listed in the fourth row of Table 5.12 (which is reproduced here):

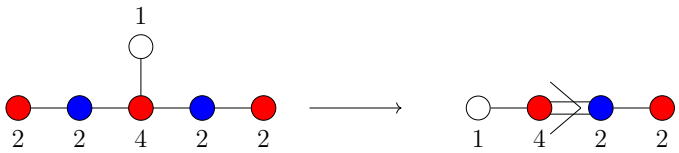

(5.27)

One can verify that the Coulomb branch of the folded orthosymplectic quiver is also $\overline{\mathcal{O}}_{\text{min}}^{\mathfrak{so}(8)}$.

As a comment, (5.26) has the D_5 Dynkin diagram on the left and the twisted affine $D_4^{(2)}$ Dynkin diagram on the right [151]. This pattern generalises to any n, meaning that the affine D_n Dynkin quiver, whose Coulomb branch is $\overline{\mathcal{O}}_{\text{min}}^{\mathfrak{so}(2n)}$, can be folded to the twisted affine $D_{n-1}^{(2)}$ Dynkin quiver, whose Coulomb branch is $\overline{\mathcal{O}}_{\text{min}}^{\mathfrak{so}(2n-2)}$.

E_4 orbit. The unitary quiver is the affine A_4 Dynkin diagram, which after framing does not have identical legs attached to a pivot node, and hence cannot be folded in the common way. The orthosymplectic quiver with the same Coulomb branch is listed in the fifth row of Table 5.12, which does have two identical legs that one can fold. The wiggly line denotes a charge 2 hypermultiplet, see [3] for more details. The Coulomb branch of the folded non-simply laced orthosymplectic quiver is $\overline{\mathcal{O}}_{\text{min}}^{\mathfrak{sl}(4)}$.

A feature of orthosymplectic quivers whose Coulomb branches are closures of exceptional algebras is that they always have two identical legs one can fold. This reflection symmetry is not always present in the unitary quiver counterparts.

$\mathbb{Z}_2$ projection on representations

The results can be explained using representation theory. In [138], 5d $\mathcal{N}=1$ theories are compactified on a circle with $\mathbb{Z}_2$ twist. First, one seeks to find a subgroup $H_{5\text{d}}$ of the global symmetry group $G_{5\text{d}}$ of the 5d SCFT such that $H_{5\text{d}} \cong H_1 \times H_1 \times H_2$. In other words, $H_{5\text{d}}$ must contain two identical groups. Next, consider the $\mathbb{Z}_2$ invariant part of $H_1 \times H_1$. This way, during the compactification, the $\mathbb{Z}_2$ acts diagonally and only representations invariant under this action remain.

Consider the E_8 quiver. E_8 contains the following subgroup:

$$E_8 \supset \mathrm{SO}(8)_A \times \mathrm{SO}(8)_B \,. \tag{5.28}$$

The adjoint representation of E_8 decomposes as:

$$\begin{aligned}(\mu_8)_{E_8} \to &(\mu_1)_{\mathrm{SO}(8)_A}(\mu_1)_{\mathrm{SO}(8)_B} + (\mu_2)_{\mathrm{SO}(8)_A} + (\mu_2)_{\mathrm{SO}(8)_B} \\ &+ (\mu_3)_{\mathrm{SO}(8)_A}(\mu_4)_{\mathrm{SO}(8)_B} + (\mu_4)_{\mathrm{SO}(8)_A}(\mu_3)_{\mathrm{SO}(8)_B}\end{aligned} \tag{5.29}$$

where $(\mu_i)_{E_8}$, $(\mu_i)_A$, $(\mu_i)_B$ are the highest weight fugacities of E_8, $\mathrm{SO}(8)_A$, and $\mathrm{SO}(8)_B$ respectively. The $\mathbb{Z}_2$ group acts on the adjoint representation as follows:

$$\begin{aligned}(\mu_2)_{\mathrm{SO}(8)_A} + (\mu_2)_{\mathrm{SO}(8)_B} &\to (\mu_2)_{\mathrm{SO}(8)_{\text{diag}}} \\ (\mu_1)_{\mathrm{SO}(8)_A}(\mu_1)_{\mathrm{SO}(8)_B} &\to (\mu_1^2)_{\mathrm{SO}(8)_{\text{diag}}} \\ (\mu_3)_{\mathrm{SO}(8)_A}(\mu_4)_{\mathrm{SO}(8)_B} + (\mu_4)_{\mathrm{SO}(8)_A}(\mu_3)_{\mathrm{SO}(8)_B} &\to (\mu_3^2)_{\mathrm{SO}(8)_{\text{diag}}} + (\mu_4^2)_{\mathrm{SO}(8)_{\text{diag}}}\end{aligned} \tag{5.30}$$

Since $\mathrm{SO}(8)_{\text{diag}} \subset \mathrm{SU}(8) \subset E_7$, the irreducible representation after the projection precisely gives

the adjoint representation for E_7:

$$(\rho_1)_{E_7} = (\kappa_1\kappa_7)_{\mathrm{SU}(8)} + (\kappa_4)_{\mathrm{SU}(8)} = (\mu_2)_{\mathrm{SO}(8)} + (\mu_1^2)_{\mathrm{SO}(8)} + (\mu_3^2)_{\mathrm{SO}(8)} + (\mu_4^2)_{\mathrm{SO}(8)} \tag{5.31}$$

where ρ_i, κ_i are highest weight fugacities of E_7 and SU(8) respectively.

This process is beautifully encoded in the folding procedure. When given a quiver, the balance of the gauge nodes determines the global symmetry group[7]. If one singles out a subset of balanced nodes, then this subquiver gives a subgroup of the global symmetry. For the E_8 quiver, one natural branching to subgroups is to identify the identical legs:

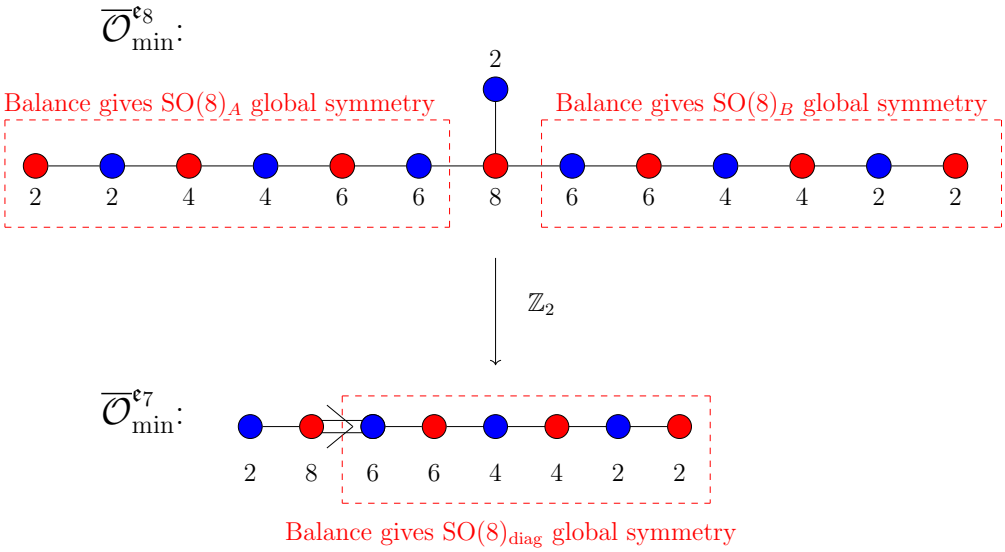

(5.32)

For a unitary magnetic quiver of E_8, the quiver takes the form of the E_8 affine Dynkin diagram which does not have a natural $\mathrm{SO}(8) \times \mathrm{SO}(8)$ subgroup one can identify and fold. This is an advantage of the E_n orthosymplectic quivers in general which always has a natural $\mathbb{Z}_2$ symmetry one can fold.

One can repeat this procedure for the remaining E_n families and the result reproduce the global symmetry of the folded quivers.

[7]To be more precise, it gives the algebra of the global symmetry group.

Table 5.13: *Generalised families of E_n orthosymplectic quivers of those in Table 5.12. The orthosymplectic quivers before folding are magnetic quivers of certain 5d $\mathcal{N}=1$ SQCD theories at infinite gauge coupling. The subscript next to the gauge group is the Chern-Simons level. For the E_{3-2l} family, the Coulomb branch of the magnetic quiver is only one of the two cones in the Higgs branch of the 5d theory. The global symmetry is given for $k>1$ and $k>l+1$, it enhances for $k=1$ or $k=l+1$ as shown in Table 5.12.*

	Before folding			After folding	
Family	Magnetic quiver (infinite coupling)	5d quiver	Global Symmetry	Magnetic quiver	Global Symmetry
E_8	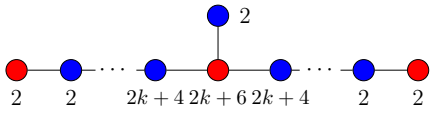	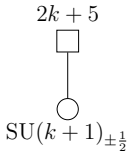	$\mathfrak{so}(4k+12)$	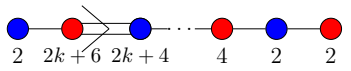	$\mathfrak{su}(2k+6)$
E_7	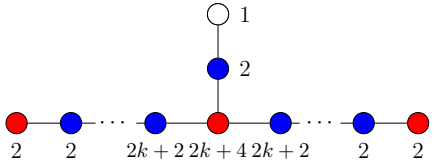	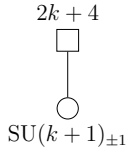	$\mathfrak{so}(4k+8)\oplus\mathfrak{su}(2)$	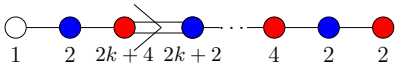	$\mathfrak{su}(2k+4)\oplus\mathfrak{su}(2)$
E_6	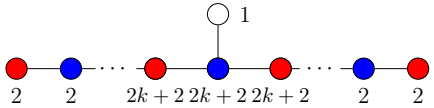	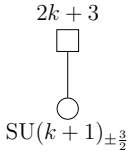	$\mathfrak{so}(4k+6)\oplus\mathfrak{u}(1)$	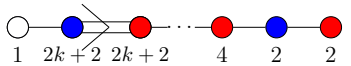	$\mathfrak{u}(2k+3)$
E_5	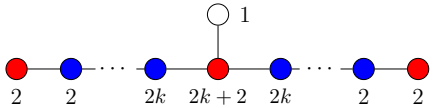	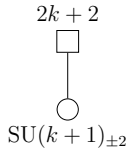	$\mathfrak{so}(4k+4)\oplus\mathfrak{u}(1)$	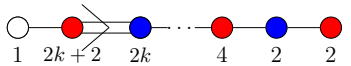	$\mathfrak{u}(2k+2)$
E_{4-2l}	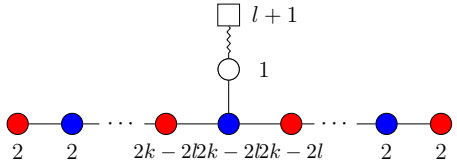	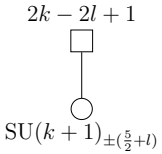	$\mathfrak{so}(4k-4l+2)\oplus\mathfrak{u}(1)$	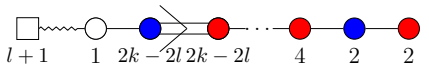	$\mathfrak{u}(2k-2l+1)$
E_{3-2l}	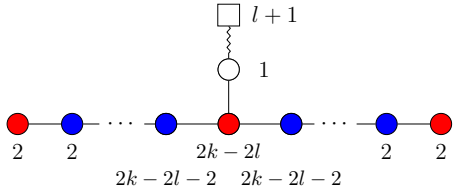	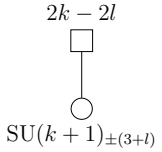	$\mathfrak{so}(4k-4l)\oplus\mathfrak{u}(1)$	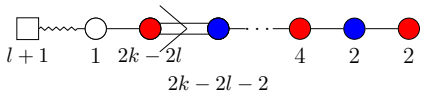	$\mathfrak{u}(2k-2l)$

Table 5.14: *The non-simply laced orthosymplectic quiver families and the unitary quiver family which have the same Coulomb branches. The highest weight generating function (HWG) is presented in the form of a plethystic logarithm (PL). The fugacities correspond to the global symmetry given in the last column of Table 5.13, with q denoting a $\mathfrak{u}(1)$ factor and ν denoting an $\mathfrak{su}(2)$ factor when present.*

Magnetic quiver (orthosymplectic)	Magnetic quiver (unitary)	PL[HWG]
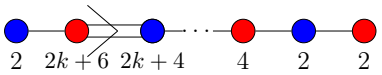	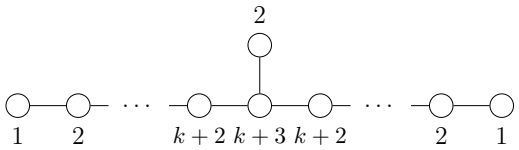	$\sum_{i=1}^{k+2} \mu_i \mu_{2k+6-i} t^{2i} + t^4 + \mu_{k+3}(t^{k+1} + t^{k+3})$
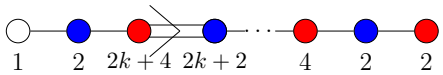	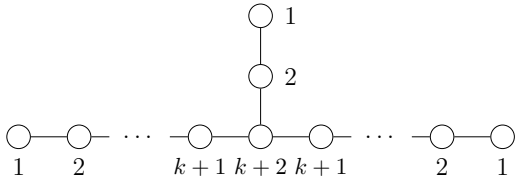	$\sum_{i=1}^{k+2} \mu_i \mu_{2k+4-i} t^{2i} + \nu^2 t^2 + t^4$ $+\nu\mu_{k+2}(t^{k+1} + t^{k+3}) - \nu^2 \mu_{k+2}^2 t^{2k+6}$
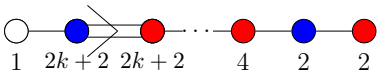	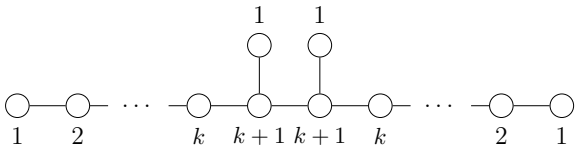	$\sum_{i=1}^{k} \mu_i \mu_{2k+3-i} t^{2i} + t^2 + (\mu_{k+1} q + \mu_{k+2}/q) t^{k+1}$
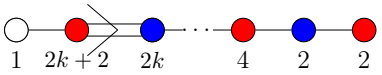	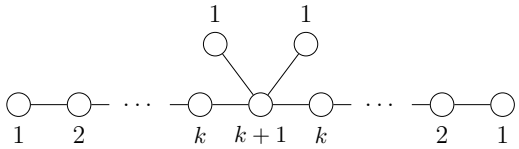	$\sum_{i=1}^{k} \mu_i \mu_{2k+2-i} t^{2i} + t^2 + \mu_{k+1}(q + 1/q) t^{k+1}$
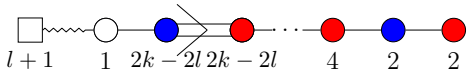	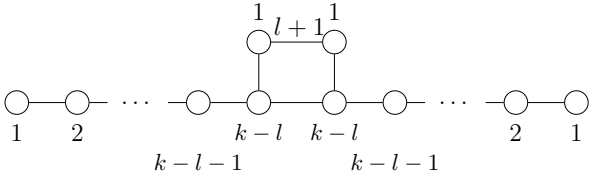	$\sum_{i=1}^{k-l} \mu_i \mu_{2k-2l+1-i} t^{2i} + t^2$ $+(\mu_{k-l} q) t^{k+1} + (\mu_{k-l+1}/q) t^{k+1} - \mu_{k-l}\mu_{k-l+1} t^{2k+2}$
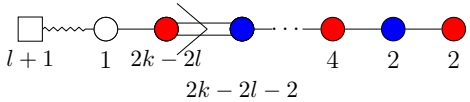	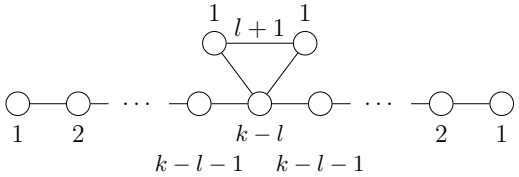	$\sum_{i=1}^{k-l} \mu_i \mu_{2k-2l-i} t^{2i} + t^2$ $+\mu_{k-l}(q + 1/q) t^{k+1} - \mu_{k-l}^2 t^{2k+2}$

5.3.5 E_n families and Magnetic quivers of 4d $\mathcal{N} = 2$

In the previous section, a class of unitary magnetic quivers of 5d $\mathcal{N} = 1$ SQCD has been folded to produce general sequences whose limiting cases are 4d $\mathcal{N} = 2$ rank 1 theories. In cases where the folding involves two identical legs, this procedure produces the Higgs branches of 5d theories compactified on a circle with a $\mathbb{Z}_2$ twist [138]. However, note that folding magnetic quivers of 5d $\mathcal{N} = 1$ theories does not always give rise to magnetic quivers of 4d $\mathcal{N} = 2$ theories.

As seen in Table 4.9, some unitary magnetic quivers, which do not have identical legs, have orthosymplectic counterparts that do have identical legs. The orthosymplectic quivers studied here are examples like that where the unitary counterparts (tabulated in [3, Tab. 1]) lack this symmetry. In this section, the generalized families of orthosymplectic quivers are considered and folded. The results are summarized in Table 5.13.

Like the unitary quivers, one conjectures that some of the folded orthosymplectic quivers are magnetic quivers of known 4d $\mathcal{N} = 2$ theories. In other words, the Coulomb branch of these folded orthosymplectic quivers are the Higgs branch of 4d $\mathcal{N} = 2$ theories. To be concrete, focus on the rank 1 cases in Table 5.12. After folding the E_8, E_7, D_5 orthosymplectic quivers, the resulting Coulomb branches are minimal nilpotent orbit closures of E_7, E_6, D_4 respectively. These are Higgs branches of known 4d $\mathcal{N} = 2$ rank 1 theories. On the other hand, folding the E_6, A_4 orthosymplectic quivers give Coulomb branches that are minimal nilpotent orbit closures of D_5, A_3 respectively which are not the Higgs branches of known rank 1 4d theories [131]. It has been shown in [152], via anomaly matching on the Higgs branch, that D_5, A_3 minimal nilpotent orbit closures (or equivalently, one-instanton moduli spaces) are excluded as Higgs branches of rank 1 4d $\mathcal{N} = 2$ theories. This shows only a subset of the folded orthosymplectic quivers are actually magnetic quivers for 4d $\mathcal{N} = 2$ theories.

Following this argument, one can generalize each E_n non-simply laced orthosymplectic quiver to infinite families as in Table 5.13 where the corresponding 5d theories are given as well. The families obtained from folding the E_8, E_7 and $E_5 \cong D_5$ families give rise to known 4d $\mathcal{N} = 2$ theories. These are all class S theories. For E_8 and E_7 folded families, these are Sicilian theories with A-type punctures (A-type $6d$ $\mathcal{N} = (2, 0)$ theories compactified on a sphere with 3 punctures) as studied in [115]. Using the parameterisation given in Table 5.14, the folded E_8

family gives the $[k+3],[k+3],[2^2,1^{k-1}]$ Sicilian theory where punctures are labelled by their partition data. The folded E_7 family gives $[k+2],[k+2],[3,1^{k-1}]$ Sicilian theory. Finally, the $E_5 \cong D_5$ folded family is the magnetic quiver for the 4d $\mathcal{N}=2$ SCFT of $\mathrm{SU}(k+1)$ with $2k+2$ flavours.

For the remaining three families in Table 5.14, the theories do not resemble magnetic quivers of known 4d $\mathcal{N}=2$ theories. Nevertheless, they are magnetic quivers for 5d $\mathcal{N}=1$ theories. For the E_6 folded family, the corresponding 5d theory is $\mathrm{SU}(k+1)_{\pm 1}$ with $2k+2$ flavours at infinite gauge coupling. The E_{4-2l} folded family is a magnetic quiver of one of the two cones of the Higgs branch of the 5d $\mathrm{SU}(k+1)_{\pm\frac{1}{2}}$ with $2k-2l+1$ flavours at infinite gauge coupling. The E_{3-2l} folded family is a magnetic quiver of one of the two cones of the Higgs branch of the 5d $\mathrm{SU}(k+1)_0$ with $2k-2l+1$ flavours at infinite gauge coupling.

The HWGs in Table 5.14 can be obtained by taking the Coulomb branch HWG of the magnetic quiver before folding, see [2], and applying appropriate $\mathbb{Z}_2$ projections. Due to the unitary counterpart, the HWGs that are equivalent to those of the folded quivers are already computed in [122, 153, 22, 11].

5.4 Class $\mathcal{S}$ orthosymplectic quivers

Based on our paper [2]

The seminal paper of [70] opens the door to constructing arbitrary 4d $\mathcal{N}=2$ SCFTs through gluing together elementary building blocks called *fixtures* [115] (or triskelions in [94]). These theories are known as class $\mathcal{S}$ theories. The purpose of this section is to study the Higgs branch of class $\mathcal{S}$ theories using magnetic quivers. Many of these magnetic quivers are unframed orthosymplectic quivers, which is the focus of this section. Choosing $H=\mathbb{Z}_2$, we find their Coulomb branch Hilbert series to be consistent with expectations on the Higgs branch of the class $\mathcal{S}$ theory [115, 114]. This provides an explicit check of the 3d mirror symmetry claim between class $\mathcal{S}$ theories on S^1 and star-shaped orthosymplectic quivers [113].

Class $\mathcal{S}$ theories are $6d$ $\mathcal{N}=(2,0)$ theories with gauge algebra J compactified on a three-punctured Riemann sphere. By computing the 3d $\mathcal{N}=4$ Coulomb branch of the star-shaped

magnetic quiver that is derived from the class $\mathcal{S}$ data along the lines proposed in [113], we obtain the Higgs branch of the corresponding 4d class $\mathcal{S}$ theories:

$$\mathcal{H}^{4d}\left(\begin{array}{c}\rho_2\\ \rho_1\\ \rho_3\end{array}\right) = \mathcal{C}^{3d}\left(\begin{array}{c}\text{Three-legged magnetic quiver}\\ \text{with } T_{\rho_1}(J),\, T_{\rho_2}(J)\,,\, T_{\rho_3}(J)\\ \text{joined at central node } J\end{array}\right). \tag{5.33}$$

where the quivers $T_\rho(J)$ are linear quivers whose structure is indicated by the partition ρ. More detail can be found in [62][8].

So far in this thesis we have looked at several orthosymplectic quivers that corresponds to class $\mathcal{S}$ theory with untwisted D_r-type punctures. These are star shaped quivers with an SO($2r$) gauge group in the centre. As a set of different examples, we consider A_{2r-1} twisted fixtures, which have a central USp(2r) gauge group. Our paper [2] is the first time the magnetic quivers of such fixtures appear in the literature.

Twisted A_{odd} fixtures

The quivers investigated here are known as A_{2r-1} twisted fixtures. These include two twisted A_{2r-1} punctures and an untwisted A_{2r-1} puncture. The twisting map folds A_{2r-1} onto C_r via outer automorphism. As a result, when we study the three-legged magnetic quiver, the two twisted A_{2r-1} punctures have USp($2r$) flavor nodes, and the fixture acquires a $J = \text{USp}(2r)$ central gauge node. The untwisted puncture has a SU($2r$) flavor node. During gluing, only the USp($2r$) $\subset$ SU($2r$) subgroup of the untwisted A_{2r-1} puncture is gauged[9]. This produces an unitary-orthosymplectic quiver. For $r = 2$, the linear quivers corresponding to different twisted punctures are tabulated in Figure 5.1 and for untwisted punctures in Figure 5.2.

The magnetic quivers are constructed by gluing such quivers. For example, the magnetic quiver for the fixture containing two maximal A_3 twisted punctures $T_{(1^5)}(\text{USp}(4))$ and one

[8]One important feature of $T_\rho(J)$ is that their $3d$ $\mathcal{N} = 4$ Higgs branch are closures of the nilpotent orbit with partition ρ of $\mathfrak{j} = \text{Lie}(J)$ which we denote as $\overline{\mathcal{O}}^{\mathfrak{j}}_{\rho}$

[9]This reproduces a similar procedure in [113] when treating twisted D_r punctures. The quiver corresponding to twisted D_r punctures have SO($2r-1$) flavor nodes whereas untwisted D_r have SO($2r$) flavor nodes. As a result, when constructing the three-legged magnetic quiver, only the SO($2r-1$) $\subset$ SO($2r$) subgroup is gauged in the untwisted puncture. We thank a discussion with Gabi Zafrir in coming out with this result.

Orbit σ	Dual Orbit $d_{BV}(\sigma)$	Dual Slice Dimension	Dual Slice Symmetry	Quiver
(1^4)	(5)	0	$\emptyset$	Trivial
(2^2)	$(3,1^2)$	1	SO(2)	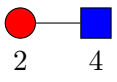
(4)	(1^5)	4	SO(5)	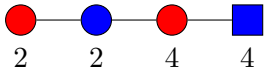

Figure 5.1: *$T(\mathrm{USp}(4))$ linear quivers. These are used in twisted A_3 fixtures. The quivers $T_{d_{BV}(\sigma)}(\mathrm{USp}(4))$ have non-diverging monopole formula. The partitions identify special orbits of* USp(4) *and its GNO dual* SO(5)*.*

Orbit σ	Dual Orbit $d_{BV}(\sigma)$	Dual Slice Dimension	Dual Slice Symmetry	Quiver
(1^4)	(4)	0	$\emptyset$	Trivial
$(2,1^2)$	$(3,1)$	1	U(1)	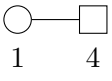
(2^2)	(2^2)	2	SU(2)	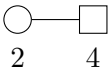
$(3,1)$	$(2,1^2)$	3	SU(2) × U(1)	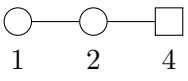
(4)	(1^4)	6	SU(4)	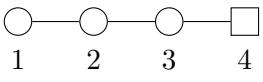

Figure 5.2: *$T(\mathrm{SU}(4))$ linear quivers. These quivers correspond to untwisted A_3 punctures. All the quivers $T_{d_{BV}(\sigma)}(\mathrm{SU}(4)) = T_{\sigma^T}(\mathrm{SU}(4))$ have non-diverging monopole formula;*

maximal A_3 untwisted puncture $T_{(1^5)}(\mathrm{SU}(4))$ can be glued together in the following way:

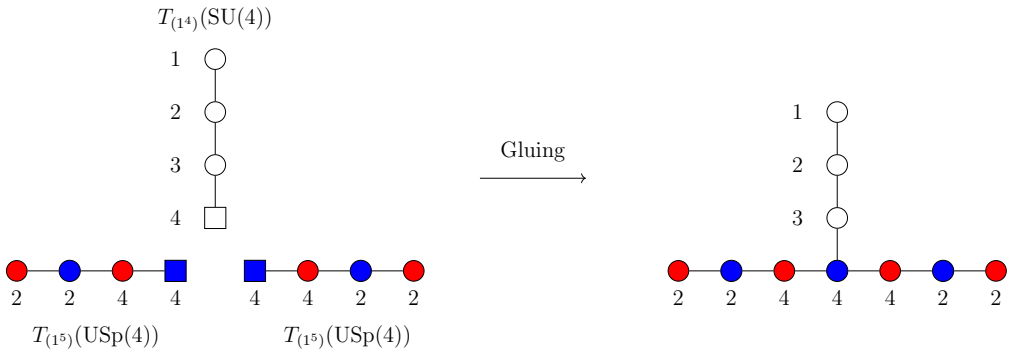

(5.34)

where the quiver after gluing is the three-legged magnetic quiver.

We tabulate twisted fixtures of A_3 in Figure 5.3. The global symmetries match those in [154]. We only provide the algebra of the global symmetry group as we often do not have the HWG required to precisely identify the group. With the monopole formula, we are unable to refine a Hilbert series with (special) orthogonal and symplectic gauge nodes. However, when there are unitary gauge nodes, we may be able to partially refine the Hilbert series by assigning the usual root fugacities to the unitary gauge nodes. The lack of HWG here is in contrary to previous orthosymplectic quivers where we were always able to find an unitary counterpart.

For A_{2n} twisted punctures we obtain $\mathrm{SO}(2n+1)$ flavor nodes and therefore the central node of our star-shaped magnetic quiver will be $\mathrm{SO}(2n+1)$ [155, 156]. We will not look at this family of quivers in this thesis.

The first row of Figure 5.3 is the E_6 quiver already investigated in Section 4.5.1. The unitary-orthosymplectic quiver in the second row has a non-simply laced unitary quiver counterpart with the same Coulomb branch and is a member of the $C_{n+1} \times A_1$ rank 1 $4d$ $\mathcal{N} = 2$ SCFT sequence we saw in the previous section.

Quiver	Global Symmetry	$\dim_{\mathbb{H}}(\mathcal{C})$	Hilbert Series	Plethystic Logarithm
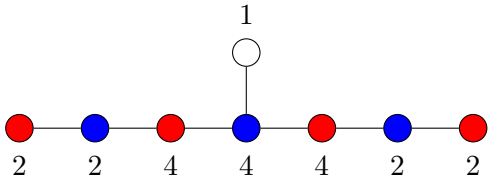	$\mathfrak{e}_6$	11	$\frac{(1+t^2)\,\mathcal{P}_{20}(t)}{(1-t^2)^{22}}$ $= 1 + 78t^2 + 2430t^4 + 43758t^6 + 537966t^8 + 4969107t^{10} + O\left(t^{12}\right)$	$78t^2 - 651t^4 + 12376t^6 - 296946t^8 + 7755189t^{10} + O\left(t^{12}\right)$
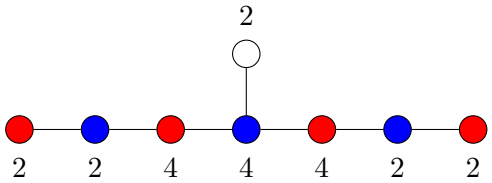	$\mathfrak{usp}(8)$ $\times$ $\mathfrak{su}(2)$	12	$\frac{\mathcal{P}_{48}(t)}{(1-t^2)^{24}(1+t^2)^{12}}$ $= 1 + 39t^2 + 878t^4 + 13396t^6 + 152412t^8 + 1370975t^{10} + O\left(t^{12}\right)$	$39t^2 + 98t^4 - 1086t^6 + 1545t^8 + 67761t^{10} + O\left(t^{12}\right)$
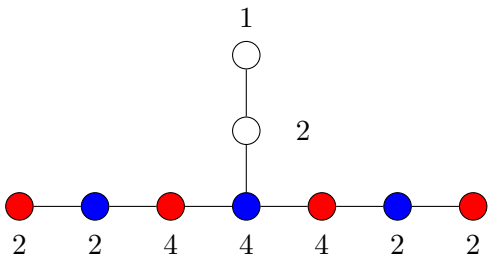	$\mathfrak{so}(5)^2$ $\times$ $\mathfrak{su}(2)$ $\times$ $\mathfrak{u}(1)$	13	$\frac{(1-t)^9\,\mathcal{P}_{86,c_2}(t)}{(1-t^2)^7(1-t^3)^{13}(1-t^4)^7(1-t^5)^8}$ $= 1 + 24t^2 + 36t^3 + 356t^4 + 932t^5 + 4367t^6 + 13272t^7 + 46189t^8 + 137468t^9 + 413087t^{10} + O\left(t^{12}\right)$	$24t^2+36t^3+56t^4+ 68t^5 - 243t^6 - 1176t^7 - 2357t^8 - 188t^9 + 18121t^{10} + O\left(t^{12}\right)$
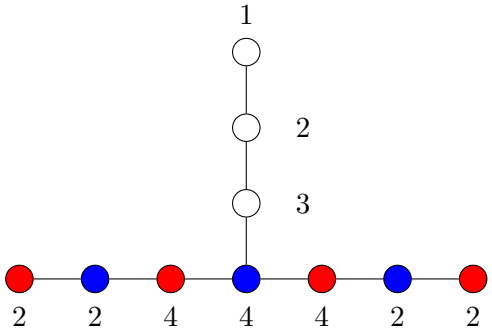	$\mathfrak{so}(5)^2$ $\times$ $\mathfrak{su}(4)$	16	$\frac{\mathcal{P}_{100}(t)}{(1-t^2)^{10}(1-t^4)^{10}(1-t^6)^{12}}$ $= 1 + 35t^2 + 724t^4 + 11242t^6 + 140062t^8 + 1453129t^{10} + 12880215t^{12} + 99473971t^{14} + 680140044t^{16} + 4172259667t^{18} + 23223084225t^{20} + O\left(t^{22}\right)$	$35t^2 + 94t^4 + 182t^6 - 3808t^8 - 7771t^{10} + O\left(t^{12}\right)$

Figure 5.3: *Magnetic quivers for twisted A_3 fixtures. We show the subset of orthosymplectic quivers whose Coulomb branch is not bad. The choice of the discrete group is $H = \ker(\phi) = \mathbb{Z}_2$. The palindromic numerator terms $\mathcal{P}_k(t)$ are very long expressions and given in Appendix E Figure 39 and 40 in [2].*

Untwisted D fixtures

The magnetic quiver of untwisted D-type fixtures are obtained by gluing together $T_\rho(\mathrm{SO}(2r))$ quivers. The linear quivers $T_\rho(\mathrm{SO}(2r))$ are listed in Figure 5.4 for $r = 3$. The magnetic quiver for a fixture with three maximal D_3 punctures is obtained by gluing three maximal legs of $T_\rho(\mathrm{SO}(6))$ [94]:

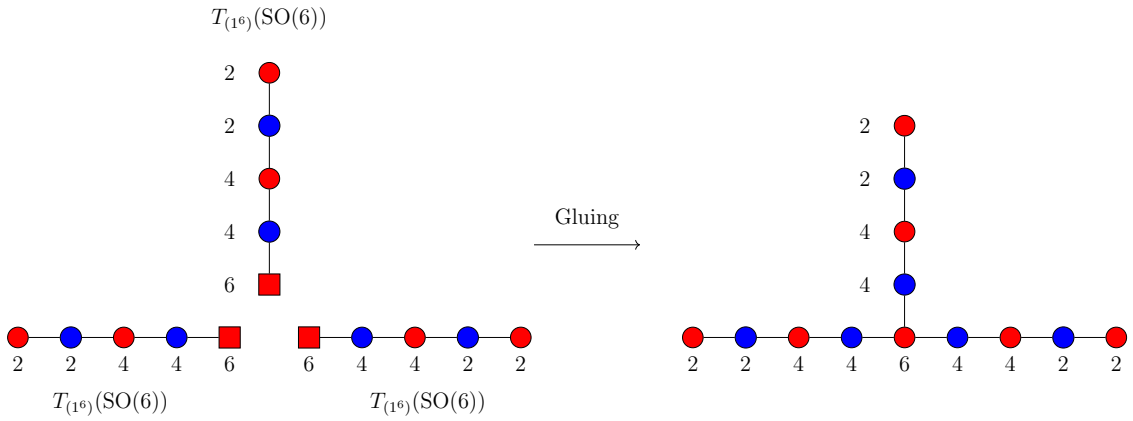

(5.35)

We have already seen several examples of magnetic quivers of such class $\mathcal{S}$ fixtures in previous sections.

Orbit σ	Dual Orbit $d_{BV}(\sigma)$	Dual Slice Dimension	Dual Slice Symmetry	Quiver
(1^6)	$(5,1)$	0	$\emptyset$	Trivial
$(2^2,1^2)$	(3^2)	1	SO(2)	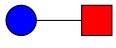
$(3,1^3)$	$(3,1^3)$	2	SO(3)	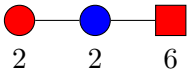
(3^2)	$(2^2,1^2)$	3	$\mathrm{USp}(2)\times\mathrm{SO}(2)$	Bad quiver
$(5,1)$	(1^6)	6	SO(6)	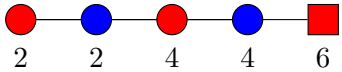

Figure 5.4: *$T(\mathrm{SO}(6))$ linear quivers. These are used in untwisted D_3 fixtures. The quivers $T_{d_{BV}(\sigma)}(\mathrm{SO}(6))$ have non-diverging monopole formula; the bad quiver with zero conformal dimension is not shown. The partitions identify special orbits of* SO(6).

Bad orthosytmplectic quivers

We encounter an interesting phenomenon where the Higgs branch of the class $\mathcal{S}$ theory is a single hyperKähler cone but nevertheless the corresponding magnetic quiver seems to be bad in the sense that the Coulomb branch Hilbert series diverges. As a result, the quivers listed here form a subset of an exhaustive list in [19] as we only list the magnetic quivers whose monopole formula is convergent. Recently in [107] and their upcoming work, a proposal is made to resolve the badness of these quivers and offer a convergent Hilbert series. It will be then be very interesting to revisit these computations and see if they match the expectations in [19].

5.4.1 Class $\mathcal{S}$ and product theories

Based on our paper [5]

Class $\mathcal{S}$ theories are meant to be constructed using fundamental building blocks of three-punctured spheres (fixtures). However, some of these building blocks are actually products of two or more SCFTs. Therefore, it is important to find which of these fundamental building blocks are not actually fundamental, but products of more fundamental SCFTs. Recalling from [126, 127] that identifying product class $\mathcal{S}$ theories is based on a systematic search without a clear smoking gun to look for. In Section 4.7 we saw that a unframed orthosymplectic quiver with a balanced set of nodes in the shape of a D-type Dynkin diagram are suggestive that the Coulomb branch is a product. And since many of these forked quivers are indeed magnetic quivers of class $\mathcal{S}$ theories, studying these families of quivers might help in the classification of class $\mathcal{S}$ theories that are products.

Under the condition that at least one of the leg be a chain of nodes ending on a balanced $SO(2)$ gauge group, we were able to classify all star-shaped orthosymplectic quivers whose Coulomb branches are products. These results can then be reinterpreted as class $\mathcal{S}$ theories using puncture data and then the statement translates to: *all* class $\mathcal{S}$ theories of classical algebra with at least one maximal puncture, whose magnetic quivers are *good*, and are the product of two SCFTs has been classified.

- The $E_8 \times E_8$ family of Table 4.11 is primarily defined as set of class $\mathcal{S}$ theories for a

three-puncture sphere with D_{2k+5} punctures. These theories factorise into two copies of the E_8 family that is understood as three-punctured sphere with D_{k+3} punctures:

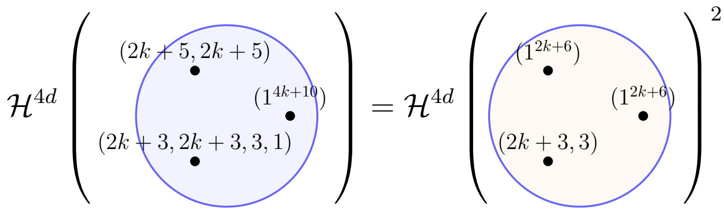

(5.36)

where the partitions are the Nahm partitions of the nilpotent orbits, following the same convention as [126, 127][10]. In particular, partition (1^{2n}) of D_n corresponds to the maximal nilpotent orbit.

- The $E_7 \times E_7$ family, see Table 4.11, is firstly defined by a three-punctured sphere with D_{2k+3} punctures. The latter factorises into two copies of the so-called E_7 family that are defined by D_{k+2} punctures:

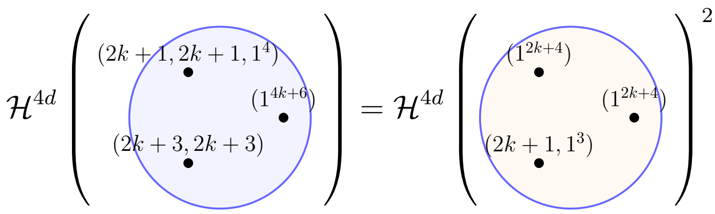

(5.37)

- The $E_6 \times E_6$ family of Table 4.11 can be understood as the class $\mathcal{S}$ theory of a three-punctured sphere with D_{2k+2} punctures. Again, it factorises into two copies of the E_6 family, defined by A_{2k+1} punctures:

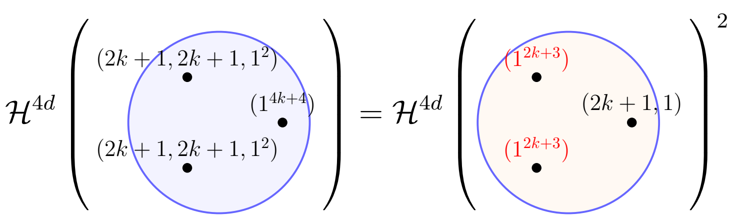

(5.38)

where the red partition denotes the B partitions of the twisted A_{2n+1} punctures.

The rarity of such decomposable three-punctured spheres has been noted in [126], where examples for D_N theories with $N = 4$ have been presented. In response to one of the observations in [126], the results of this paper show that only when $k = 1$ does the Coulomb branch carry exceptional

[10] This is not the same convention as we used in the previous subsection.

global symmetry; whereas for $k > 1$, the global symmetry is composed of classical groups.

For a four-punctured sphere with one maximal puncture, the only family that factorises is the $E_8 \times \mathrm{SO}(16)$ family given by D_{2k+1} punctures:

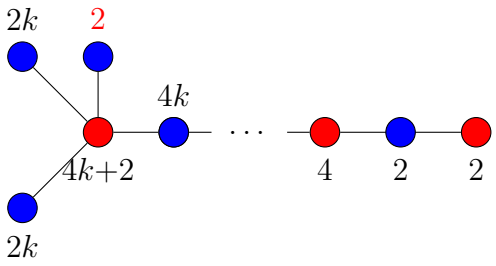

(5.39)

The moduli space is the product of the Higgs branch of a class $\mathcal{S}$ theory with D_{k+1} punctures and the nilpotent orbit closure $\overline{\mathcal{O}}^{\mathfrak{so}(4k+4l)}_{(2^{2k},1^{4l})}$.

$$\mathcal{H}^{4d}\left[\begin{array}{c}\\ \\ \end{array}\right. \quad = \mathcal{H}^{4d}\left[\begin{array}{c}\\ \\ \end{array}\right] \times \overline{\mathcal{O}}^{\mathfrak{so}(4k+4)}_{(2^{2k},1^{4})} . \tag{5.40}$$

For five or more punctures, it can be shown that the fork cannot be balanced and, therefore, the product structure does not appear. For class $\mathcal{S}$ theories without maximal punctures, we have yet to find a single example where the theory factorizes. For *bad* star-shaped quivers, no further analysis has been attempted in this work. Nonetheless, there are conjectures where product theories can arise from bad theories; for examples, a different realization of the $E_8 \times E_8$ theory as a bad quiver has been given in [106].

Interlude - Orthosymplectic program

Orthosymplectic quivers are much less studied in the literature compared to their unitary counterparts. Part of the reason is that they are more difficult to study.

In brane systems, things are more complicated because orientifold planes are always present which changes the dynamics of the branes non-trivially. However, it is precisely these phenomenons that lead to interesting new physics. For example, intersecting orientifold planes significantly complicates the brane system but leads to moduli spaces that are products. Such phenomenons can never appear in brane systems that describe unitary quivers.

Another complication arises when one tries to compute partition functions such as superconformal indices, topologically twisted indices, S^3 partition functions. Computations often takes longer and there are many subtleties involving disconnected subgroups such as $SO(n)$ vs $O(n)$. Computing S^3 partition functions is difficult due to lack of FI parameters for orthosymplectic gauge groups.

The introduction of the monopole formula resolves much of the computational difficulty of orthosymplectic quivers. Due to the Weyl action, a rank n (special) orthogonal or symplectic gauge group requires fewer magnetic charges to be summed over compared to a $U(n)$ gauge group[11]. However, an issue remains that the refinement of the monopole formula requires the gauge group to be non-simply connected so that there is a topological symmetry that the monopoles can be charged under. In the IR fixed point, the topological symmetries then enhances to the Coulomb branch global symmetry of the theory. This makes things challenging for orthosymplectic quivers since the $Sp(n)$ gauge groups are simply connected whereas the

[11]Of course, for the exact Hilbert series, the total magnetic charges to be summed over will always be infinity. But if you are only computing a perturbative series to some order, the number of charges to be summed over is finite.

$SO(n)$ gauge groups for $n > 2$ do not have a continuous topological symmetry for us to charge under (the topological symmetry is $\mathbb{Z}_2$). As a result, one can at best partially refine the Hilbert series, which is not enough to write down the HWG or write down the refined generators and relations in the chiral ring[12]. The refined Coulomb branch Hilbert series can be extracted by other means such as computing the Higgs branch of its mirror or computing the refined Coulomb branch Hilbert series of its unitary counterpart (if it exists). The latter is how we obtain all the HWGs for the orthosymplectic quivers in the previous sections, which luckily all have unitary counterparts.

Despite these difficulties, the fact that we can *quickly* compute the unrefined Hilbert series of any good orthosymplectic quiver is already very powerful. The details in computing any framed/flavoured orthosymplectic quivers were already given in the monopole formula paper [36]. In our paper [2], we extend this to unframed/flavorless orthosymplectic quiver by requiring the specification of $H \subset (\mathbb{Z}_2)_{\text{diag}}$.

Now, not only do we know how to apply the monopole formula for orthosymplectic quivers with different features (framed/unframed, non-simply laced, unitary-orthosymplectic etc), we can also carry out computations very quickly. For example, the first ten orders of the Hilbert series of a quiver with $\dim_{\mathbb{H}} = 30$ Coulomb branch will take less than 10 minutes with `Mathematica`. A perturbative series to this order is normally more than enough to try to identify the Coulomb branch with a known algebraic variety. With these tools under our belt, we set forth to **classify** orthosymplectic quivers.

One way to systematically classify orthosymplectic quivers is to follow the early developments of unitary quivers. For example, the ADE Dynkin classification of unitary quiver theories describing the low-energy theories of D-branes probing an ADE singularity $\mathbb{C}^2/\Gamma_{ADE}$ [35, 157], also known as McKay correspondence. The Dynkin type quivers are completed by unitary quivers [65] in the shape of classical BC type Dynkin diagrams and quivers in the shape of exceptional G_2, F_4 Dynkin diagrams. While the ADE-type quivers admit a Lagrangian description, the $BCFG$-type quivers do have a known Lagrangian. The Coulomb branch of a Dynkin quiver of

[12]It is still achievable with some guess work involved since the dimensions of the irreducible representations of the global symmetry are known

the Lie algebra $\mathfrak{g}$ is the (reduced) one G-instanton moduli space, or equivalently, the minimal nilpotent orbit closure of $\mathfrak{g}$ [158, 159, 160]. The relationship between Coulomb branches and moduli spaces of instantons was pointed out for ADE quivers in [91], see also [161, 162], and for $BCFG$ quivers in [65]. This classification yields a set of simple moduli spaces which are ubiquitous in quiver gauge theories.

Table 5.15: *The Dynkin classification of orthosymplectic quivers.*

Dynkin type orthosymplectic quivers	
A-type	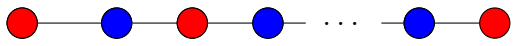
B-type	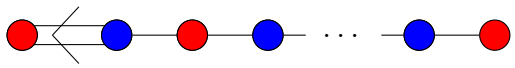
C-type	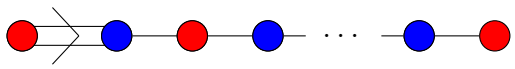
D-type	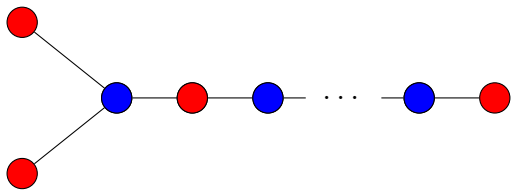

Dynkin-type classification. In this thesis, orthosymplectic quivers were explored in a similar manner — aiming to develop a Dynkin classification of balanced orthosymplectic quivers, see Tables 5.15 and 5.16:

- A**-type** orthosymplectic quivers, i.e. all edges are simply-laced and the gauge groups are arranged in a linear chain, are well known [40, 62]. These quivers, when balanced, give $SO(n)$ Coulomb branch global symmetries which can be enhanced in unframed cases by half-plus-integer contributions. Unframed cases such as the E_n families were seen in Chapter 4 which were magnetic quivers of 5d $\mathcal{N}=1$ SCFTs. They can also be magnetic quivers of $6d$ $\mathcal{N}=(1,0)$ SCFTs as shown in [163, 108, 109].

- B**-type** orthosymplectic quivers, i.e contains a balanced linear chain of nodes with a non-simply laced edge, are studied in our paper [5]. The global symmetry is $SO(n)\times SO(n-1)$ but can be enhanced in unframed cases. These are quivers whose moduli spaces can

display a product structure. We obtain B-type quivers by folding the two prongs of the fork in D-type orthosymplectic quivers, producing an outward pointing non-simply laced edge. For B-type theories, we have yet to find examples where we are confident that they are magnetic quivers of higher dimensional SCFTs[13].

- **C-type** orthosymplectic quivers, i.e contains a balanced linear chain of nodes with a non-simply laced edge, are studied in our paper [8]. We differentiate these from B-type by ensuring that the edge points towards the longer chain of the quiver whereas the direction is opposite as B-type. The global symmetry is $SU(n)$ but can be enhanced in unframed cases. They can be obtained by *folding* A-type orthosymplectic quivers. This is shown in Chapter 5 where folding the orthosymplectic magnetic quiver of a 5d SCFT can yield magnetic quiver of a 4d SCFT. This is the magnetic quiver operation corresponding to compactifing 5d theory on a circle with a discrete twist[14] .

- **D-type** orthosymplectic quivers, i.e contains a balanced fork and is studied in our paper [5]. The global symmetry is $SO(n) \times SO(n)$ and can be enhanced in unframed cases. These are quivers whose moduli spaces can display a product structure. The product may or may not be two identical moduli spaces. The D-type quivers are our forked quivers in Chapter 4 and some examples are shown to be magnetic quivers of product of SCFTs in $d = 4, 5, 6$.

We find many examples where the resulting $3d$ $\mathcal{N} = 4$ Coulomb branches often describes the Higgs branch of higher dimensional SCFTs. However, this does not mean that orthosymplectic quivers that are not magnetic quivers of higher dimensional theories aren't worth studying. They can be interesting on their own right as $3d$ $\mathcal{N} = 4$ theories, hence, the importance in a classification.

For framed/flavoured orthosymplectic quivers, most of the interesting cases we know are either $T_\rho^\sigma(G)$ theories [62] where $G = SO(n), Sp(n)$ or those whose Coulomb branch describes

[13]There are, however, some hints that the product involves a low energy 5d quiver gauge theory and another 5d theory whose coupling is tuned to infinity.

[14]Note, not all folded quivers are magnetic quivers of 4d SCFTs as discussed in the previous chapter.

slices of affine Grassmanian of type G as shown in [164]. The latter are actually unitary-orthosymplectic quivers that are framed.

For unframed/flavorless orthosymplectic quivers, it is quite miraculous that we can construct many infinite families of quivers of $ABCD$ type that have simple moduli spaces [15]. It is thus unsurprising that these theories are associated to higher dimensional SCFTs whose low energy description is a SQCD theory, rather than a multi-gauge group theory. Some of these results are summarized in Table 5.16. One interesting feature here is that all the theories contains a *maximal chain* which is a linear chain of balanced nodes that begins with SO(2). As a consequence, such a chain always results in an increasing sequence of the form

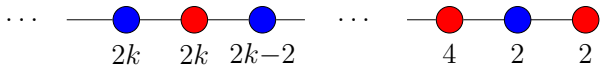

(5.41)

This is equivalent to a maximal puncture in class $\mathcal{S}$ language. Once we deviate from this property, the resulting quivers often have less desirable Coulomb branches which we were unable to match with other theories or are bad and the Hilbert series diverge.

Reverse engineering brane systems

Our approach so far is to find new quivers that describe known moduli spaces and see what it teaches us rather than finding new moduli spaces. In some cases, it taught us something about compatification $\leftrightarrow$ folding (such as B and C type), whereas other times it taught about product theories (such as D-type). Knowing these properties allows us to reverse engineer the brane systems that describe the quivers. In particular, knowing the moduli space of BCD type orthosymplectic magnetic quivers and their corresponding $d = 3, 4, 5, 6$ SCFTs, allow us to investigate the dynamics of $\mathrm{D}_d - \mathrm{D}_{d+2} -$ NS5 brane systems in the presence of $\mathrm{O}_d - \mathrm{O}_{d+2} -$ ON planes. This epitomizes the Bottom-Up approach. Now that we have a better understanding of these new brane systems, we can apply the Top-Down approach to construct new magnetic quivers with previously unknown moduli spaces.

[15] One way that we identify a simple moduli space is that the whole family can be expressed by a general HWG taking the form PE$[P(\mu_i, t)]$ where $P(\mu_i, t)$ is a polynomial in the fugacities μ_i, t

Beyond classical Dynkin type

Table 5.16: *Representative examples of ABCD-Dynkin type orthosymplectic quivers and their Coulomb branch moduli spaces. $\overline{\mathcal{O}}^{\mathfrak{g}}$ denotes the closure of a nilpotent orbit closure of the Lie algebra $\mathfrak{g}$. The subscript $_{\min}$ denotes the minimal orbit.*

Orthosymplectic quiver	Framed	Unframed
Balanced A-type	$\overline{\mathcal{O}}^{D}_{\min}$, e.g. [40]	$\overline{\mathcal{O}}^{E_n}_{\min}$, e.g. [3]
Balanced B-type	$\overline{\mathcal{O}}^{D} \times \overline{\mathcal{O}}^{B}$	$\overline{\mathcal{O}}^{E_6}_{\min} \times \overline{\mathcal{O}}^{F_4}_{\min}, \overline{\mathcal{O}}^{E_6}_{\min} \times \overline{\mathcal{O}}^{B_4}_{\min}, \overline{\mathcal{O}}^{E_8}_{\min} \times \overline{\mathcal{O}}^{B_7}, \overline{\mathcal{O}}^{F_4}_{\min} \times \overline{\mathcal{O}}^{B_4}_{\min}, \overline{\mathcal{O}}^{B} \times \overline{\mathcal{O}}^{D}$
Balanced C-type	$\overline{\mathcal{O}}^{A}_{\min}$, e.g. [8]	$\overline{\mathcal{O}}^{E_7,E_6,D_5,D_4,A_3}_{\min}$, e.g. [8]
Balanced D-type	$\overline{\mathcal{O}}^{D} \times \overline{\mathcal{O}}^{D}$	$\overline{\mathcal{O}}^{E_n}_{\min} \times \overline{\mathcal{O}}^{E_n}_{\min}, \overline{\mathcal{O}}^{E_6}_{\min} \times \overline{\mathcal{O}}^{D_5}_{\min}, \overline{\mathcal{O}}^{E_8}_{\min} \times \overline{\mathcal{O}}^{D_8}, \overline{\mathcal{O}}^{F_4}_{\min} \times \overline{\mathcal{O}}^{F_4}_{\min}, \overline{\mathcal{O}}^{B} \times \overline{\mathcal{O}}^{B}$

So far, we explored examples of all the classical Dynkin-type orthosymplectic quivers. In an upcoming work [165], we intend to study exceptional Dynkin type orthosymplectic quivers as well.

Furthermore, the balancing conditions of orthosymplectic quivers is different than that of unitary quivers, meaning it is possible to construct balanced quivers beyond Dynkin types[16]. So far, all known examples beyond Dynkin type are either bad quivers or free theories [13]. For example, take the $k = 0$ members of the E_n families where $4 \leq n \leq 8$. These are free theories of 2^{n-4} free hypermultiplets; thus, the Coulomb branch is $\mathbb{H}^{2^{n-4}}$. Similarly, for the $E_n \times E_n$ family, the theories are 2^{n-3} free hypermultiplets. The results are summarised in Table 5.17. Notice that all the nodes are balanced, and for $n = 6, 7, 8$ the balanced set of nodes do not form a Dynkin diagram of any finite algebra. For $n = 8$ case, the Dynkin diagram of E_{12} seems to arise! The discussion of balanced Dynkin diagrams beyond finite type is left for future work.

[16]This is impossible for unitary quivers as a fully balanced quiver can either be a finite or (twisted) affine Dynkin quiver depending on whether the quiver is framed or unframed.

Table 5.17: *The $k = 0$ members of the $E_n \times E_n$ family of Table 4.11 for $4 \leq n \leq 8$. These quivers are magnetic quivers for free hypermultiplets such that Coulomb branches are flat spaces. The Coulomb branch Hilbert series are given by* $\mathrm{PE}\left[2(n-3)\ t\right]$.

Family	Orthosymplectic quiver	Coulomb branch
E_8	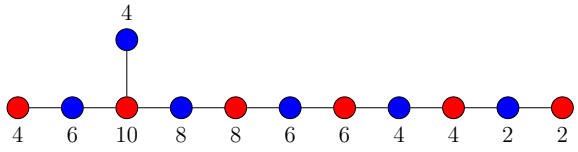	$\mathbb{H}^{32}$
E_7	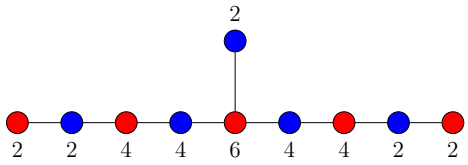	$\mathbb{H}^{16}$
E_6	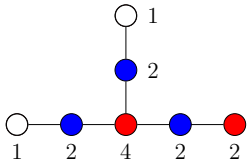	$\mathbb{H}^{8}$
E_5	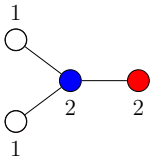	$\mathbb{H}^{4}$
E_4	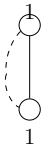	$\mathbb{H}^{2}$

Concluding remarks

Unitary quivers and special unitary quivers have been studied intensively in the last few decades. Now that we have the right tools (such as the monopole formula) and right understanding (such as presence of discrete one-form symmetries of unframed quivers that you need to ungauge), the time is ripe to explore the landscape of orthosymplectic quivers.

Chapter 6

Three dimensional gauge theories

Based on our paper [9]

In this chapter we focus *only* on 3d $\mathcal{N} = 4$ gauge theories. If the Higgs branch of the $3d$ $\mathcal{N} = 4$ electric theory[1] is a single hyperKähler cone, then the corresponding magnetic quiver is also the 3d mirror. However, if the Higgs branch is a union of several hyperKähler cones, which we will see examples of, then the magnetic quiver is no longer a 3d mirror. The indication of when there is a 3d mirror duality or the more general electric-magnetic quiver duality is summarized in Figure 6.1 for SQCD theories.

This chapter will be divided into two parts, both of which focuses on electric quivers with a *mixture* of unitary and special unitary gauge groups. The first part deal with 3d mirror pairs and the second part look at cases where there are several magnetic quivers corresponding to the same electric theory. These dual pairs are constructed through 5d brane webs and applying the fact that the classical Higgs branch is the same in 3d and in 5d.[2] This procedure is algorithmized in our `Mathematica` code that accompanied the paper.

[1] Just a reminder that the electric quivers in the previous chapters are often referred to as 'higher dimensional theory'.

[2] In this chapter, we only look at the classical Higgs branch so there are no instanton corrections, unlike in the previous chapters.

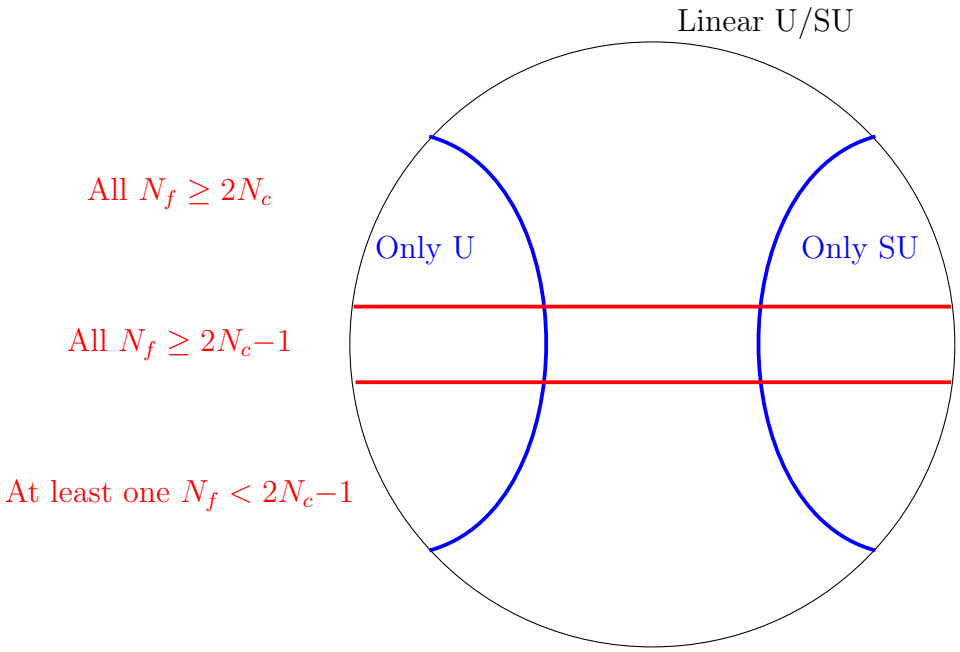

Figure 6.1: *Venn diagram of the different types of quivers discussed in this paper. N_c stands for the gauge rank of a node in the quiver, while N_f stands for the number of hypermultiplets connected to it. The circle represents all linear quivers with unitary and special unitary gauge groups, and arbitrary numbers of flavors. In the left blue region, where all gauge groups are unitary, magnetic quivers can be computed using D3-D5-NS5 systems (One can also use (fully) locked brane webs), while in the right blue region, where all the gauge groups are special unitary, one can use 5-brane webs. In the generic (middle) region, brane webs with lockings are needed. In the top region, all gauge groups have enough matter to ensure that the magnetic quiver is a 3d mirror theory. Below this, in the middle stripe, the same applies up to free hypermultiplets if only one gauge node has $N_f = 2N_c - 1$; if two gauge nodes or more satisfy this equality, the situation is more complex. In the last region, a collection of effects can happen: the Higgs branch can contain one cone or more, and the Higgs ring can possibly contain nilpotent elements, see [11].*

6.1 3d mirror of Mixed U & SU quivers

Brane set ups with D3-D5-NS5 branes produce $3d$ $\mathcal{N}=4$ gauge theories with unitary gauge groups. In the presence of O3 planes, this extends to gauge theories with (special) orthogonal and symplectic gauge groups. The lack of a natural brane construction for quivers with *special unitary* gauge groups is quite unsatisfying and makes it hard to find the $3d$ mirror of such quivers.

A partial resolution to this is given in [166, 167, 86, 168, 169] for cases where *all* the unitary gauge groups are replaced by special unitary gauge groups. We will take a different approach in chapter paper by first considering the electric quiver as a $5d$ $\mathcal{N}=1$ theory. As discussed in detail in Chapter 3, a 5d $\mathcal{N}=1$ gauge theories can be described using a brane web configuration consisting of (p,q)5-branes are stretched between $[p,q]$7-branes. Our quiver theories are now effective field theories living on the world volume of the 5-branes. With the asymptotic locations of the external legs of the brane webs fixed, a $U(1)$ factor decouples from each of the unitary gauge groups, thus yielding low energy effective theories with special unitary gauge groups. Therefore, using the brane web construction, we can find the magnetic quiver corresponding to any linear quiver with *only* special unitary gauge groups.

Now, in $3d$ $\mathcal{N}=4$, both the Coulomb branch and Higgs branch are hyperKähler manifolds. This obviously does not extend to $5d$ $\mathcal{N}=1$ and therefore we do not expect mirror symmetry to hold in $5d$ either. However, due to the hyperKähler construction of the classical Higgs branch, it is immune to quantum corrections and remains the same $d=3,4,5,6$. Therefore, the Higgs branch of the electric quiver is the same either $5d$ $\mathcal{N}=1$ or $3d$ $\mathcal{N}=4$ theory. Motivated by this fact, we conjecture that the same linear quiver with only special unitary gauge groups but as a 3d theory is mirror dual to the magnetic quiver. This is checked by an explicit computation of Coulomb branch and Higgs branch Hilbert series of both quivers. One can think of the the trip to $5d$ as a detour so that we can use brane web configuration to find the $3d$ mirror pairs.

In this paper, we will extend the brane web procedure in [25] to electric quivers containing a *mixture* of unitary gauge groups and special unitary gauge groups. The prescription turns out to be remarkably simple and systematic. This procedure can be easily generalized to finding

the $3d$ mirror quiver of any quiver that is linear. This includes the $T^{\sigma}_{\rho}(SU(n))$ quiver theories introduced in [62] with any of the unitary gauge groups replaced by special unitary gauge groups. Furthermore, it also extends to linear quivers that are 'bad'. Where possible, the results are checked by explicit computations of Higgs branch and Coulomb branch Hilbert series.

6.1.1 Web locking: first examples

In this section, we introduce the concept of brane locking on a family of basic examples, which are all good 3d $\mathcal{N} = 4$ quiver theories (in the sense described in the introduction), which means $N_f \geq 2N_c$ for every gauge node. For this kind of theory, brane locking provides 3d $\mathcal{N} = 4$ mirror pairs. We confirm these findings using Hilbert series computations for the Higgs and Coulomb branches of both quivers in the pair. More general quivers will be dealt with later on, using the same principles.

The traditional way of computing a 3d $\mathcal{N} = 4$ mirror of a linear quiver with unitary gauge groups makes use of brane set ups with D3, D5 and NS5 branes and S-duality. Let us start with a $T(\mathrm{SU}(4))$ quiver. Utilizing brane set ups, one finds that this theory is 3d self mirror:

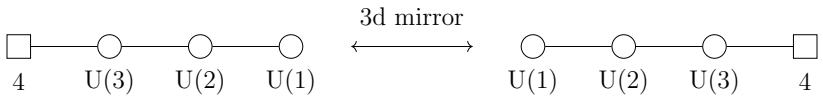

(6.1)

This can be checked through explicit Coulomb branch and Higgs branch Hilbert series computations as shown in Table 6.2.

We now want to know what happens if we replace *all* the unitary gauge nodes with special unitary gauge nodes:

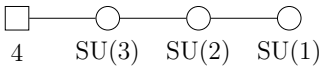

(6.2)

In 3d, we do not have a brane system for such a quiver, as stacks of D3 branes stretched between 5-branes only give rise to unitary gauge groups. However we can construct a brane configuration in 5d using brane webs [170, 171, 172]. With the basics of brane systems explained in Chapter

3, the brane web of this theory is as follows:

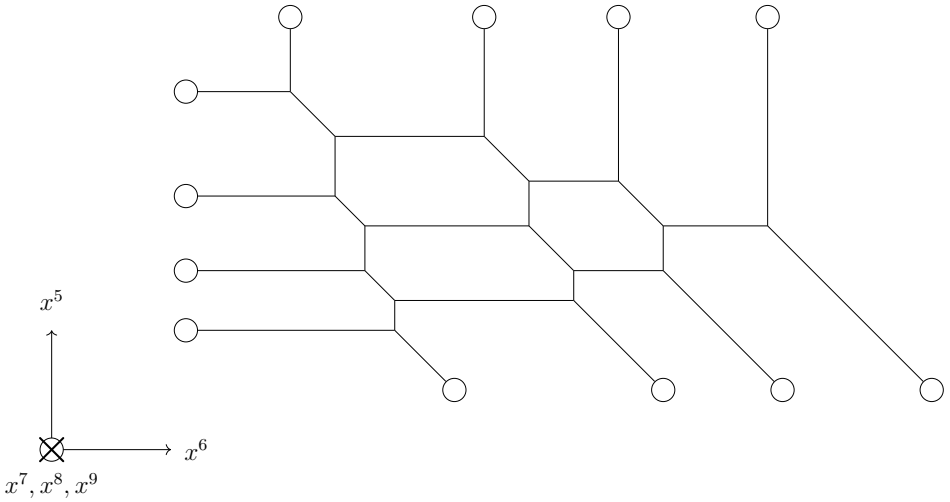

(6.3)

where nodes represent 7-branes and lines represent 5-branes (specifically, horizontal lines are D5 branes, vertical lines are NS5 branes, and lines at an angle here are $(1, -1)$ 5-branes.) The coordinate system we adopted here are the same as in Chapter 3. The stretching and contracting of the polygons represent moduli of the Coulomb branch. For the case above we see three polygons and hence the Coulomb branch has real dimension 3.

Going to the Higgs branch

As outlined in Chapter 3, we can go to the Higgs branch by first setting all the masses (given by the vertical distance between the D7 branes) to zero. The resulting configuration is:

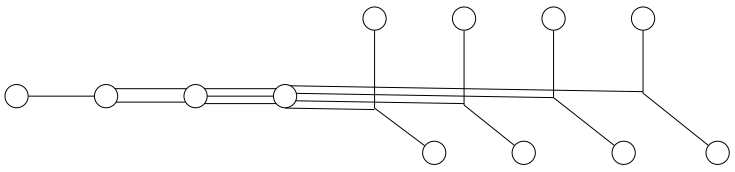

(6.4)

This diagram can be made clearer by pulling the fourth 7-brane from the left all the way to the right. The process involves several brane creations and annihilations [37]. As a result, $(1, -1)$ branes become NS5 branes after passing through the monodromy cuts originating from the 7-branes:

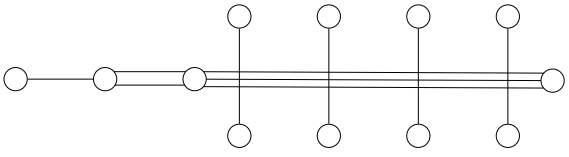

(6.5)

The Higgs branch moduli correspond to brane segments moving in the x^7, x^8, x^9 directions.

Getting the magnetic quiver

Following the algorithm in [25], which we also described in Chapter 3, we first do a maximal decomposition into subwebs that are free to move with respect to each together:

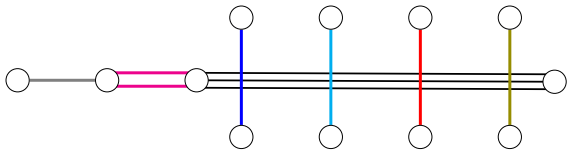

(6.6)

We now read off the magnetic quiver where each subweb represents a unitary gauge node with rank given by the number of coincident branes. The multiplicity of hypermultiplets between the gauge nodes are then given by the intersection number between each pair of subwebs. For the current example, each pair of subwebs intersect at most once, so the edges in the quiver have multiplicity at most one. The resulting magnetic quiver is:

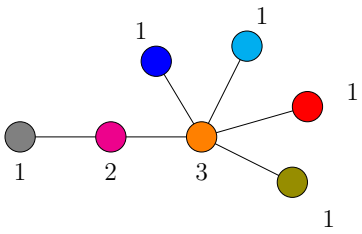

(6.7)

where the coloured nodes correspond to the different subwebs in (6.6). In this chapter, all the gauge groups in the magnetic quivers are unitary, and as usual a diagonal U(1) should be ungauged. (6.7) reproduces results computed in [168, 169].

Now, (6.7) is only the magnetic quiver for (6.2) when the gauge couplings of the special unitary gauge groups are all finite. Crucially, at finite gauge coupling, the Higgs branch of the 5d quiver is classical and thus the same in $3-6$ dimensions. This allows us to establish the following relationship:

$$\mathcal{H}^{5d}_{\text{classical}}(6.2) = \mathcal{H}^{3d}(6.2) = \mathcal{C}^{3d}(6.7) \tag{6.8}$$

The right equality of (6.8) is now an equality amongst 3d $\mathcal{N} = 4$ theories. This motivates us to

conjecture that the two quivers form a 3d mirror pair:

$$\mathcal{C}^{3d}(6.2) = \mathcal{H}^{3d}(6.7) \tag{6.9}$$

This is checked explicitly through Hilbert series computations in Table 6.2.

Changing SU(3) **to** U(3)

Now, consider gauging the SU(3) node to a U(3):

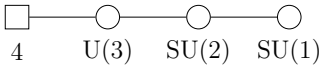

(6.10)

The Higgs branch of this quiver is now a subspace of the Higgs branch of (6.2). To demonstrate this gauging process in the brane set up, we introduce the notion of *locking*. Two subwebs are locked if they are forced to move together. The gauging of SU(3) to U(3) then translates to locking the two left most NS5 branes (coloured in blue). On the other hand, the two remaining NS5 branes (in red and olive) are still free to move independently.

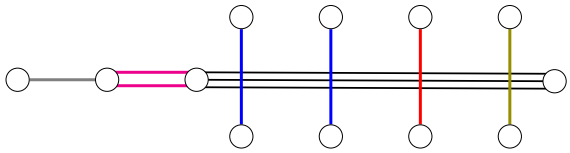

(6.11)

Physically, the explanation for locking is that separating the NS5 branes in the x^7, x^8, x^9 direction corresponds to moving on the baryonic branches of the 5d theory; as a consequence, preventing the NS5 from moving apart is equivalent to removing one of the baryonic branches, removing a baryonic U(1) global symmetry by gauging it, therefore producing the Higgs branch of a theory with a unitary gauge group. Indeed, the Higgs branches of an SU(3) gauge theory and the Higgs branch of a U(3) gauge theory share the same mesonic branch, and the only difference is that the SU(3) theory has a baryonic branch in addition. We can read off the magnetic quiver from (6.11):

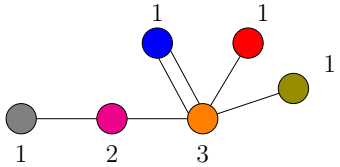

(6.12)

One of the U(1) nodes is now connected to the U(3) node with an edge of multiplicity two, which simply means there are twice as many hypermultiplets. This is because the intersection number between the blue subweb and orange subweb is two. Edge multiplicity naturally arises when studying magnetic quivers [25, 173]. Once again, the Coulomb branch and Higgs branch computation shows that, at least on the level of Hilbert series, (6.11) and (6.12) are indeed mirror pairs.

Changing SU(3) **to** U(3) **and** SU(1) **to** U(1)

Let's see what happens if we gauge the baryonic U(1)s associated to both the SU(3) and SU(1) nodes:

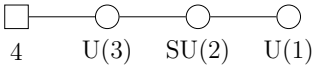

(6.13)

In the brane set up, this is equivalent to locking both the pair of branes on the left (blue) and on the right (green):

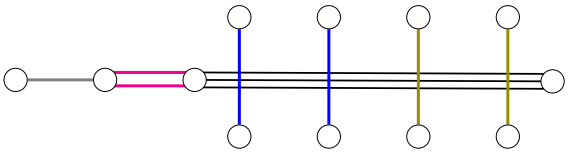

(6.14)

Now, amongst the NS5 branes, there are only two pieces (rather than three in (6.11)) that move independently. Looking at the intersection numbers, one quickly obtains the magnetic quiver:

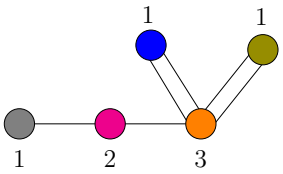

(6.15)

where the edges of both U(1)s connecting the U(3) have multiplicity two. The unrefined Coulomb and Higgs branch Hilbert series are presented in Table 6.2 and is consistent with the conjecture that they are 3d mirror pairs.

Summary

We summarize all the different combinations of U / SU nodes for $T(SU(4))$ theories in Table 6.1, along with their unrefined Coulomb and Higgs branch Hilbert series in Table 6.2 and global symmetries in Table 6.3. As is clear from the magnetic quivers in Table 6.1 and 3d mirror symmetry, the Higgs and Coulomb branches of these quivers only depend on the partition of 4 which defines the locking (see the coloured cells in the second column).

6.1.2 Linear quivers with nodes of non-negative balance

Good linear quivers with all nodes U go under the name $T_\rho^\sigma(SU(n))$ theories. Each unitary gauge group is either balanced or overbalanced. 3d mirror symmetry for these theories was studied in [62] using the classic NS5-D3-D5 HW brane system. If we take the NS5-D3-D5 brane system for any $T_\rho^\sigma(SU(n))$ and we go to the Higgs phase (i.e. all D3 branes are suspended between D5 branes, and any D3 branes stuck between a D5 and a NS5 are annihilated by a HW transition) then all the NS5 branes have no D3 branes ending on them.[3] T-dualizing this system to a brane web, we obtain the brane system of the electric quiver with all U nodes replaced by SU. The NS5 branes present in this system have no D5 branes ending on them, which means the only 5-branes are NS5 and D5. This greatly simplifies obtaining the magnetic quiver for any choice of locking, i.e. any choice of U and SU nodes in the electric quiver. We proceed with some examples.

$T(SU(n))$ theories

The $T(SU(n))$ family has a single SU(n) flavor group and is 3d self mirror. This makes it the simplest example to see how the different arrangements of U/SU have on the mirror. The $n = 4$ case is already studied in detail in Section 6.1.1. When all the gauge nodes are unitary,

[3]Note that we can only reach such a Higgs phase, when there is complete Higgsing. Otherwise there are always some D3 branes suspended between NS5 branes.

Table 6.1: *The left column shows extensions of the $T(SU(4))$ quiver with different combinations of U/SU nodes. The middle column shows their respective magnetic quivers, which in this particular case are in fact 3d mirrors. These magnetic quivers are derived from 5d brane webs, which yield quivers with all unitary gauge nodes. The right column shows the maximal decompositions of the brane webs into subwebs, with the necessary locking imposed. Note that the two magnetic quivers in blue cells and the three magnetic quivers in yellow cells are identical: this shows that Higgs branches for the family of theories considered in this table depends only on partitions of 4. This is reflected in the next three tables by merging the corresponding cells.*

Electric Quiver	Magnetic Quiver	Brane web
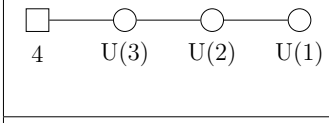	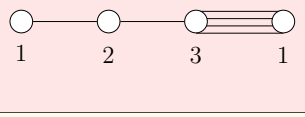	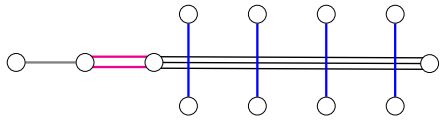
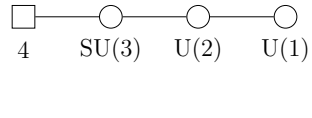	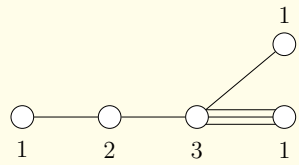	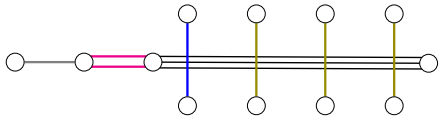
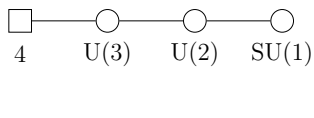	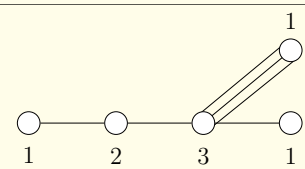	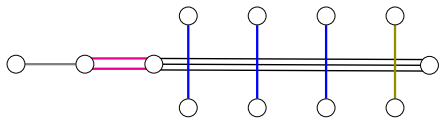
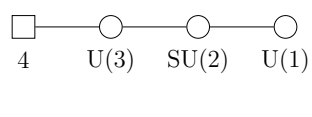	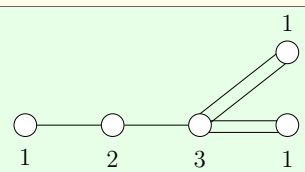	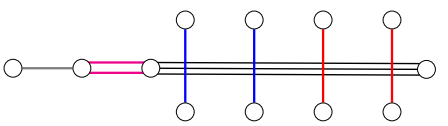
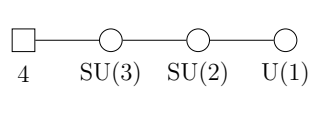	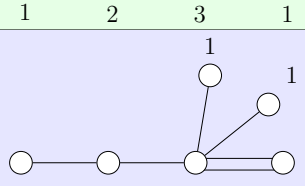	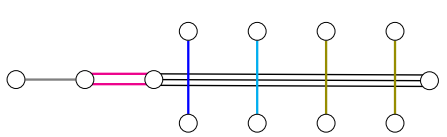
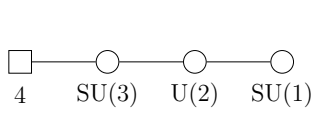	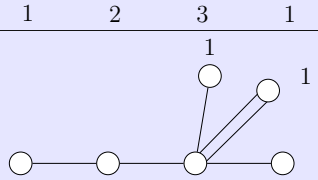	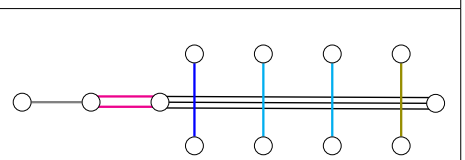
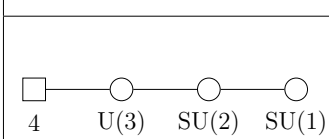	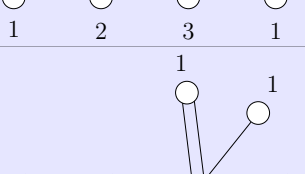	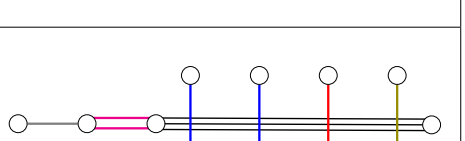
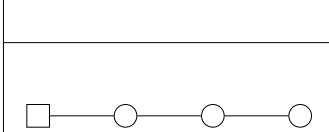	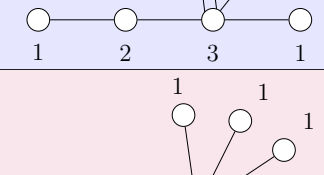	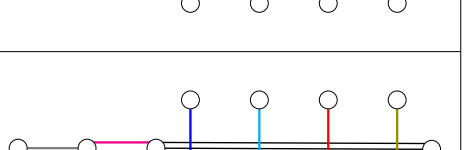

Table 6.2: *Extensions of the $T(SU(4))$ quiver are shown with different combinations of U/SU nodes, along with their Higgs and Coulomb branch unrefined Hilbert series. These correspond to the Coulomb and Higgs branch Hilbert series, respectively, of their mirror quivers shown in Table 6.1. For brevity, unrefined Hilbert series are shown. Under the appropriate fugacity maps, this correspondence extends to refined Hilbert series.*

Electric Quiver	Higgs branch unrefined Hilbert Series	Coulomb branch unrefined Hilbert Series
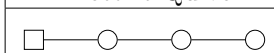	$\frac{(1-t^4)(1-t^6)(1-t^8)}{(1-t^2)^{15}}$	$\frac{(1-t^4)(1-t^6)(1-t^8)}{(1-t^2)^{15}}$
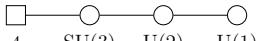	$\frac{1+3t^2+4t^3+7t^4+4t^5+7t^6+4t^7+3t^8+t^{10}}{(1-t^2)^{13}(1-t^3)^4(1-t^4)^{-2}(1-t^6)^{-1}}$	$\frac{(1-t^6)(1-t^8)(1+4t^4+t^8)}{(1-t^2)^8(1-t^4)^4}$
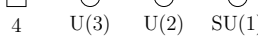		
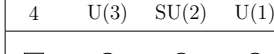	$\frac{1+5t^2+23t^4+62t^6+110t^8+130t^{10}+110t^{12}+62t^{14}+23t^{16}+5t^{18}+t^{20}}{(1-t^2)^{11}(1-t^4)^3}$	$\frac{(1-t^6)(1-t^8)^2(1+8t^4+t^8)}{(1-t^2)^6(1-t^4)^7}$
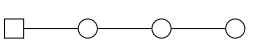	$\frac{\left(\begin{array}{c}(1+3t+15t^2+46t^3+148t^4+386t^5+954t^6+2064t^7+4183t^8+7649t^9+13081t^{10}+20490t^{11}\\ +30060t^{12}+40738t^{13}+51804t^{14}+61138t^{15}+67790t^{16}+69920t^{17}+\ldots\text{palindrome}+\ldots+t^{34})\end{array}\right)}{(1-t)^{-3}(1-t^2)^8(1-t^3)^7(1-t^4)^4}$	$\frac{1+t^2+4t^4+9t^6+13t^8+12t^{10}+13t^{12}+9t^{14}+4t^{16}+t^{18}+t^{20}}{(1-t^2)^2(1-t^4)^5(1-t^6)^2(1-t^8)^{-1}}$
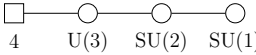		
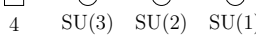		
	$\frac{\left(\begin{array}{c}(1-t+13t^2+12t^3+96t^4+172t^5+572t^6+1072t^7+2479t^8+4265t^9+7813t^{10}+11874t^{11}\\ +18146t^{12}+24124t^{13}+31540t^{14}+36640t^{15}+41456t^{16}+42064t^{17}+\ldots\text{palindrome}\ldots-t^{33}+t^{34})\end{array}\right)}{(1-t)(1-t^2)^5(1-t^3)^7(1-t^4)^5}$	$\frac{(1-t^2+t^4+4t^6+t^8-t^{10}+t^{12})}{(1-t^2)(1-t^4)^4(1-t^6)^2(1-t^{12})^{-1}}$

the quiver is balanced and the theory is self-dual:

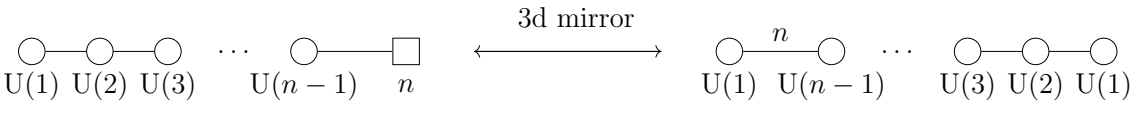

(6.16)

As before, we first turn all the gauge nodes from U to SU. In this case, the 3d mirror obtained from the brane web takes the following form:

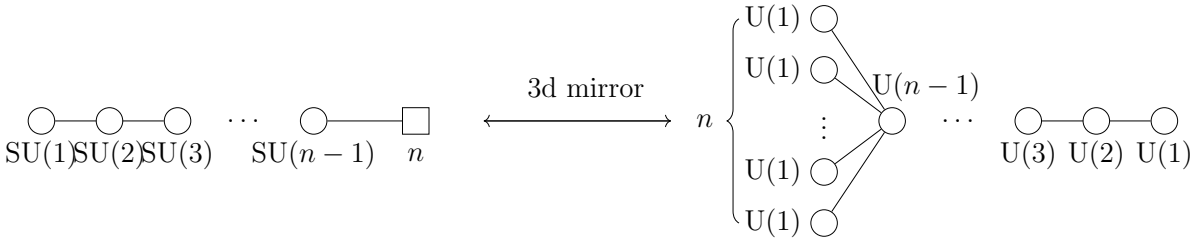

(6.17)

which appeared in [168]. Comparing (6.16) and (6.17) we see that the only difference in the mirror quivers is the U($n-1$) connected to a U(1) with n links exploded into a bouquet of n U(1)s. Regardless of the choice of U/SU groups, the U(N_i) gauge nodes with $1 \leq N_i \leq n-1$, in the mirror theory remain the same because they correspond to D5 branes in the brane web and not NS5 branes, hence are not affected by locking. When all gauge nodes are SU, the brane web has n independent (unlocked) NS5 branes, each corresponding to a U(1) in the bouquet.

Starting from (6.17), we then turn some of the SU into U. The only change to the 3d mirror is in the U(1) bouquet which is connected to the U($n-1$) node. The number of U(1) nodes in the new bouquet and the multiplicity of the edges connected to the U($n-1$) can be determined solely from the different ways the NS5 branes are locked. To illustrate this, it is sufficient to draw an *incomplete* brane diagram with only NS5 branes. When all the gauge groups are SU,

the NS5 branes are unlocked and is denoted by different colours:

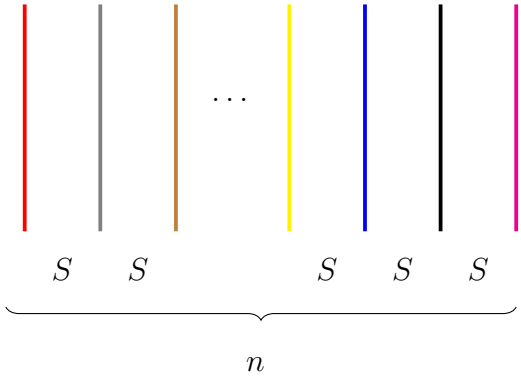

(6.18)

where S stand for special unitary group in the electric quiver. For $n-1$ balanced nodes in the electric quiver, there are n NS5 branes in the brane web. The dictionary between the figure and the electric quiver is as follows. For adjacent NS5s with different/same colour, a D brane stretched between them has a special unitary/unitary gauge group, respectively. Changing the gauge groups in the original quiver from special unitary to unitary is equivalent to setting the adjacent branes to the same colour. The adjacent branes are locked, hence corresponding to a single U(1) node in the bouquet of the mirror quiver. The multiplicity of the edge is then the number of NS5 branes that move together. This is because in the full brane web, this number is the intersection number between the locked NS5s and the D5 branes.

The changes in the mirror quiver are dictated solely by the arrangement of U/SU nodes in the electric quiver. The ranks of the gauge and flavor groups are irrelevant here. For example, if the electric quiver has a $USUSUU$ structure (where U/S stand for unitary/special unitary group, respectively), then the NS5 branes takes the form:

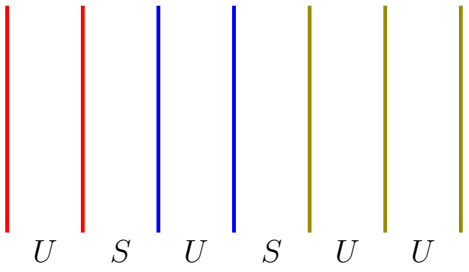

(6.19)

The mirror quiver has the following bouquet:

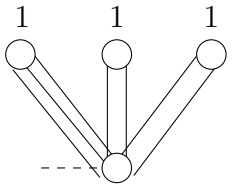

(6.20)

where the rest of the quiver remains the same. Notice that the order of the links with multiplicities (triple, double, double) in (6.20) is in reverse to the multiplicities read from (6.19). This order reversal is just to be consistent with the way the brane webs are drawn throughout this paper and in the `Mathematica` code. The reverse order does not make a difference here since all gauge nodes are balanced. However, this becomes important below when there are overbalanced nodes. We can illustrate this with $T(SU(7))$ with a particular choice of U/SU:

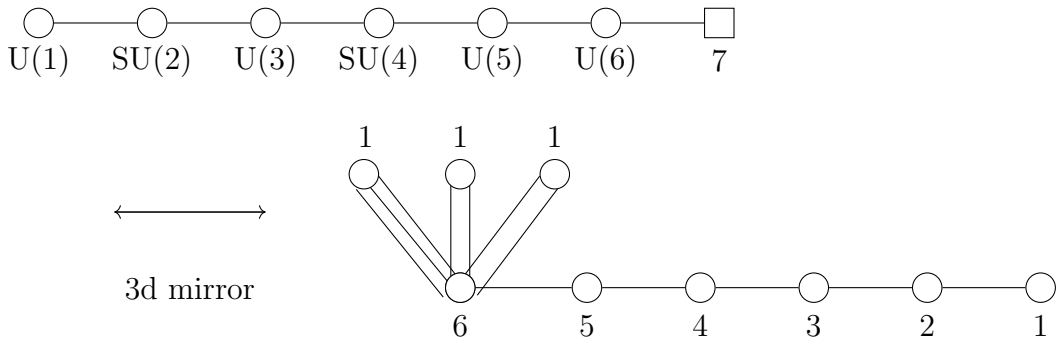

(6.21)

For $T(SU(n))$ theories, we can easily write down the prescription for any general U/SU combination:

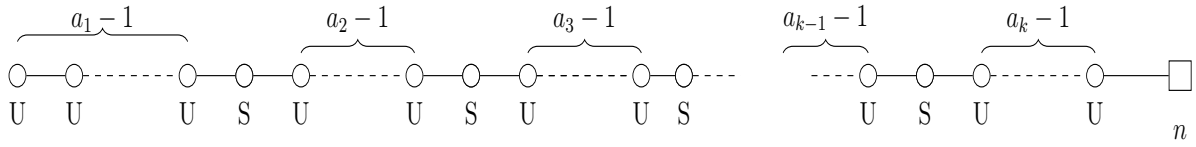

(6.22)

where $a_i - 1$ counts the number of unitary nodes in between neighbouring special unitary nodes such that

$$\sum_{i=1}^{k} a_i = n \tag{6.23}$$

and the gauge node starts with (U or SU)(1), (U or SU)(2), ..., (U or SU)$(n-1)$. The mirror

quiver takes the following form:

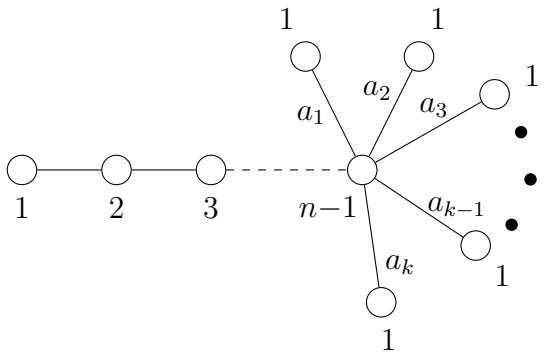

(6.24)

Linear quiver where all gauge nodes are balanced

A linear quiver where *all* k gauge nodes are unitary and balanced has a 3d mirror with only one SU$(k+1)$ flavor node. Written as an unframed quiver, this means there is a U(1) gauge group connected to *one* of the other gauge groups with $k+1$ links. This is because the Coulomb branch global symmetry of an electric theory with k consecutive balanced nodes is SU$(k+1)$. The Higgs branch global symmetry of the mirror theory is SU$(k+1)$ as well, which translates to a single flavor node[4]. If k unitary gauge nodes are replaced with special unitary nodes, then the single flavor node in the mirror will become a bouquet of k U(1)s with multiplicities a_i such that $\sum_i^k a_i = n$. The procedure described above in this subsection can then be straightforwardly applied to any linear quiver where all gauge nodes are balanced. For example, consider the following balanced quiver and its mirror:

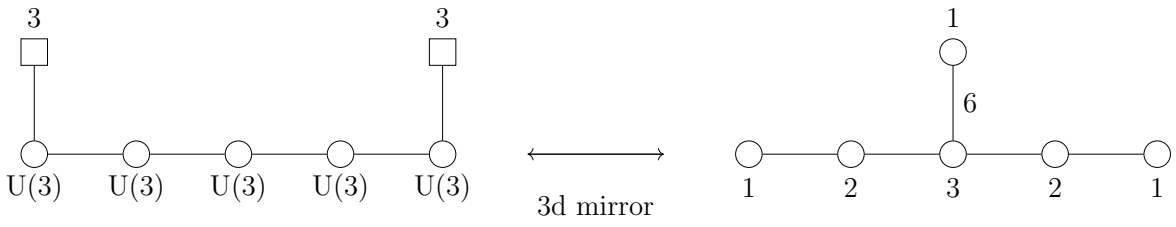

(6.25)

[4]Recall, the global symmetry of the Coulomb branch can be read off from the number of balanced nodes in the quiver. The global symmetry of the Higgs branch is the same as the flavor symmetry.

and when all gauge nodes are SU[5]:

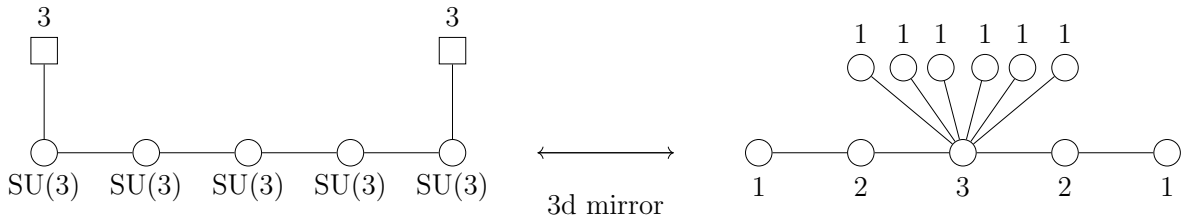

(6.26)

An arbitrary selection of U/SU gives a bouquet of U(1)s connected to the U(3) with links of different multiplicities. For instance,

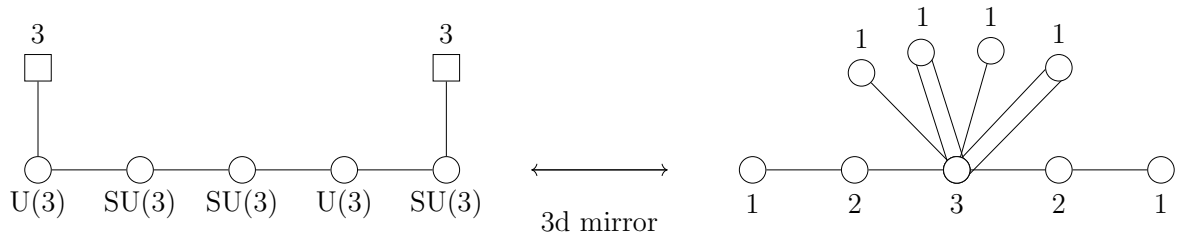

(6.27)

One or more overbalanced nodes

As mentioned above, for good linear quivers the different combinations of U/SU only affect the way U(1) bouquets behave in the mirror. When all gauge nodes are balanced, there is only a single bouquet. When there are one or more overbalanced gauge nodes then there are more bouquets in the mirror. For the remainder of this subsection, it is sufficient just to focus on the different kinds of bouquets that can arise under different combinations of U/SU and balanced/overbalanced nodes.

A good linear quiver with only unitary gauge nodes with one or more being overbalanced, has a mirror quiver with more than one flavor node. Written as an unframed quiver, this means the U(1) node connects to several other gauge nodes. Let us start with a linear theory with gauge nodes $USUSUU$ where the cyan node is overbalanced. Once again, the rank of the gauge nodes and the flavor nodes do not affect the results. The configuration of NS5 branes takes the

[5]The quiver on the right is also the 3d mirror of the A_2 class $\mathcal{S}$ theory with 2 maximal and 6 minimal punctures

form:

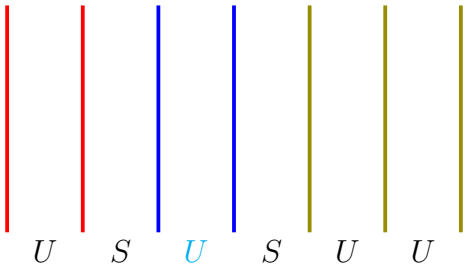

(6.28)

It is now important to pay attention to the interval between the two blue NS branes. This is now an additional information beyond the colour coding of the NS5s that needs to be taken into consideration. The number of gauge nodes in the mirror theory that have U(1) bouquets is $u+1$ where u is the number of overbalanced nodes in the electric quiver. Here, we have two bouquets in the mirror quiver. The novelty compared to the all balanced case is that the U(1) nodes in the bouquet may have edges connected to more than one gauge node. For (6.28) the mirror quiver always has the following bouquets:

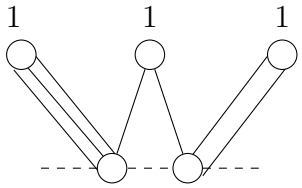

(6.29)

Depending on the ranks of the gauge groups and flavor groups in the electric theory, there can be many gauge nodes between the two unmarked nodes in (6.29) but they will not have any links to the three U(1)s. In other words, they won't have any U(1) bouquets irrespective of the U/SU combination in the electric quiver.

Next up, we place two unbalanced unitary nodes next to each other. For a quiver with $USUUUU$, the NS5 configuration is:

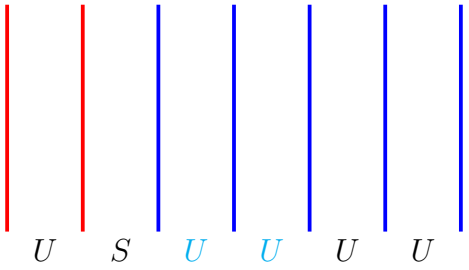

(6.30)

Following the same set of rules, there are three gauge nodes in the mirror with bouquets. The

mirror quiver has the structure:

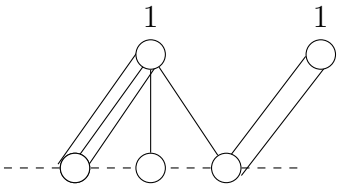

(6.31)

Unbalanced special unitary gauge group

If we look at $USSUU$ where the overbalanced node is now special unitary, the NS5s read:

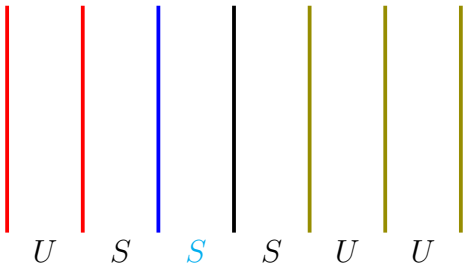

(6.32)

Like before, the special unitary node means the nearby NS5 branes will move independently from each other, yielding a mirror quiver with the following bouquets:

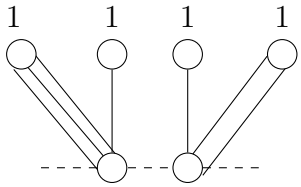

(6.33)

Therefore, an unbalanced special unitary node results in the two U(1) nodes being connected to two separate gauge nodes.

Generalization

In general, the procedure of finding the mirror pair of a good linear quiver is the following:

1. Set all the gauge nodes in the electric quiver to be unitary. This is now a $T_\rho^\sigma(SU(n))$ quiver whose mirror quiver is $T_\sigma^\rho(SU(n))$ and can be easily obtained following [62, 96].

2. Switch all the U nodes in the electric quiver to SU which translates to exploding all the $U(N_i)$ flavor nodes in the mirror into bouquets of N_i U(1)s.

3. Identify which gauge groups in the electric quiver are overbalanced.

4. Draw the *incomplete* brane configurations introduced above with only NS5 branes and alter the bouquets depending on the U/SU and balanced/overbalanced conditions outlined above. This reproduces the mirror quiver of the mixed U/SU electric theory.

Reverse algorithm

Note, the procedure above is completely included in a general algorithm detailed in our paper [9]. Nevertheless, working with only linear electric quivers that are good allows us to simplify the algorithm immensely using incomplete brane configurations with only NS5s. Another advantage is that the algorithm for a good linear quiver can be reversed: given a quiver, one can decide whether it is the mirror of a good linear quiver, and if so we can find it.

1. The reverse algorithm only works if all the gauge groups are either balanced or overbalanced (we are now talking about the mirror quiver but this still needs to be true). Look for a set of U(1) gauge nodes, each not connected to any other in that set, such that ungauging all of them (i.e turning U(1) gauge groups into U(1) flavors) produces a framed linear quiver with only multiplicity 1 links. If this is not possible, i.e. (a) the remaining gauge groups do not form a linear quiver, or (b) there are multiple links between the remaining gauge groups, then there is no mirror that is a good linear quiver and the algorithm stops here. [6]

2. Whenever multiple $U(1)$ flavor nodes are attached to a single gauge node they should be aggregated into a single $U(k)$ flavor, taking account of linking multiplicities.

3. The resulting quiver will be a linear chain of unitary gauge nodes with flavors. If it is a good linear quiver, then it is a $T^{\rho}_{\sigma}(SU(n))$ theory. The mirror theory $T^{\sigma}_{\rho}(SU(n))$ is straightforward to obtain once the quiver is expressed using partitions (n, ρ, σ). $T^{\sigma}_{\rho}(SU(n))$ is identical to the desired electric quiver under the reverse algorithm, but with all its

[6] If there are links between two U(1)s with multiplicity $k > 0$, then ungauging both of them gives rise to 1 —(k)— 1. If such a feature arises when creating a linear quiver, the electric quiver will be an ugly/bad quiver and the reverse algorithm will not work. Another way to think about this is that the information contained in the links between the U(1)s is lost after the ungauging.

gauge groups set to unitary. Therefore, the next step is to figure out which arrangement of U/SU nodes in $T^{\sigma}_{\rho}(SU(n))$ will reproduce our mirror quiver under the forward algorithm.

4. Return to the mirror quiver in the beginning but highlight the gauge nodes that form the linear chain in step 1. The U(1)s attached to this chain will be the bouquets. This brings the quiver into a familiar form which we see throughout the paper. By studying how the bouquets connect to the rest of the quiver, we can reconstruct the incomplete brane diagram where the number of NS5s is equal to the total number of links to the U(1)s in the bouquets. With the incomplete brane diagram, we can now identify which of the gauge groups in the electric quiver are unitary or special unitary. Replacing the electric quiver in step 3 with the correct U/SU arrangement recovers the electric quiver.

We demonstrate this with the following example:

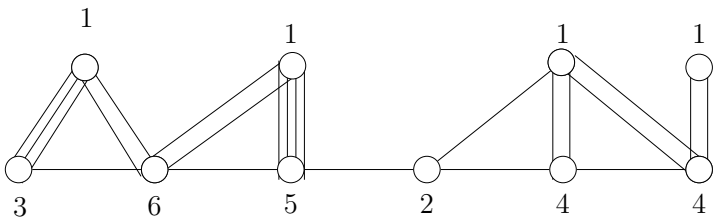

(6.34)

Step 1-2: Ungauge the U(1)s until we have a linear quiver without links with multiplicity:

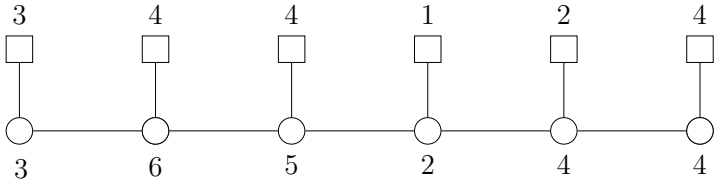

(6.35)

Step 3. (6.35) is a linear quiver where all gauge nodes are unitary and are either balanced or overbalanced and thus a $T^{\rho}_{\sigma}(SU(N))$ theory. The 3d mirror (which can be obtained either by following [62, 96] or using the `Mathematica` code) is:

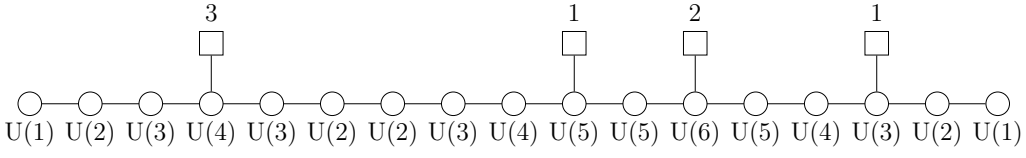

(6.36)

Step 4: From the structure of the four bouquets in (6.34), we read off the following incomplete brane diagram with only NS5s:

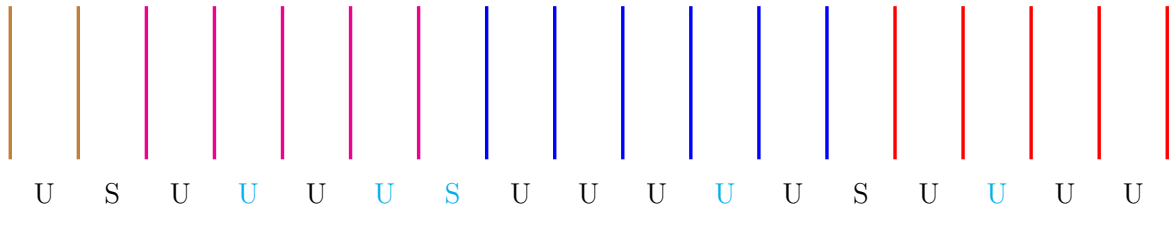

(6.37)

This information specifies the U/SU nodes in (6.36) that makes it the electric quiver of (6.34):

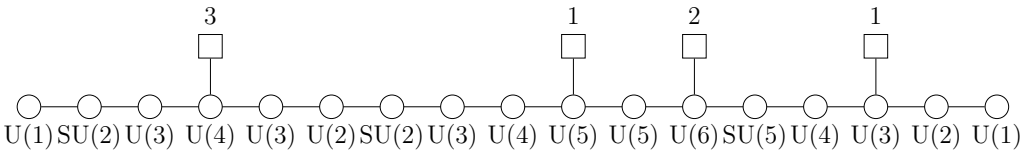

(6.38)

As a consistency check, the position of the overbalanced nodes (cyan) predicted in (6.37) matches with those in (6.38). (6.38) is indeed the 3d mirror of (6.34) which can now be checked by putting it as an input in the `Mathematica` code for the forward algorithm.

6.1.3 Some underbalanced nodes and several Magnetic quivers

The Higgs branch of a 3d $\mathcal{N} = 4$ quiver where all gauge nodes are either balanced or overbalanced is a single cone. If one or more gauge groups are underbalanced, the Higgs branch could be the union of several cones as first observed for SQCD in [34]. As a result, we have one magnetic quiver for each of the cones. The concept of 3d mirror pairs is ill defined in this case and we will therefore only speak of magnetic quivers.

The multitude of hyper-Kähler cones and hence magnetic quivers come from inequivalent choices of maximal decomposition of our brane web into subwebs [25]. Consider the following quiver:

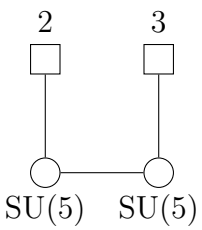

(6.39)

We see that both gauge nodes are underbalanced. When drawing the brane web, choose a convention that move all the D7 branes to the left:

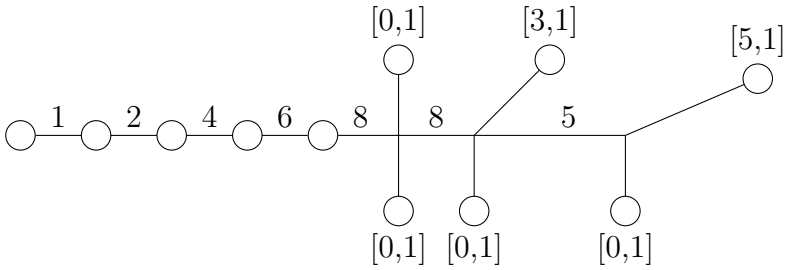

(6.40)

The brane web has four inequivalent maximal decompositions, each giving rise to a magnetic quiver, listed in the first row of Table 6.4. (This statement, and subsequent statements in this section, can be obtained immediately using the attached code). An immediate observation is that the subwebs associated with NS5s now have non-trivial intersection number between them. In other words, the bouquets of U(1) nodes in the magnetic quiver can now have edges between them, which is something we do not observe in good linear quivers where all nodes are balanced or overbalanced.

The next step is to turn the SU(5)s into U(5)s by locking the branes. In contrast to good quivers where locking makes minor changes to the magnetic quivers, for bad quivers it can also leave the magnetic quiver unchanged or it can change the structure drastically.

As already stated in this section, for a good linear quiver there is always a set of HW transitions such that there is an unbound state of D5 and NS5 branes. As a corollary, the NS5 branes move independently from each other. If the electric quiver contains underbalanced nodes, this no longer holds and there may be bound states one cannot get rid of. This, in return, can allow for more than one maximal decomposition with some of the 5-branes forced to move together. Note, we are not doing any locking here, but this is a natural feature of a maximal decomposition of a brane web, even when all the gauge nodes in the electric quiver are SU. In particular, for an SQCD electric quiver, the hyper-Kähler cone where all the NS5 move independently from each other is called the baryonic branch. If some of the NS5 move together, it is the mesonic branch. In Table 6.4, the baryonic cone is given by Magnetic Quiver 4 in the first row. The remaining magnetic quivers all have some or all of the NS5 branes moving

together. As a result, if the NS5 branes that are already moving together are locked when going from SU to U, the resulting magnetic quiver will stay the same. For example, Magnetic Quiver 1 remains the same when the second SU(5) in the electric quiver is turned to U(5).

In the case of good linear quivers, we have seen that changing nodes in the electric quiver from SU to U simply translates to merging some of the U(1)s in the bouquet. For a quiver with bad nodes, the s-rule plays a crucial role which can result in a complete change to the structure of the magnetic quiver. For example, Magnetic Quiver 3 changes drastically when the second SU(5) in the electric quiver is changed to U(5).

When all the SU nodes are changed to U in the electric quiver, all four magnetic quivers become identical. In other words, the four hyper-Kähler cones coalesce into a single cone. This is expected as the Higgs branch of a bad quiver with only unitary gauge nodes should be a single hyper-Kähler cone as observed in [173]. This is shown in the fourth line of Table 6.4. As a consistency check, the Higgs branch of any linear bad quiver with only unitary gauge nodes is equivalent to the Higgs branch of a good quiver. The good quiver can be obtained through a set of operations outlined in [174]. Basically, assuming vanishing FI parameters, a bad node of U(k) with N_f flavor is replaced with U($\lfloor N_f/2 \rfloor$). This process is repeated until all gauge nodes are good. For our electric quiver, the following equivalence in Higgs branches hold:

$\mathcal{H}$ 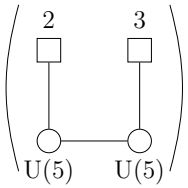

$=$ $\mathcal{H}$ 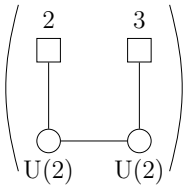

$=$ $\mathcal{C}$ 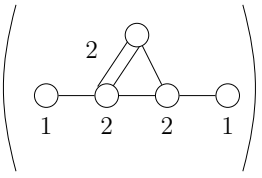

(6.41)

where the right side is the known 3d mirror of the good theory in the middle.

For good linear quivers with different combinations of U/SU nodes, we can check the conjectured mirror pairs through explicit Hilbert series computations. For electric quivers with bad nodes, however, computational difficulties prevent us from doing the same explicit checks. Nevertheless, we find consistency when comparing to the magnetic quivers found using other methods.

Table 6.3: *Extensions of the $T(SU(4))$ quiver are shown with different combinations of U/SU nodes, along with their Higgs and Coulomb branch global symmetry. Notice that the ranks of the global symmetries always add to* 6*.*

Electric Quiver	Higgs branch global symmetry	Coulomb branch global symmetry
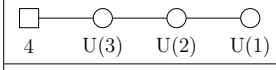	A_3	A_3
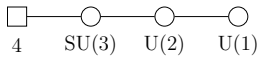	A_3U_1	A_2
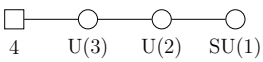		
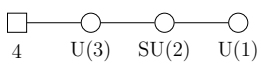	A_3U_1	A_1A_1
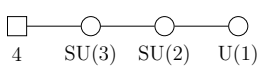	$A_3U_1U_1$	A_1
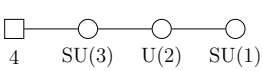		
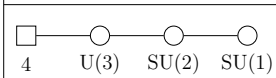		
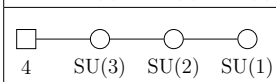	$A_3U_1U_1U_1$	

Table 6.4: *The first row displays the electric theory and the four corresponding magnetic quivers. The next few rows show how the magnetic quivers change as the SU nodes in the electric theory are turned into U nodes. We observe how distinct subdivisions of the brane web (and hence their magnetic quivers) become identical when some of the SU nodes are turned to U nodes. The light blue colored box indicates the same magnetic quiver.*

Electric Quiver	Magnetic Quiver 1	Magnetic Quiver 2	Magnetic Quiver 3	Magnetic Quiver 4

Argyres-Douglas theories

The Higgs branch of certain Argyres-Douglas (AD) theories has been argued to coincide with the Higgs branch of U/SU linear quivers where one or more nodes have negative balance [116, 175, 176, 177]. The above algorithm can then be applied to find their magnetic quivers. The results are consistent with the those given in [116, 175, 176, 177], which use different techniques.

`Mathematica` algorithm

One of the most useful outcome of [9] is the `Mathematica` algorithm that comes with it. This algorithm takes any linear quiver with any mixture of U & SU gauge groups and outputs the 3d mirror/magnetic quiver(s). The algorithm is extremely efficient, for example a long linear quiver with Higgs branch dimension $\dim_{\mathbb{H}}(\text{Higgs}) \approx 50$ will take less than one second to output the 3d mirror/magnetic quiver(s). Naturally, if one is only interested in quivers with unitary gauge groups or quivers with only special unitary gauge groups, the algorithm will also output their 3d mirror/magnetic quiver(s).

Extension to non-linear U & SU quivers

Ongoing work in [178] repeats the above procedure but for electric quivers of BCD type Dynkin quivers with mixed U & SU groups. This exercise greatly expands the literature of known 3d mirror pairs. One may wonder if this procedure can be repeated for any of the known 3d pairs. For example, quivers corresponding to k-instanton moduli spaces on ALE spaces whose mirrors are known as sunshine quivers [92].

Chapter 7

Hasse diagrams

Based on our paper [10]

Our goal is to study the Higgs branch of electric quivers in $d = 3, 4, 5, 6$ using magnetic quivers. So far, the focus has been on computing the Hilbert series, identifying the geometry of the moduli space and studying its chiral ring. In this chapter, we discuss a very different method of studying the Higgs branch: by focusing on its Hasse diagram. Put simply, the Hasse diagram studies the different phases of the Higgs branch where new massless states arise.

Hasse diagram basics

Let us look at the Hasse diagram of a simple set $\{a, b\}$. The Hasse diagram takes subspaces that are partially ordered by inclusion of their closures and arrange them into a tree like diagram:

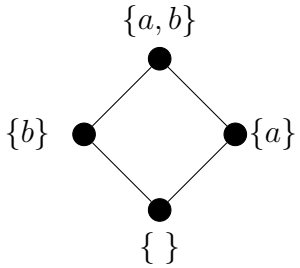

(7.1)

The node at the top of the diagram represents the full set whilst the node at the bottom is the empty/trivial set.

7.1 Hasse diagram of moduli spaces

Higgs branches have the property that they are *symplectic singularities*[1]. As such, they have a natural foliation into *symplectic leaves* induced by the symplectic form. These leaves are then related to each other by *transverse slices*. In the Higgs branch Hasse diagram, the symplectic leaves are the nodes/dots and the transverse slice between two leaves are the line(s) between them.

The physics encoded in the Hasse diagram is the pattern of partial Higgsing. In Higgs mechanism, scalar fields acquire VEVs which cause gauge bosons to become massive, thus breaking the gauge group into a subgroup. If the gauge group is fully broken, then we say there is complete Higgsing. However, it is possible that there aren't enough scalar fields in the hypers to fully break the gauge group, such theories are said to have incomplete Higgsing. Theories with incomplete Higgsing are closely related to the bad theories we mentioned in the previous chapter.

Rather than turning on the VEVs of all scalars in the hypers at the same time, one can also turn on *some* of the scalars to break the gauge group G into a subgroup H such that $G \supset H \supset H_{\text{max.broken}}$. Such a process is called *partial Higgsing*. The Hasse diagram encodes all possible H that the gauge group can be broken into.

7.1.1 Example with $SU(3)$ with 6 flavors

Let us study the classical Higgs branch of $G = SU(3)$ with 6 flavors which is the same in $d = 3, 4, 5, 6$. The Hasse diagram can be obtained using representation theory arguments with the different fields transforming in irreducible representations of $SU(3)$. The irreps are expressed using Dynkin labels $[\dots]_{\text{G}}$.

For this theory, we have 18 hypers and thus 36 complex scalars transforming in $6 \times ([1,0]_{SU(3)} + [0,1]_{SU(3)})$ and gauge bosons transforming in the $[1,1]_{SU(3)}$ irrep.

[1]We provide a brief introduction to symplectic singularities in Appendix E.

Breaking $SU(3) \to SU(2)$

One of the subgroups is $SU(2) \subset SU(3)$. To see what happens if we break into this subgroup, we need to project the irreps above into $SU(2)$ irreps. The 36 complex scalars in the hypers decomposes as

$$6\times([1,0]_{SU(3)}+[0,1]_{SU(3)}) \to 6\times([1]_{SU(2)}+[0]_{SU(2)}+[1]_{SU(2)}+[0]_{SU(2)}) = 12\times[1]_{SU(2)}+12\times[0]_{SU(2)} \tag{7.2}$$

The gauge bosons transform in the adjoint representation of the gauge group which decomposes as:

$$[1,1]_{SU(3)} \to \times([2]_{SU(2)} + 2[1]_{SU(2)} + [0]_{SU(2)}) \tag{7.3}$$

Like before, the adjoint representation of $[2]_{SU(2)}$ are assigned to the gauge bosons of the broken group $SU(2)$ whereas the remaining gauge bosons eats the scalar fields to become massive. The process is analogous to Higgs mechanism in electroweak theory. The gauge bosons and the scalars fields that are eaten must be in the same irreps.

$$12 \times [1]_{SU(2)} + 12 \times [0]_{SU(2)} - 2 \times ([2[1]_{SU(2)} + [0]_{SU(2)}) = 8[1]_{SU(2)} + 10[0]_{SU(2)} \tag{7.4}$$

where the factor of two comes from integration over complexified gauge group and imposing F-term conditions. From the scalar fields that remains, we see 16 complex scalars transforming in $8 \times [1]_{SU(2)}$ and 10 complex scalar fields which transforms trivially.

Breaking to other subgroups of $SU(3)$

Other subgroups include $SU(2) \times U(1)$, $U(1) \times U(1)$ and $U(1)$. Repeating the analysis above, one will find that the irreps of the gauge bosons that acquires mass cannot be matched with the irreps from the scalars. Hence, partial Higgsing to these subgroups are not allowed.

Breaking from $SU(2)$ to $\{1\}$

The $SU(2)$ gauge group can then be completely broken to the trivial group where 6 of the 16 complex scalar fields will give mass to the W bosons. The 10 complex scalars remains that

does not transform under irreps of any group.

The Hasse diagram is:

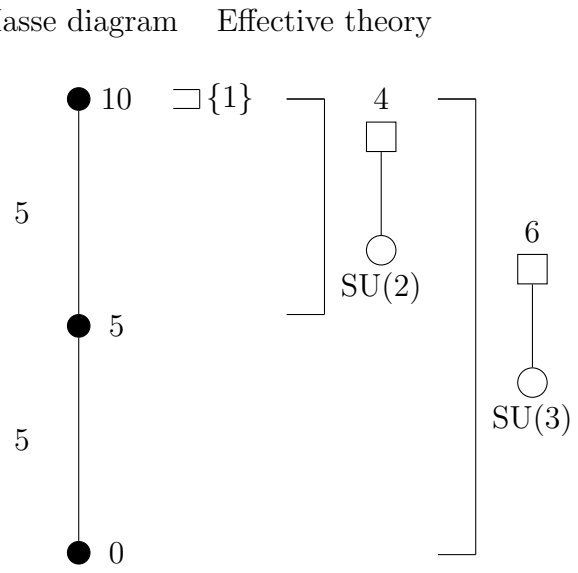

(7.5)

Let us explain this diagram in more detail. The Higgs branch of the theories on the right is given by the transverse slice between the top node and the node at the bottom of the bracket. For example, the largest Higgs branch ($SU(3)$ with 6 flavors) is the transverse slice between the top node and the bottom node. In other words, this is the slice between the full space and the trivial space. The Higgs branches of other theories are subspaces of this Higgs branch, hence the slice is taken from the top node to some other node above the bottom node.

When conducting partial Higgsing from $SU(3)$ with 6 flavors to $SU(2)$ with 4 flavors, the Higgs branch is now the slice between the top node and the middle node. The leftover transverse space between the bottom node and the middle node has 5 quaterionic dimension (10 complex) and is parameterized by the 10 complex scalar fields that transform as singlets in (7.4).

When the $SU(2)$ with 4 flavor theory is Higgsed to a trivial theory, the Higgs branch is trivial, indicated by the transverse slice between the top node and itself. The 10 complex scalars parameterizes the 5 quaterionic dimensional transverse space between the top node and the middle node.

To sum up, the Hasse diagram shows the pattern of partial Higgsing and the dimension of the Higgs branch of the broken theories.

7.2 Hasse diagrams from magnetic quivers

Higgs branch Hasse diagrams can be obtained using representation theory techniques as we have just seen. However, there are other methods of obtaining them as well. Since the Higgs branch of the electric quiver is the same as the Coulomb branch of the magnetic quiver, their Hasse diagrams must be the same as well. The Coulomb branch Hasse diagram can be obtained using brane systems and applying *Kraft-Procesi transitions* [42], or through an algorithm called *quiver subtraction* pioneered in[43].

Transverse slices

A crucial property of our Hasse diagrams is that the transverse slices in the Higgs branch are symplectic singularities as well. The transverse slice between two adjacent leaves is called an *elementary slice*. It is an ongoing challenge in the mathematics community to classify all possible elementary slices for symplectic singularities. As physicists, the challenge is then for us to find a 3d $\mathcal{N} = 4$ quiver whose Coulomb branch (which is also a symplectic singularity) corresponds to these elementary slices.

7.2.1 Hasse diagram from Brane systems

The classical Higgs branch of $SU(3)$ with 6 flavors can be studied using brane webs as shown on the top left corner of Figure 7.1. For this example we are only interested in the classical Higgs branch so the gauge coupling (spacing between the NS5s) is kept finite. The brane system is that of the Higgs branch phase. In this phase, you select the minimal set of subwebs that allows you to subsequently open up a 5d Coulomb branch direction[2]. For brane webs, a Coulomb branch moduli corresponds to opening up a polygon that can shrink or expand freely. This is the green piece in the figure. The resulting magnetic quiver can then be read off where the green piece is treated as a single subweb moving along the 7-branes, hence contributing a $U(1)$ degree of freedom. Doing a second transition, we see that in order to open up the second moduli in the Coulomb branch, the entire brane web need to be merged into a single web. As a

[2]This was first done in 3d brane systems in [42] and then for 5d and 6d brane systems in [10].

result, the Higgs branch becomes trivial and the magnetic quiver is trivial as well. Knowing the magnetic quivers after each transition, we can write down the 3d $\mathcal{N} = 4$ Coulomb branch Hasse diagram, which is equivalent to the Higgs branch Hasse diagram of our original theory.

Before doing that, let us discuss a point that is often a source of confusion. The 3d $\mathcal{N} = 4$ Coulomb branch of the magnetic quiver corresponds to the *closure* of a symplectic leaf $\mathcal{L}$, meaning the transverse space between $\mathcal{L}$ and the bottom/trivial leaf. This distinguishes with how we study the Higgs branch which is given by the slice between $\mathcal{L}$ and the top leaf. This important distinction is why this brane manoeuvre is a partial *un-Higgsing* procedure where the gauge symmetry is enhanced rather than broken in each step. In the central column of the figure, we begin at a generic point on the Higgs branch where the gauge group is completely broken and the theory is trivial. Then, by doing one minimal transition, we reach a particular singular loci on the Higgs branch and the gauge theory is enhanced to $SU(2)$ with 4 flavors. Another minimal transition and we obtain the $SU(3)$ theory with 6 flavors. A minimal transition (which goes from a leaf to its adjacent leaf in the Hasse diagram) is called a Kraft-Procesi (KP) transition and more details can be found in [42, 179].

In terms of the magnetic quivers, on the top right corner we have the magnetic quiver whose Coulomb branch is the closure of the top leaf in the Hasse diagram (7.5) with 10 quaterionic dimensions. After a KP transition, we reach the magnetic quiver whose Coulomb branch is the closure of the middle leaf with 5 quaterionic dimensions. And finally, after a second transition we have the trivial magnetic quiver corresponding to the trivial leaf with 0 quaterionic dimensions. Thus, the three magnetic quivers at different steps of the partial-unhiggsing reproduces the Hasse diagram.

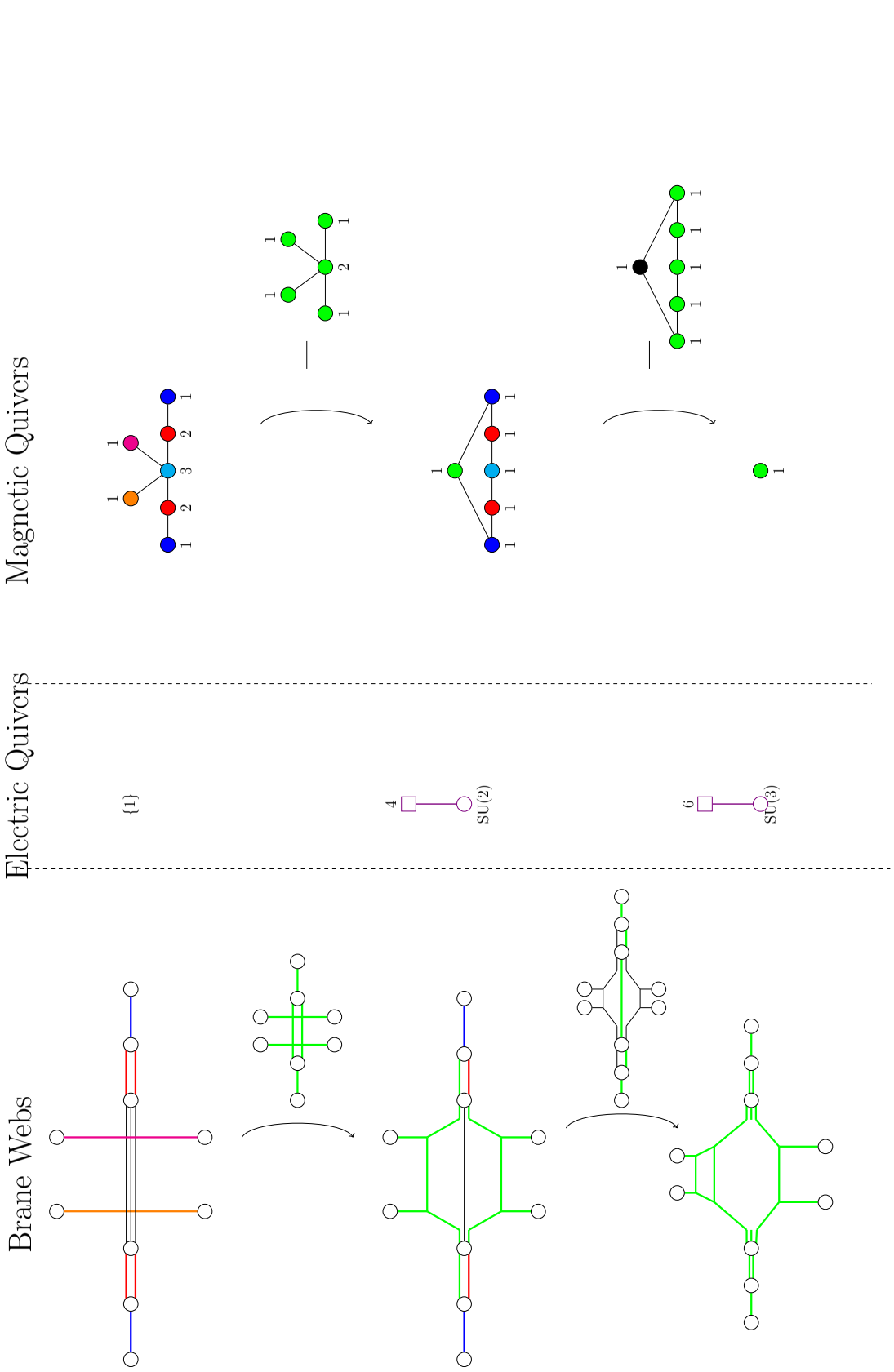

Figure 7.1: *Depiction of the different 5-brane webs in the gauge enhancements up to* SU(3) *with* 6 *fundamentals. The methods developed in [25] allow us to read magnetic quivers for the closure of all symplectic leaves in the Higgs branch as well as the transverse slices. This process can be translated into an operation between the magnetic quivers, called quiver subtraction. Coloured branes are assumed to be on different positions along the 7-branes.*

7.2.2 Hasse diagram from Quiver subtraction

Enough familiarity with the Kraft-Procesi transitions in brane systems leads one to realize the same transitions can be performed directly on the magnetic quiver. This leads to the *Quiver Subtraction* algorithm. The detailed algorithm is given in [43, 10] which we outline in the steps below. Note the algorithm is only for unitary magnetic quivers.

1. Find the magnetic quiver to your electric quiver and make sure it is unframed. If you are given a framed unitary quiver, you can unframe it by *gauging* all the flavor nodes with a single diagonal $U(1)$.

2. Write down all the balances of the gauge groups. For a $U(k)$ gauge group connected to $U(n_i)$ gauge nodes with edges of multiplicity l_i and a $U(m)$ flavor node, the balance is $\sum_i l_i n_i + m - 2k$.

3. The KP transitions in brane systems now corresponds to subtracting quivers whose Coulomb branches are elementary slices. Figure 7.1 shows all known 3d $\mathcal{N} = 4$ quivers whose Coulomb branch corresponds to an elementary slice. Find a subquiver in the magnetic quiver that has the same shape as one of the elementary slice quivers. Align the elementary slice quiver node for node and subtract the ranks of the gauge groups. This is allowed as long as the resulting gauge group has non-negative rank. In Figure 7.1, this is the subtraction of the affine D_4 Dynkin quiver from the magnetic quiver.

4. After subtraction, write down the balance of all the gauge groups again. Identify all gauge nodes whose balance changed during the subtraction. Introduce a new $U(1)$ gauge group to the quiver whose function is to rebalance the gauge nodes so that they are the same as before subtraction. This is done by connecting all gauge groups whose balance changed by x_i with an x_i multiplicity edge to the new $U(1)$. In our example, after subtracting the affine D_4, the only nodes whose balances changed are the two blue $U(1)$ nodes, each with $x_1 = x_2 = 1$. Hence, each of them is connected to the new $U(1)$ (green) with a multiplicity 1 edge.

5. Repeat step (3)-(4) for any other elementary slices that you can subtract. Each different

choice causes a new branching of the Hasse diagram. In our example, there are no new branchings.

6. After you obtain a new 3d $\mathcal{N} = 4$ quiver after subtraction, repeat (2)-(5) until there is no quiver left.

Each magnetic quiver corresponds to a node in the Hasse diagram. The elementary slice quivers you subtract are the transverse space (lines) between adjacent nodes in the diagram.

Summary of elementary slices

The known elementary slices and their associated 3d $\mathcal{N} = 4$ quivers are given in Table 7.1. We know this table is not complete as there are many other slices, some even non-normal, that are identified in the mathematics literature such as [180]. However, the quivers for those slices are not known. Furthermore, there can also be elementary slice quivers with matter fields in the adjoint representation. For example, the slice k_n that appears when performing quiver subtraction for $\mathcal{S}$-fold theory is denoted as:

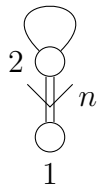

(7.6)

where n is the multiplicity of the non-simply laced edge. For $n = 2$, this slice is studied above where the Coulomb branch is $a_1 \times a_1$. For $n > 2$, the Coulomb branch global symmetry is A_1. It is not yet clear what the Coulomb branch Hasse diagram of (7.6) is, and there is the possibility that it can be a new elementary slice.

The search of new elementary slices is currently ongoing and one can either look for evidence in the mathematical literature, or by find quivers where a new elementary slice is required in order for one to proceed with quiver subtraction. The latter is used to find a few of the slices in Table 7.1.

Table 7.1: *Most up-to-date, but incomplete list of unitary quivers without loops for elementary slices usable in the quiver subtraction algorithm. In each case we provide two quivers, a framed version and an equivalent unframed version, where a* U(1) *should be ungauged on the long node. For* a_n, b_n, c_n, d_n, ac_n, $h_{n,k}$ *and* $\overline{h}_{n,k}$ *there are* n *gauge nodes in the framed quiver and* $n+1$ *gauge nodes in the unframed quiver. Notice that* $h_{n,1} = \mathbb{H}^n$, $h_{n,2} = c_n$, $h_{2,3} = cg_2$, $\overline{h}_{n,1} = a_n$, $\overline{h}_{n,2} = ac_n$, *and* $\overline{h}_{2,3} = ag_2$.

Slice	Framed quiver	Unframed quiver
a_n	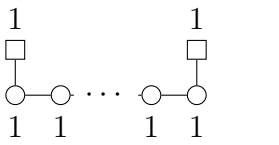	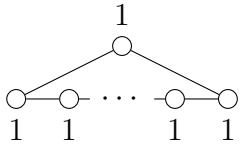
b_n	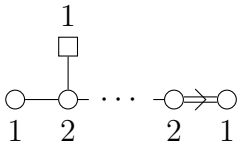	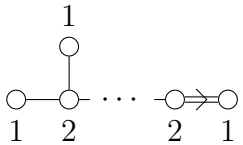
c_n	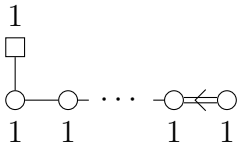	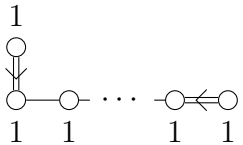
d_n	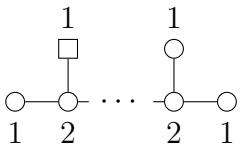	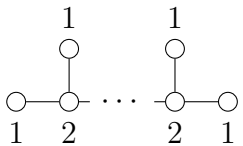
e_6	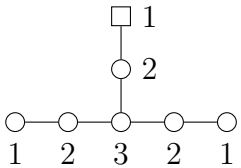	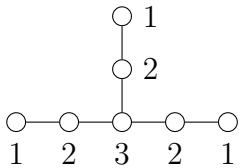
e_7	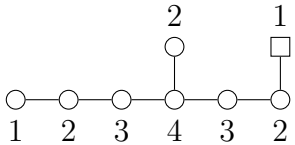	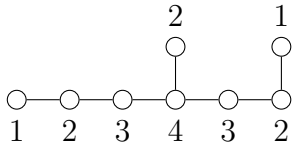
e_8	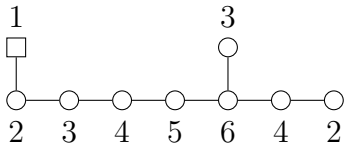	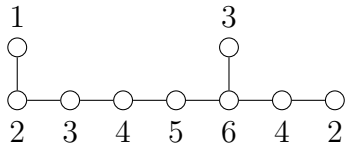

Slice	Framed quiver	Unframed quiver
f_4	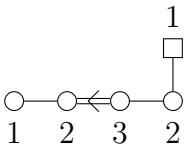	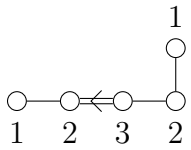
g_2	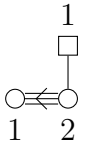	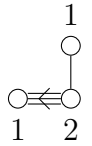
ac_n	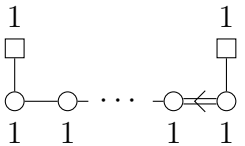	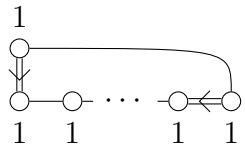
ag_2	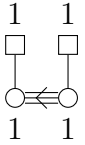	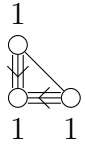
cg_2	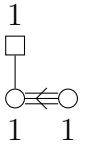	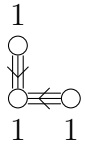
$h_{n,k}$	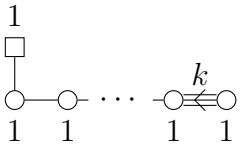	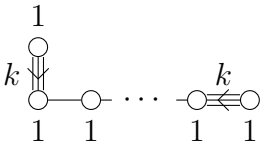
$\overline{h}_{n,k}$	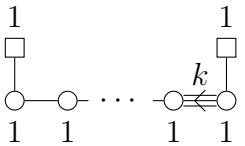	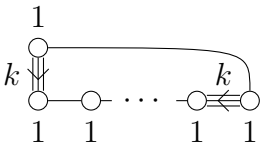
A_n		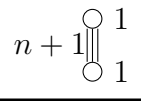

Advantage of Quiver Subtraction

The partial Higgsing procedure where we used representation theory is limited to Higgs branches of theories which have quiver descriptions. In particular, most of the 4d, 5d and 6d SCFTs do not belong in this category. On the other hand, the brane systems and magnetic quivers for these SCFTs are known so we can perform KP transitions or quiver subtractions to obtain their Hasse diagrams. This is the main advantage of our tools and was only made possible because we know the magnetic quivers. Furthermore, it can deal with more than just SCFTs as one can look at 5d or 6d gauge theories where only some of the gauge couplings are tuned to infinity. For example, the magnetic quivers of 5d and 6d theories at different coupling limits and their Hasse diagrams were obtained in [3, 109].

The quiver subtraction algorithm has two further advantages over brane systems as a) it is much easier to execute which leads us to the develop a `Mathematica` algorithm that automates the process and b) in many cases, such as class $\mathcal{S}$ theories, the brane systems are not known but we can still perform quiver subtraction. In fact, the short coming of brane systems occurs whenever we deviate significantly from linear unitary quivers (such as T_4 theory).

Orthosymplectic quiver subtraction

Quiver subtraction for orthosymplectic quivers are not yet fully developed. This is due to more complicated balancing condition and the fact that gauge nodes can change between SO(even) and SO(odd) before and after subtraction. For simpler cases, the correct Hasse diagram (since we know their unitary counterparts) have been extracted using orthosymplectic quiver subtraction in [163, 8].

Global symmetry

One can read off the Coulomb branch global symmetry of the 3d quiver (and equivalently the Higgs branch global symmetry of the electric quiver) from the elementary slice(s) with algebra $\mathfrak{g}_i$ connected to the bottom leaf/node. The non-Abelian global symmetry is then $\prod_i \mathfrak{g}_i$. Unfortunately, our current construction is unable to reveal the Abelian groups in the global symmetry. In our searches, we did find one case where we cannot read off even the correct

non-Abelian symmetry, this is the magnetic quiver corresponding to $C_3 \times A_1$ 4d SCFT and the infinite family associated with it. This shows that one needs to take care when identifying the global symmetry solely based on the Hasse diagram. On the other hand, a Hilbert series computation at order t^2 will always reveal the global symmetry group if refined and its dimension if unrefined.

7.3 Examples

We can now take the magnetic quivers we studied in the previous chapters and compute their Hasse diagrams.

7.3.1 6d theories

So far in the thesis, we only lightly touched upon the topic of 6d $\mathcal{N} = (1, 0)$ SCFTs, however many of their magnetic quivers are known in previous [163, 108, 109] and here we present some of them with their Hasse diagram.

Cancellation of gauge anomalies imposes strong restrictions on the gauge groups and matter contents, giving a list of allowed theories [181]. This list has been reproduced from F-theory constructions [84]. The theories can be labelled by their rank, which by definition is the dimension of the tensor branch. Theories of rank 1 can be realized on complex curves $\mathbb{P}^1$ with negative self-intersection. See, for instance, [182] for a review.

In this section, no attempt is made to compute the Hasse diagrams for the Higgs branches of all these theories. Instead, focus is placed on a few examples as a proof of concept. Theories realized on so-called -1 curves experience a small E_8 instanton transition at the origin of the tensor branch, see [183] and also [184, 185, 186, 187]. This transition implies a jump by 29 quaterionic dimensions of the Higgs branch between a generic point and the origin of the tensor branch. (Higgs branches at the origin of the tensor branch have been addressed recently in [188, 189, 163].) In the Hasse diagram this is expected to be manifested by a presence of an e_8 transition on the top of the Hasse diagram which describes the classical Higgs branch.

Table 7.2: *Hasse diagrams of* 6*d SCFTs:* SU(N) *with* $N + 8$ *fundamentals and one 2nd rank antisymmetric. Note that the two diagrams differ only at the bottom.*

6d SCFT	SU($2k$) with N=$2k$+8 and Λ^2	SU($2k$+1) with N=$2k$+9 and Λ^2
Magnetic quiver	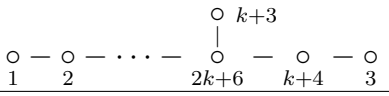	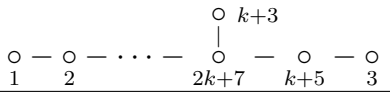
Hasse diagram	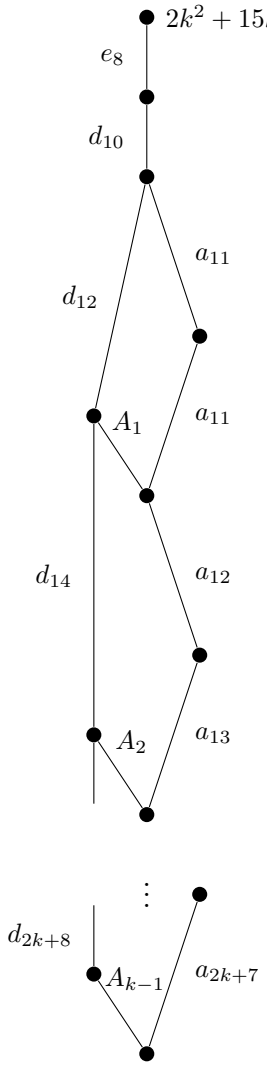	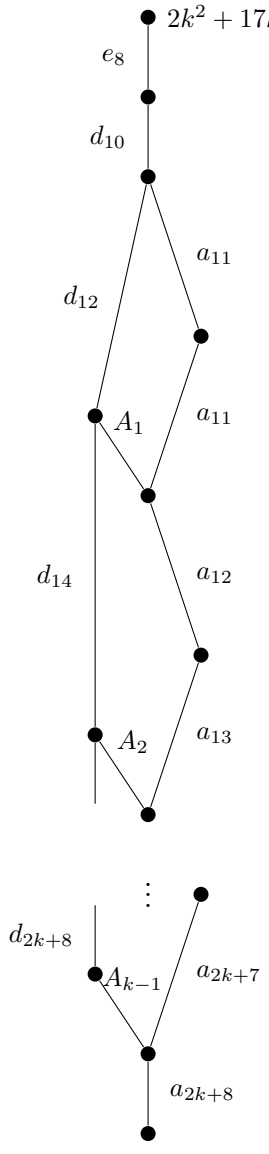

As an illustration, we first consider two infinite families of rank one theories on a -1 curve. These are the following:

- The 6d SU(N) gauge theory with $N+8$ fundamental hypermultiplets and a 2nd rank antisymmetric hypermultiplet, denoted by Λ^2. The Hasse diagrams for this theory is given in Table 7.2, using the magnetic quiver of [108, Sec. 3.6.2] for SU($2k$) and of [108, Sec. 3.6.4] for SU($2k+1$). Note that the Hasse diagram of the SU(N_1) theory is entirely included into the Hasse diagram of the SU(N_2) provided $N_1 \leq N_2$. This means that one can Higgs the SU(N_2) theory with N_2+8 fundamentals and one Λ^2 to the SU(N_1) theory with exactly N_1+8 fundamentals and one Λ^2. Alternatively, this can be checked directly by decomposing the representations, see for instance [85, Fig. 5].

- The Sp(k) with $N = 4k+16$ fundamental 6d half-hypermultiplets, with magnetic quivers derived in [108, Sec. 3.6.1 and 3.6.3]. The Hasse diagram for this family of theories is given in Table 7.3. Again, theories defined by various k-values display Hasse diagrams included into one another.

As a consistency check, the global symmetry of the theories is reproduced by the bottom part of the diagrams as discussed in the previous section.

7.3.2 5d theories

For 5d theories, we look at the SQCD theories at infinite gauge coupling as discussed in the Section 4.1 of Chapter 4. The orthosymplectic quivers in that chapter has the same Hasse diagram as their unitary counterparts in Section 4.1 which is given by Table 7.17 to Table 7.21. The Hasse diagram of all the magnetic quivers are as follows.

Table 7.3: *Hasse diagrams of 6d SCFTs:* Sp(k) *family and* G_2 *theory.*

6d SCFT	Sp(k) with $N = 4k + 16$ flavours	G_2 with 7 flavours
Magnetic quiver	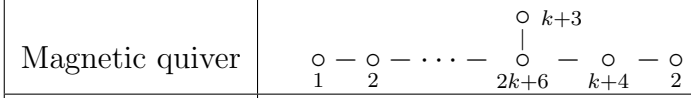	Not known
Hasse diagram	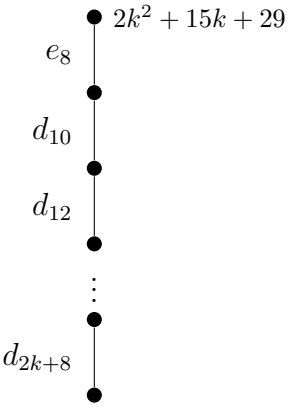	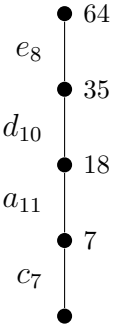

Table 7.4: *Components of* $\mathcal{H}_\infty$ *for* $\frac{1}{2} < |k| < N_c - \frac{N_f}{2}$*, part 1. Component I is present for* $\frac{N_f}{2} \geq |k|$*, Component II is present for* $N_f \geq N_c$*. The three dots denote a chain of balanced gauge nodes.*

Phase	Quiver	Hasse diagram
I	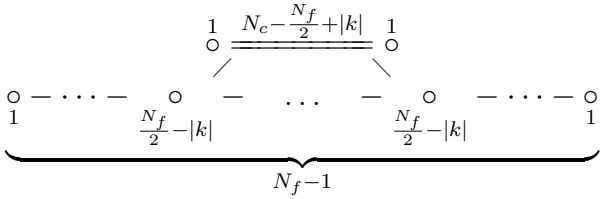	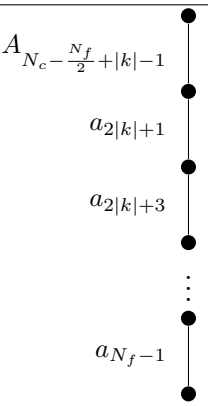
II	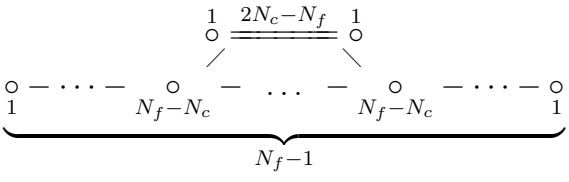	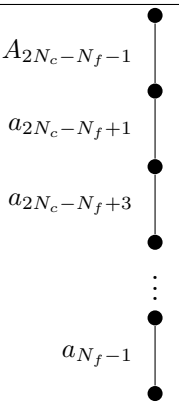

Table 7.5: *Components of $\mathcal{H}_\infty$ for $\frac{1}{2} < |k| < N_c - \frac{N_f}{2}$, part 2. Component III is present for $N_f \geq 2$. The three dots denote a chain of balanced gauge nodes.*

Phase	Quiver	Hasse diagram
III (N_f even)	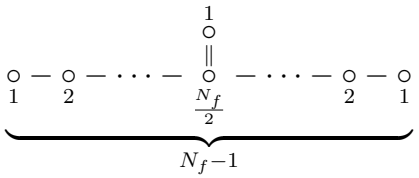	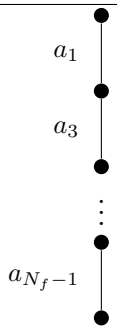
III (N_f odd)	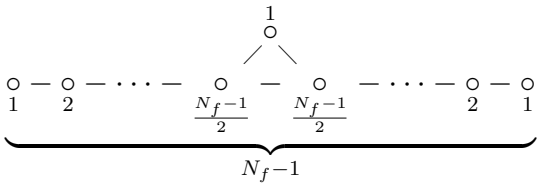	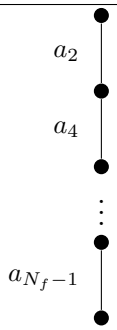

Table 7.6: *Components of $\mathcal{H}_\infty$ for $\frac{1}{2} = |k| < N_c - \frac{N_f}{2}$. Component I appears for $N_f \geq 1$, Component II appears for $N_f \geq N_c$.*

Phase	Quiver	Hasse diagram
I	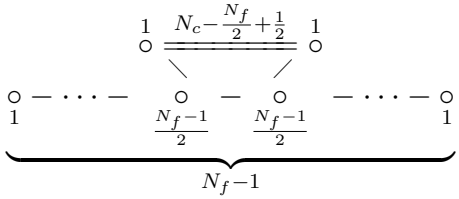	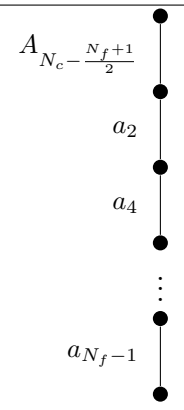
II	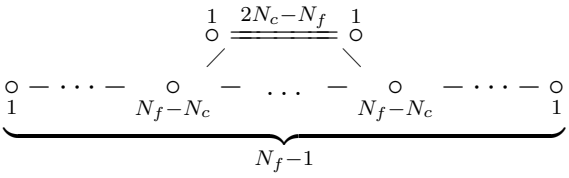	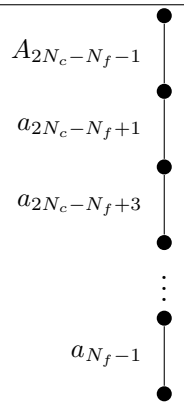

Table 7.7: *Components of $\mathcal{H}_\infty$ for $0 = |k| < N_c - \frac{N_f}{2}$. Component II is present for $N_f \geq N_c$*

Phase	Quiver	Hasse diagram, $N_c \neq \frac{N_f+2}{2}$	Hasse diagram, $N_c = \frac{N_f+2}{2}$
I	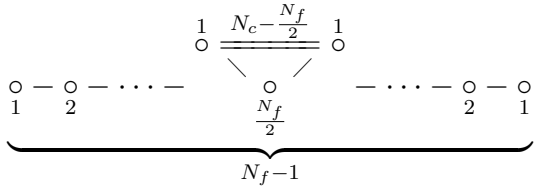	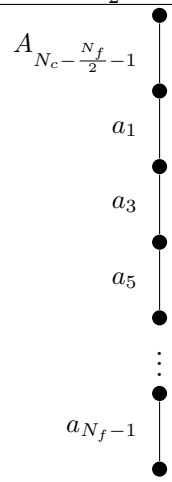	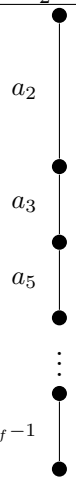
II	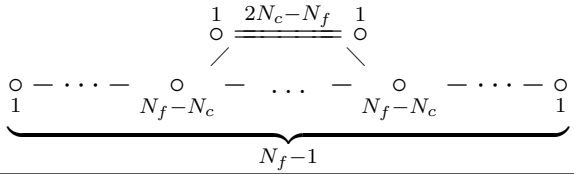	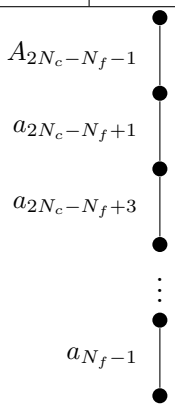	

Table 7.8: *Components of $\mathcal{H}_\infty$ for $1 < |k| = N_c - \frac{N_f}{2}$. Component I is present for $N_f \geq N_c$, which means $\frac{N_f}{2} \geq |k|$, and Component III appears for $N_f \geq 1$.*

Phase	Quiver	Hasse diagram
I	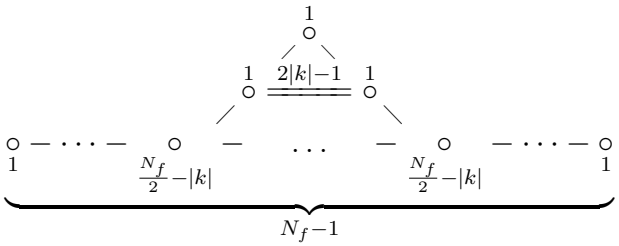	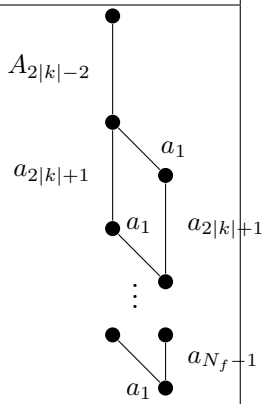
III (N_f even)	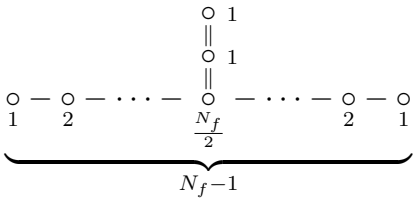	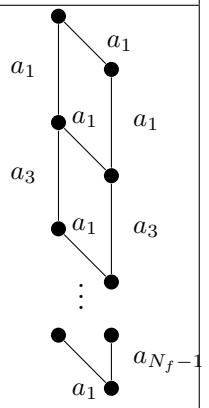
III (N_f odd)	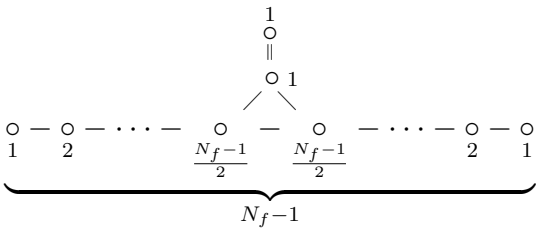	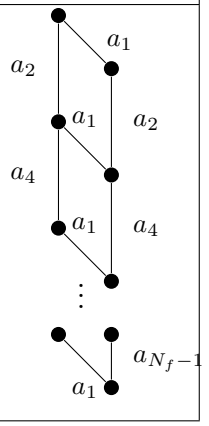

Table 7.9: *Components of $\mathcal{H}_\infty$ for $1 = |k| = N_c - \frac{N_f}{2}$.*

Phase	Quiver	Hasse diagram
I	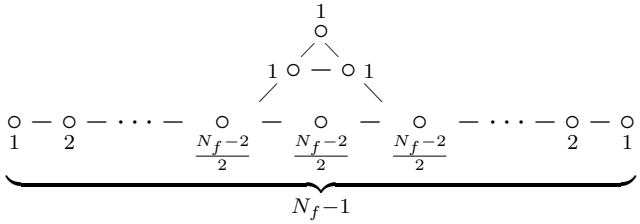	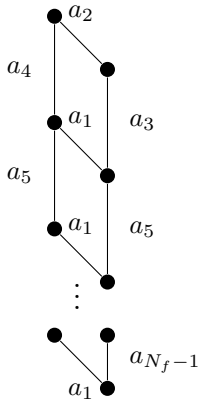
III (N_f even)	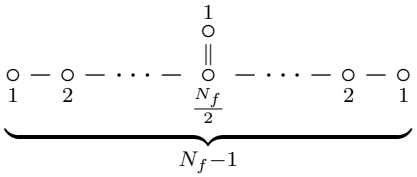	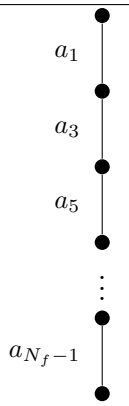

Table 7.10: *Component of $\mathcal{H}_\infty$ for $\frac{1}{2} = |k| = N_c - \frac{N_f}{2}$.*

Phase	Quiver	Hasse diagram
I	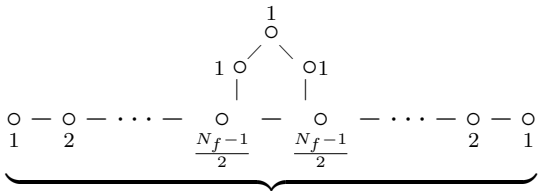	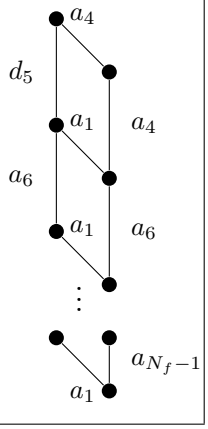

Table 7.11: *The component of $\mathcal{H}_\infty$ for $0 = |k| = N_c - \frac{N_f}{2}$. Note that for $N_f = 2$ there is no e_6 nor e_7 elementary slice, as expected for the* SU(2) *theory with 4 flavours. For $N_f = 3$ there is no e_7 elementary slice. Also note that since the quiver has an $\mathbb{Z}_2$ automorphism symmetry, there is branching into two e_6 transitions. As a consequence, the non-Abelian part of the global symmetry is $A_{N_f-1} \times A_1 \times A_1$.*

Phase	Quiver	Hasse diagram
I′	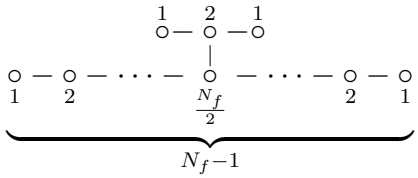	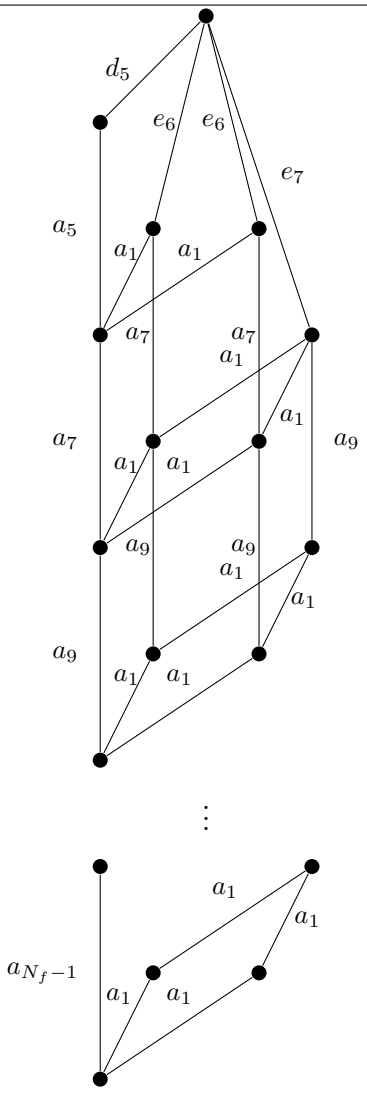

Table 7.12: *Components of $\mathcal{H}_\infty$ for $\frac{3}{2} < |k| = N_c - \frac{N_f}{2} + 1$. Component I is present for $N_f \geq N_c$, which means $\frac{N_f}{2} \geq |k| - 1$, and Component III is present for $N_f \geq 1$*

Phase	Quiver	Hasse diagram
I	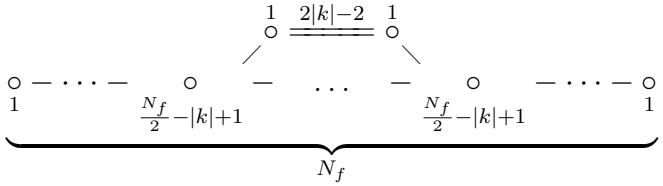	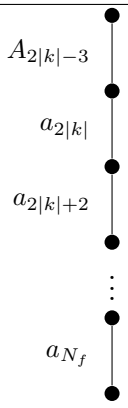
III (N_f even)	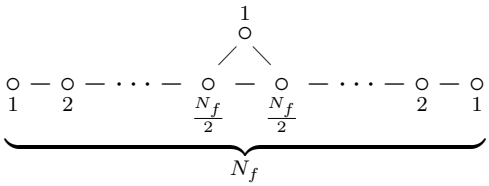	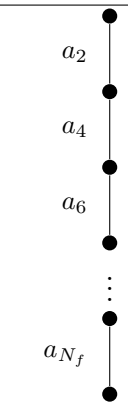
III (N_f odd)	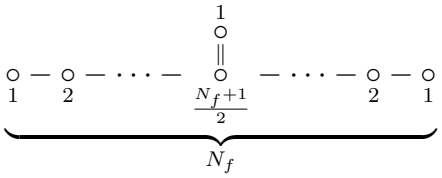	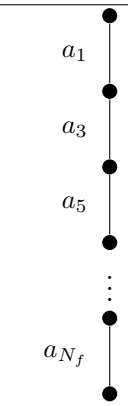

Table 7.13: *The component of $\mathcal{H}_\infty$ for $\frac{3}{2} = |k| = N_c - \frac{N_f}{2} + 1$.*

Phase	Quiver	Hasse diagram
I	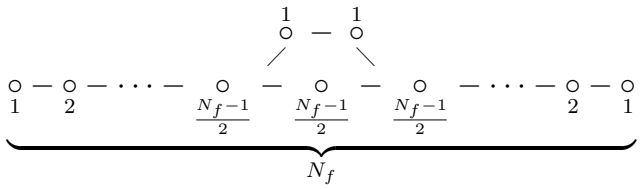	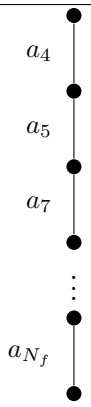

Table 7.14: *The component of $\mathcal{H}_\infty$ for $1 = |k| = N_c - \frac{N_f}{2} + 1$.*

Phase	Quiver	Hasse diagram
I	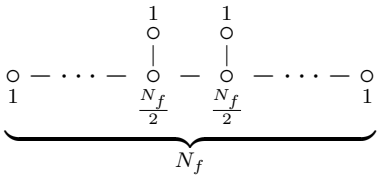	

Table 7.15: *The component of $\mathcal{H}_\infty$ for $\frac{1}{2} = |k| = N_c - \frac{N_f}{2} + 1$.*

Phase	Quiver	Hasse diagram
I′	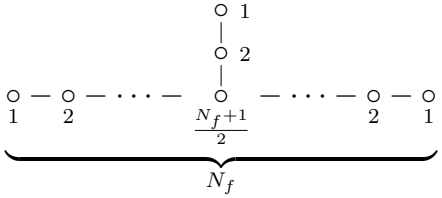	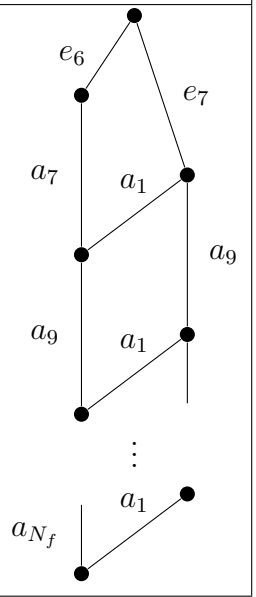

Table 7.16: *The component of* $\mathcal{H}_\infty$ *for* $0 = |k| = N_c - \frac{N_f}{2} + 1$.

Phase	Quiver	Hasse diagram
I′	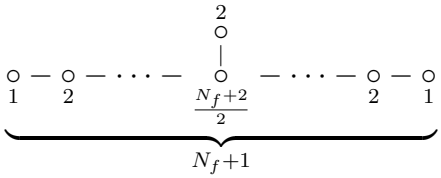	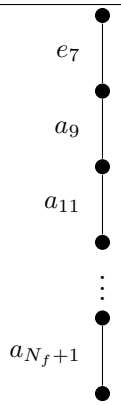

Table 7.17: *Components of $\mathcal{H}_\infty$ for $2 < |k| = N_c - \frac{N_f}{2} + 2$. Component IV is present for $N_f \geq 2$ with N_f even. Component V (N_f even) is present for $N_f \geq 0$ if k is even and is present for $N_f \geq 2$ if k is odd. Component V (N_f odd) is present for $N_f \geq 1$.*

Phase	Quiver	Hasse diagram
IV (N_f even)	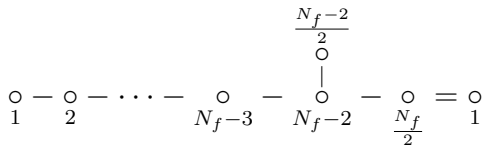	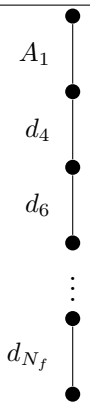
V (N_f even)	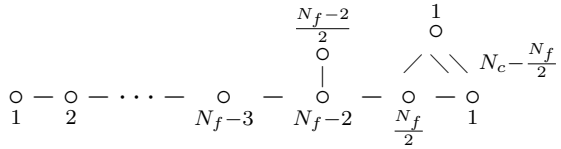	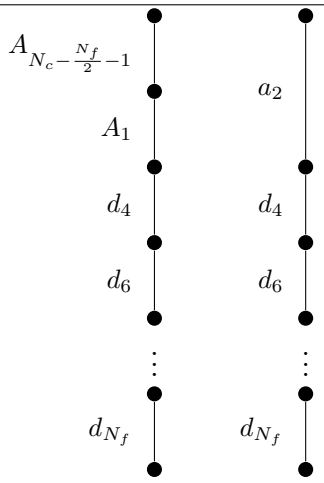
V (N_f odd)	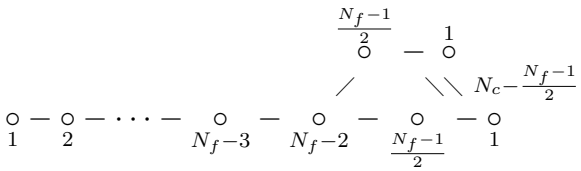	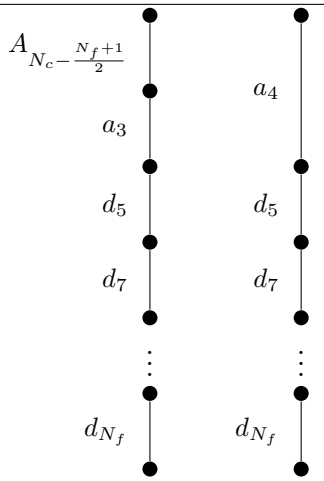

Table 7.18: *The component of $\mathcal{H}_\infty$ for $2 = |k| = N_c - \frac{N_f}{2} + 2$.*

Phase	Quiver	Hasse diagram
V (N_f even)	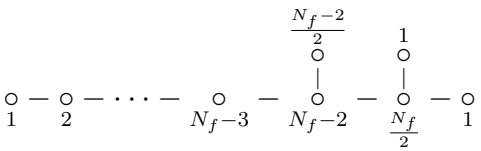	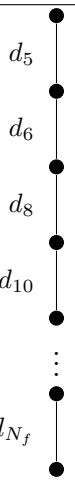

Table 7.19: *The component of $\mathcal{H}_\infty$ for $\frac{3}{2} = |k| = N_c - \frac{N_f}{2} + 2$.*

Phase	Quiver	Hasse diagram
V (N_f odd)	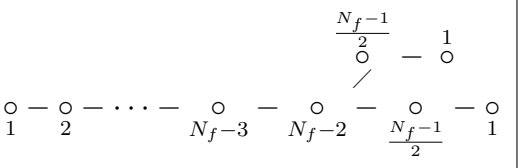	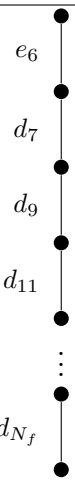

Table 7.20: *The component of $\mathcal{H}_\infty$ for $1 = |k| = N_c - \frac{N_f}{2} + 2$.*

Phase	Quiver	Hasse diagram
V′ (N_f even)	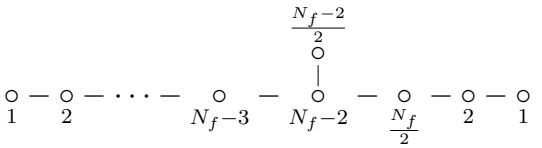	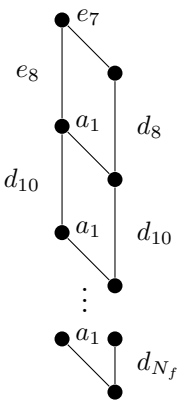

Table 7.21: *The component of $\mathcal{H}_\infty$ for $\frac{1}{2} = |k| = N_c - \frac{N_f}{2} + 2$.*

Phase	Quiver	Hasse diagram
V′ (N_f odd)	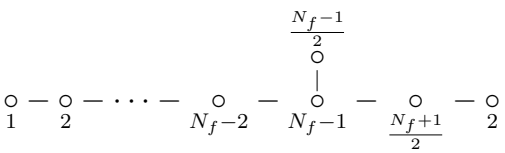	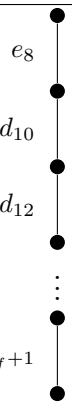

7.3.3 4d theories

The Hasse diagrams of the rank one SCFTs we studied in Chapter 5 are given in Table 7.22 to Table 7.26. For their extension to infinite families, only the extension of C_5, $C_2 \times A_1$, $C_n \times U_1$ and $\mathbb{H}/\mathbb{Z}_2$ has simple Hasse diagrams which we give in Table 7.27.

Complexity in Hasse diagram and HWG

One important observation here is that the families with simple Hasse diagrams also have simple HWGs. In particular, if the Hasse diagram for the general family is known, the general HWG is known as well. This once again ties us to the notion of simplicity when it comes to moduli spaces, and makes drawing the Hasse diagram a test of such simplicity.

$\mathcal{S}$-fold theories

When discussing moduli spaces, two common objects often arise in the literature. k-instanton moduli spaces and Higgs branch of SQCD theories. Both spaces are well studied. However, from our analysis, we see that instanton moduli spaces has a significantly more complicated moduli spaces, both in terms of the HWG and the Hasse diagrams, compared to SQCD theories. The moduli spaces of $\mathcal{S}$-fold theories are closely related to instanton moduli spaces, where within the same infinite family, the number of gauge nodes in the magnetic quiver does not change but their rank increases. We do not have the general Hasse diagram for the infinite family of these theories, but as a show of its complexity, we provide the $r = 2$ cases of $\mathring{\mathcal{S}}^{(r)}_{G,\ell}$ theory in Figure 7.2.

Quiver subtraction for non-simply laced quivers

In general, the quiver subtraction rules for non-simply laced quivers is the same as for simply laced. In chapter 5, we saw that for $\mathring{\mathcal{S}}^{(r)}_{G,\ell}$ theories, there are two equivalent sets of magnetic quivers: one with a flavor node on the short side and the other an unframed version. As mentioned in the quiver subtraction rules, it is important to use the unframed version as otherwise the algorithm will miss several symplectic leaves in the Hasse diagram.

Table 7.22: *C_5 theory. Hasse diagram for the Higgs branch of the 4d $\mathcal{N} = 2$ rank 1 theory. To the right of the Hasse diagram are the magnetic quivers for the closures of the leaves and to the left are magnetic quivers for the slices. This Hasse diagram is already explored in [10, 24].*

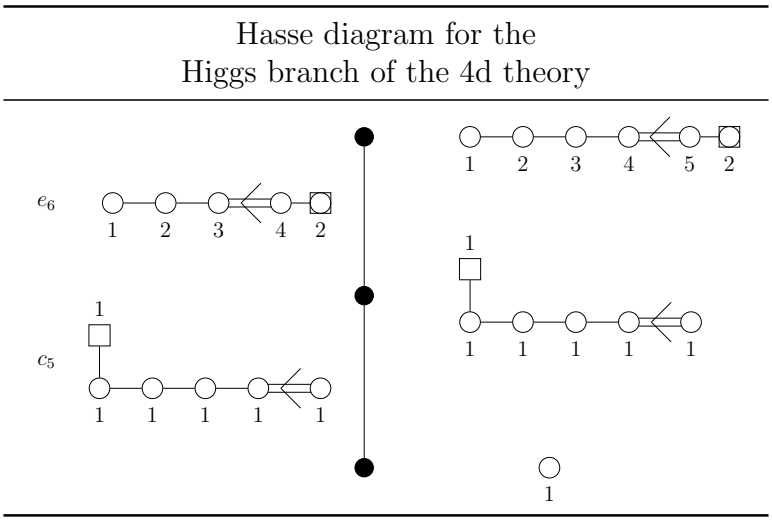

There is an additional caveat in the quiver subtraction algorithm for a non-simply laced quiver with l multiplicity edge. If one of the short nodes needs rebalancing after subtraction, the short node needs to be connected to the $U(1)$ node (which as discussed above, is a new node added to rebalance all the other nodes) with a non-simply laced edge of multiplicity l pointing outward of the $U(1)$.

Another interesting phenomenon that arises when dealing with $\mathcal{S}$-fold magnetic quivers and quivers of k-instanton moduli spaces is that you can often subtract two or more of the same quiver at the same set of nodes. If this happens for k' successive times, then the rebalanced node in the end would be a $U(k)$ node with hypers transforming in the adjoint representation. This was first discussed in [7] and studied in more detail in [15].

Folded orthosymplectic quivers

The Coulomb branch of folded orthosymplectic quivers discussed in Chapter 5 have been identified as magnetic quivers of both 5d and 4d SCFTs. The Hasse diagrams of the unitary counterparts of the E_n folded quivers are given in the 5d section above and we will not repeat it here. However, the quiver subtraction of orthosymplectic quivers is studied for these cases in [8] and the Hasse diagrams obtained are consistent with the unitary counterparts.

Table 7.23: *$C_3 \times A_1$ theory. Hasse diagram for the Higgs branch of the 4d $\mathcal{N} = 2$ rank 1 theory. To the right of the Hasse diagram are the magnetic quivers for the closures of the leaves and to the left are magnetic quivers for the slices.*

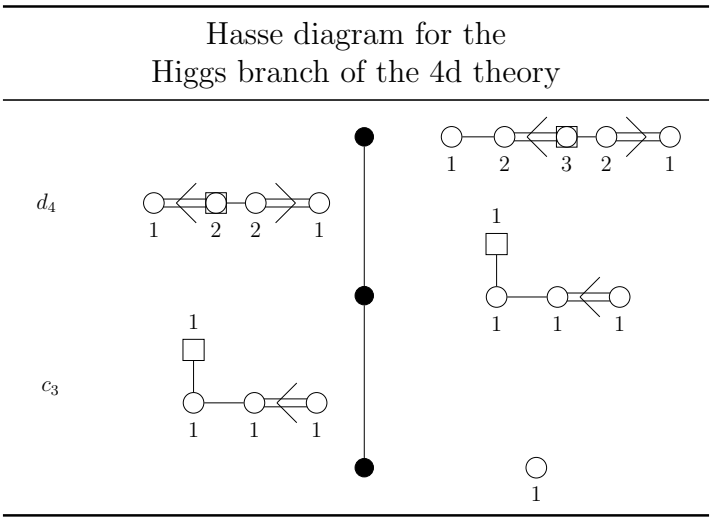

Class $\mathcal{S}$ Hasse diagrams

Class $\mathcal{S}$ Hasse diagrams can be obtained using the same methods as above. However, most of them do not have infinite families that can be nicely expressed in a single general Hasse diagram as in 5d or 6d examples above. Therefore, the best method is to study them is on a case by case basis which can be done efficiently using our `Mathematica` code.

7.3.4 3d theories

For mixed U and SU quivers in chapter 6, the Hasse diagrams are quite involved as well. We look at the Hasse diagram of the $T(SU(4))$ quiver with various choices of unitary and special unitary nodes specified by the partition $\{\dots\}$. The same notation and colouring are used in Table 6.1.

Table 7.24: *A_3 theory. Hasse diagram for the Higgs branch of the 4d $\mathcal{N}=2$ rank 1 theory. To the right of the Hasse diagram are the magnetic quivers for the closures of the leaves and to the left are magnetic quivers for the slices.*

Hasse diagram for the Higgs branch of the 4d theory
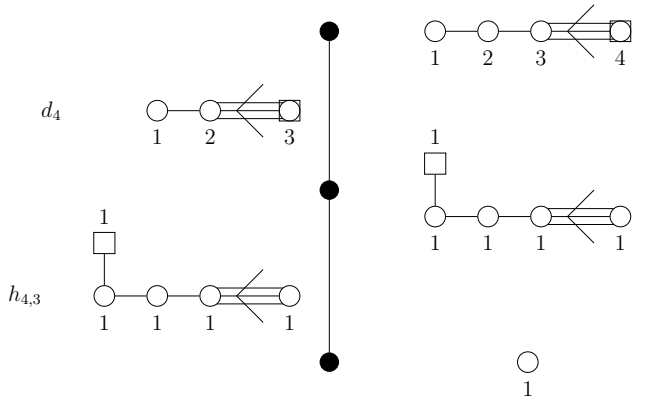

Table 7.25: *$A_1 \times U_1$ theory. Hasse diagram for the Higgs branch of the 4d $\mathcal{N}=2$ rank 1 theory. To the right of the Hasse diagram are the magnetic quivers for the closures of the leaves and to the left are magnetic quivers for the slices.*

Hasse diagram for the Higgs branch of the 4d theory
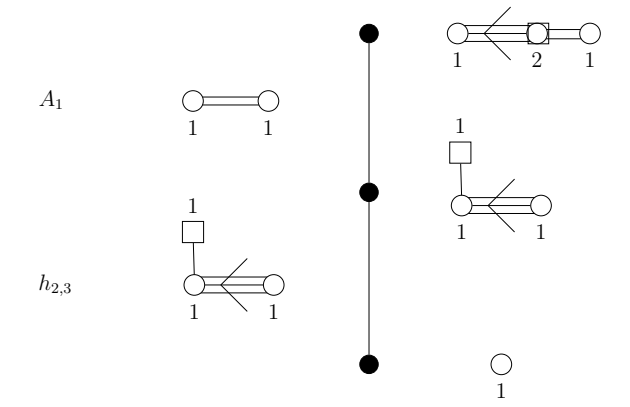

Table 7.26: *A_2 theory. Hasse diagram for the Higgs branch of the 4d $\mathcal{N}=2$ rank 1 theory. To the right of the Hasse diagram are the magnetic quivers for the closures of the leaves and to the left are magnetic quivers for the slices.*

Hasse diagram for the Higgs branch of the 4d theory
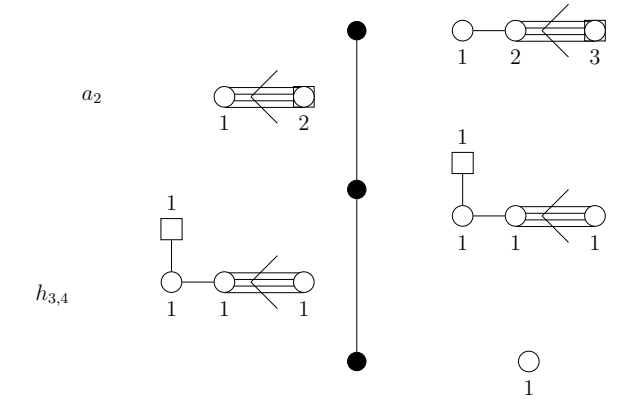

Table 7.27: *Hasse diagrams for the first three families of quivers in Table 5.5, and for the generalised $\mathbb{H}/\mathbb{Z}_2$ family of quivers in Table 5.7.*

C_{n+3}	$C_{n+1} \times A_1$	$C_n \times U_1$	$\mathbb{H}/\mathbb{Z}_2$
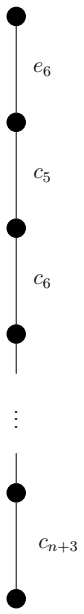	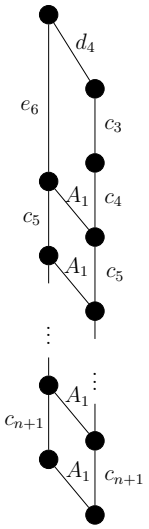		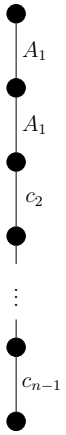

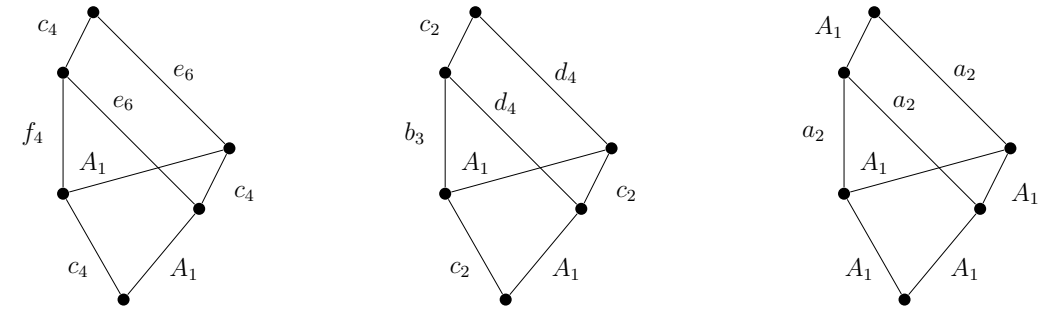

(a) $\mathring{\mathcal{S}}^{(1)}_{E_6,2}$ ***(b)*** $\mathring{\mathcal{S}}^{(1)}_{D_4,2}$ ***(c)*** $\mathring{\mathcal{S}}^{(1)}_{A_2,2}$

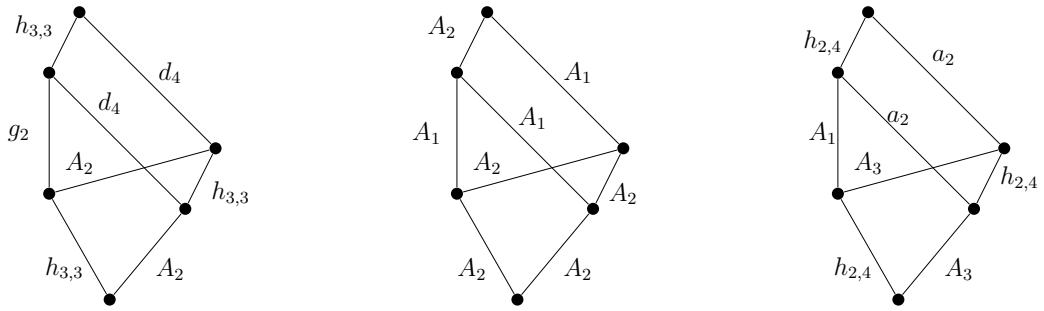

(d) $\mathring{\mathcal{S}}^{(1)}_{D_4,3}$ ***(e)*** $\mathring{\mathcal{S}}^{(1)}_{A_1,3}$ ***(f)*** $\mathring{\mathcal{S}}^{(1)}_{A_2,4}$

Figure 7.2: *Proposed Hasse diagram for* $\mathring{\mathcal{S}}^{(1)}_{G,\ell}$ *theories.*

Table 7.28: *Hasse diagrams of symplectic leaves (black dots) for the Higgs branches of theories shown in Tables 6.1, 6.3 and 6.2. The elementary slices between adjacent leaves are labeled A_n for the Klein singularity $\mathbb{C}^2/\mathbb{Z}_{n+1}$ and a_n (respectively d_n) for the closure of the minimal nilpotent orbit of $\mathfrak{sl}(n+1,\mathbb{C})$ (resp. $\mathfrak{so}(2n,\mathbb{C})$). The partition refers to hypers connecting the $\mathrm{U}(3)$ node and the bouquet of $\mathrm{U}(1)$ nodes in the second column of Table 6.1, as indicated by the colouring of the cells.*

Partition	$[4]$	$[3,1]$	$[2,2]$	$[2,1,1]$	$[1,1,1,1]$
Hasse Diagram	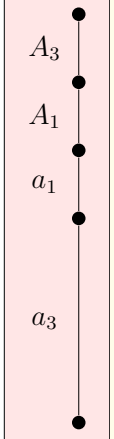	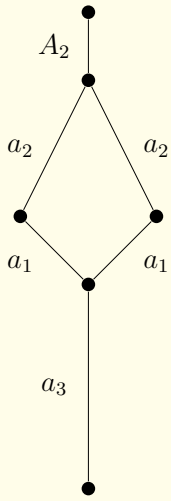	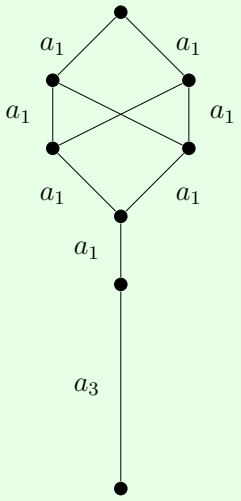	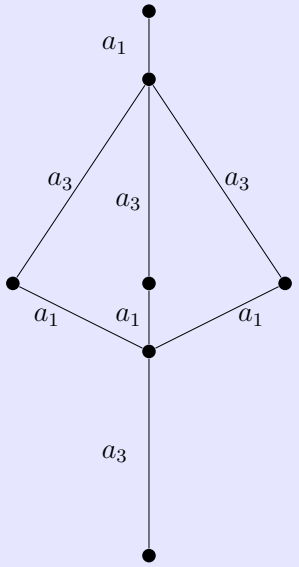	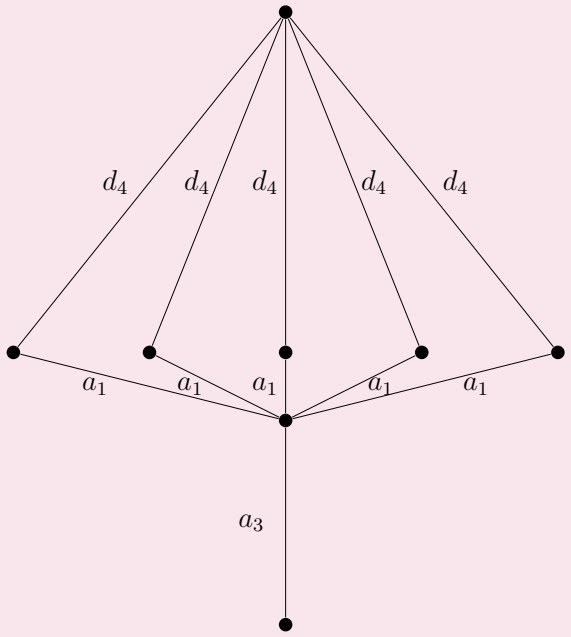

Conclusion

The focus of this thesis is to study supersymmetric gauge theories from a new perspective. The new perspective is that rather than studying very detailed properties of simple gauge theories, we use **magnetic quivers** to study very simple properties – moduli space of vacua – of very complicated gauge theories.

Given a supersymmetric gauge theory with eight supercharges, we studied their moduli spaces of vacua in $d = 3, 4, 5, 6$ dimensions with a particular focus on their Higgs branch. However, the Higgs branch can receive non-perturbative instanton/tensionless string corrections in $d = 5, 6$. Whereas in $d = 4$, most of the interesting theories are non-Lagrangian. This means a hyperKähler quotient construction is not known for these theories and a new direction is needed to study them. The magnetic quiver is a unifying approach that allows us to study the Higgs branch of all these gauge theories. In this thesis, we extracted the magnetic quivers and studied the chiral ring by computing the Hilbert series. The goals we achieved are two fold:

1) We created a large database of magnetic quivers, Hilbert series, Hasse diagrams, thus unveiling detailed properties of the Higgs branch of popular gauge theories in the literature such as rank one 4d SCFTs, class $\mathcal{S}$ theories, Argyres-Douglas theories, $\mathcal{S}$-folds, 5d SQCDs, 6d SCFTs etc. These computations will lay the foundation for future research. For example, if one finds a new gauge theory or SCFT and knows some of its properties such as global symmetry, moduli space dimension etc, they can then try to match it with one of our magnetic quivers in the database. If the result matched, the Hilbert series and Hasse diagram of its magnetic quiver will be readily available which provide a lot more non-trivial information about that gauge theory/ SCFT.

2) With the magnetic quivers at hand, we had already obtained non-trivial results about

the corresponding electric quivers as follows:

- The magnetic quivers for 5d SQCD theories at superconformal fixed point were known in the literature. We found that each one of the infinite families of magnetic quivers can be expressed by a general HWG and Hasse diagram. This is an indication of simplicity of these moduli spaces. Whenever a new idea occurs, one would always test them on the simplest set of theories they can think of. In terms of moduli spaces, the literature often favours the moduli spaces of k-instantons as the simplest moduli spaces to study. However, we will now argue that the moduli spaces related to SQCD theories of gauge group G with arbitrary rank k are the simplest non-trivial theories to study.

  In our paper [11], which was not discussed in this thesis, we find that $3d$ $\mathcal{N} = 4$ SQCD theories have nilpotent operators in the chiral ring when the number of flavors are too small. Such features were also explored in 4d $\mathcal{N} = 2$ theories (see [190]). It will be interesting to see if such features appear for 5d SQCD theories as well[3].

- 4d $\mathcal{N} = 2$ SCFTs were often studied through compatification of 5d $\mathcal{N} = 1$ SCFTs on S^1. The compatification can also include a $\mathbb{Z}_k$ topological twist. We are now able to perform the same procedure on the magnetic quivers of 5d SCFTs through folding $\mathbb{Z}_k$ identical legs to give the magnetic quiver of 4d $\mathcal{N} = 2$ SCFTs. One future exercise is to take all known magnetic quivers of 5d SCFTs with identical legs and fold them to see if we get can get magnetic quivers of any new 4d SCFTs.

- The majority of 4d SCFTs in the literature are $\mathcal{S}$ theories whose magnetic quivers take the shape of star-shaped quivers. By investigating all rank one SCFTs and $\mathcal{S}$-fold theories, we find that non-simply laced quivers are ubiquitous as magnetic quivers of 4d theories as well. Extending this observation to higher ranks may allow us to use the non-simply laced magnetic quivers as a starting point to produce a whole new zoo of 4d SCFTs.

- Orthosymplectic quivers had always been less studied than their unitary counterpart. In this thesis, we highlighted subtle issues involving orthosymplectic quivers, such as the

[3]In addition to the nilpotent element S from the gaugino superfield which we already know.

existence of a $(\mathbb{Z})_{\text{diag}}$ subgroup when quivers are made of $U(n)$, $SO(2n)$ and $USp(2n)$ gauge groups and are unframed/flavorless. Identifying this discrete subgroup and correctly modifying the magnetic lattice of the monopole formula allowed us to find orthosymplectic magnetic quivers corresponding to various 4d, 5d and 6d SCFTs.

- We also made a Dynkin classification of orthosymplectic quivers where a systematic study of BCD type orthosymplectic quivers appear for the first time in the literature. The fact that these quivers yield interesting results: C-type (non-simply laced) orthosymplectic quivers are magnetic quivers of 4d SCFTs and D-type (forked) quivers have Coulomb branches that are products, shows that they are objects worth studying now that we have the right tools to study them.

- We also completely answered the question: what are the 3d mirrors of quivers containing a mixture of unitary and special unitary gauge groups. The brane locking mechanism, along with our `Mathematica` code, can be applied to *any* linear quivers with mixed U & SU gauge groups. The output will either be the 3d mirror or the magnetic quiver depending on whether the linear quiver is good/ugly/bad.

- We obtained Hasse diagrams for a myriad of Higgs branches in this thesis. There are other approaches in obtaining Hasse diagrams in the literature as well such as using vertex operator algebra (VOA) [191]. It will be important to compare Higgs branch Hasse diagrams, whenever possible, with others to see if we get consistent results.

Future outlooks

The obvious next steps are a) take the Hilbert series and reconstruct the generators and relations that define chiral rings and b) take the Hasse diagrams and study the pattern of partial Higgsing of different theories and how one theory can be Higgsed to the other.

Here, we give three additional future prospects that follows the work in this thesis.

- So far we always take a magnetic quiver and derive the corresponding Hasse diagram using quiver subtraction. But perhaps one can reverse the order and start "building" Hasse diagrams from the bottom-up. For example, if we study gauge theories whose Higgs branch

has a single non-Abelian global symmetry $SU(n)$, then we know the slice between the trivial leaf and the first non-trivial leaf is an elementary slice with a_{n-1}. Now, we can ask the question: what are the possible slices that we can add to this first slice. In other words, we are growing the Hasse diagram one slice at a time to see all possible slices that can be added. The answer is *not* an infinite number of slices, because arbitrarily adding slices through *quiver addition* will easily change the global symmetry of the magnetic quiver and hence the bottom slice. So in order make sure the global symmetry is $SU(n)$ upon adding slices, it turns out only a very finite classes of elementary slices can be added. This can be an interesting way in classifying 3d $\mathcal{N} = 4$ gauge theories based on the number of slices in the Hasse diagram. For instance, one can go through and classify all possible Hasse diagrams with two slices. In fact, the Hasse diagram of rank one SCFTs in $d = 4, 5, 6$ all seem to have very few number of slices, so perhaps such a classification can help in classifying all possible lower rank SCFTs in various dimensions!

One interesting observation we found in this thesis is that simple Hasse diagrams (for example, with no bifurcations) leads to simple HWG. Perhaps, coupled with the previous proposal, one can also construct new HWGs based on the Hasse diagrams. This is a plausible goal since the HWG for elementary slices are all known. The non-trivial step here is that the Hasse diagrams we drew does not uniquely identify a moduli space. However, with some additional labellings in the Hasse diagram, this can become possible. If the Hasse diagram $\leftrightarrow$ HWG correspondence can be made, then we can obtain the refined Hilbert series of arbitrarily complicated moduli spaces as long as the Hasse diagram is known. The latter is a much simpler computation using our `Mathematica` code.

- In terms of orthosymplectic quivers, they are starting to play a more and more important role in understanding gauge theories in different dimensions. There are also evidences of theories which only has a orthosymplectic magnetic quiver and not a unitary one (e.g G_2 with 5 flavors at infinite coupling in 5d [192])[4]. Furthermore, there is a wide range of discrete factors beyond our $(\mathbb{Z}_2)_{\text{diag}}$ such as SO(2n) vs O(2n) vs Spin(2n) etc. The interplay

[4]Of course, by construction one can create many such examples by looking at class $\mathcal{S}$ theories with (un)twisted D-type punctures or twisted A-type punctures

of discrete factors is tightly related to the recent explosion of activities around higher-form symmetries, 2-groups and non-invertible symmetries. Some of the recent works that are more relevant to the work in this thesis can be found in [193, 194, 195, 196, 197, 198]. I believe orthosymplectic quivers can play an important role in understanding these features in gauge theories.

- Finally, after extending the number of known 3d mirror pairs in the literature, one can ask how far can we push forward in systematically deriving 3d mirror pairs. One extension is to take all known 3d mirror pairs with unitary gauge groups and turn some or all of them into special unitary and ask whats their 3d mirror. However, pretty much all known quivers in the literature that has a 3d mirror pair has gauge groups linked together to form a finite or affine Dynkin quiver. The question is then if we deviate from a Dynkin type quiver significantly, such as a star-shaped quiver, can we find a Lagrangian (quiver gauge theory) 3d mirror dual? I would argue that this can't be done as long as we are able to subtract a $E_{6,7,8}$ affine Dynkin diagram from the quiver. However, this should be tested further which may explain the lack of such mirror pairs in the literature.

Bibliography

[1] A. Hanany and Z. Zhong, *Highest Weight Generating function for tropical quivers*, *(in preparation)* .

[2] A. Bourget, J. F. Grimminger, A. Hanany, R. Kalveks, M. Sperling and Z. Zhong, *Magnetic Lattices for Orthosymplectic Quivers*, *JHEP* **12** (2020) 092, [2007.04667].

[3] A. Bourget, J. F. Grimminger, A. Hanany, M. Sperling and Z. Zhong, *Magnetic Quivers from Brane Webs with O5 Planes*, *JHEP* **07** (2020) 204, [2004.04082].

[4] S. Nawata, M. Sperling, H. E. Wang and Z. Zhong, *Magnetic quivers and line defects — On a duality between 3d $\mathcal{N} = 4$ unitary and orthosymplectic quivers*, *JHEP* **02** (2022) 174, [2111.02831].

[5] M. Sperling and Z. Zhong, *Balanced B and D-type orthosymplectic quivers — magnetic quivers for product theories*, *JHEP* **04** (2022) 145, [2111.00026].

[6] A. Bourget, J. F. Grimminger, A. Hanany, M. Sperling, G. Zafrir and Z. Zhong, *Magnetic quivers for rank 1 theories*, *JHEP* **09** (2020) 189, [2006.16994].

[7] A. Bourget, S. Giacomelli, J. F. Grimminger, A. Hanany, M. Sperling and Z. Zhong, *S-fold magnetic quivers*, *JHEP* **02** (2021) 054, [2010.05889].

[8] A. Bourget, J. F. Grimminger, A. Hanany, R. Kalveks, M. Sperling and Z. Zhong, *Folding orthosymplectic quivers*, *JHEP* **12** (2021) 070, [2107.00754].

[9] A. Bourget, J. F. Grimminger, A. Hanany, R. Kalveks and Z. Zhong, *Higgs Branches of U/SU Quivers via Brane Locking*, 2111.04745.

[10] A. Bourget, S. Cabrera, J. F. Grimminger, A. Hanany, M. Sperling, A. Zajac et al., *The Higgs mechanism — Hasse diagrams for symplectic singularities*, *JHEP* **01** (2020) 157, [1908.04245].

[11] A. Bourget, S. Cabrera, J. F. Grimminger, A. Hanany and Z. Zhong, *Brane Webs and Magnetic Quivers for SQCD*, *JHEP* **03** (2020) 176, [1909.00667].

[12] A. Bourget, J. F. Grimminger, A. Hanany, M. Sperling and Z. Zhong, *Branes, Quivers, and the Affine Grassmannian*, 2102.06190.

[13] A. Bourget, A. Dancer, J. F. Grimminger, A. Hanany, F. Kirwan and Z. Zhong, *Orthosymplectic implosions*, *JHEP* **08** (2021) 012, [2103.05458].

[14] A. Bourget, A. Dancer, J. F. Grimminger, A. Hanany and Z. Zhong, *Partial Implosions and Quivers*, 2112.10825.

[15] A. Bourget, J. F. Grimminger, A. Hanany and Z. Zhong, *The Hasse Diagram of the Moduli Space of Instantons*, 2202.01218.

[16] O. Aharony, A. Hanany and B. Kol, *Webs of (p,q) five-branes, five-dimensional field theories and grid diagrams*, *JHEP* **01** (1998) 002, [hep-th/9710116].

[17] D. Gaiotto and H.-C. Kim, *Duality walls and defects in 5d $\mathcal{N} = 1$ theories*, *JHEP* **01** (2017) 019, [1506.03871].

[18] H. Hayashi, S.-S. Kim, K. Lee and F. Yagi, *6d SCFTs, 5d Dualities and Tao Web Diagrams*, *JHEP* **05** (2019) 203, [1509.03300].

[19] O. Chacaltana and J. Distler, *Tinkertoys for the D_N series*, *JHEP* **02** (2013) 110, [1106.5410].

[20] O. Chacaltana, J. Distler and Y. Tachikawa, *Gaiotto duality for the twisted A_{2N-1} series*, *JHEP* **05** (2015) 075, [1212.3952].

[21] O. Aharony and Y. Tachikawa, *S-folds and 4d N=3 superconformal field theories*, *JHEP* **06** (2016) 044, [1602.08638].

[22] G. Ferlito, A. Hanany, N. Mekareeya and G. Zafrir, *3d Coulomb branch and 5d Higgs branch at infinite coupling*, *JHEP* **07** (2018) 061, [1712.06604].

[23] S. Giacomelli, C. Meneghelli and W. Peelaers, *New N=2 superconformal field theories from S-folds*, 2007.00647.

[24] J. F. Grimminger and A. Hanany, *Hasse diagrams for 3d $\mathcal{N}$ = 4 quiver gauge theories — Inversion and the full moduli space*, *JHEP* **09** (2020) 159, [2004.01675].

[25] S. Cabrera, A. Hanany and F. Yagi, *Tropical Geometry and Five Dimensional Higgs Branches at Infinite Coupling*, *JHEP* **01** (2019) 068, [1810.01379].

[26] P. A. M. Dirac, *The quantum theory of the electron*, *Proceedings of the Royal Society of London. Series A, Containing Papers of a Mathematical and Physical Character* **117** (1928) 610–624.

[27] R. P. Feynman et al., *Qed: The strange theory of light and matter*, 1985.

[28] F. Combley, F. J. M. Farley and E. Picasso, *The CERN muon (g-2) experiments*, *Phys. Rep.* **68** (Jun, 1980) 93–119. 46 p.

[29] Muon g-2 collaboration, B. Abi et al., *Measurement of the Positive Muon Anomalous Magnetic Moment to 0.46 ppm*, *Phys. Rev. Lett.* **126** (2021) 141801, [2104.03281].

[30] S. Borsanyi, Z. Fodor, J. N. Guenther, C. Hoelbling, S. D. Katz, L. Lellouch et al., *Leading hadronic contribution to the muon magnetic moment from lattice QCD*, *Nature* **593** (apr, 2021) 51–55.

[31] W. Nahm, *Supersymmetries and their Representations*, *Nucl. Phys. B* **135** (1978) 149.

[32] N. Seiberg and E. Witten, *Electric - magnetic duality, monopole condensation, and confinement in N=2 supersymmetric Yang-Mills theory*, *Nucl. Phys. B* **426** (1994) 19–52, [hep-th/9407087].

[33] N. Seiberg and E. Witten, *Monopoles, duality and chiral symmetry breaking in N=2 supersymmetric QCD*, *Nucl. Phys. B* **431** (1994) 484–550, [hep-th/9408099].

[34] P. C. Argyres, M. R. Plesser and N. Seiberg, *The Moduli space of vacua of N=2 SUSY QCD and duality in N=1 SUSY QCD*, *Nucl. Phys.* **B471** (1996) 159–194, [hep-th/9603042].

[35] M. R. Douglas and G. W. Moore, *D-branes, quivers, and ALE instantons*, hep-th/9603167.

[36] S. Cremonesi, A. Hanany and A. Zaffaroni, *Monopole operators and Hilbert series of Coulomb branches of* $3d$ $\mathcal{N} = 4$ *gauge theories*, *JHEP* **01** (2014) 005, [1309.2657].

[37] A. Hanany and E. Witten, *Type IIB superstrings, BPS monopoles, and three-dimensional gauge dynamics*, *Nucl. Phys.* **B492** (1997) 152–190, [hep-th/9611230].

[38] A. Kapustin, *D(n) quivers from branes*, *JHEP* **12** (1998) 015, [hep-th/9806238].

[39] A. Hanany and A. Zaffaroni, *Issues on orientifolds: On the brane construction of gauge theories with SO(2n) global symmetry*, *JHEP* **07** (1999) 009, [hep-th/9903242].

[40] B. Feng and A. Hanany, *Mirror symmetry by O3 planes*, *JHEP* **11** (2000) 033, [hep-th/0004092].

[41] H. Kraft and C. Procesi, *On the geometry of conjugacy classes in classical groups*, *Commentarii mathematici Helvetici* **57** (1982) 539–602.

[42] S. Cabrera and A. Hanany, *Branes and the Kraft-Procesi Transition*, *JHEP* **11** (2016) 175, [1609.07798].

[43] S. Cabrera and A. Hanany, *Quiver Subtractions*, *JHEP* **09** (2018) 008, [1803.11205].

[44] B. Feng, A. Hanany and Y.-H. He, *Counting gauge invariants: The Plethystic program*, *JHEP* **03** (2007) 090, [hep-th/0701063].

[45] S. Cremonesi, *3d supersymmetric gauge theories and Hilbert series*, *Proc. Symp. Pure Math.* **98** (2018) 21–48, [1701.00641].

[46] J. Gray, A. Hanany, Y.-H. He, V. Jejjala and N. Mekareeya, *SQCD: A Geometric Apercu*, *JHEP* **05** (2008) 099, [0803.4257].

[47] D. Eisenbud, *Commutative Algebra with a View Toward Algebraic Geometry*. Springer, 1995.

[48] R. Stanley, *Hilbert functions of graded algebras*, *Advances in Mathematics* **28** (1978) 57–83.

[49] A. Hanany and R. Kalveks, *Highest Weight Generating Functions for Hilbert Series*, *JHEP* **10** (2014) 152, [1408.4690].

[50] A. Hanany and R. Kalveks, *Highest Weight Generating Functions for Hilbert Series*, *JHEP* **10** (2014) 152, [1408.4690].

[51] S. Benvenuti, B. Feng, A. Hanany and Y.-H. He, *Counting BPS Operators in Gauge Theories: Quivers, Syzygies and Plethystics*, *JHEP* **11** (2007) 050, [hep-th/0608050].

[52] A. Hanany and R. Kalveks, *Quiver Theories for Moduli Spaces of Classical Group Nilpotent Orbits*, *JHEP* **06** (2016) 130, [1601.04020].

[53] A. Hanany and R. Kalveks, *Quiver Theories and Formulae for Nilpotent Orbits of Exceptional Algebras*, *JHEP* **11** (2017) 126, [1709.05818].

[54] A. Hanany and A. Zajac, *Discrete Gauging in Coulomb branches of Three Dimensional $\mathcal{N} = 4$ Supersymmetric Gauge Theories*, *JHEP* **08** (2018) 158, [1807.03221].

[55] A. Hanany and N. Mekareeya, *Complete Intersection Moduli Spaces in N=4 Gauge Theories in Three Dimensions*, *JHEP* **01** (2012) 079, [1110.6203].

[56] S. Cabrera, A. Hanany and Z. Zhong, *Nilpotent orbits and the Coulomb branch of $T^\sigma(G)$ theories: special orthogonal vs orthogonal gauge group factors*, *JHEP* **11** (2017) 079, [1707.06941].

[57] S. Cabrera, A. Hanany and R. Kalveks, *Quiver Theories and Formulae for Slodowy Slices of Classical Algebras*, *Nucl. Phys. B* **939** (2019) 308–357, [1807.02521].

[58] N. Seiberg and E. Witten, *Gauge dynamics and compactification to three-dimensions*, in *Conference on the Mathematical Beauty of Physics (In Memory of C. Itzykson)*, pp. 333–366, 6, 1996. hep-th/9607163.

[59] G. 't Hooft, *On the Phase Transition Towards Permanent Quark Confinement*, *Nucl. Phys. B* **138** (1978) 1–25.

[60] F. Englert and P. Windey, *Quantization Condition for 't Hooft Monopoles in Compact Simple Lie Groups*, *Phys. Rev. D* **14** (1976) 2728.

[61] P. Goddard, J. Nuyts and D. I. Olive, *Gauge Theories and Magnetic Charge*, *Nucl. Phys. B* **125** (1977) 1–28.

[62] D. Gaiotto and E. Witten, *S-Duality of Boundary Conditions In N=4 Super Yang-Mills Theory*, *Adv. Theor. Math. Phys.* **13** (2009) 721–896, [0807.3720].

[63] D. H. Collingwood and W. M. McGovern, *Nilpotent Orbits In Semisimple Lie Algebra: An Introduction*. CRC Press, 1993.

[64] J. McKay, *Graphs, singularities, and finite groups*, in *The Santa Cruz Conference on Finite Groups (Univ. California, Santa Cruz, Calif, 19'79)*, vol. 37, p. 183486.

[65] S. Cremonesi, G. Ferlito, A. Hanany and N. Mekareeya, *Coulomb Branch and The Moduli Space of Instantons*, *JHEP* **12** (2014) 103, [1408.6835].

[66] P. Argyres, M. Lotito, Y. Lü and M. Martone, *Geometric constraints on the space of $\mathcal{N} = 2$ SCFTs. Part I: physical constraints on relevant deformations*, *JHEP* **02** (2018) 001, [1505.04814].

[67] Y. Tachikawa, *N=2 supersymmetric dynamics for pedestrians*. 12, 2013, 10.1007/978-3-319-08822-8.

[68] M. Akhond, G. Arias-Tamargo, A. Mininno, H.-Y. Sun, Z. Sun, Y. Wang et al., *The Hitchhiker's Guide to 4d $\mathcal{N} = 2$ Superconformal Field Theories*, 12, 2021. 2112.14764.

[69] N. A. Nekrasov, *Seiberg-Witten prepotential from instanton counting*, *Adv. Theor. Math. Phys.* **7** (2003) 831–864, [hep-th/0206161].

[70] D. Gaiotto, *N=2 dualities*, *JHEP* **08** (2012) 034, [0904.2715].

[71] P. C. Argyres, Y. Lü and M. Martone, *Seiberg-Witten geometries for Coulomb branch chiral rings which are not freely generated*, *JHEP* **06** (2017) 144, [1704.05110].

[72] A. Bourget, A. Pini and D. Rodríguez-Gómez, *Gauge theories from principally extended disconnected gauge groups*, *Nucl. Phys. B* **940** (2019) 351–376, [1804.01108].

[73] P. C. Argyres and M. R. Douglas, *New phenomena in SU(3) supersymmetric gauge theory*, *Nucl. Phys. B* **448** (1995) 93–126, [hep-th/9505062].

[74] N. Seiberg, *Five-dimensional SUSY field theories, nontrivial fixed points and string dynamics*, *Phys. Lett. B* **388** (1996) 753–760, [hep-th/9608111].

[75] K. A. Intriligator, D. R. Morrison and N. Seiberg, *Five-dimensional supersymmetric gauge theories and degenerations of Calabi-Yau spaces*, *Nucl. Phys. B* **497** (1997) 56–100, [hep-th/9702198].

[76] P. Jefferson, H.-C. Kim, C. Vafa and G. Zafrir, *Towards Classification of 5d SCFTs: Single Gauge Node*, 1705.05836.

[77] P. Jefferson, S. Katz, H.-C. Kim and C. Vafa, *On Geometric Classification of 5d SCFTs*, *JHEP* **04** (2018) 103, [1801.04036].

[78] L. Bhardwaj and P. Jefferson, *Classifying* 5*d SCFTs via* 6*d SCFTs: Rank one*, *JHEP* **07** (2019) 178, [1809.01650].

[79] L. Bhardwaj and P. Jefferson, *Classifying 5d SCFTs via 6d SCFTs: Arbitrary rank*, *JHEP* **10** (2019) 282, [1811.10616].

[80] L. Bhardwaj, *On the classification of 5d SCFTs*, *JHEP* **09** (2020) 007, [1909.09635].

[81] L. Bhardwaj, *Do all 5d SCFTs descend from 6d SCFTs?*, *JHEP* **04** (2021) 085, [1912.00025].

[82] L. Bhardwaj and G. Zafrir, *Classification of 5d $\mathcal{N} = 1$ gauge theories*, *JHEP* **12** (2020) 099, [2003.04333].

[83] H. Hayashi, S.-S. Kim, K. Lee and F. Yagi, *Complete prepotential for 5d $\mathcal{N} = 1$ superconformal field theories*, *JHEP* **02** (2020) 074, [1912.10301].

[84] J. J. Heckman, D. R. Morrison, T. Rudelius and C. Vafa, *Atomic Classification of 6D SCFTs*, *Fortsch. Phys.* **63** (2015) 468–530, [1502.05405].

[85] M. Del Zotto and G. Lockhart, *Universal Features of BPS Strings in Six-dimensional SCFTs*, *JHEP* **08** (2018) 173, [1804.09694].

[86] A. Hanany and G. Zafrir, *Discrete Gauging in Six Dimensions*, *JHEP* **07** (2018) 168, [1804.08857].

[87] A. Hanany and A. Zajac, *Discrete Gauging in Coulomb branches of Three Dimensional $\mathcal{N} = 4$ Supersymmetric Gauge Theories*, *JHEP* **08** (2018) 158, [1807.03221].

[88] A. Hanany and M. Sperling, *Discrete quotients of 3-dimensional $\mathcal{N} = 4$ Coulomb branches via the cycle index*, *JHEP* **08** (2018) 157, [1807.02784].

[89] S. J. Gates, Jr., C. M. Hull and M. Rocek, *Twisted Multiplets and New Supersymmetric Nonlinear Sigma Models*, *Nucl. Phys. B* **248** (1984) 157–186.

[90] A. Giveon and D. Kutasov, *Brane Dynamics and Gauge Theory*, *Rev. Mod. Phys.* **71** (1999) 983–1084, [hep-th/9802067].

[91] K. A. Intriligator and N. Seiberg, *Mirror symmetry in three-dimensional gauge theories*, *Phys. Lett. B* **387** (1996) 513–519, [hep-th/9607207].

[92] A. Dey, A. Hanany, N. Mekareeya, D. Rodríguez-Gómez and R.-K. Seong, *Hilbert Series for Moduli Spaces of Instantons on C^2/Z_n*, *JHEP* **01** (2014) 182, [1309.0812].

[93] A. Braverman, M. Finkelberg and H. Nakajima, *Coulomb branches of 3d $\mathcal{N} = 4$ quiver gauge theories and slices in the affine Grassmannian*, *Adv. Theor. Math. Phys.* **23** (2019) 75–166, [1604.03625].

[94] F. Benini, Y. Tachikawa and D. Xie, *Mirrors of 3d Sicilian theories*, *JHEP* **09** (2010) 063, [1007.0992].

[95] C. Hwang, S. Pasquetti and M. Sacchi, *4d mirror-like dualities*, *JHEP* **09** (2020) 047, [2002.12897].

[96] S. Cremonesi, A. Hanany, N. Mekareeya and A. Zaffaroni, T_ρ^σ *(G) theories and their Hilbert series*, *JHEP* **01** (2015) 150, [1410.1548].

[97] E. Witten, *Solutions of four-dimensional field theories via M theory*, *Nucl. Phys. B* **500** (1997) 3–42, [hep-th/9703166].

[98] M. Van Beest, A. Bourget, J. Eckhard and S. Schäfer-Nameki, *(5d RG-flow) Trees in the Tropical Rain Forest*, *JHEP* **03** (2021) 241, [2011.07033].

[99] A. Braverman, M. Finkelberg and H. Nakajima, *Towards a mathematical definition of Coulomb branches of* 3*-dimensional* $\mathcal{N} = 4$ *gauge theories, II*, *Adv. Theor. Math. Phys.* **22** (2018) 1071–1147, [1601.03586].

[100] S. Cremonesi, G. Ferlito, A. Hanany and N. Mekareeya, *Instanton Operators and the Higgs Branch at Infinite Coupling*, *JHEP* **04** (2017) 042, [1505.06302].

[101] F. Cachazo, M. R. Douglas, N. Seiberg and E. Witten, *Chiral rings and anomalies in supersymmetric gauge theory*, *JHEP* **12** (2002) 071, [hep-th/0211170].

[102] G. Zafrir, *Brane webs and* $O5$*-planes*, *JHEP* **03** (2016) 109, [1512.08114].

[103] H. Hayashi, S.-S. Kim, K. Lee and F. Yagi, *5-brane webs for 5d* $\mathcal{N} = 1$ G_2 *gauge theories*, *JHEP* **03** (2018) 125, [1801.03916].

[104] G. Bertoldi, B. Feng and A. Hanany, *The Splitting of branes on orientifold planes*, *JHEP* **04** (2002) 015, [hep-th/0202090].

[105] M. Akhond, F. Carta, S. Dwivedi, H. Hayashi, S.-S. Kim and F. Yagi, *Five-brane webs, Higgs branches and unitary/orthosymplectic magnetic quivers*, *JHEP* **12** (2020) 164, [2008.01027].

[106] M. Akhond, F. Carta, S. Dwivedi, H. Hayashi, S.-S. Kim and F. Yagi, *Factorised 3d $\mathcal{N} = 4$ orthosymplectic quivers*, *JHEP* **05** (2021) 269, [2101.12235].

[107] M. Akhond, F. Carta, S. Dwivedi, H. Hayashi, S.-S. Kim and F. Yagi, *Exploring the orthosymplectic zoo*, 2203.01951.

[108] S. Cabrera, A. Hanany and M. Sperling, *Magnetic quivers, Higgs branches, and 6d N=(1,0) theories*, *JHEP* **06** (2019) 071, [1904.12293].

[109] S. Cabrera, A. Hanany and M. Sperling, *Magnetic Quivers, Higgs Branches, and 6d N=(1,0) Theories – Orthogonal and Symplectic Gauge Groups*, *JHEP* **02** (2020) 184, [1912.02773].

[110] O. Bergman and G. Zafrir, *Lifting 4d dualities to 5d*, *JHEP* **04** (2015) 141, [1410.2806].

[111] A. Hanany and A. Pini, *HWG for Coulomb branch of* 3*d Sicilian theory mirrors*, 1707.09784.

[112] G. Ferlito and A. Hanany, *A tale of two cones: the Higgs Branch of Sp(n) theories with 2n flavours*, 1609.06724.

[113] F. Benini, Y. Tachikawa and D. Xie, *Mirrors of 3d Sicilian theories*, *JHEP* **09** (2010) 063, [1007.0992].

[114] O. Chacaltana and J. Distler, *Tinkertoys for the D_N series*, *JHEP* **02** (2013) 110, [1106.5410].

[115] O. Chacaltana and J. Distler, *Tinkertoys for Gaiotto Duality*, *JHEP* **11** (2010) 099, [1008.5203].

[116] C. Closset, S. Giacomelli, S. Schafer-Nameki and Y.-N. Wang, *5d and 4d SCFTs: Canonical Singularities, Trinions and S-Dualities*, *JHEP* **05** (2021) 274, [2012.12827].

[117] O. Aharony, N. Seiberg and Y. Tachikawa, *Reading between the lines of four-dimensional gauge theories*, *JHEP* **08** (2013) 115, [1305.0318].

[118] S. Cremonesi, A. Hanany, N. Mekareeya and A. Zaffaroni, *Coulomb branch Hilbert series and Three Dimensional Sicilian Theories*, *JHEP* **09** (2014) 185, [1403.2384].

[119] A. Hanany and R. Kalveks, *Quiver Theories and Hilbert Series of Classical Slodowy Intersections*, *Nucl. Phys.* **B952** (2020) 114939, [1909.12793].

[120] S. Cremonesi, A. Hanany, N. Mekareeya and A. Zaffaroni, *Coulomb branch Hilbert series and Hall-Littlewood polynomials*, *JHEP* **09** (2014) 178, [1403.0585].

[121] E. Witten, *An SU(2) Anomaly*, *Phys. Lett. B* **117** (1982) 324–328.

[122] S. Benvenuti, A. Hanany and N. Mekareeya, *The Hilbert Series of the One Instanton Moduli Space*, *JHEP* **06** (2010) 100, [1005.3026].

[123] O. Bergman and G. Zafrir, *5d fixed points from brane webs and O7-planes*, *JHEP* **12** (2015) 163, [1507.03860].

[124] C. Closset and H. Kim, *Comments on twisted indices in 3d supersymmetric gauge theories*, *JHEP* **08** (2016) 059, [1605.06531].

[125] V. Pestun et al., *Localization techniques in quantum field theories*, *J. Phys. A* **50** (2017) 440301, [1608.02952].

[126] J. Distler, B. Ergun and F. Yan, *Product SCFTs in Class-S*, *JHEP* **02** (2021) 164, [1711.04727].

[127] J. Distler and B. Ergun, *Product SCFTs for the E_7 Theory*, 1803.02425.

[128] B. Ergun, Q. Hao, A. Neitzke and F. Yan, *Factorized class S theories and surface defects*, *JHEP* **12** (2021) 041, [2010.06722].

[129] D. R. Gulotta, C. P. Herzog and T. Nishioka, *The ABCDEF's of Matrix Models for Supersymmetric Chern-Simons Theories*, *JHEP* **04** (2012) 138, [1201.6360].

[130] P. C. Argyres, M. Lotito, Y. Lü and M. Martone, *Geometric constraints on the space of $\mathcal{N}$ = 2 SCFTs. Part II: construction of special Kähler geometries and RG flows*, *JHEP* **02** (2018) 002, [1601.00011].

[131] P. C. Argyres, M. Lotito, Y. Lü and M. Martone, *Expanding the landscape of $\mathcal{N} = 2$ rank 1 SCFTs*, *JHEP* **05** (2016) 088, [1602.02764].

[132] P. Argyres, M. Lotito, Y. Lü and M. Martone, *Geometric constraints on the space of $\mathcal{N} = 2$ SCFTs. Part III: enhanced Coulomb branches and central charges*, *JHEP* **02** (2018) 003, [1609.04404].

[133] J. A. Minahan and D. Nemeschansky, *Superconformal fixed points with E(n) global symmetry*, *Nucl. Phys.* **B489** (1997) 24–46, [hep-th/9610076].

[134] D. Xie, *General Argyres-Douglas Theory*, *JHEP* **01** (2013) 100, [1204.2270].

[135] F. Apruzzi, S. Giacomelli and S. Schäfer-Nameki, *4d $\mathcal{N} = 2$ S-folds*, *Phys. Rev. D* **101** (2020) 106008, [2001.00533].

[136] K. Ohmori, Y. Tachikawa and G. Zafrir, *Compactifications of 6d $N = (1, 0)$ SCFTs with non-trivial Stiefel-Whitney classes*, *JHEP* **04** (2019) 006, [1812.04637].

[137] A. Hanany and A. Zajac, *Ungauging Schemes and Coulomb Branches of Non-simply Laced Quiver Theories*, *JHEP* **09** (2020) 193, [2002.05716].

[138] G. Zafrir, *Compactifications of 5d SCFTs with a twist*, *JHEP* **01** (2017) 097, [1605.08337].

[139] R. Brylinski and B. Kostant, *Nilpotent orbits, normality, and Hamiltonian group actions*, *arXiv Mathematics e-prints* (Mar., 1992) math/9204227, [math/9204227].

[140] K. Maruyoshi, Y. Tachikawa, W. Yan and K. Yonekura, *N=1 dynamics with T_N theory*, *JHEP* **10** (2013) 010, [1305.5250].

[141] S. Cabrera, A. Hanany and A. Zajac, *Minimally Unbalanced Quivers*, *JHEP* **02** (2019) 180, [1810.01495].

[142] O. Chacaltana, J. Distler and A. Trimm, *A Family of 4D $\mathcal{N} = 2$ Interacting SCFTs from the Twisted A_{2N} Series*, 1412.8129.

[143] O. Chacaltana, J. Distler and A. Trimm, *Tinkertoys for the Z3-twisted D4 Theory*, 1601.02077.

[144] A. Hanany and R. Kalveks, *Construction and Deconstruction of Single Instanton Hilbert Series*, *JHEP* **12** (2015) 118, [1509.01294].

[145] A. Hanany, S. Ramgoolam and D. Rodriguez-Gomez, *Highest weight generating functions for hyperKähler T*(G/H) spaces*, *JHEP* **10** (2016) 021, [1601.02531].

[146] O. Chacaltana, J. Distler and A. Trimm, *Tinkertoys for the Twisted D-Series*, *JHEP* **04** (2015) 173, [1309.2299].

[147] Y. Tachikawa, Y. Wang and G. Zafrir, *Comments on the twisted punctures of A_{even} class S theory*, *JHEP* **06** (2018) 163, [1804.09143].

[148] Y. Wang and D. Xie, *Codimension-two defects and Argyres-Douglas theories from outer-automorphism twist in 6d* $(2, 0)$ *theories*, *Phys. Rev. D* **100** (2019) 025001, [1805.08839].

[149] H. Sakai, *Rational Surfaces Associated with Affine Root Systems and Geometry of the Painlevé Equations*, *Communications in Mathematical Physics* **220** (2001) 165–229.

[150] P. Boalch, *Quivers and Difference Painlevé Equations*, *Groups and Symmetries: From Neolithic Scots to John McKay* **47** (2009) 25.

[151] J. Fuchs and C. Schweigert, *Symmetries, Lie Algebras and Representations: A Graduate Course for Physicists*. Cambridge Monographs on Mathematical Physics. Cambridge University Press, 2003.

[152] H. Shimizu, Y. Tachikawa and G. Zafrir, *Anomaly matching on the Higgs branch*, *JHEP* **12** (2017) 127, [1703.01013].

[153] A. Hanany and A. Pini, *HWG for Coulomb branch of* 3*d Sicilian theory mirrors*, 1707.09784.

[154] O. Chacaltana, J. Distler and Y. Tachikawa, *Gaiotto duality for the twisted A_{2N-1} series*, *JHEP* **05** (2015) 075, [1212.3952].

[155] O. Chacaltana, J. Distler and A. Trimm, *A Family of 4D $\mathcal{N} = 2$ Interacting SCFTs from the Twisted A_{2N} Series*, 1412.8129.

[156] Y. Tachikawa, Y. Wang and G. Zafrir, *Comments on the twisted punctures of A_{even} class S theory*, *JHEP* **06** (2018) 163, [1804.09143].

[157] C. V. Johnson and R. C. Myers, *Aspects of type IIB theory on ALE spaces*, *Phys. Rev. D* **55** (1997) 6382–6393, [hep-th/9610140].

[158] P. B. Kronheimer, *Instantons and the geometry of the nilpotent variety*, *J. Diff. Geom.* **32** (1990) 473–490.

[159] R. Brylinski, *Instantons and Kaehler Geometry of Nilpotent Orbits*, *arXiv Mathematics e-prints* (Nov., 1998) math/9811032, [math/9811032].

[160] P. Kobak and A. Swann, *The HyperKähler Geometry Associated to Wolf Spaces*, *arXiv Mathematics e-prints* (Jan., 2000) math/0001025, [math/0001025].

[161] J. de Boer, K. Hori, H. Ooguri and Y. Oz, *Mirror symmetry in three-dimensional gauge theories, quivers and D-branes*, *Nucl. Phys. B* **493** (1997) 101–147, [hep-th/9611063].

[162] M. Porrati and A. Zaffaroni, *M theory origin of mirror symmetry in three-dimensional gauge theories*, *Nucl. Phys. B* **490** (1997) 107–120, [hep-th/9611201].

[163] A. Hanany and N. Mekareeya, *The small E_8 instanton and the Kraft Procesi transition*, *JHEP* **07** (2018) 098, [1801.01129].

[164] H. Nakajima, *Towards a mathematical definition of Coulomb branches of 3-dimensional $\mathcal{N} = 4$ gauge theories, I*, *Adv. Theor. Math. Phys.* **20** (2016) 595–669, [1503.03676].

[165] A. Bourget and Z. Zhong, *Highest Weight Generating function for tropical quivers, (in preparation)* .

[166] A. Dey, A. Hanany, P. Koroteev and N. Mekareeya, *Mirror Symmetry in Three Dimensions via Gauged Linear Quivers*, *JHEP* **06** (2014) 059, [1402.0016].

[167] S. Cremonesi, A. Hanany, N. Mekareeya and A. Zaffaroni, *Coulomb branch Hilbert series and Hall-Littlewood polynomials*, *JHEP* **09** (2014) 178, [1403.0585].

[168] A. Dancer, A. Hanany and F. Kirwan, *Symplectic duality and implosions*, 2004.09620.

[169] A. Collinucci and R. Valandro, *A string theory realization of special unitary quivers in 3 dimensions*, *JHEP* **11** (2020) 157, [2008.10689].

[170] O. Aharony and A. Hanany, *Branes, superpotentials and superconformal fixed points*, *Nucl. Phys. B* **504** (1997) 239–271, [hep-th/9704170].

[171] O. Aharony, A. Hanany and B. Kol, *Webs of (p,q) five-branes, five-dimensional field theories and grid diagrams*, *JHEP* **01** (1998) 002, [hep-th/9710116].

[172] O. DeWolfe, A. Hanany, A. Iqbal and E. Katz, *Five-branes, seven-branes and five-dimensional E(n) field theories*, *JHEP* **03** (1999) 006, [hep-th/9902179].

[173] A. Bourget, S. Cabrera, J. F. Grimminger, A. Hanany and Z. Zhong, *Brane Webs and Magnetic Quivers for SQCD*, *JHEP* **03** (2020) 176, [1909.00667].

[174] B. Assel and S. Cremonesi, *The Infrared Physics of Bad Theories*, *SciPost Phys.* **3** (2017) 024, [1707.03403].

[175] S. Giacomelli, N. Mekareeya and M. Sacchi, *New aspects of Argyres–Douglas theories and their dimensional reduction*, *JHEP* **03** (2021) 242, [2012.12852].

[176] D. Xie, *3d mirror for Argyres-Douglas theories*, 2107.05258.

[177] A. Dey, *Higgs Branches of Argyres-Douglas theories as Quiver Varieties*, 2109.07493.

[178] Z. Zhong, *Mixed U/SU quivers of Dynkin type and their mirrors*, *(in preparation)* .

[179] S. Cabrera and A. Hanany, *Branes and the Kraft-Procesi transition: classical case*, *JHEP* **04** (2018) 127, [1711.02378].

[180] B. Fu, D. Juteau, P. Levy and E. Sommers, *Generic singularities of nilpotent orbit closures*, *Advances in Mathematics* **305** (2017) 1–77.

[181] U. H. Danielsson, G. Ferretti, J. Kalkkinen and P. Stjernberg, *Notes on supersymmetric gauge theories in five-dimensions and six-dimensions*, *Phys. Lett.* **B405** (1997) 265–270, [hep-th/9703098].

[182] J. J. Heckman and T. Rudelius, *Top Down Approach to 6D SCFTs*, *J. Phys.* **A52** (2019) 093001, [1805.06467].

[183] O. J. Ganor and A. Hanany, *Small E(8) instantons and tensionless noncritical strings*, *Nucl. Phys.* **B474** (1996) 122–140, [hep-th/9602120].

[184] N. Seiberg and E. Witten, *Comments on string dynamics in six-dimensions*, *Nucl. Phys.* **B471** (1996) 121–134, [hep-th/9603003].

[185] K. A. Intriligator, *RG fixed points in six-dimensions via branes at orbifold singularities*, *Nucl. Phys. B* **496** (1997) 177–190, [hep-th/9702038].

[186] J. D. Blum and K. A. Intriligator, *New phases of string theory and 6-D RG fixed points via branes at orbifold singularities*, *Nucl. Phys. B* **506** (1997) 199–222, [hep-th/9705044].

[187] A. Hanany and A. Zaffaroni, *Branes and six-dimensional supersymmetric theories*, *Nucl. Phys. B* **529** (1998) 180–206, [hep-th/9712145].

[188] N. Mekareeya, T. Rudelius and A. Tomasiello, *T-branes, Anomalies and Moduli Spaces in 6D SCFTs*, *JHEP* **10** (2017) 158, [1612.06399].

[189] N. Mekareeya, K. Ohmori, H. Shimizu and A. Tomasiello, *Small instanton transitions for M5 fractions*, *JHEP* **10** (2017) 055, [1707.05785].

[190] C. Beem and L. Rastelli, *Vertex operator algebras, Higgs branches, and modular differential equations*, *JHEP* **08** (2018) 114, [1707.07679].

[191] C. Beem, C. Meneghelli and L. Rastelli, *Free Field Realizations from the Higgs Branch*, *JHEP* **09** (2019) 058, [1903.07624].

[192] C. Closset, S. Schafer-Nameki and Y.-N. Wang, *Coulomb and Higgs Branches from Canonical Singularities: Part 0*, *JHEP* **02** (2021) 003, [2007.15600].

[193] C. Cordova, T. T. Dumitrescu and K. Intriligator, *2-Group Global Symmetries and Anomalies in Six-Dimensional Quantum Field Theories*, *JHEP* **04** (2021) 252, [2009.00138].

[194] L. Bhardwaj, M. Hubner and S. Schafer-Nameki, *1-form Symmetries of 4d N=2 Class S Theories*, *SciPost Phys.* **11** (2021) 096, [2102.01693].

[195] F. Apruzzi, L. Bhardwaj, J. Oh and S. Schafer-Nameki, *The Global Form of Flavor Symmetries and 2-Group Symmetries in 5d SCFTs*, 2105.08724.

[196] F. Apruzzi, L. Bhardwaj, D. S. W. Gould and S. Schafer-Nameki, *2-Group Symmetries and their Classification in 6d*, 2110.14647.

[197] L. Bhardwaj, S. Giacomelli, M. Hübner and S. Schäfer-Nameki, *Relative Defects in Relative Theories: Trapped Higher-Form Symmetries and Irregular Punctures in Class S*, 2201.00018.

[198] L. Bhardwaj, L. Bottini, S. Schafer-Nameki and A. Tiwari, *Non-Invertible Higher-Categorical Symmetries*, 2204.06564.

[199] A. Hanany and M. Sperling, *Algebraic properties of the monopole formula*, *JHEP* **02** (2017) 023, [1611.07030].

[200] P. Argyres and M. Martone, *Construction and classification of Coulomb branch geometries*, 2003.04954.

[201] K. Dasgupta and S. Mukhi, *F theory at constant coupling*, *Phys. Lett. B* **385** (1996) 125–131, [hep-th/9606044].

[202] P. C. Argyres and M. Martone, *4d $\mathcal{N}$ =2 theories with disconnected gauge groups*, *JHEP* **03** (2017) 145, [1611.08602].

[203] D. Eisenbud and J. Harris, *The geometry of schemes*, vol. 197. Springer Science & Business Media, 2006.

[204] D. A. Cox, J. Little and D. O'shea, *Using algebraic geometry*, vol. 185. Springer Science & Business Media, 2006.

[205] P. Vanhaecke, *Integrable systems in the realm of algebraic geometry*. Springer Science & Business Media, 2001.

[206] I. Vaisman, *Lectures on the geometry of Poisson manifolds*, vol. 118. Birkhäuser, 2012.

[207] R. L. Fernandes and I. Marcut, *Lectures on poisson geometry*, 2014.

[208] A. Beauville, *Symplectic singularities*, *Invent. Math.* **139** (2000) 541–549, [`math/9903070`].

[209] Y. Namikawa, *Extension of 2-forms and symplectic varieties*, *arXiv preprint math/0010114* (2000) .

[210] B. Fu, *A survey on symplectic singularities and symplectic resolutions*, vol. 13, pp. 209–236, 2006. `math/0510346`.

[211] G. Bellamy, "Symplectic singularities and their quantization." https://www.maths.gla.ac.uk/ gbellamy/Padova.pdf.

[212] D. Kaledin, *Symplectic singularities from the poisson point of view*, *Journal für die reine und angewandte Mathematik (Crelles Journal)* **2006** (2006) 135–156.

[213] H. Nakajima, *Questions on provisional Coulomb branches of* 3*-dimensional* $\mathcal{N} = 4$ *gauge theories*, `1510.03908`.

Appendix A

Monopole formula cheat sheet

In this section, we provide some very useful information to compute the monopole formula. The monopole formula contains three main ingredients:

- Conformal dimension Δ
- Magnetic lattice to sum over the magnetic charges $\Gamma_{G^\vee}/\mathcal{W}_{G^\vee}$
- Classical (dressing) factors P_G

We will now provide the conformal dimension and magnetic lattice for all classical gauge groups. For the dressing factors this is already done in great detail in Appendix A of the original paper [36] and we will not repeat it here.

A.1 Conformal dimension

The contribution to the conformal dimension comes from the vector multiplets and the hypermultiplets. The results for classical gauge groups are provided in Figure A.1.

In [65], the conformal dimension for quivers with non-simply laced edges was proposed. For a l multiplicity edge from G_1 to G_2, the vector multiplet contribution to the conformal dimension remains the same and given in Figure A.1 but the hypermultiplet contribution has an additional l factor in front of the magnetic charges of G_1. The details for different classical gauge groups is given in Figure A.2.

Group	Δ_{vec}
$\mathrm{U}(r)$	$-\sum_{i<j}^{r} \lvert m_i - m_j \rvert$
$\mathrm{SO}(2r)$	$-\sum_{i<j}^{r} (\lvert m_i + m_j \rvert + \lvert m_i - m_j \rvert)$
$\mathrm{O}(2r)$	$-\sum_{i<j}^{r} (\lvert m_i + m_j \rvert + \lvert m_i - m_j \rvert)$
$\mathrm{SO}(2r+1)$	$-\sum_{i<j}^{r} (\lvert m_i + m_j \rvert + \lvert m_i - m_j \rvert) - \sum_{i=1}^{r} \lvert m_i \rvert$
$\mathrm{USp}(2r)$	$-\sum_{i<j}^{r} (\lvert m_i + m_j \rvert + \lvert m_i - m_j \rvert) - 2\sum_{i=1}^{r} \lvert m_i \rvert$

(a) *The contribution of vector multiplets for various gauge groups.*

Representation	Δ_{hyp}
$\mathrm{SO}(2r)_m \times \mathrm{USp}(2k)_n$ bifundamental	$\frac{1}{2}\sum_{i=1}^{k}\sum_{j=1}^{r} (\lvert n_i - m_j \rvert + \lvert n_i + m_j \rvert)$
$\mathrm{SO}(2r)_m \times \mathrm{U}(k)_n$ bifundamental	$\frac{1}{2}\sum_{i=1}^{k}\sum_{j=1}^{r} (\lvert n_i - m_j \rvert + \lvert n_i + m_j \rvert)$
$\mathrm{U}(r)_m \times \mathrm{USp}(2k)_n$ bifundamental	$\frac{1}{2}\sum_{i=1}^{k}\sum_{j=1}^{r} (\lvert n_i - m_j \rvert + \lvert n_i + m_j \rvert)$
$\mathrm{SO}(2r+1)_m \times \mathrm{USp}(2k)_n$ bifundamental	$\frac{1}{2}\sum_{i=1}^{k}\sum_{j=1}^{r} (\lvert n_i - m_j \rvert + \lvert n_i + m_j \rvert) + \frac{1}{2}\sum_{i=1}^{k} \lvert n_i \rvert$

(b) *The contribution of hypermultiplets in bifundamental representations.*

Representation	$\Delta_{\text{vec}} + \Delta_{\text{hyp}}$
$\mathrm{SO}(2r)_m$ with antisymmetric Λ^2	0
$\mathrm{USp}(2k)_m$ with antisymmetric Λ^2	$-2\sum_{i=1}^{k} \lvert m_i \rvert$
$\mathrm{U}(k)_m$ with l charge 2 hypermultiplets	$l\sum_{i=1}^{k} \lvert m_i \rvert - \sum_{i<j}^{k} \lvert m_i - m_j \rvert$

(c) *The combined contribution of the vector and hypermultiplets for special representations.*

Figure A.1: *Contributions to the conformal dimension Δ that appear in the monopole formula. (a) summarizes the vector multiplet contributions, (b) collects the hypermultiplet contributions, and (c) provides the combined parts for certain special representations. Note in particular that a bifundamental of $\mathrm{SO}(2r)_m \times \mathrm{U}(k)_n$ contributes exactly the same as a bifundamental of $\mathrm{SO}(2r)_m \times \mathrm{USp}(2k)_n$ and of $\mathrm{USp}(2r)_m \times \mathrm{U}(k)_n$, as required by the fact that $\mathrm{U}(k)$ should be seen as a subgroup of $\mathrm{USp}(2k)$.*

A.2 Magnetic lattice

For a gauge group G or rank r, we label the magnetic charges by $m_1, \ldots, m_r$. The following are the lattices of their GNO dual $G^\vee$ group quotiented out by their respective Weyl action $\Gamma_{G^\vee}/\mathcal{W}_{G^\vee}$.

$U(r)$

The magnetic lattice sums over magnetic charges that obey : $(\infty > m_1 \geq m_2 \geq \cdots \geq m_r \geq -\infty)$.

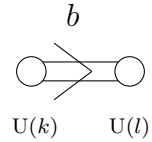

$$\Delta_{\text{edge}} = \tfrac{1}{2}\sum_{i=1}^{k}\sum_{j=1}^{l}|b\, m_{1,i} - m_{2,j}|$$

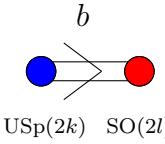

$$\Delta_{\text{edge}} = \tfrac{1}{2}\sum_{i=1}^{k}\sum_{j=1}^{l}(|b\, m_{1,i} - m_{2,j}| + |b\, m_{1,i} + m_{2,j}|)$$

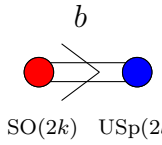

$$\Delta_{\text{edge}} = \tfrac{1}{2}\sum_{i=1}^{k}\sum_{j=1}^{l}(|b\, m_{1,i} - m_{2,j}| + |b\, m_{1,i} + m_{2,j}|)$$

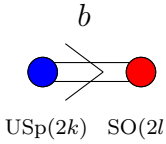

$$\Delta_{\text{edge}} = \tfrac{1}{2}\sum_{i=1}^{k}\sum_{j=1}^{l}(|b\, m_{1,i} - m_{2,j}| + |b\, m_{1,i} + m_{2,j}|) + \tfrac{1}{2}\sum_{i=1}^{k}|b\, m_{1,i}|$$

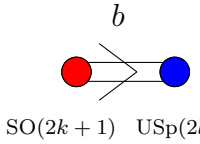

$$\Delta_{\text{edge}} = \tfrac{1}{2}\sum_{i=1}^{k}\sum_{j=1}^{l}(|b\, m_{1,i} - m_{2,j}| + |b\, m_{1,i} + m_{2,j}|) + \tfrac{1}{2}\sum_{j=1}^{l}|m_{2,j}|$$

Figure A.2: *The contribution of the edges to the conformal dimension Δ_{edge} is given for the two-node quivers on the left. The magnetic charges for the left nodes are denoted by $\{m_{1,i}\}$ and for the right node by $\{m_{2,j}\}$. The non-simply laced edge has multiplicity b, which then appears as a multiplicative factor for the $m_{1,i}$ magnetic charges. The contribution of the vector multiplets is not affected by non-simply laced edges.*

$SU(r)$

The magnetic lattice sums over magnetic charges that obey : $(\infty > m_1 \geq m_2 \geq \cdots \geq m_r \geq -\infty)$ and $\sum_i^r m_i = 0$.

$SO(2r)$

The magnetic lattice sums over magnetic charges that obey : $(\infty > m_1 \geq m_2 \geq \cdots \geq |m_r| \geq 0)$.

$SO(2r+1)$

The magnetic lattice sums over magnetic charges that obey : $(\infty > m_1 \geq m_2 \geq \cdots \geq m_r \geq 0)$.

$O(2r)$

The magnetic lattice sums over magnetic charges that obey : $(\infty > m_1 \geq m_2 \geq \cdots \geq m_r \geq 0)$.

$O(2r+1)$

In [56], we argue that the lattice for $O(2r+1)$ is the same as that of $SO(2r+1)$. However, a lack of examples in the literature where we know the gauge group needs to be one or the other makes it difficult to test this conjecture.

$USp(2r)$

The magnetic lattice sums over magnetic charges that obey : $(\infty > m_1 \geq m_2 \geq \cdots \geq m_r \geq 0)$.

The above results are the magnetic lattices for each gauge group. However, as we have seen in Section 4.4, when a quiver is unframed/flavorless, there is often a diagonal subgroup that one can ungauge. This ungauging will affect the magnetic lattice as well.

Unframed unitary quiver, $H = U(1)$

An overall $U(1)$ must be ungauged which can be done on any of the unitary gauge groups. We often put a 'squircle' around the chosen gauge node. For a $U(r)$ gauge group with a $U(1)$ ungauged, the magnetic lattice is then $(\infty > m_1 \geq m_2 \geq \cdots \geq m_{r-1} \geq 0)$ with $m_r = 0$.

Unframed quiver with one $SU(k)$ node and rest are unitary nodes, $H = \mathbb{Z}_k$

The presence of a single $SU(k)$ gauge node means there is now a $\mathbb{Z}_k$ one-form symmetry in the quiver. If we do not quotient out the $\mathbb{Z}_k$ from the gauge groups, the magnetic lattice Λ is obtained using the results above. If we choose to quotient out this $\mathbb{Z}_k$, the magnetic lattice

will now be a sum over k lattices. Each lattice is the same as Λ but with magnetic charges shifted by $\Lambda_b = \Lambda + b/k$, $b = 0, \ldots, k-1$. If the unframed quiver contains several special unitary gauge groups $SU(k_i)$, $i = 1, \ldots, x$, then the one-form symmetry is $\mathbb{Z}_{\mathrm{gcd(k_1,\ldots,k_x)}}$ and the magnetic lattice is split into $\gcd(k_1, \ldots, k_x)$ pieces.

Unframed quiver with $U(k)$, $SO(2k)$, $USp(2k)$ nodes, $H = \mathbb{Z}_2$.

Following the same line of thought above, the magnetic lattice is split into an integer lattice Λ and an integer-plus-half lattice $\Lambda + \frac{1}{2}$. This is discussed in more detail in Section 4.4.

A.3 Computational complexity and the Gluing technique

When one talks about various computational methods, a comparison shouldn't just be based on what one can compute, but also on the complexity of the computation. For example, computing the $3d$ $\mathcal{N} = 4$ superconformal index tells us a lot about the spectrum of operators in an SCFT but such a computation for a quiver with multiple gauge groups, even perturbatively, will be extremely difficult. For example, the superconformal index for 3d $\mathcal{N} = 4$ E_8 Dynkin quiver up to q^{10} , where q is the fugacity in the superconformal index that always has a positive power in a Taylor expansion, will take at least a few days to compute. Throughout this thesis, we see many examples whose Coulomb branch dimensions greatly exceeds that of the E_8 quiver, but nevertheless we can make efficient Coulomb branch Hilbert series computations using the monopole formula.

Perturbative computation

The first advantage of the monopole formula is the perturbative Hilbert series. When computing the monopole formula, one in principle sum over all the magnetic charges in an infinite lattice as shown above. The resulting Hilbert series can then be expressed as a rational function whose palindromic numerator is an indication that the moduli space is hyperKähler. However, summing over infinite magnetic charges is difficult when your function contain absolute values, which is the case for our conformal dimension $\Delta(m)$. As a result, `Mathematica` has a

hard time doing the computation for a quiver with more than one gauge group. A way out is to devise an algorithm that splits $\Delta(m)$ into different chambers/fans of magnetic charges which will always result in $\Delta(m)$ being positive even without taking the absolute values. This is done to a certain degree in [144, 199] but only for small number of gauge groups. A remarkable `Mathematica` code developed by our collaborator Rudolph Kalveks was able to make this process efficient for several gauge groups with low ranks. However, even though it was able to generate all the Hilbert series of the magnetic quivers to the rank 1 SCFTs in Chapter 5, any larger quiver would take longer than a day to compute. When a computation increases to several days, it is also limited by the physical memory of the computer.

This is where the advantage of a perturbative computation comes in. Rather than summing the magnetic charges to infinity, we set a limit $m \to gg$ where gg is a cut-off. Then, the magnetic charges summed over is a finite sum and `Mathematica` will output the Hilbert series up to t^{2gg}. It may come as a surprise that magnetic charges of $gg+1$ and above does not contribute to the Hilbert series up to t^{2gg} but we found this to be true for simply-laced quivers with classical gauge groups. If there is a non-simply laced edge of multiplicity l, then the magnetic charges on the short nodes needs to be summed to $l \times gg$ whereas the charges on the long nodes remains as gg. In summary, we were able to compute the monopole formula at a cut-off and obtain the perturbative Hilbert series that is always correct up to (twice) that cut-off.

Gluing technique

Another essential technique is the *gluing technique*. Such a technique had already been applied to the Molien-Weyl integral by taking hyperKähler quotients over gauge groups one at a time. It was also used in the Hall-Littlewood formula where the Hilbert series (with background charges n_i of the flavor group G) for three $T_\rho(G)$ legs were computed first and then the diagonal subgroup G of the three flavor groups are gauged together by summing over the background magnetic charges n_i [118].

This gluing process can be applied straightforwardly for the monopole formula as well! Consider the following quiver of $T(SU(4))$ with the magnetic charges labelled on top of each

node:

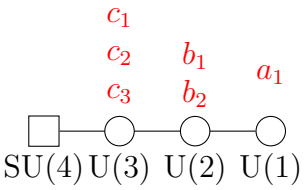

(A.1)

1. Compute the subquiver:

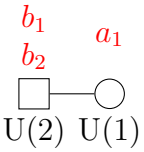

$$\mathrm{HS}_1(t, b_1, b_2) = \sum_{a_1}^{gg} t^{2(\Delta_{U(1)-[2]}(a_1,b_1,b_2)+\Delta_{U(1)}(a_1))} P_{U(1)}(a_1) \tag{A.2}$$

where the $\Delta_{U(1)-[2]}(a_1, b_1, b_2)$ is the hypermultiplet contribution where b_1, b_2 are not summed over and treated instead as background magnetic charges of the $U(2)$ flavor group. $\Delta_{U(1)}(a_1)$ is the vector contribution (which is trivial in this case). Since we are doing a perturbative computation, the cut-off is already set at gg.

2. Next, we gauge the $U(2)$ flavor group but add an additional $U(3)$ flavor group:

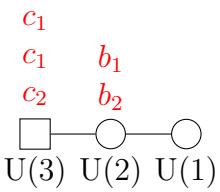

$$\mathrm{HS}_2(t, c_1, c_2, c_3) = \sum_{b_1 \geq b_2}^{gg} t^{2(\Delta_{U(2)-[3]}(b_1,b_2,c_1,c_2,c_3)+\Delta_{U(2)}(b_1,b_2))} P_{U(2)}(b_1, b_2) \mathrm{HS}_1(t, b_1, b_2) \tag{A.3}$$

In the equation, we take the previous Hilbert series and gauge the $U(2)$ by summing over b_1, b_2. In addition, we include the $U(3)$ flavor node with c_1, c_2, c_3 being the background magnetic charges.

3. Finally, we gauge over the $U(3)$ and add an $SU(4)$ flavor node:

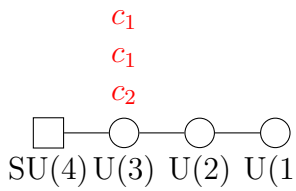

$$\mathrm{HS}(t) = \sum_{c_1 \geq c_2 \geq c_3}^{gg} t^{2(\Delta_{U(3)-[4]}(c_1,c_2,c_3)+\Delta_{U(3)}(c_1,c_2,c_3))} P_{U(3)}(c_1,c_2,c_3)\mathrm{HS}_2(t,c_1,c_2,c_3) \tag{A.4}$$

The summation now sums over the c_1, c_2, c_3 charges of $U(3)$. Since the $SU(4)$ remains a flavor node, we will not assign anymore background magnetic charges to them. The Coulomb branch Hilbert series up to order t^{2gg} is now obtained.

This is the gluing technique. It may seem trivial at first since the ordering in a summation is always commutative (you can always sum over one set of magnetic charges before the other). However, for computer softwares such as `Mathematica`, this is not so trivial. If we do not do this summation step by step, `Mathematica` will assign values to all the magnetic charges before evaluating them for the conformal dimension. Roughly, the number of magnetic charges to be summed over is shortened from $\Lambda_{U(1)} \times \Lambda_{U(2)} \times \Lambda_{U(3)}$ to $\Lambda_{U(1)} \oplus \Lambda_{U(2)} \oplus \Lambda_{U(3)}$. For instance, using the above method and an average computer[1], the Coulomb branch Hilbert series to order t^{10} of an E_8 Dynkin quiver, which has Coulomb branch dimension $\dim_{\mathbb{H}} = 29$, should take less than one minute.

This gluing technique allowed us to make high order perturbative computations for the many complicated magnetic quivers seen throughout this thesis. It is only possible because of the simplicity of the monopole formula. In fact, the computation really boils down to assigning integer or half-plus-integer numbers to a piece-wise linear function! Such computation should also be parallelizable, allowing efficient use of supercomputers and clusters to speed things up even more. The usage of supercomputers also prevent `Mathematica` from crashing due to memory issues and can allow the computation to go on for days or even weeks!

[1]Say, a 2015 Windows computer with i3 processor. Or equivalently, a 2022 Mac with state of the art M1 processor.

Appendix B

Hilbert series and other generating functions

Based on our paper [1] and [4] In this appendix, we provide all the Coulomb branch Hilbert series computations of the magnetic quivers provided in this thesis. The computations are mostly unrefined and therefore the Hilbert series HS(t) is just parameterized by the counting fugacity t.

B.1 SQCD quivers

The magnetic quivers corresponding to Section 4.1. The exact Hilbert series as well as perturbative refined PL are given for various members of the Trapezium, Kite and Truck family.

B.1.1 Exact unrefined Hilbert series

Exact unrefined Hilbert series for the 'Trapzeium' family

Table B.1: *Exact unrefined Hilbert series for the $m = 2$ case in the 'Trapezium' family of quivers for $\mathfrak{v} = 1, 2, 3$*

n	$\mathfrak{v}$	Unrefined Hilbert Series
1	1	$\frac{1}{(-1+t)^4}$
	2	$\frac{1+t^2}{(-1+t)^4(1+t)^2}$
	3	$\frac{1-t+t^2}{(-1+t)^4\,(1+t+t^2)}$

Table B.2: *Exact unrefined Hilbert series for the $m = 3$ case in the 'Trapezium' family of quivers for $\mathfrak{v} = 1, 2, 3$*

n	$\mathfrak{v}$	Unrefined Hilbert Series
1	1	$\frac{(1+t^2)\,(1+8t^2+t^4)}{(-1+t)^6(1+t)^6}$
	2	$\frac{1+t+6t^2+9t^3+15t^4+12t^5+15t^6+9t^7+6t^8+t^9+t^{10}}{(-1+t)^6(1+t)^4\,(1+t+t^2)^3}$
	3	$\frac{1+6t^2+15t^4+18t^6+15t^8+6t^{10}+t^{12}}{(-1+t)^6(1+t)^6\,(1+t^2)^3}$

Table B.3: *Exact unrefined Hilbert series for the $m = 4, k = 1$ case in the 'Trapezium' family of quivers for $\mathfrak{v} = 1, 2, 3$*

n	$\mathfrak{v}$	Unrefined Hilbert Series
1	1	$\frac{1+16t^2+36t^4+16t^6+t^8}{(-1+t)^8(1+t)^8}$
	2	$(1+2t+13t^2+28t^3+62t^4+88t^5+128t^6+132t^7+128t^8+88t^9+62t^{10}+28t^{11}+13t^{12}+2t^{13}+t^{14})/(-1+t)^8(1+t)^6(1+t+t^2)^4$
	3	$\frac{1+12t^2+46t^4+92t^6+116t^8+92t^{10}+46t^{12}+12t^{14}+t^{16}}{(-1+t)^8(1+t)^8\,(1+t^2)^4}$

Table B.4: *Exact unrefined Hilbert series for the $m = 4, k = 2$ case in the 'Trapezium' family of quivers for $\mathfrak{v} = 1, 2, 3$*

n	$\mathfrak{v}$	Unrefined Hilbert Series
2	1	$(1+3t+14t^2+41t^3+104t^4+207t^5+367t^6+540t^7+684t^8+730t^9+684t^{10}+540t^{11}+367t^{12}+207t^{13}+104t^{14}+41t^{15}+14t^{16}+3t^{17}+t^{18})/((-1+t)^{10}(1+t)^8(1+t+t^2)^5)$
	2	$\frac{1+11t^2+57t^4+170t^6+324t^8+398t^{10}+324t^{12}+170t^{14}+57t^{16}+11t^{18}+t^{20}}{(-1+t)^{10}(1+t)^{10}\,(1+t^2)^5}$
	3	$(1+3t+14t^2+34t^3+83t^4+168t^5+316t^6+531t^7+841t^8+1202t^9+1632t^{10}+2052t^{11}+2420t^{12}+2652t^{13}+2754t^{14}+2652t^{15}+2420t^{16}+2052t^{17}+1632t^{18}+1202t^{19}+841t^{20}+531t^{21}+316t^{22}+168t^{23}+83t^{24}+34t^{25}+14t^{26}+3t^{27}+t^{28})/((-1+t)^{10}(1+t)^8(1+t+t^2+t^3+t^4)^5)$

Table B.5: *Exact unrefined Hilbert series for the $m = 5, k = 1$ case in the 'Trapezium' family of quivers for $\mathfrak{v} = 1, 2, 3$*

n	$\mathfrak{v}$	Unrefined Hilbert Series
1	1	$\frac{(1+t^2)\,(1+24t^2+76t^4+24t^6+t^8)}{(-1+t)^{10}(1+t)^{10}}$
	2	$(1+3t+23t^2+66t^3+185t^4+365t^5+665t^6+950t^7+1220t^8+1280t^9+1220t^{10}+950t^{11}+665t^{12}+365t^{13}+185t^{14}+66t^{15}+23t^{16}+3t^{17}+t^{18})/(-1+t)^{10}(1+t)^8(1+t+t^2)^5$
	3	$\frac{1+20t^2+115t^4+340t^6+620t^8+750t^{10}+620t^{12}+340t^{14}+115t^{16}+20t^{18}+t^{20}}{(-1+t)^{10}(1+t)^{10}\,(1+t^2)^5}$

Table B.6: *Exact unrefined Hilbert series for the $m = 5, k = 2$ case in the 'Trapezium' family of quivers for $\mathfrak{v} = 1, 2, 3$*

n	$\mathfrak{v}$	Unrefined Hilbert Series
2	1	$(1+5t+28t^2+113t^3+396t^4+1145t^5+2895t^6+6296t^7+12023t^8+20153t^9+30040t^{10}+39761t^{11}+47035t^{12}+49670t^{13}+47035t^{14}+39761t^{15}+30040t^{16}+20153t^{17}+12023t^{18}+6296t^{19}+2895t^{20}+1145t^{21}+396t^{22}+113t^{23}+28t^{24}+5t^{25}+t^{26})/(-1+t)^{14}(1+t)^{12}(1+t+t^2)^7$
	2	$(1+18t^2+159t^4+818t^6+2711t^8+6140t^{10}+9895t^{12}+11570t^{14}+9895t^{16}+6140t^{18}+2711t^{20}+818t^{22}+159t^{24}+18t^{26}+t^{28})/(-1+t)^{14}(1+t)^{14}(1+t^2)^7$
	3	$(1+5t+28t^2+100t^3+331t^4+924t^5+2329t^6+5282t^7+11012t^8+21089t^9+37624t^{10}+62611t^{11}+97850t^{12}+143938t^{13}+200145t^{14}+263356t^{15}+329025t^{16}+390530t^{17}+441100t^{18}+474255t^{19}+485950t^{20}+474255t^{21}+441100t^{22}+390530t^{23}+329025t^{24}+263356t^{25}+200145t^{26}+143938t^{27}+97850t^{28}+62611t^{29}+37624t^{30}+21089t^{31}+11012t^{32}+5282t^{33}+2329t^{34}+924t^{35}+331t^{36}+100t^{37}+28t^{38}+5t^{39}+t^{40})/((-1+t)^{14}(1+t)^{12}(1+t+t^2+t^3+t^4)^7))$

Table B.7: *Exact unrefined Hilbert series for the $m = 6, k = 1$ case in the 'Trapezium' family of quivers for $\mathfrak{v} = 1, 2, 3$*

n	$\mathfrak{v}$	Unrefined Hilbert Series
1	1	$\frac{1+36t^2+225t^4+400t^6+225t^8+36t^{10}+t^{12}}{(-1+t)^{12}(1+t)^{12}}$
	2	$(1+4t+36t^2+130t^3+445t^4+1116t^5+2489t^6+4526t^7+7290t^8+10000t^9+12247t^{10}+12960t^{11}+12247t^{12}+10000t^{13}+7290t^{14}+4526t^{15}+2489t^{16}+1116t^{17}+445t^{18}+130t^{19}+36t^{20}+4t^{21}+t^{22})/(-1+t)^{12}(1+t)^{10}(1+t+t^2)^6$
	3	$(1+30t^2+246t^4+1010t^6+2535t^8+4272t^{10}+5062t^{12}+4272t^{14}+2535t^{16}+1010t^{18}+246t^{20}+30t^{22}+t^{24})/(-1+t)^{12}(1+t)^{12}(1+t^2)^6$

Table B.8: *Exact unrefined Hilbert series for the $m = 6, k = 2$ case in the 'Trapezium' family of quivers for $\mathfrak{v} = 1, 2, 3$*

n	$\mathfrak{v}$	Unrefined Hilbert Series
2	1	$(1 + 7t + 48t^2 + 245t^3 + 1091t^4 + 4086t^5 + 13382t^6 + 38204t^7 + 96585t^8 + 217249t^9 + 438784t^{10} + 798855t^{11} + 1318069t^{12} + 1976404t^{13} + 2702163t^{14} + 3373477t^{15} + 3852319t^{16} + 4025730t^{17} + 3852319t^{18} + 3373477t^{19} + 2702163t^{20} + 1976404t^{21} + 1318069t^{22} + 798855t^{23} + 438784t^{24} + 217249t^{25} + 96585t^{26} + 38204t^{27} + 13382t^{28} + 4086t^{29} + 1091t^{30} + 245t^{31} + 48t^{32} + 7t^{33} + t^{34})/(-1 + t)^{18}(1 + t)^{16}(1 + t + t^2)^9$
	2	$(1 + 27t^2 + 363t^4 + 2827t^6 + 14238t^8 + 49872t^{10} + 127390t^{12} + 244479t^{14} + 359118t^{16} + 407782t^{18} + 359118t^{20} + 244479t^{22} + 127390t^{24} + 49872t^{26} + 14238t^{28} + 2827t^{30} + 363t^{32} + 27t^{34} + t^{36})/(-1 + t)^{18}(1 + t)^{18}(1 + t^2)^9$
	3	$(1+7t+48t^2+224t^3+944t^4+3381t^5+10823t^6+31058t^7+81213t^8+194813t^9+432962t^{10} + 896394t^{11} + 1739592t^{12} + 3178077t^{13} + 5488182t^{14} + 8986233t^{15} + 13991895t^{16} + 20762811t^{17} + 29423016t^{18} + 39881511t^{19} + 51778977t^{20} + 64462347t^{21} + 77028096t^{22} + 88406421t^{23} + 97512231t^{24} + 103403109t^{25} + 105443112t^{26} + 103403109t^{27} + 97512231t^{28} + 88406421t^{29} + 77028096t^{30} + 64462347t^{31} + 51778977t^{32} + 39881511t^{33} + 29423016t^{34} + 20762811t^{35} + 13991895t^{36} + 8986233t^{37} + 5488182t^{38} + 3178077t^{39} + 1739592t^{40} + 896394t^{41} + 432962t^{42} + 194813t^{43} + 81213t^{44} + 31058t^{45} + 10823t^{46} + 3381t^{47} + 944t^{48} + 224t^{49} + 48t^{50} + 7t^{51} + t^{52})/(-1 + t)^{18}(1 + t)^{16}(1 + t + t^2 + t^3 + t^4)^9)$

Table B.9: *Exact unrefined Hilbert series for the $m = 6, k = 3$ case in the 'Trapezium' family of quivers for $\mathfrak{v} = 1, 2, 3$*

n	$\mathfrak{v}$	Unrefined Hilbert Series
3	1	$(1 + 26t^2 + 345t^4 + 2835t^6 + 15863t^8 + 63865t^{10} + 192048t^{12} + 442283t^{14} + 793768t^{16} + 1122615t^{18} + 1259282t^{20} + 1122615t^{22} + 793768t^{24} + 442283t^{26} + 192048t^{28} + 63865t^{30} + 15863t^{32} + 2835t^{34} + 345t^{36} + 26t^{38} + t^{40})/(-1 + t)^{20}(1 + t)^{20}(1 + t^2)^{10}$
	2	$(1 + 8t + 54t^2 + 264t^3 + 1113t^4 + 4062t^5 + 13283t^6 + 39404t^7 + 107433t^8 + 271254t^9 + 639012t^{10} + 1411762t^{11} + 2938876t^{12} + 5785934t^{13} + 10807824t^{14} + 19205498t^{15} + 32543067t^{16} + 52685460t^{17} + 81634614t^{18} + 121240970t^{19} + 172812329t^{20} + 236660856t^{21} + 311687899t^{22} + 395095814t^{23} + 482356231t^{24} + 567488012t^{25} + 643670661t^{26} + 704102126t^{27} + 742982247t^{28} + 756401528t^{29} + 742982247t^{30} + 704102126t^{31} + 643670661t^{32} + 567488012t^{33} + 482356231t^{34} + 395095814t^{35} + 311687899t^{36} + 236660856t^{37} + 172812329t^{38} + 121240970t^{39} + 81634614t^{40} + 52685460t^{41} + 32543067t^{42} + 19205498t^{43} + 10807824t^{44} + 5785934t^{45} + 2938876t^{46} + 1411762t^{47} + 639012t^{48} + 271254t^{49} + 107433t^{50} + 39404t^{51} + 13283t^{52} + 4062t^{53} + 1113t^{54} + 264t^{55} + 54t^{56} + 8t^{57} + t^{58})/(-1 + t)^{20}(1 + t)^{18}(1 + t + t^2 + t^3 + t^4)^{10}$
	3	$(1 + 26t^2 + 315t^4 + 2405t^6 + 13254t^8 + 56731t^{10} + 197168t^{12} + 573138t^{14} + 1422221t^{16} + 3057599t^{18} + 5757435t^{20} + 9572116t^{22} + 14135651t^{24} + 18621181t^{26} + 21945131t^{28} + 23175984t^{30} + 21945131t^{32} + 18621181t^{34} + 14135651t^{36} + 9572116t^{38} + 5757435t^{40} + 3057599t^{42} + 1422221t^{44} + 573138t^{46} + 197168t^{48} + 56731t^{50} + 13254t^{52} + 2405t^{54} + 315t^{56} + 26t^{58} + t^{60})/(-1 + t)^{20}(1 + t)^{20}(1 - t + t^2)^{10}(1 + t + t^2)^{10}$

Table B.10: *Exact unrefined Hilbert series for the $m = 7, k = 1$ case in the 'Trapezium' family of quivers for $\mathfrak{v} = 1, 2, 3$*

n	$\mathfrak{v}$	Unrefined Hilbert Series
1	1	$\frac{(1+t^2)\,(1+48t^2+393t^4+832t^6+393t^8+48t^{10}+t^{12})}{(-1+t)^{14}(1+t)^{14}}$
	2	$(1+5t+52t^2+227t^3+922t^4+2801t^5+7441t^6+16422t^7+31927t^8+53767t^9+80682t^{10}+106771t^{11}+126707t^{12}+133630t^{13}+126707t^{14}+106771t^{15}+80682t^{16}+53767t^{17}+31927t^{18}+16422t^{19}+7441t^{20}+2801t^{21}+922t^{22}+227t^{23}+52t^{24}+5t^{25}+t^{26})/(-1+t)^{14}(1+t)^{12}(1+t+t^2)^7$
	3	$1+42t^2+469t^4+2562t^6+8491t^8+18942t^{10}+30079t^{12}+34986t^{14}+30079t^{16}+18942t^{18}+8491t^{20}+2562t^{22}+469t^{24}+42t^{26}+t^{28}/(-1+t)^{14}(1+t)^{14}\,(1+t^2)^7$

Table B.11: *Exact unrefined Hilbert series for the $m = 7, k = 2$ case in the 'Trapezium' family of quivers for $\mathfrak{v} = 1, 2, 3$*

n	$\mathfrak{v}$	Unrefined Hilbert Series
2	1	$(1+9t+74t^2+457t^3+2465t^4+11294t^5+45343t^6+159791t^7+501073t^8+1407196t^9+3568687t^{10}+8215777t^{11}+17261755t^{12}+33227158t^{13}+58806645t^{14}+95951209t^{15}+144678726t^{16}+201962853t^{17}+261406665t^{18}+314053002t^{19}+350499186t^{20}+363541404t^{21}+350499186t^{22}+314053002t^{23}+261406665t^{24}+201962853t^{25}+144678726t^{26}+95951209t^{27}+58806645t^{28}+33227158t^{29}+17261755t^{30}+8215777t^{31}+3568687t^{32}+1407196t^{33}+501073t^{34}+159791t^{35}+45343t^{36}+11294t^{37}+2465t^{38}+457t^{39}+74t^{40}+9t^{41}+t^{42})/(-1+t)^{22}(1+t)^{20}(1+t+t^2)^{11}$
	2	$(1+38t^2+723t^4+7914t^6+56015t^8+277316t^{10}+1011173t^{12}+2811056t^{14}+6100550t^{16}+10502324t^{18}+14492450t^{20}+16124444t^{22}+14492450t^{24}+10502324t^{26}+6100550t^{28}+2811056t^{30}+1011173t^{32}+277316t^{34}+56015t^{36}+7914t^{38}+723t^{40}+38t^{42}+t^{44})/(-1+t)^{22}(1+t)^{22}(1+t^2)^{11}$
	3	$(1+9t+74t^2+426t^3+2186t^4+9577t^5+37345t^6+130238t^7+412089t^8+1192953t^9+3188421t^{10}+7920183t^{11}+18399822t^{12}+40177265t^{13}+82823481t^{14}+161782977t^{15}+300413759t^{16}+531742918t^{17}+899328939t^{18}+1456340667t^{19}+2262118536t^{20}+3375587774t^{21}+4845670980t^{22}+6699404229t^{23}+8929693641t^{24}+11485012548t^{25}+14264042022t^{26}+17117445468t^{27}+19858360146t^{28}+22280924058t^{29}+24184925310t^{30}+25402327314t^{31}+25821230736t^{32}+25402327314t^{33}+24184925310t^{34}+22280924058t^{35}+19858360146t^{36}+17117445468t^{37}+14264042022t^{38}+11485012548t^{39}+8929693641t^{40}+6699404229t^{41}+4845670980t^{42}+3375587774t^{43}+2262118536t^{44}+1456340667t^{45}+899328939t^{46}+531742918t^{47}+300413759t^{48}+161782977t^{49}+82823481t^{50}+40177265t^{51}+18399822t^{52}+7920183t^{53}+3188421t^{54}+1192953t^{55}+412089t^{56}+130238t^{57}+37345t^{58}+9577t^{59}+2186t^{60}+426t^{61}+74t^{62}+9t^{63}+t^{64})/((-1+t)^{22}(1+t)^{20}(1+t+t^2+t^3+t^4)^{11})$

Table B.12: *Exact unrefined Hilbert series for the $m = 7, k = 3$ case in the 'Trapezium' family of quivers for $\mathfrak{v} = 1, 2, 3$*

n	$\mathfrak{v}$	Unrefined Hilbert Series
3	1	$(1 + 36t^2 + 674t^4 + 8058t^6 + 67083t^8 + 409192t^{10} + 1896763t^{12} + 6865446t^{14} + 19809204t^{16} + 46278352t^{18} + 88564471t^{20} + 140010256t^{22} + 183886760t^{24} + 201306308t^{26} + 183886760t^{28} + 140010256t^{30} + 88564471t^{32} + 46278352t^{34} + 19809204t^{36} + 6865446t^{38} + 1896763t^{40} + 409192t^{42} + 67083t^{44} + 8058t^{46} + 674t^{48} + 36t^{50} + t^{52})/(-1 + t)^{26}(1 + t)^{26}(1 + t^2)^{13}$
	2	$(1+11t+91t^2+561t^3+2927t^4+13246t^5+53624t^6+197160t^7+666602t^8+2089844t^9+6116574t^{10}+16799980t^{11}+43494373t^{12}+106532655t^{13}+247657723t^{14}+547966929t^{15}+1156824845t^{16}+2335327528t^{17}+4517017030t^{18}+8385844508t^{19}+14966597581t^{20}+25715853133t^{21}+42593091071t^{22}+68083277137t^{23}+105137384039t^{24}+156998522990t^{25}+226892433564t^{26}+317582322118t^{27}+430819057114t^{28}+566752262418t^{29}+723399678478t^{30}+896289495964t^{31}+1078386828737t^{32}+1260384026411t^{33}+1431379225435t^{34}+1579894499783t^{35}+1695112427945t^{36}+1768151474440t^{37}+1793175996572t^{38}+1768151474440t^{39}+1695112427945t^{40}+1579894499783t^{41}+1431379225435t^{42}+1260384026411t^{43}+1078386828737t^{44}+896289495964t^{45}+723399678478t^{46}+566752262418t^{47}+430819057114t^{48}+317582322118t^{49}+226892433564t^{50}+156998522990t^{51}+105137384039t^{52}+68083277137t^{53}+42593091071t^{54}+25715853133t^{55}+14966597581t^{56}+8385844508t^{57}+4517017030t^{58}+2335327528t^{59}+1156824845t^{60}+547966929t^{61}+247657723t^{62}+106532655t^{63}+43494373t^{64}+16799980t^{65}+6116574t^{66}+2089844t^{67}+666602t^{68}+197160t^{69}+53624t^{70}+13246t^{71}+2927t^{72}+561t^{73}+91t^{74}+11t^{75}+t^{76})/(-1+t)^{26}(1+t)^{24}(1+t+t^2+t^3+t^4)^{13}$
	3	$(1 + t^2)(1 + 35t^2 + 582t^4 + 6195t^6 + 47615t^8 + 282512t^{10} + 1351477t^{12} + 5375881t^{14} + 18190425t^{16} + 53270070t^{18} + 136826005t^{20} + 311485461t^{22} + 633692332t^{24} + 1159674887t^{26} + 1918949593t^{28} + 2882895862t^{30} + 3944502108t^{32} + 4926762778t^{34} + 5626421830t^{36} + 5880455132t^{38} + 5626421830t^{40} + 4926762778t^{42} + 3944502108t^{44} + 2882895862t^{46} + 1918949593t^{48} + 1159674887t^{50} + 633692332t^{52} + 311485461t^{54} + 136826005t^{56} + 53270070t^{58} + 18190425t^{60} + 5375881t^{62} + 1351477t^{64} + 282512t^{66} + 47615t^{68} + 6195t^{70} + 582t^{72} + 35t^{74} + t^{76})/(-1+t)^{26}(1+t)^{26}(1-t+t^2)^{13}(1+t+t^2)^{13}$

Table B.13: *Exact unrefined Hilbert series for the $m = 8, k = 1$ case in the 'Trapezium' family of quivers for $\mathfrak{v} = 1, 2, 3$*

n	$\mathfrak{v}$	Unrefined Hilbert Series
1	1	$\dfrac{1 + 64t^2 + 784t^4 + 3136t^6 + 4900t^8 + 3136t^{10} + 784t^{12} + 64t^{14} + t^{16}}{(-1 + t)^{16}(1 + t)^{16}}$
	2	$(1 + 6t + 71t^2 + 364t^3 + 1715t^4 + 6118t^5 + 18921t^6 + 49120t^7 + 112090t^8 + 223476t^9 + 397390t^{10} + 629272t^{11} + 897456t^{12} + 1151416t^{13} + 1337884t^{14} + 1404648t^{15} + 1337884t^{16} + 1151416t^{17} + 897456t^{18} + 629272t^{19} + 397390t^{20} + 223476t^{21} + 112090t^{22} + 49120t^{23} + 18921t^{24} + 6118t^{25} + 1715t^{26} + 364t^{27} + 71t^{28} + 6t^{29} + t^{30})/(-1+t)^{16}(1+t)^{14}(1+t+t^2)^8$
	3	$(1 + 56t^2 + 820t^4 + 5768t^6 + 24430t^8 + 69608t^{10} + 141988t^{12} + 215000t^{14} + 246388t^{16} + 215000t^{18} + 141988t^{20} + 69608t^{22} + 24430t^{24} + 5768t^{26} + 820t^{28} + 56t^{30} + t^{32})/(-1 + t)^{16}(1 + t)^{16}(1 + t^2)^8$

Table B.14: *Exact unrefined Hilbert series for the $m = 8, k = 2$ case in the 'Trapezium' family of quivers for $\mathfrak{v} = 1, 2, 3$*

n	$\mathfrak{v}$	Unrefined Hilbert Series
2	1	$(1+11t+106t^2+769t^3+4870t^4+26349t^5+125167t^6+524126t^7+1959039t^8+6583221t^9+20048090t^{10}+55649341t^{11}+141558271t^{12}+331404638t^{13}+716773143t^{14}+1436706861t^{15}+2676153506t^{16}+4643110405t^{17}+7518379995t^{18}+11380827210t^{19}+16127350871t^{20}+21418138241t^{21}+26682386938t^{22}+31202417689t^{23}+34267633179t^{24}+35353713606t^{25}+34267633179t^{26}+31202417689t^{27}+26682386938t^{28}+21418138241t^{29}+16127350871t^{30}+11380827210t^{31}+7518379995t^{32}+4643110405t^{33}+2676153506t^{34}+1436706861t^{35}+716773143t^{36}+331404638t^{37}+141558271t^{38}+55649341t^{39}+20048090t^{40}+6583221t^{41}+1959039t^{42}+524126t^{43}+125167t^{44}+26349t^{45}+4870t^{46}+769t^{47}+106t^{48}+11t^{49}+t^{50})/(-1+t)^{26}(1+t)^{24}(1+t+t^2)^{13}$
	2	$(1+51t^2+1305t^4+19098t^6+180400t^8+1193460t^{10}+5838416t^{12}+21924814t^{14}+64900197t^{16}+154355499t^{18}+299050701t^{20}+476577756t^{22}+628777824t^{24}+689356068t^{26}+628777824t^{28}+476577756t^{30}+299050701t^{32}+154355499t^{34}+64900197t^{36}+21924814t^{38}+5838416t^{40}+1193460t^{42}+180400t^{44}+19098t^{46}+1305t^{48}+51t^{50}+t^{52})/(-1+t)^{26}(1+t)^{26}(1+t^2)^{13}$
	3	$(1+11t+106t^2+726t^3+4397t^4+22802t^5+105048t^6+432315t^7+1610556t^8+5478757t^9+17167046t^{10}+49893312t^{11}+135347363t^{12}+344514490t^{13}+826650208t^{14}+1877220773t^{15}+4048499143t^{16}+8316987406t^{17}+16318496360t^{18}+30650902710t^{19}+55226032655t^{20}+95623733693t^{21}+159368755448t^{22}+256018477786t^{23}+396931979707t^{24}+594595783344t^{25}+861426558034t^{26}+1208052724209t^{27}+1641198188584t^{28}+2161422161175t^{29}+2761091165060t^{30}+3423021031082t^{31}+4120212940265t^{32}+4816982233122t^{33}+5471569442574t^{34}+6040041454719t^{35}+6481019072541t^{36}+6760543909128t^{37}+6856310658000t^{38}+6760543909128t^{39}+6481019072541t^{40}+6040041454719t^{41}+5471569442574t^{42}+4816982233122t^{43}+4120212940265t^{44}+3423021031082t^{45}+2761091165060t^{46}+2161422161175t^{47}+1641198188584t^{48}+1208052724209t^{49}+861426558034t^{50}+594595783344t^{51}+396931979707t^{52}+256018477786t^{53}+159368755448t^{54}+95623733693t^{55}+55226032655t^{56}+30650902710t^{57}+16318496360t^{58}+8316987406t^{59}+4048499143t^{60}+1877220773t^{61}+826650208t^{62}+344514490t^{63}+135347363t^{64}+49893312t^{65}+17167046t^{66}+5478757t^{67}+1610556t^{68}+432315t^{69}+105048t^{70}+22802t^{71}+4397t^{72}+726t^{73}+106t^{74}+11t^{75}+t^{76})/(-1+t)^{26}(1+t)^{24}(1+t+t^2+t^3+t^4)^{13}$

Table B.15: *Exact unrefined Hilbert series for the $m = 8, k = 3$ case in the 'Trapezium' family of quivers for $\mathfrak{v} = 1, 2, 3$.*

n	$\mathfrak{v}$	Unrefined Hilbert Series
3	1	$(1 + 48t^2 + 1208t^4 + 19743t^6 + 227168t^8 + 1931399t^{10} + 12580080t^{12} + 64562900t^{14} + 266897534t^{16} + 904235932t^{18} + 2545058368t^{20} + 6014719671t^{22} + 12034445136t^{24} + 20514838759t^{26} + 29933441440t^{28} + 37503583980t^{30} + 40422495006t^{32} + 37503583980t^{34} + 29933441440t^{36} + 20514838759t^{38} + 12034445136t^{40} + 6014719671t^{42} + 2545058368t^{44} + 904235932t^{46} + 266897534t^{48} + 64562900t^{50} + 12580080t^{52} + 1931399t^{54} + 227168t^{56} + 19743t^{58} + 1208t^{60} + 48t^{62} + t^{64})/(-1 + t)^{32}(1 + t)^{32}(1 + t^2)^{16}$
	2	$(1 + 14t + 139t^2 + 1036t^3 + 6481t^4 + 35138t^5 + 170178t^6 + 748458t^7 + 3026960t^8 + 11353526t^9 + 39756383t^{10} + 130634524t^{11} + 404513133t^{12} + 1184673946t^{13} + 3291788257t^{14} + 8702687284t^{15} + 21946370354t^{16} + 52912020120t^{17} + 122217163848t^{18} + 270968772584t^{19} + 577651645684t^{20} + 1185925640608t^{21} + 2348113723918t^{22} + 4489753883188t^{23} + 8300228830574t^{24} + 14852491088896t^{25} + 25750576405212t^{26} + 43296460223480t^{27} + 70657910401852t^{28} + 112007208027552t^{29} + 172588931030870t^{30} + 258666465974628t^{31} + 377295339955958t^{32} + 535880589134880t^{33} + 741497845665856t^{34} + 999993847146816t^{35} + 1314928529144676t^{36} + 1686470775920728t^{37} + 2110403197757586t^{38} + 2577416334823284t^{39} + 3072869074307126t^{40} + 3577153496238128t^{41} + 4066729392717320t^{42} + 4515794807753280t^{43} + 4898450189357624t^{44} + 5191115780313904t^{45} + 5374895866791466t^{46} + 5437565804318652t^{47} + 5374895866791466t^{48} + 5191115780313904t^{49} + 4898450189357624t^{50} + 4515794807753280t^{51} + 4066729392717320t^{52} + 3577153496238128t^{53} + 3072869074307126t^{54} + 2577416334823284t^{55} + 2110403197757586t^{56} + 1686470775920728t^{57} + 1314928529144676t^{58} + 999993847146816t^{59} + 741497845665856t^{60} + 535880589134880t^{61} + 377295339955958t^{62} + 258666465974628t^{63} + 172588931030870t^{64} + 112007208027552t^{65} + 70657910401852t^{66} + 43296460223480t^{67} + 25750576405212t^{68} + 14852491088896t^{69} + 8300228830574t^{70} + 4489753883188t^{71} + 2348113723918t^{72} + 1185925640608t^{73} + 577651645684t^{74} + 270968772584t^{75} + 122217163848t^{76} + 52912020120t^{77} + 21946370354t^{78} + 8702687284t^{79} + 3291788257t^{80} + 1184673946t^{81} + 404513133t^{82} + 130634524t^{83} + 39756383t^{84} + 11353526t^{85} + 3026960t^{86} + 748458t^{87} + 170178t^{88} + 35138t^{89} + 6481t^{90} + 1036t^{91} + 139t^{92} + 14t^{93} + t^{94})/(-1 + t)^{32}(1 + t)^{30}(1 + t + t^2 + t^3 + t^4)^{16}$
	3	$1 + 48t^2 + 1112t^4 + 16687t^6 + 181000t^8 + 1507623t^{10} + 10052864t^{12} + 55362916t^{14} + 257958930t^{16} + 1036323060t^{18} + 3643898608t^{20} + 11349745079t^{22} + 31621466460t^{24} + 79433727887t^{26} + 181088582688t^{28} + 376688580160t^{30} + 718154701658t^{32} + 1259512364088t^{34} + 2038256985200t^{36} + 3051192424019t^{38} + 4233565727024t^{40} + 5453236925459t^{42} + 6528751430088t^{44} + 7270994941632t^{46} + 7536301866630t^{48} + 7270994941632t^{50} + 6528751430088t^{52} + 5453236925459t^{54} + 4233565727024t^{56} + 3051192424019t^{58} + 2038256985200t^{60} + 1259512364088t^{62} + 718154701658t^{64} + 376688580160t^{66} + 181088582688t^{68} + 79433727887t^{70} + 31621466460t^{72} + 11349745079t^{74} + 3643898608t^{76} + 1036323060t^{78} + 257958930t^{80} + 55362916t^{82} + 10052864t^{84} + 1507623t^{86} + 181000t^{88} + 16687t^{90} + 1112t^{92} + 48t^{94} + t^{96})/(-1 + t)^{32}(1 + t)^{32}(1 - t + t^2)^{16}(1 + t + t^2)^{16}$

Table B.16: *Exact unrefined Hilbert series for the $m = 8, k = 4$ case in the 'Trapezium' family of quivers for $\mathfrak{v} = 1$.*

n	$\mathfrak{v}$	Plethystic logarithm
4	1	$(1 + 15t + 152t^2 + 1160t^3 + 7364t^4 + 40348t^5 + 196359t^6 + 864004t^7 + 3484191t^8 + 13007946t^9 + 45325235t^{10} + 148366997t^{11} + 458742668t^{12} + 1345992193t^{13} + 3762574196t^{14} + 10055406237t^{15} + 25769503470t^{16} + 63499676293t^{17} + 150811449701t^{18} + 345957406842t^{19} + 768015026643t^{20} + 1652823026444t^{21} + 3453593931514t^{22} + 7016489417347t^{23} + 13878153081271t^{24} + 26755720185551t^{25} + 50331596319853t^{26} + 92476299632454t^{27} + 166102913283119t^{28} + 291904573071183t^{29} + 502287878574675t^{30} + 846872912713515t^{31} + 1399973601024399t^{32} + 2270485259783765t^{33} + 3614570497585323t^{34} + 5651428840412064t^{35} + 8682238199966561t^{36} + 13112049739724701t^{37} + 19473992039434201t^{38} + 28454599213758157t^{39} + 40918442761073825t^{40} + 57929562904111103t^{41} + 80766531110661053t^{42} + 110927423585176322t^{43} + 150120655632113963t^{44} + 200237635878415679t^{45} + 263303656656781351t^{46} + 341404425523047539t^{47} + 436587200360391991t^{48} + 550737590279981553t^{49} + 685435622944164987t^{50} + 841797470158528088t^{51} + 1020312005792106173t^{52} + 1220683824185574317t^{53} + 1441696128166564247t^{54} + 1681107673690404151t^{55} + 1935597465128123495t^{56} + 2200768971381957873t^{57} + 2471222265015961059t^{58} + 2740697831177675992t^{59} + 3002290180522421129t^{60} + 3248723313751306131t^{61} + 3472674117041238221t^{62} + 3667124555274860425t^{63} + 3825719681403191979t^{64} + 3943106494958295009t^{65} + 4015228882757614815t^{66} + 4039556353976212676t^{67} + 4015228882757614815t^{68} + 3943106494958295009t^{69} + 3825719681403191979t^{70} + 3667124555274860425t^{71} + 3472674117041238221t^{72} + 3248723313751306131t^{73} + 3002290180522421129t^{74} + 2740697831177675992t^{75} + 2471222265015961059t^{76} + 2200768971381957873t^{77} + 1935597465128123495t^{78} + 1681107673690404151t^{79} + 1441696128166564247t^{80} + 1220683824185574317t^{81} + 1020312005792106173t^{82} + 841797470158528088t^{83} + 685435622944164987t^{84} + 550737590279981553t^{85} + 436587200360391991t^{86} + 341404425523047539t^{87} + 263303656656781351t^{88} + 200237635878415679t^{89} + 150120655632113963t^{90} + 110927423585176322t^{91} + 80766531110661053t^{92} + 57929562904111103t^{93} + 40918442761073825t^{94} + 28454599213758157t^{95} + 19473992039434201t^{96} + 13112049739724701t^{97} + 8682238199966561t^{98} + 5651428840412064t^{99} + 3614570497585323t^{100} + 2270485259783765t^{101} + 1399973601024399t^{102} + 846872912713515t^{103} + 502287878574675t^{104} + 291904573071183t^{105} + 166102913283119t^{106} + 92476299632454t^{107} + 50331596319853t^{108} + 26755720185551t^{109} + 13878153081271t^{110} + 7016489417347t^{111} + 3453593931514t^{112} + 1652823026444t^{113} + 768015026643t^{114} + 345957406842t^{115} + 150811449701t^{116} + 63499676293t^{117} + 25769503470t^{118} + 10055406237t^{119} + 3762574196t^{120} + 1345992193t^{121} + 458742668t^{122} + 148366997t^{123} + 45325235t^{124} + 13007946t^{125} + 3484191t^{126} + 864004t^{127} + 196359t^{128} + 40348t^{129} + 7364t^{130} + 1160t^{131} + 152t^{132} + 15t^{133} + t^{134})/((-1+t)^{34}(1+t)^{32}(1+t+t^2+t^3+t^4+t^5+t^6)^{17})$

Table B.17: *Exact unrefined Hilbert series for the $m = 8, k = 4$ case in the 'Trapezium' family of quivers for $\mathfrak{v} = 2$.*

n	$\mathfrak{v}$	Plethystic logarithm
4	2	$((1+t^2)(1+46t^2+1018t^4+14584t^6+152566t^8+1244181t^{10}+8245081t^{12}+45712517t^{14}+216671424t^{16}+892779426t^{18}+3240426292t^{20}+10471368239t^{22}+30390038371t^{24}+79783099549t^{26}+190609276314t^{28}+416493317778t^{30}+835854880029t^{32}+1546137559346t^{34}+2643912606549t^{36}+4189874945272t^{38}+6165893566076t^{40}+8440176638093t^{42}+10760606764255t^{44}+12790358679749t^{46}+14183755473858t^{48}+14680505470988t^{50}+14183755473858t^{52}+12790358679749t^{54}+10760606764255t^{56}+8440176638093t^{58}+6165893566076t^{60}+4189874945272t^{62}+2643912606549t^{64}+1546137559346t^{66}+835854880029t^{68}+416493317778t^{70}+190609276314t^{72}+79783099549t^{74}+30390038371t^{76}+10471368239t^{78}+3240426292t^{80}+892779426t^{82}+216671424t^{84}+45712517t^{86}+8245081t^{88}+1244181t^{90}+152566t^{92}+14584t^{94}+1018t^{96}+46t^{98}+t^{100})/(-1+t)^{34}(1+t)^{34}(1-t+t^2)^{17}(1+t+t^2)^{17}$

Table B.18: *Exact unrefined Hilbert series for the $m = 8, k = 4$ case in the 'Trapezium' family of quivers for $\mathfrak{v} = 3$.*

n	$\mathfrak{v}$	Plethystic logarithm
4	3	$(1 + 15t + 152t^2 + 1160t^3 + 7364t^4 + 40348t^5 + 196359t^6 + 864004t^7 + 3484191t^8 + 13007946t^9 + 45325235t^{10} + 148366997t^{11} + 458742668t^{12} + 1345992193t^{13} + 3762574196t^{14} + 10055406237t^{15} + 25769503470t^{16} + 63499676293t^{17} + 150811449701t^{18} + 345957406842t^{19} + 768015026643t^{20} + 1652823026444t^{21} + 3453593931514t^{22} + 7016489417347t^{23} + 13878153081271t^{24} + 26755720185551t^{25} + 50331596319853t^{26} + 92476299632454t^{27} + 166102913283119t^{28} + 291904573071183t^{29} + 502287878574675t^{30} + 846872912713515t^{31} + 1399973601024399t^{32} + 2270485259783765t^{33} + 3614570497585323t^{34} + 5651428840412064t^{35} + 8682238199966561t^{36} + 13112049739724701t^{37} + 19473992039434201t^{38} + 28454599213758157t^{39} + 40918442761073825t^{40} + 57929562904111103t^{41} + 80766531110661053t^{42} + 110927423585176322t^{43} + 150120655632113963t^{44} + 200237635878415679t^{45} + 263303656656781351t^{46} + 341404425523047539t^{47} + 436587200360391991t^{48} + 550737590279981553t^{49} + 685435622944164987t^{50} + 841797470158528088t^{51} + 1020312005792106173t^{52} + 1220683824185574317t^{53} + 1441696128166564247t^{54} + 1681107673690404151t^{55} + 1935597465128123495t^{56} + 2200768971381957873t^{57} + 2471222265015961059t^{58} + 2740697831177675992t^{59} + 3002290180522421129t^{60} + 3248723313751306131t^{61} + 3472674117041238221t^{62} + 3667124555274860425t^{63} + 3825719681403191979t^{64} + 3943106494958295009t^{65} + 4015228882757614815t^{66} + 4039556353976212676t^{67} + 4015228882757614815t^{68} + 3943106494958295009t^{69} + 3825719681403191979t^{70} + 3667124555274860425t^{71} + 3472674117041238221t^{72} + 3248723313751306131t^{73} + 3002290180522421129t^{74} + 2740697831177675992t^{75} + 2471222265015961059t^{76} + 2200768971381957873t^{77} + 1935597465128123495t^{78} + 1681107673690404151t^{79} + 1441696128166564247t^{80} + 1220683824185574317t^{81} + 1020312005792106173t^{82} + 841797470158528088t^{83} + 685435622944164987t^{84} + 550737590279981553t^{85} + 436587200360391991t^{86} + 341404425523047539t^{87} + 263303656656781351t^{88} + 200237635878415679t^{89} + 150120655632113963t^{90} + 110927423585176322t^{91} + 80766531110661053t^{92} + 57929562904111103t^{93} + 40918442761073825t^{94} + 28454599213758157t^{95} + 19473992039434201t^{96} + 13112049739724701t^{97} + 8682238199966561t^{98} + 5651428840412064t^{99} + 3614570497585323t^{100} + 2270485259783765t^{101} + 1399973601024399t^{102} + 846872912713515t^{103} + 502287878574675t^{104} + 291904573071183t^{105} + 166102913283119t^{106} + 92476299632454t^{107} + 50331596319853t^{108} + 26755720185551t^{109} + 13878153081271t^{110} + 7016489417347t^{111} + 3453593931514t^{112} + 1652823026444t^{113} + 768015026643t^{114} + 345957406842t^{115} + 150811449701t^{116} + 63499676293t^{117} + 25769503470t^{118} + 10055406237t^{119} + 3762574196t^{120} + 1345992193t^{121} + 458742668t^{122} + 148366997t^{123} + 45325235t^{124} + 13007946t^{125} + 3484191t^{126} + 864004t^{127} + 196359t^{128} + 40348t^{129} + 7364t^{130} + 1160t^{131} + 152t^{132} + 15t^{133} + t^{134})/((-1+t)^{34}(1+t)^{32}(1+t+t^2+t^3+t^4+t^5+t^6)^{17})$

Exact unrefined Hilbert series of the 'Kite' family

Table B.19: *Exact unrefined Hilbert series for the $k = 1$ case of the 'Kite' Family of quivers for $\mathfrak{v} = 1, 2, 3$.*

n	$\mathfrak{v}$	Unrefined Hilbert Series
1	1	$\frac{1}{(-1+t)^4}$
	2	$\frac{1+t^2}{(-1+t)^4(1+t)^2}$
	3	$\frac{1-t+t^2}{(-1+t)^4\,(1+t+t^2)}$

Table B.20: *Exact unrefined Hilbert series for the $k = 2$ case of the 'Kite' Family of quivers for $\mathfrak{v} = 1, 2, 3$.*

n	$\mathfrak{v}$	Unrefined Hilbert Series
2	1	$(1 + 5t + 32t^2 + 129t^3 + 452t^4 + 1291t^5 + 3231t^6 + 6962t^7 + 13239t^8 + 22155t^9 + 33026t^{10} + 43743t^{11} + 51799t^{12} + 54726t^{13} + 51799t^{14} + 43743t^{15} + 33026t^{16} + 22155t^{17} + 13239t^{18} + 6962t^{19} + 3231t^{20} + 1291t^{21} + 452t^{22} + 129t^{23} + 32t^{24} + 5t^{25} + t^{26})/((-1 + t)^{14}(1 + t)^{12}(1 + t + t^2)^7)$
	2	$(1 + 22t^2 + 191t^4 + 952t^6 + 3101t^8 + 7000t^{10} + 11297t^{12} + 13228t^{14} + 11297t^{16} + 7000t^{18} + 3101t^{20} + 952t^{22} + 191t^{24} + 22t^{26} + t^{28})/((-1 + t)^{14}(1 + t)^{14}(1 + t^2)^7)$
	3	$(1 + 5t + 32t^2 + 120t^3 + 407t^4 + 1140t^5 + 2857t^6 + 6412t^7 + 13222t^8 + 25077t^9 + 44382t^{10} + 73395t^{11} + 114204t^{12} + 167526t^{13} + 232593t^{14} + 305874t^{15} + 382137t^{16} + 453682t^{17} + 512626t^{18} + 551333t^{19} + 564998t^{20} + 551333t^{21} + 512626t^{22} + 453682t^{23} + 382137t^{24} + 305874t^{25} + 232593t^{26} + 167526t^{27} + 114204t^{28} + 73395t^{29} + 44382t^{30} + 25077t^{31} + 13222t^{32} + 6412t^{33} + 2857t^{34} + 1140t^{35} + 407t^{36} + 120t^{37} + 32t^{38} + 5t^{39} + t^{40})/((-1 + t)^{14}(1 + t)^{12}(1 + t + t^2 + t^3 + t^4)^7)$

Table B.21: *Exact unrefined Hilbert series for the $k = 3$ case of the 'Kite' Family of quivers for $\mathfrak{v} = 1, 2, 3$.*

n	$\mathfrak{v}$	Unrefined Hilbert Series
3	1	$(1 + 51t^2 + 1296t^4 + 20743t^6 + 231124t^8 + 1903143t^{10} + 12057442t^{12} + 60501689t^{14} + 245693944t^{16} + 820951913t^{18} + 2286178042t^{20} + 5359408861t^{22} + 10658876246t^{24} + 18091269915t^{26} + 26320135410t^{28} + 32920932321t^{30} + 35463630834t^{32} + 32920932321t^{34} + 26320135410t^{36} + 18091269915t^{38} + 10658876246t^{40} + 5359408861t^{42} + 2286178042t^{44} + 820951913t^{46} + 245693944t^{48} + 60501689t^{50} + 12057442t^{52} + 1903143t^{54} + 231124t^{56} + 20743t^{58} + 1296t^{60} + 51t^{62} + t^{64})/((-1 + t)^{32}(1 + t)^{32}(1 + t^2)^{16})$
	2	$(1 + 14t + 142t^2 + 1078t^3 + 6890t^4 + 38086t^5 + 187357t^6 + 832736t^7 + 3385801t^8 + 12707230t^9 + 44350540t^{10} + 144818330t^{11} + 444678628t^{12} + 1289602686t^{13} + 3545584183t^{14} + 9271806532t^{15} + 23127796402t^{16} + 55169434408t^{17} + 126134480468t^{18} + 276955374784t^{19} + 585065134420t^{20} + 1191008765112t^{21} + 2339754367128t^{22} + 4441577302552t^{23} + 8156972077880t^{24} + 14508108156088t^{25} + 25015273150194t^{26} + 41850121721300t^{27} + 67988450794850t^{28} + 107334490282680t^{29} + 164778170391600t^{30} + 246139285532776t^{31} + 357951379993072t^{32} + 507046900471928t^{33} + 699926045061460t^{34} + 941924905819456t^{35} + 1236241035837868t^{36} + 1582920058383320t^{37} + 1977946173840456t^{38} + 2412601815148008t^{39} + 2873257851765004t^{40} + 3341719963018176t^{41} + 3796189697954922t^{42} + 4212808113183628t^{43} + 4567650441066094t^{44} + 4838950821685912t^{45} + 5009276034502816t^{46} + 5067351262074456t^{47} + 5009276034502816t^{48} + 4838950821685912t^{49} + 4567650441066094t^{50} + 4212808113183628t^{51} + 3796189697954922t^{52} + 3341719963018176t^{53} + 2873257851765004t^{54} + 2412601815148008t^{55} + 1977946173840456t^{56} + 1582920058383320t^{57} + 1236241035837868t^{58} + 941924905819456t^{59} + 699926045061460t^{60} + 507046900471928t^{61} + 357951379993072t^{62} + 246139285532776t^{63} + 164778170391600t^{64} + 107334490282680t^{65} + 67988450794850t^{66} + 41850121721300t^{67} + 25015273150194t^{68} + 14508108156088t^{69} + 8156972077880t^{70} + 4441577302552t^{71} + 2339754367128t^{72} + 1191008765112t^{73} + 585065134420t^{74} + 276955374784t^{75} + 126134480468t^{76} + 55169434408t^{77} + 23127796402t^{78} + 9271806532t^{79} + 3545584183t^{80} + 1289602686t^{81} + 444678628t^{82} + 144818330t^{83} + 44350540t^{84} + 12707230t^{85} + 3385801t^{86} + 832736t^{87} + 187357t^{88} + 38086t^{89} + 6890t^{90} + 1078t^{91} + 142t^{92} + 14t^{93} + t^{94})/((-1 + t)^{32}(1 + t)^{30}(1 + t + t^2 + t^3 + t^4)^{16})$
	3	$(1 + 51t^2 + 1248t^4 + 19111t^6 + 206352t^8 + 1690175t^{10} + 11035612t^{12} + 59501547t^{14} + 271886436t^{16} + 1073671689t^{18} + 3719961686t^{20} + 11443193055t^{22} + 31551477938t^{24} + 78576217741t^{26} + 177863314892t^{28} + 367829950013t^{30} + 697950292696t^{32} + 1219406743321t^{34} + 1967342741456t^{36} + 2937983789307t^{38} + 4068994310590t^{40} + 5234145983089t^{42} + 6260623079224t^{44} + 6968599528959t^{46} + 7221583960034t^{48} + 6968599528959t^{50} + 6260623079224t^{52} + 5234145983089t^{54} + 4068994310590t^{56} + 2937983789307t^{58} + 1967342741456t^{60} + 1219406743321t^{62} + 697950292696t^{64} + 367829950013t^{66} + 177863314892t^{68} + 78576217741t^{70} + 31551477938t^{72} + 11443193055t^{74} + 3719961686t^{76} + 1073671689t^{78} + 271886436t^{80} + 59501547t^{82} + 11035612t^{84} + 1690175t^{86} + 206352t^{88} + 19111t^{90} + 1248t^{92} + 51t^{94} + t^{96})/((-1 + t)^{32}(1 + t)^{32}(1 - t + t^2)^{16}(1 + t + t^2)^{16})$

Exact unrefined Hilbert series for the 'Truck' family

Table B.22: *Exact unrefined Hilbert series for the $k = 1$ case of the 'Truck' Family of quivers for $\mathfrak{v} = 1, 2, 3$.*

n	$\mathfrak{v}$	Unrefined Hilbert Series
1	1	$\frac{(1+t^2)\,(1+48t^2+393t^4+832t^6+393t^8+48t^{10}+t^{12})}{(-1+t)^{14}(1+t)^{14}}$
	2	$(1+5t+52t^2+227t^3+922t^4+2801t^5+7441t^6+16422t^7+31927t^8+53767t^9+80682t^{10}+106771t^{11}+126707t^{12}+133630t^{13}+126707t^{14}+106771t^{15}+80682t^{16}+53767t^{17}+31927t^{18}+16422t^{19}+7441t^{20}+2801t^{21}+922t^{22}+227t^{23}+52t^{24}+5t^{25}+t^{26})/(-1+t)^{14}(1+t)^{12}(1+t+t^2)^7$
	3	$1+42t^2+469t^4+2562t^6+8491t^8+18942t^{10}+30079t^{12}+34986t^{14}+30079t^{16}+18942t^{18}+8491t^{20}+2562t^{22}+469t^{24}+42t^{26}+t^{28}/(-1+t)^{14}(1+t)^{14}\,(1+t^2)^7$

Table B.23: *Exact unrefined Hilbert series for the $k = 2$ case of the 'Truck' Family of quivers for $\mathfrak{v} = 1, 2, 3$.*

n	$\mathfrak{v}$	Unrefined Hilbert Series
2	1	$(1+9t+71t^2+420t^3+2150t^4+9412t^5+36337t^6+124051t^7+379003t^8+1041724t^9+2594425t^{10}+5881681t^{11}+12196521t^{12}+23215826t^{13}+40700792t^{14}+65885464t^{15}+98702871t^{16}+137075325t^{17}+176728177t^{18}+211739308t^{19}+235928860t^{20}+244576472t^{21}+235928860t^{22}+211739308t^{23}+176728177t^{24}+137075325t^{25}+98702871t^{26}+65885464t^{27}+40700792t^{28}+23215826t^{29}+12196521t^{30}+5881681t^{31}+2594425t^{32}+1041724t^{33}+379003t^{34}+124051t^{35}+36337t^{36}+9412t^{37}+2150t^{38}+420t^{39}+71t^{40}+9t^{41}+t^{42})/((-1+t)^{22}(1+t)^{20}(1+t+t^2)^{11})$
	2	$(1+35t^2+596t^4+6104t^6+41488t^8+199913t^{10}+715079t^{12}+1960640t^{14}+4213746t^{16}+7207530t^{18}+9909462t^{20}+11012276t^{22}+9909462t^{24}+7207530t^{26}+4213746t^{28}+1960640t^{30}+715079t^{32}+199913t^{34}+41488t^{36}+6104t^{38}+596t^{40}+35t^{42}+t^{44})/((-1+t)^{22}(1+t)^{22}(1+t^2)^{11})$
	3	$(1+9t+71t^2+399t^3+1961t^4+8262t^5+31072t^6+105118t^7+324312t^8+919586t^9+2416068t^{10}+5916870t^{11}+13582512t^{12}+29359058t^{13}+59998484t^{14}+116320918t^{15}+214588740t^{16}+377665670t^{17}+635546260t^{18}+1024655182t^{19}+1585431217t^{20}+2357783503t^{21}+3374542499t^{22}+4653398305t^{23}+6188648811t^{24}+7944308554t^{25}+9850599616t^{26}+11805276716t^{27}+13680836596t^{28}+15337126350t^{29}+16638049846t^{30}+17469499684t^{31}+17755538748t^{32}+17469499684t^{33}+16638049846t^{34}+15337126350t^{35}+13680836596t^{36}+11805276716t^{37}+9850599616t^{38}+7944308554t^{39}+6188648811t^{40}+4653398305t^{41}+3374542499t^{42}+2357783503t^{43}+1585431217t^{44}+1024655182t^{45}+635546260t^{46}+377665670t^{47}+214588740t^{48}+116320918t^{49}+59998484t^{50}+29359058t^{51}+13582512t^{52}+5916870t^{53}+2416068t^{54}+919586t^{55}+324312t^{56}+105118t^{57}+31072t^{58}+8262t^{59}+1961t^{60}+399t^{61}+71t^{62}+9t^{63}+t^{64})/((-1+t)^{22}(1+t)^{20}(1+t+t^2+t^3+t^4)^{11})$

B.2 Refined Plethystic Logarithm (PL)

Refined PL of 'Trapezium' family

Table B.24: *Refined Plethystic Logarithm (PL) of the $m = 2$ case in the 'Trapezium' family of quivers.*

n	ϑ	Plethystic logarithm
1	1	
	2	$t^2 : [0] + [2]$ $t^3 : (q + 1/q)[1]$ $t^4 : -[0]$ $t^5 : -(q + 1/q)[1]$ $t^6 : -[0] - [2]$ $t^7 : (q + 1/q)[1]$ $t^8 : 2[0] + 2[2]$
	3	$t^2 : [0] + [2]$ $t^3 :$ $t^4 : -[0] + (q + 1/q)[1]$ $t^5 :$ $t^6 : -(q + 1/q)[1]$ $t^7 :$ $t^8 : -[0] + (q + 1/q)[1] - [2]$

Table B.25: *Refined Plethystic Logarithm (PL) of the $m = 3$ case in the 'Trapezium' family of quivers.*

n	$\mathfrak{v}$	Plethystic logarithm
1	1	$t^2 : [0,0] + (1/q)[0,1] + q[1,0] + [1,1]$ t^3 : $t^4 : -2[0,0] - (1/q)([0,1] + [2,0]) - q([0,2] + [1,0]) - 2[1,1]$ t^5 : $t^6 : 2[0,0] + (3/q + q^2)[0,1] + 3q[0,2] + [0,3] + (1/q^2 + 3q)[1,0] + 6[1,1] + (1/q)[1,2] + (3/q)[2,0] + q[2,1] + [3,0]$ t^7 : $t^8 : -8[0,0] - (11/q + 4q^2)[0,1] - (1/q^2 + 9q)[0,2] - 6[0,3] - (4/q^2 + 11q)[1,0] - 20[1,1] - (7/q + 2q^2)[1,2] - 2q[1,3] - (9/q + q^2)[2,0] - (2/q^2 + 7q)[2,1] - 3[2,2] - 6[3,0] - 2/q[3,1]$
	2	t^2 : [0,0]+[1,1] t^3 : (1/q)[0,1]+q[1,0] t^4 : -[0,0]-[1,1] $t^5 : -[1/q][0,1] - q[0,2] - q[1,0] - 1/q[2,0]$ t^6 :-[0,0]+[1,1] $t^7 : (2/q)[0,1] + 2q[0,2] + 2q[1,0] + (1/q)[1,2] + (2/q)[2,0] + q[2,1]$ $t^8 : [0,0] + q^2[0,1] + (1/q^2)[1,0] + [1,1]$
	3	$t^2 : [0,0] + [1,1]$ t^3 : $t^4 : -[0,0] + (1/q)[0,1] + q[1,0] - [1,1]$ t^5 : $t^6 : -(1/q)[0,1] - q[0,2] - q[1,0] + 2[1,1] - (1/q)[2,0]$ t^7 : $t^8 : -2[0,0] + (2/q)[0,1] + 2q[0,2] - [0,3] + 2q[1,0] - 4[1,1] + (1/q)[1,2] + (2/q)[2,0] + q[2,1] - [3,0]$

Table B.26: *Refined Plethystic Logarithm (PL) of the $m = 4, k = 1$ case in the 'Trapezium' family of quivers.*

n	$\mathfrak{v}$	Plethystic logarithm
1	1	$t^2 : [0,0,0] + (1/q)[0,0,1] + q[1,0,0] + [1,0,1]$ t^3 : t^4 :$-2[0,0,0] - (1/q)[0,0,1] - q[0,1,1] - [0,2,0] - q[1,0,0] - 2[1,0,1] - (1/q)[1,1,0]$ t^5 : t^6 :(all positive terms)
	2	t^2 :$[0,0,0] + [1,0,1]$ t^3 :$(1/q)[0,0,1] + q[1,0,0]$ t^4 :$-[0,0,0] - [0,2,0] - [1,0,1]$ t^5 :$-(1/q)[0,0,1] - q[0,1,1] - q[1,0,0] - (1/q)[1,1,0]$ t^6 :$-[0,0,0] + [0,1,2] + 2[0,2,0] + [1,0,1] + [2,1,0]$ t^7 :(all positive terms) $t^8$$-3[0,1,2] - [0,2,0] - 2[1,0,1] - 2[1,2,1] - [2,0,2] - 3[2,1,0] + q^2[0,0,2] + (1/q^2 + q^2)[0,1,0] + (1/q^2)[2,0,0] + [0,0,0]$
	3	t^2 :$[0,0,0] + [1,0,1]$ t^3 : t^4 :$-[0,0,0] + (1/q)[0,0,1] - [0,2,0] + q[1,0,0] - [1,0,1]$ t^5 : t^6 :$(-(1/q)[0,0,1] - q[0,1,1] + [0,1,2] + 2[0,2,0] - q[1,0,0] + 2[1,0,1] - (1/q)[1,1,0] + [2,1,0]$ t^7 : t^8 :$-2[0,0,0] - 4[0,1,2] - 3[0,2,0] - 7[1,0,1] - 2[1,2,1] - [2,0,2] - 4[2,1,0]$ + positive terms

Table B.27: *Refined Plethystic Logarithm (PL) of the $m = 4, k = 2$ case in the 'Trapezium' family of quivers.*

n	$\mathfrak{v}$	Plethystic logarithm
2	1	t^2 :$[0,0,0]+[1,0,1]$ t^3 :$(q+1/q)[0,1,0]$ t^4 :$-[0,0,0]-[1,0,1]$ t^5 :$-(1/q+q)[0,0,2]-(1/q+q)[0,1,0]-(1/q+q)[2,0,0]$ t^6 :$-[0,0,0]-(1/q^2)[0,0,0]-q^2[0,0,0]$ t^7 :$(1/q+q)(2[0,0,2]+2[0,1,0]+2[2,0,0]+[1,1,1])$ t^8 :$(1+1/q^2+q^2)[0,0,0]+[0,1,2]_[0,2,0]+(5+2/q^2+2q^2)[1,0,1]+[2,1,0]$
	2	t^2 :$[0,0,0]+[1,0,1]$ t^3 : t^4 :$-[0,0,0]+(1/q+q)[0,1,0]-[1,0,1]$ t^5 : t^6 :$-(1/q+q)([0,0,2]+[0,1,0]+[2,0,0])+[0,2,0]+[1,0,1]$ t^7 : $t^8-(2+1/q^2+q^2)[0,0,0]+(1/q+q)(2[0,0,2]+[0,1,0]+[1,1,1]+2[2,0,0])-[0,1,2]-2[0,2,0]-2[1,0,1]-[2,1,0]$
	3	t^2 :$[0,0,0]+[1,0,1]$ t^3 : t^4 :$-[0,0,0]-[1,0,1]$ t^5 :$(1/q+q)[0,1,0]$ t^6 :$[0,2,0]+[1,0,1]$ t^7 :$-(1/q+q)([0,0,2]+[0,1,0]+[2,0,0]$ $t^8-[0,0,0]-[0,1,2]-[0,2,0]-[1,0,1]-[2,1,0]$

Table B.28: *Refined Plethystic Logarithm (PL) of the $m = 5, k = 1$ case in the 'Trapezium' family of quivers.*

n	$\mathfrak{v}$	Plethystic logarithm
1	1	t^2 :$[0,0,0,0] + 1/q[0,0,0,1] + q[1,0,0,0] + [1,0,0,1]$ t^3 : t^4 :$-2[0,0,0,0] - 1/q([0,0,0,1] + [1,0,1,0]) - q([0,1,0,1] + [1,0,0,0]) - [0,1,1,0] - 2[1,0,0,1]$ t^5 : t^6 : All positive terms
	2	t^2 :$[0,0,0,0] + [1,0,0,1]$ t^3 :$1/q[0,0,0,1] + q[1,0,0,0]$ t^4 :$-[0,0,0,0] - [0,1,1,0] - [1,0,0,1]$ t^5 : $-1/q([0,0,0,1] + [1,0,1,0]) - q([0,1,0,1] + [1,0,0,0])$ t^6 :$-[0,0,0,0] + [0,0,2,1] + [0,1,0,2] + 2[0,1,1,0] + [1,0,0,1] + [1,2,0,0] + [2,0,1,0]$
	3	t^2 :$[0,0,0,0] + [1,0,0,1]$ t^3 : t^4 :$-[0,0,0,0] + 1/q[0,0,0,1] - [0,1,1,0] + q[1,0,0,0] - [1,0,0,1]$ t^5 : t^6 :$[0,0,0,0] - 1/q([0,0,0,1] + [1,0,1,0]) - q([0,1,0,1] + [1,0,0,0]) + [0,0,2,1] + [0,1,0,2] + 2[0,1,1,0] + 2[1,0,0,1] + [1,2,0,0] + [2,0,1,0]$

Table B.29: *Refined Plethystic Logarithm (PL) of the $m = 5, k = 2$ case in the 'Trapezium' family of quivers.*

n	$\mathfrak{v}$	Plethystic logarithm
2	1	t^2 :$[0,0,0,0]+[1,0,0,1]$ t^3 :$1/q[0,0,1,0]+q[0,1,0,0]$ t^4 : $-[0,0,0,0]-[1,0,0,1]$ t^5 :$-1/q([0,0,0,2]+[0,0,1,0]+[1,1,0,0])-q([0,0,1,1]+[0,1,0,0]+[2,0,0,0])$ t^6 :$-[0,0,0,0]-q^2[0,0,0,1]-[0,1,1,0]-(1/q^2)[1,0,0,0]$
	2	t^2 :$[0,0,0,0]+[1,0,0,1]$ t^3 : t^4 :$-[0,0,0,0]+1/q[0,0,1,0]+q[0,1,0,0]-[1,0,0,1]$ t^5 : t^6 :$-1/q([0,0,0,2]+[0,0,1,0]+[1,1,0,0])-q([0,0,1,1]+[0,1,0,0]+[2,0,0,0])+[1,0,0,1]$
	3	t^2 :$[0,0,0,0]+[1,0,0,1]$ t^3 : t^4 :$-[0,0,0,0]-[1,0,0,1]$ t^5 :$1/q[0,0,1,0]+q[0,1,0,0]$ t^6 :$[1,0,0,1]$ t^7 :$-1/q([0,0,0,2]+[0,0,1,0]+[1,1,0,0])-q([0,0,1,1,]+[0,1,0,0]+[2,0,0,0])$ $t^8$$-[0,0,0,0]+[0,1,1,0]-[1,0,0,1]$

Table B.30: *Refined Plethystic Logarithm (PL) of the $m = 6, k = 1$ case in the 'Trapezium' family of quivers.*

n	$\mathfrak{v}$	Plethystic logarithm
1	1	t^2 :$[0,0,0,0,0] + 1/q[0,0,0,0,1] + q[1,0,0,0,0] + [1,0,0,0,1]$ t^3 : t^4 :$-2[0,0,0,0,0] - 1/q([0,0,0,0,1] + [1,0,0,1,0]) - q([0,1,0,0,1] + [1,0,0,0,0]) - [0,1,0,1,0] - 2[1,0,0,0,1]$ t^5 :
	2	t^2 :$[0,0,0,0,0] + [1,0,0,0,1]$ t^3 :$1/q[0,0,0,0,1] + q[1,0,0,0,0]$ t^4 :$-[0,0,0,0,0] - [0,1,0,1,0] - [1,0,0,0,1]$ t^5 :$-1/q([0,0,0,0,1] + [1,0,0,1,0]) - q([0,1,0,0,1] + [1,0,0,0,0])$ t^6 :$-[0,0,0,0,0] + [0,0,1,1,1,] + [0,1,0,0,2] + 2[0,1,0,1,0] + [1,0,0,0,1] + [1,1,1,0,0] + [2,0,0,1,0]$
	3	t^2 :$[0,0,0,0,0] + [1,0,0,0,1]$ t^3 : t^4 :$-[0,0,0,0,0] + 1/q[0,0,0,0,1] - [0,1,0,1,0] + q[1,0,0,0,0] - [1,0,0,0,1]$

Table B.31: *Refined Plethystic Logarithm (PL) of the $m = 6, k = 2$ case in the 'Trapezium' family of quivers.*

n	$\mathfrak{v}$	Plethystic logarithm
2	1	t^2 :$[0,0,0,0,0] + [1,0,0,0,1]$ t^3 :$1/q[0,0,0,1,0] + q[0,1,0,0,0]$ t^4 :$-[0,0,0,0,0] - [1,0,0,0,1]$ t^5 :$-1/q([0,0,0,0,2] + [0,0,0,1,0] + [1,0,1,0,0]) - q([0,0,1,0,1] + [0,1,0,0,0] + [2,0,0,0,0]$ t^6 :$-[0,0,0,0,0] - q^2[0,0,0,1,0] - [0,0,2,0,0] - 1/q^2[0,1,0,0,0] - [0,1,0,1,0]$
	2	t^2 :$[0,0,0,0,0] + [1,0,0,0,1]$ t^3 : t^4 :$-[0,0,0,0,0] + 1/q[0,0,0,1,0] + q[0,1,0,0,0] - [1,0,0,0,1]$ t^5 : t^6 : $-1/q([0,0,0,0,2] + [0,0,0,1,0] + [1,0,1,0,0] - q([0,0,1,0,1] + [2,0,0,0,0] + [0,1,0,0,0]) - [0,0,2,0,0]$
	3	t^2 :$[0,0,0,0,0] + [1,0,0,0,1]$ t^3 : t^4 :$-[0,0,0,0,0] - [1,0,0,0,1]$ t^5 :$1/q[0,0,0,1,0] + q[0,1,0,0,0]$ t^6 :$-[0,0,2,0,0] + [1,0,0,0,1]$

Table B.32: *Refined Plethystic Logarithm (PL) of the $m = 6, k = 3$ case in the 'Trapezium' family of quivers.*

n	$\mathfrak{v}$	Plethystic logarithm
3	1	t^2 :$[0,0,0,0,0] + [1,0,0,0,1]$ t^3 : t^4 :$-[0,0,0,0,0] + (1/q + q)[0,0,1,0,0] - [1,0,0,0,1]$ t^5 : t^6 :$-(1/q + q)([0,0,0,1,1] + [0,0,1,0,0] + [1,1,0,0,0]) + [1,0,0,0,1]$
	2	t^2 :$[0,0,0,0,0] + [1,0,0,0,1]$ t^3 : t^4 :$-[0,0,0,0,0] - [1,0,0,0,1]$ t^5 :$(1/q + q)[0,0,1,0,0]$ t^6 : $[1,0,0,0,1]$
	3	t^2 :$[0,0,0,0,0] + [1,0,0,0,1]$ t^3 : t^4 :$-[0,0,0,0,0] - [1,0,0,0,1]$ t^5 : t^6 :$(1/q + q)[0,0,1,0,0] + [1,0,0,0,1]$

Table B.33: *Refined Plethystic Logarithm (PL) of the $m = 7, k = 1$ case in the 'Trapezium' family of quivers.*

n	$\mathfrak{v}$	Plethystic logarithm
1	1	t^2 :$[0,0,0,0,0,0] + [1,0,0,0,0,1] + 1/q[0,0,0,0,0,1] + q[1,0,0,0,0,0]$ t^3 : t^4 :$-2[0,0,0,0,0,0] - 1/q([0,0,0,0,0,1] + [1,0,0,0,1,0]) - q([0,1,0,0,0,1] + [1,0,0,0,0,0]) - 2[1,0,0,0,0,1] - [0,1,0,0,1,0]$ t^5 :
	2	t^2 :$[0,0,0,0,0,0] + [1,0,0,0,0,1]$ t^3 :$1/q[0,0,0,0,0,1] + q[1,0,0,0,0,0]$ t^4 :$-[0,0,0,0,0,0] - [0,1,0,0,1,0] - [1,0,0,0,0,1]$ t^5 :$-1/q([0,0,0,0,0,1] + [1,0,0,0,1,0]) - q([0,1,0,0,0,1] + [1,0,0,0,0,0])$ t^6 : $-[0,0,0,0,0,0] + [0,0,1,0,1,1] + [0,1,0,0,0,2] + 2[0,1,0,0,1,0] + [1,0,0,0,0,1] + [1,1,0,1,0,0] + [2,0,0,0,1,0]$
	3	t^2 :$[0,0,0,0,0,0] + [1,0,0,0,0,1]$ t^3 : t^4 : $-[0,0,0,0,0,0] + 1/q[0,0,0,0,0,1] - [0,1,0,0,1,0] + q[1,0,0,0,0,0] - [1,0,0,0,0,1]$ t^5 : t^6 :

Table B.34: *Refined Plethystic Logarithm (PL) of the $m = 7, k = 2$ case in the 'Trapezium' family of quivers.*

n	$\mathfrak{v}$	Plethystic logarithm
2	2	t^2 :$[0,0,0,0,0] + [1,0,0,0,1]$ t^3 :$1/q[0,0,0,0,1,0]$ + $q[0,1,0,0,0,0,0]$ t^4 :$-[0,0,0,0,0,0] - [1,0,0,0,0,1]$ t^5 :$-1/q([0,0,0,0,0,2]$ + $[0,0,0,0,1,0] + [1,0,0,1,0,0]) -$ $q([0,0,1,0,0,1] + [0,1,0,0,0,0] +$ $[2,0,0,0,0,0]$ t^6 :$-[0,0,0,0,0,0,]$ − $q^2[0,0,0,1,0,0]$ − $1/q^2[0,0,1,0,0,0,0]$ − $[0,0,1,1,0,0] - [0,1,0,0,1,0]$
	2	t^2 :$[0,0,0,0,0,0] + [1,0,0,0,0,1]$ t^3 : t^4 :$-[0,0,0,0,0,0,]$ + $1/q[0,0,0,0,1,0]$ + $q[0,1,0,0,0,0] - [1,0,0,0,0,1]$ t^5 :
	3	t^2 :$[0,0,0,0,0,0] + [1,0,0,0,0,1]$ t^3 : t^4 :$-[0,0,0,0,0,0] - [1,0,0,0,0,1]$ t^5 :$1/q[0,0,0,0,1,0] + q[0,1,0,0,0,0]$ t^6 :$-[0,0,1,1,0,0] + [1,0,0,0,0,1]$

Table B.35: *Refined Plethystic Logarithm (PL) of the $m = 7, k = 3$ case in the 'Trapezium' family of quivers.*

n	$\mathfrak{v}$	Plethystic logarithm
3	1	t^2 :$[0,0,0,0,0] + [1,0,0,0,1]$ t^3 : t^4 :$-[0,0,0,0,0,0,] +$ $1/q[0,0,0,1,0,0] +$ $q[0,0,1,0,0,0] - [1,0,0,0,0,1]$ t^5 : t^6 :$-1/q([0,0,0,0,1,1,] +$ $[0,0,0,1,0,0] + [1,0,1,0,0,0]) -$ $q([0,0,0,1,0,1] + [0,0,1,0,0,0] +$ $[1,1,0,0,0,0]) + [1,0,0,0,0,1]$
	2	t^2 :$[0,0,0,0,0,0] + [1,0,0,0,0,1]$ t^3 : t^4 :$-[0,0,0,0,0,0,] - [1,0,0,0,0,1]$ t^5 :$1/q[0,0,0,1,0,0] +$ $q[0,0,1,0,0,0,0]$ t^6 : $[1,0,0,0,0,1]$
	3	t^2 : t^3 : t^4 : t^5 : t^6 :

B.3 D-type orthosymplectic quivers

D-type orthosymplectic quivers from Section 4.7 whose Coulomb branch are product of moduli spaces. Note that even if one computes the perturbative Hilbert series, it can still be factorized into the perturbative Hilbert series of each moduli space.

Table B.36: *Hilbert series results for theories of Tables 4.10 and 4.11. The first line displays the Coulomb branch Hilbert series for the proposed quiver, while the second line displays the factorisation into a product. The known Hilbert series for the factors match these findings.*

	Coulomb branch Hilbert series
$E_{3-2l}^{k=2,l=0}$	$1+58t^2+32t^3+1569t^4+1600t^5+27220t^6+37856t^7+348124t^8+577920t^9+3540936t^{10}+6502720t^{11}+29981572t^{12}+58099072t^{13}+217747736t^{14}+432151456t^{15}+1385881186t^{16}+2764473568t^{17}+7858110900t^{18}+15572468640t^{19}+40224531398t^{20}+\dots$ $=(1+29t^2+16t^3+364t^4+336t^5+2926t^6+3360t^7+17584t^8+22400t^9+85260t^{10}+114240t^{11}+349572t^{12}+479232t^{13}+1251816t^{14}+1729488t^{15}+4008081t^{16}+5534496t^{17}+11680405t^{18}+16045920t^{19}+31415582t^{20}+\dots)^2$
$E_{3-2l}^{k=3,l=1}$	$1+58t^2+1601t^4+28424t^6+369156t^8+3771348t^{10}+31759488t^{12}+227801304t^{14}+1425775758t^{16}+7933063516t^{18}+39822908626t^{20}+\dots$ $=(1+29t^2+380t^4+3192t^6+19810t^8+98224t^{10}+409016t^{12}+1480548t^{14}+4776849t^{16}+13998385t^{18}+37805264t^{20}+\dots)^2$
$E_{3-2l}^{k=3,l=0}$	$1+134t^2+9017t^4+403982t^6+13508026t^8+358747158t^{10}+\dots$ $=(1+67t^2+2264t^4+50303t^6+820864t^8+10489699t^{10}+\dots)^2$
$E_{3=2l}^{k=4,l=1}$	$1+134t^2+8889t^4+128t^5+388366t^6+15616t^7+12558722t^8+943360t^9+320512966t^{10}+\dots$ $=(1+67t^2+2200t^4+64t^5+46783t^6+3520t^7+724900t^8+95040t^9+8763535t^{10}+\dots)^2$
$E_{4-2l}^{k=1,l=0}$	$1+48t^2+976t^4+11600t^6+95350t^8+598352t^{10}+3053296t^{12}+13224752t^{14}+50129875t^{16}+170108000t^{18}+525728128t^{20}+\dots$ $=(1+24t^2+200t^4+1000t^6+3675t^8+10976t^{10}+28224t^{12}+64800t^{14}+136125t^{16}+266200t^{18}+490776t^{20}+\dots)^2$
$E_{4-2l}^{k=2,l=1}$	$1+32t^2+16t^3+456t^4+416t^5+4104t^6+4960t^7+27490t^8+38400t^9+148792t^{10}+223840t^{11}+681924t^{12}+1062432t^{13}+2729368t^{14}+4305376t^{15}+9754099t^{16}+15374976t^{17}+31652168t^{18}+49482864t^{19}+94506536t^{20}+\dots$ $=(1+16t^2+8t^3+100t^4+80t^5+420t^6+400t^7+1385t^8+1440t^9+3836t^{10}+4200t^{11}+9366t^{12}+10528t^{13}+20728t^{14}+23632t^{15}+42345t^{16}+48672t^{17}+81088t^{18}+93480t^{19}+147106t^{20}+\dots)^2$
$E_{4-2l}^{k=2,l=0}$	$1+92t^2+64t^3+4168t^4+5248t^5+125140t^6+211968t^7+2809296t^8+5635008t^9+50260590t^{10}+\dots$ $=(1+46t^2+32t^3+1026t^4+1152t^5+14862t^6+20160t^7+157794t^8+232608t^9+1314687t^{10}+\dots)^2$
$E_{4-2l}^{k=3,l=1}$	$1+92t^2+4232t^4+128860t^6+2910592t^8+51921078t^{10}+\dots$ $=(1+46t^2+1058t^4+15762t^6+170562t^8+1438491t^{10}+\dots)^2$
$E_5^{k=1}$	$1+90t^2+3565t^4+84588t^6+1386700t^8+17100048t^{10}+167857416t^{12}+1365541740t^{14}+9486469554t^{16}+57589566980t^{18}+311107661634t^{20}+\dots$ $=(1+45t^2+770t^4+7644t^6+52920t^8+282744t^{10}+1241460t^{12}+4671810t^{14}+15520791t^{16}+46521475t^{18}+127891764t^{20}+\dots)^2$
$E_5^{k=2}$	$1+134t^2+128t^3+8889t^4+15616t^5+394310t^6+943360t^7+13220746t^8+37713280t^9+357061474t^{10}+1123982464t^{11}+8061468875t^{12}+26656882432t^{13}+155821066386t^{14}+524237477376t^{15}+2622606331104t^{16}+8795126835840t^{17}+38944260460754t^{18}+128525072279296t^{19}+515800796930805t^{20}+\dots$ $=(1+67t^2+64t^3+2200t^4+3520t^5+47707t^6+95040t^7+768724t^8+1691712t^9+9793069t^{10}+22431552t^{11}+102616722t^{12}+237022656t^{13}+910198783t^{14}+2083699904t^{15}+6988000316t^{16}+15707153088t^{17}+47277765667t^{18}+103827525120t^{19}+286056524848t^{20}+\dots)^2$
$E_6^{k=1}$	$1+156t^2+10944t^4+466596t^6+13807080t^8+306524790t^{10}+5377829028t^{12}+77405354312t^{14}+940221343776t^{16}+9853246779220t^{18}+90680857312617t^{20}+\dots$ $=(1+78t^2+2430t^4+43758t^6+537966t^8+4969107t^{10}+36685506t^{12}+225961450t^{14}+1198006524t^{16}+5597569328t^{18}+23474156784t^{20}+\dots)^2$
$E_6^{k=2}$	$1+184t^2+256t^3+16810t^4+43520t^5+1040056t^6+3674112t^7+49469875t^8+206409216t^9+1925805206t^{10}+8703438848t^{11}+63418779630t^{12}+294056655104t^{13}+1801033108182t^{14}+8290154332416t^{15}+44696692490453t^{16}+200425546653440t^{17}+979719926063866t^{18}+4237436679956480t^{19}+19144937799760589t^{20}+\dots$ $=(1+92t^2+128t^3+4173t^4+9984t^5+127920t^6+384384t^7+2981381t^8+9804288t^9+55764111t^{10}+186920448t^{11}+863386770t^{12}+2844037120t^{13}+11315720064t^{14}+35984655616t^{15}+127863652644t^{16}+389538715904t^{17}+1265346923490t^{18}+3684348495360t^{19}+11116073388432t^{20}+\dots)^2$
$E_7^{k=1}$	$1+266t^2+32431t^4+2437890t^6+128297273t^8+5085058160t^{10}+159309437560t^{12}+4084414731904t^{14}+87979394611180t^{16}+1625455257184024t^{18}+26192135424825720t^{20}+\dots$ $=(1+133t^2+7371t^4+238602t^6+5248750t^8+85709988t^{10}+1101296924t^{12}+11604306012t^{14}+103402141164t^{16}+797856027500t^{18}+5431803835220t^{20}+\dots)^2$
$E_8^{k=1}$	$1+496t^2+115504t^4+16918250t^6+1761796000t^8+139749232560t^{10}+\dots$ $=(1+248t^2+27000t^4+1763125t^6+79143000t^8+2642777280t^{10}+\dots)^2$

B.4 Unitary vs orthosymplectic quivers

In Section 4.3 we mentioned that not only the Hilbert series matches between E_n orthosymplectic quivers and their unitary counterparts but other functions such as superconformal indices matches as well.

B.4.1 Superconformal index

E_4 quiver. To begin with, consider $k = 1$ and $N_f = 3$. The $E_4 \cong \mathfrak{su}(5)$ quiver is given by the Dynkin diagram of $\mathfrak{su}(5)$:

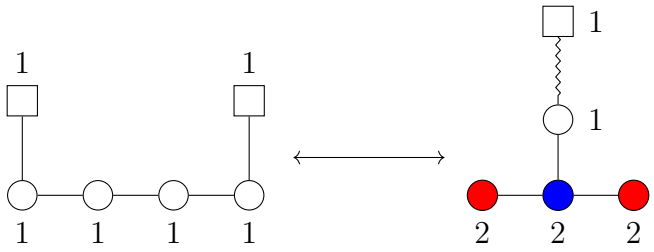

(B.1)

The wiggly line denotes a charge 2 hypermultiplet (under the U(1) gauge node). The definition of the index for the framed unitary quiver is standard; in contrast, the index for the orthosymplectic quiver requires a careful consideration of the magnetic lattice as emphasised in Section 4.4. After these preliminary remarks, a straightforward perturbative computation shows that both quivers have the same superconformal indices

$$\mathbb{I} = 1 + \sqrt{\mathfrak{q}}\left(\frac{24}{\mathfrak{t}^2} + \mathfrak{t}^2\right) + \mathfrak{q}\left(-26 + \frac{200}{\mathfrak{t}^4} + \mathfrak{t}^4\right) + 2\mathfrak{q}^{\frac{5}{4}}\mathfrak{t}^5 + \mathfrak{q}^{\frac{3}{2}}\left(\frac{1000}{\mathfrak{t}^6} - \frac{451}{\mathfrak{t}^2} + \mathfrak{t}^6\right) + \mathfrak{q}^{\frac{7}{4}}\left(-2\mathfrak{t}^3 + 2\mathfrak{t}^7\right) + \mathfrak{q}^2\left(373 + \frac{3675}{\mathfrak{t}^8} - \frac{2824}{\mathfrak{t}^4} + \mathfrak{t}^8\right) + \ldots \tag{B.2}$$

up to order $\mathfrak{q}^2$.

E_5 quiver. In the case of $N_f = 4$, the unitary quiver is the affine Dynkin quiver of D_5, whereas the orthosymplectic quiver is different. Again, to evaluate the superconformal index of the

unframed orthosymplectic, we need to adjust the magnetic lattice.

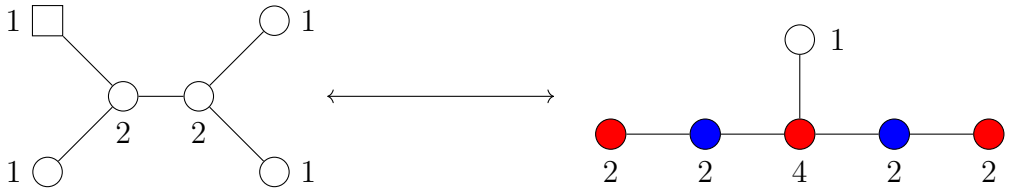

(B.3)

It is then straightforward but tedious to verify that the superconformal index of the orthosymplectic quiver below agrees up to $\mathcal{O}(\mathfrak{q}^{3/2})$.

$$1+\frac{45\sqrt{\mathfrak{q}}}{\mathfrak{t}^2}+\mathfrak{q}\left(-46+\frac{770}{\mathfrak{t}^4}+\mathfrak{t}^4\right)+\mathfrak{q}^{3/2}\left(\frac{7644}{\mathfrak{t}^6}-\frac{1714}{\mathfrak{t}^2}+\mathfrak{t}^6\right)\\+\mathfrak{q}^2\left(988+\frac{52920}{\mathfrak{t}^8}-\frac{24574}{\mathfrak{t}^4}-\mathfrak{t}^4+2\mathfrak{t}^8\right)+\cdots \tag{B.4}$$

E_6 quiver. Consider the unitary quiver whose Coulomb branch is $\overline{\mathcal{O}}^{\mathfrak{e}_6}_{\text{min}}$:

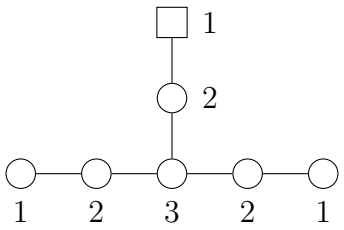

(B.5)

The unitary-orthosymplectic quiver whose Coulomb branch is the closure of the E_6 minimal nilpotent orbit $\overline{\mathcal{O}}^{\mathfrak{e}_6}_{\text{min}}$ takes the following form [3] (see also [20, A.1.5] for class $\mathcal{S}$ description):

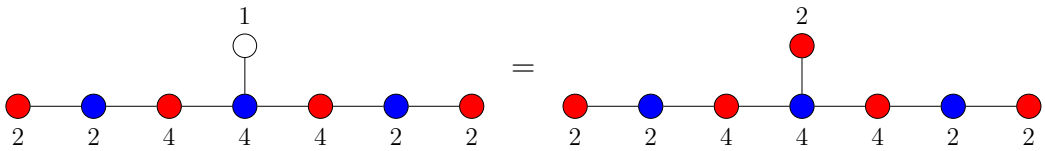

(B.6)

Since the orthosymplectic quiver is rather large, the perturbative calculation of the superconformal indices of these theories is limited to order $\mathcal{O}(\mathfrak{q})$. Nonetheless, both computations yield the same result

$$\mathbb{I}=1+\frac{78\sqrt{\mathfrak{q}}}{\mathfrak{t}^2}+\mathfrak{q}\left(-79+\frac{2430}{\mathfrak{t}^4}\right)+\dots\,. \tag{B.7}$$

Appendix C

Review: Rank 1 $\mathcal{N} = 2$ SCFTs

Based on our paper [10]

A brief review of the classification of rank one 4d $\mathcal{N} = 2$ SCFTs [66, 130, 131, 132, 200]. It is a geometric classification, based on the geometry of the Coulomb branch $\mathcal{C}$, which by definition is a complex singular space of dimension 1. In the case where there is no enhanced Coulomb branch, at a generic point on $\mathcal{C}$ the theory is a free $U(1)$ gauge theory, and interesting physics emerges at singular points. Scale invariance indicates that the singular locus is reduced to a single point, which we take to be the origin O of the Coulomb branch. On the non simply connected regular locus $\mathcal{C} - \{O\}$, the locally trivial physics undergoes non-trivial topological effects, incarnated by a non-trivial monodromy in the electromagnetic duality group $\mathrm{SL}(2,\mathbb{Z})$. Scale invariance constrains the geometry of the Coulomb branch to be one of those listed in the left part of Table 5.1. These geometries can be characterized by their Kodaira type [201]

$$K \in \{II^*, III^*, IV^*, I_0^*, IV, III, II\}\,. \tag{C.1}$$

When there is an enhanced Coulomb branch, on a generic point of the Coulomb branch there are also $d > 0$ hypermultiplets which can take vacuum expectation values, parametrizing a geometry which can be globally non-trivial (in the rank 1 case, studied in this paper, these take the form of orbifolds $h_{d,k}$, see [6]).

The geometry of the scale-invariant geometry $\mathcal{C}$ is not sufficient to fully characterize the SCFT: one also needs to understand possible $\mathcal{N} = 2$ preserving mass deformations. These

deformations break conformal invariance, so the geometry after deformation does not need to contain a single singular point. Rather, it contains a finite number of singularities which can be characterized by a finite set of Kodaira classes. The deformation parameters are invariant under (the Weyl group of) a flavor symmetry F. There can also be chiral deformation parameters. Barring the issue of discrete gauging [202], a pair $[K, F]$ entirely identifies a 4d $\mathcal{N} = 2$ rank-1 SCFT. For instance, the $\mathfrak{su}(2)$ gauge theory with $N_f = 4$ has $K = I_0^*$ (which can be deformed to $\{I_1^6\}$), $F = D_4$ and has an exactly marginal deformation parameter.

The classification gives a list of 17 rank 1 $\mathcal{N} = 2$ SCFTs (not counting IR-free theories) and can be uniquely identified by the flavor symmetry F (which is also the global symmetry of the Higgs branch).

Appendix D

Crash course on algebraic varieties

Based on our paper [11]

In this Appendix, we give a brief review of algebraic varieties and nilpotent orbits. This is based on [203, 204, 63] in which the reader will find more details and proofs.

D.1 Ideals and Varieties

We are mainly interested in two classes of objects:

- Polynomial rings of the form $\mathbb{C}[X_1, \ldots, X_n]/I$ where I is an ideal. For instance, the ring $\mathbb{C}[q, \tilde{q}]/\langle \text{F-terms} \rangle$ where $q, \tilde{q}$ are the scalars in the chiral and anti-chiral multiplets.

  Or, the ring $\mathbb{C}[M, B, \tilde{B}]$ modulo relations. This defines our chiral ring where $M, B, \tilde{B}$ are gauge invariant objects constructed from $q, \tilde{q}$ and form irreducible representations of the global symmetry group. The relations between them can be extracted from the first few negative terms in the refined plethystic logarithm of the Hilbert series.

- Algebraic varieties, i.e. the subset of $\mathbb{C}^n$ of zeroes of a finite family of polynomials.

At the heart of algebraic geometry is the correspondence between these two classes of objects. An ideal in $\mathbb{C}[X_1, \ldots, X_n]$ is always generated by a finite number of polynomials $P_1, \ldots, P_r$. In this case, we denote the ideal by $I = \langle P_1, \ldots, P_r \rangle$. Therefore to each ideal one can associate an algebraic variety. Conversely, to every algebraic variety one can associate the ideal of polynomials

which vanish on this variety. Therefore, in this thesis we often refer to a moduli space as an algebraic variety but also expresses it as a chiral ring.

However the first class contains more objects, because certain polynomials in the rings can be nilpotent, and as a consequence two ideals can correspond to the same variety. For instance the rings $\mathbb{C}[X]/\langle X\rangle$ and $\mathbb{C}[X]/\langle X^2\rangle$ both correspond to the algebraic variety $\{0\}$, but they are not isomorphic rings. The Hilbert series is sensitive to such a difference: if X is given weight 1, then the Hilbert series of $\mathbb{C}[X]/\langle X\rangle$ is 1 while the Hilbert series of $\mathbb{C}[X]/\langle X^2\rangle$ is $1+t$.

Radical To remedy this, one needs to introduce the concept of radical of an ideal. The radical of I is the ideal defined by

$$\sqrt{I} = \{f \mid f^m \in I \text{ for some integer } m > 0\} \,. \tag{D.1}$$

If an algebraic variety is defined by a set of polynomial equations $P_i = 0$ for $i = 1, \ldots, r$ in some variables $X_1, \ldots, X_n$ then the coordinate ring of this variety is

$$\mathbb{C}[X_1, \ldots, X_n]/\sqrt{\langle P_1, \ldots, P_r\rangle}\,. \tag{D.2}$$

For instance, we can check that $\sqrt{\langle X^2\rangle} = \langle X\rangle$. There is a one-to-one correspondence between the algebraic varieties and the radical ideals (this is the Nullstellensatz). In particular, the Hilbert series of an algebraic variety coincides with the Hilbert series of the ring defined by the radical ideal.

A ring without non-zero nilpotent elements is called a *reduced* ring. It follows directly from the definition that a quotient ring R/I is reduced if and only if I is a radical ideal.

The importance of radical ideals arise when we look at the classical Higgs branch of SQCD theories when the number of flavors are too small. This was discussed in great detail in our work [11] but such examples do not arise in this thesis.

Intersections and Unions of varieties In chapter 4 we looked at Higgs branches that are unions of several hyperKähler cones. These unions have non-trivial intersections and

mathematically they can be understood as the following. Given two algebraic varieties V_1 and V_2, their intersection $V_1 \cap V_2$ is again an algebraic variety. At the level of ideals, this translates into a sum. Namely, let I_1 and I_2 be the (radical) ideals associated to V_1 and V_2. The sum $I_1 + I_2$ is simply the set of all polynomials $P+Q$ for $P \in I_1$, $Q \in I_2$. We note the useful property that if $I_1 = \langle P_1, \ldots, P_r \rangle$ and $I_2 = \langle Q_1, \ldots, Q_s \rangle$, then

$$I_1 + I_2 = \langle P_1, \ldots, P_r, Q_1, \ldots, Q_s \rangle \,. \tag{D.3}$$

This makes it clear that $I_1 + I_2$ is associated with the intersection $V_1 \cap V_2$.

Similarly, a the *union* $V_1 \cup V_2$ is associated to the *intersection* of ideals $I_1 \cap I_2$. Correspondingly, the variety is written as a union of irreducible varieties (which are cones in this thesis).

D.2 Nilpotent orbits

We give a brief review on nilpotent orbits focusing on $\mathfrak{g} = \mathfrak{sl}(n, \mathbb{C})$[1]. An $\mathfrak{sl}(n, \mathbb{C})$ nilpotent adjoint orbit is characterised by a partition of n, $\lambda \in \mathcal{P}(n)$, where $\mathcal{P}(n)$ is the set of all tuples of positive integers λ_i, such that $\lambda_i > \lambda_j \forall i < j$ and $\sum_i \lambda_i = n$. As an example

$$\begin{aligned} \mathcal{P}(5) =& \{(1,1,1,1,1), (2,1,1,1), (2,2,1), (3,1,1), (3,2), (4,1), (5)\} \\ =& \{(1^5), (2,1^3), (2^2,1), (3,1^2), (4,1), (5)\} \qquad \text{(exponent notation)} \end{aligned} \tag{D.4}$$

An elementary Jordan block of order d, J_d, is a $d \times d$ matrix with all entries 0 except for super diagonal entries, which are 1

$$J_d = \begin{pmatrix} 0 & 1 & 0 & \ldots & 0 & 0 \\ 0 & 0 & 1 & \ldots & 0 & 0 \\ \vdots & \vdots & \vdots & \ddots & \vdots & \vdots \\ 0 & 0 & 0 & \ldots & 0 & 1 \\ 0 & 0 & 0 & \ldots & 0 & 0 \end{pmatrix} \in \mathbb{R}^{d \times d}. \tag{D.5}$$

[1] In the text, we simply denote these algebra as $\mathfrak{su}(n)$.

for every partition $\lambda = (\lambda_1, \lambda_2, \ldots, \lambda_k)$ we can build the nilpotent matrix

$$X_\lambda = \begin{pmatrix} J_{\lambda_1} & 0 & \ldots & 0 \\ 0 & J_{\lambda_2} & \ldots & 0 \\ \vdots & \vdots & \ddots & \vdots \\ 0 & 0 & \ldots & J_{\lambda_k} \end{pmatrix} \in \mathfrak{sl}(n, \mathbb{C}). \tag{D.6}$$

A nilpotent adjoint orbit of $\mathfrak{sl}(n, \mathbb{C})$ is now given as

$$\mathcal{O}_\lambda = \{M \in \mathfrak{sl}(n, \mathbb{C}) | M = \mathrm{Ad}_g(X_\lambda), g \in \mathrm{PSL}(n, \mathbb{C})\}. \tag{D.7}$$

Two nilpotent orbits corresponding to different partitions are disjoint sets in $\mathfrak{sl}(n, \mathbb{C})$. However, the Zariski closures of nilpotent orbits are partially ordered by inclusion. A graphical representation of this partial order is given by a Hasse diagram. The closure of an orbit is its union with all of its lower orbits in the Hasse diagram.

Appendix E

Symplectic singularities

Based on our paper [6]

In this subsection, we provide a brief guide to the mathematics of Hasse diagrams employed in the main text, referring the reader to references for the details.

In classical mechanics, a central tool is the Poisson bracket $\{f, g\}$ for f and g two functions on the phase space. This bracket satisfies

1. Skew-symmetry $\{f, g\} + \{g, f\} = 0$
2. The Jacobi identity $\{f, \{g, h\}\} + \{g, \{h, f\}\} + \{h, \{f, g\}\} = 0$
3. The Leibniz rule $\{h, fg\} = \{h, f\}g + f\{h, g\}$

More generally, a Poisson variety is any variety whose coordinate ring possesses a bracket satisfying the above three properties. Note that the Poisson bracket can be seen as a two-vector defined on the variety, called the *Poisson bivector*.

Dualising the Poisson bivector, one obtains a two-form, and vice versa. Recalling that a symplectic variety is a variety with a non-degenerate two-form, we immediately see that any symplectic variety is a Poisson variety. However, the converse is not true, because the Poisson bivector can be degenerate. For reviews of Poisson geometry, we refer to [205, 206, 207]. In this sense, Poisson geometry generalises symplectic geometry, by "allowing" the symplectic form to be degenerate.

A Poisson structure on a smooth manifold gives rise to a foliation by symplectic leaves, and these leaves can have jumps in dimensionality. This extends to symplectic singularities [208, 209], see also [210, 211] for a review. Given an affine normal variety X over $\mathbb{C}$ of even complex dimension with a non-degenerate closed two-form, we say that X is a symplectic singularity if the two-form extends to a two-form on a resolution of X. We stress that this two form does not have to be non-degenerate in general.

According to [212, Thm. 2.3], every (normal) symplectic singularity admits a finite stratification $\{0\} = X_0 \subset X_1 \subset \cdots \subset X_n = X$ such that

(i) the singular part of X_i is X_{i-1}, and

(ii) the normalisation of any irreducible component of X_i is a symplectic singularity.

In general, there exists more than one such stratification. The set of all the spaces involved in these stratifications are nevertheless partially ordered by the operation of taking the singular part. This partial order is represented by a Hasse diagram.

Questions about the properties of the symplectic leaves of a 3d $\mathcal{N} = 4$ Coulomb branch have already been raised in [213, Sec. 2].